Veröffentlichungen des Instituts für Geologie und Paläontologie der Universität Innsbruck und des Naturmuseums Südtirol/Museo Scienze Naturali Alto Adige, Bozen/Bolzano

ISSN 1824-7741

Geo.Alp

Festschrift Rainer Brandner

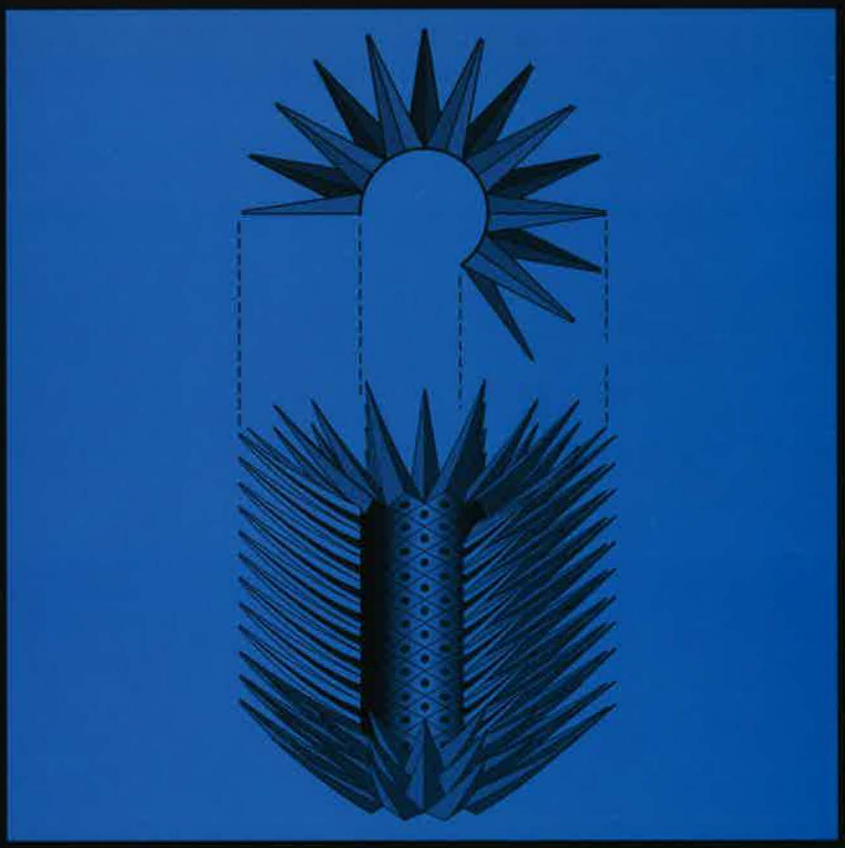

Volume 3 2006

universität innsbruck

NATURMUSEUM SÜDTIROL
MUSEO SCIENZE NATURALI ALTO ADIGE
MUSEUM NATÖRA SÜDTIROL

Geo.Alp

A yearly journal devoted to Alpine geology

Jahreszeitschrift zur Alpengeologie

La rivista per la Geologia delle Alpi

Geo.Alp

Herausgeber, Eigentümer und Verleger:
Institut für Geologie und Paläontologie, Universität Innsbruck, Naturmuseum Bozen

Chefredakteure Geo.Alp 3: Diethard Sanders, Karl Krainer

Erscheinungsweise und Bezug:
Geo.Alp erscheint einmal jährlich und kann bei beiden herausgebenden Institutionen im Abonnement oder einzeln bezogen werden:
Institut für Geologie und Paläontologie, Innrain 52, A-6020 Innsbruck, Austria
Naturmuseum Südtirol/Museo Scienze Naturali Alto Adige, Bindergasse/via Bottai 1, I-39100 Bozen/Bolzano, Italy

Genehmigung des Landesgerichts Bozen Nr. 12/2004 vim 05/11/2004
Verantwortlicher Direktor: Dr. Vito Zingerle

ISSN 1824-7741

Umschlagbild: Monika Tessadri-Wackerle, verwendete Abbildung von Petra Nittel

Druck: Walser Druck KG

INSTRUCTIONS TO AUTHORS

Articles may be submitted in English, German or Italian. In case of a German or Italian text, the captions to all figures, plates and tables must be also in English, and an English abridged version (1000–1500 words) and abstract are to be delivered.

Articles shall be submitted in three copies to:

Karl Krainer, Diethard Sanders, Institute of Geology and Palaeontology, University of Innsbruck, Innrain 52, A-6020 Innsbruck, Austria. E-mail: Karl.Krainer@uibk.ac.at; Diethard.G.Sanders@uibk.ac.at
or to:
Benno Baumgarten, Naturmuseum Südtirol/Museo Scienze Naturali Alto Adige, Bindergasse 1/Via Bottai 1, I-39100 Bozen/Bolzano, Italy: E-mail: benno.baumgarten@naturmuseum.it

Articles must be typed double-space. The quality of line-drawings must be ready for print. In line-drawings and figures of any sort, all labellings, numbers and letters should be readable upon 50% reduction in size.

Photographs and line-drawings can be submitted in original hardcopy, or in an electronic format. All photographs must be clearly labelled on the backside.

For photographic tables (plate header - e.g. "Plate 1" - included) and for text-figures: please note that the page setup of Geo.Alp is 23,47 x 16,70 cm (8 cm column width).

The final text (Word file) must be submitted on CD or Zip disk. The name of the author, the name and version of the word processing program(s) and type of computer on which the text was prepared must be indicated. To avoid obsolete passages in the manuscript please note that Word files should be saved after using the option "Accept Changes" in the Tools Menu.

Word tables must be on single pages for transformation into pdf format or already in pdf format.

The text should be submitted in single column format, and should be formatted as simple as possible (e.g. no bullets and no automatic numbering). Electronic versions of figures and/or photographs must be submitted as separate files (file format: tif (high-resolution jpg files are also possible), photographs with a resolution of 300 dpi (due to print size), line drawings at least 600 dpi; colour images all in CMYK mode.

Referencing:

Articles:
Author 1, X. Y., Author 2, Z. A. (2002): Title of article. – International journal abbreviation (e.g. Sediment. Geol.), vol.: pp–pp.

Articles in books:
Author 1, X. Y., Author 2, Z. A. (2002): Title of article. – In: Person A, Person B. (eds.): Title of book, pp–pp, publisher, place of publication.

Books:
Author 1, X. Y., Author 2, Z. A. (2002): Title of book. – no. of pages, publisher, place of publication.

Reprints: 50 reprints are free of charge

Geo.Alp

Inhalt

Geo.Alp, Vol. 3, S. 1–2, 2006

RAINER BRANDNER: EINE KURZE WURDIGUNG

Gerhard Eisbacher

Kommt ein Lehrer oder Forscher in die Jahre – und das passiert den Besten –, so fragt er sich gelegentlich, ob Begeisterung und Hingabe noch ausreichen, um die immer anonyer werdende Fangemeinde weiter an der Stange zu halten. Da ist es vor allem im Hobbyberuf des Geologen gut zu wissen, dass man mit Kollegen und Studierenden einen Arbeitsstil teilt, der es erlaubt, auch mit kürzeren Tritten alte Probleme mit neuen Fragen zu umkreisen. Dazu dient vielleicht eine Festschrift als guter Ansatzpunkt!

Rainer Brandner ist Geländegeologe in der besten Tiroler Tradition. Wie für viele Geologen seiner Generation kamen die ersten fruchtbaren Impulse für seine Arbeit jedoch nicht aus einer oft philosophisch tiefschürfenden, mit Jargon durchtränkten und semantisch isolierten „Alpengeologie". Seine Hinneigung zum Fach ergab sich vielmehr aus der Entwicklung einer neuen Sedimentologie, welche der internationalen Explorationstätigkeit entstammte und bald Eingang in die akademische Forschung und Lehre gefunden hatte. Rainer Brandners Arbeitsstil beruhte schon deshalb früh auf der engen Verbindung von detaillierter Profilaufnahme und genauen Kartierung des Umfelds. Er hat diesem Stil über Jahre die Treue gehalten. Dabei wurden auch seine Studenten darauf vorbereitet, dass jede Geologie immer auch eine regionale Geologie ist. Der erfolgreiche Einstieg vieler Absolventen aus Innsbruck in so unterschiedliche Bereiche wie die Wildbachverbauung oder die Exploration auf Kohlenwasserstoffe basiert auf dieser gesunden Mischung allgemein geowissenschaftlicher und reginalgeologischer Kenntnisse. Diese Mischung richtig zu dosieren scheint Rainer gut gelungen zu sein!

Kein Mann der pompösen Selbstvermarktung, stellt Rainer Brandner auch im Angesicht einfachster Aufschlussverhältnisse fast immer frustrierende Fragen, wo von anderer Seite bereits großmundige Lösungen angeboten werden. Diese Art des Nachfragens kostet natürlich Zeit und mancher Studierende oder Koautor wurde dabei von Symptomen zunehmender Ermüdung überwältigt. Trotzdem war es vielleicht gerade in der anwendung der Geologie auf praktische Fragen, wie die Auslage von Verkehrswegen oder Tunnelstrecken, wo Rainer – umgeben von bunt schillernden Modellen – sich der vielfachen Unsicherheiten geologische Prognosen bewusst bleiben musste.

Rainer Brandner hat immer wieder versucht, sein wissenschaftliches Arbeitsgebiet auszuweiten, vor allem in Richtung einer Tektonik, die, aufbauend von der kartierung, über ein kinematisches Verständnis der Lokalstrukturen wiederum zurück in

die Sedimentologie geführt hat. Aus der Verbindung verschiedener Arbeitsweisen ergab sich für die Geologie in Innsbruck so ein breites fachliches Fundament, das gegen Personalkürzung scheinbar immun geblieben ist, während sich viele andere Institute durch immer enger definierte Arbeitsrichtungen bis zur Irrelevanz und personellen Nullsituation durchgekämpft haben! Die Frage „welche Vorlesungen und Übungen brauchen die Leut'?" taucht in allen Diskussionen mit Rainer Brandner auf und dieses Thema wird für ihn wahrscheinlich auch weiterhin interessant bleiben. Auf der von ihm bereits geschaffenen Basis ist aber vieles viel leichter zu erhalten als an anderen Institutionen.

So kann man nur hoffen, dass Rainer noch viele Jahre der Gesundheit und ein nur von ihm selbst beschränktes Schaffen genießen kann!

Geo.Alp, Vol. 3, S. 3–8, 2006

A FURTHER ONCOCERID NAUTILOID FROM THE UPPER SILURIAN OF SOUTHWEST SARDINIA

Maurizio Gnoli & Paolo Serventi

With 2 figures and 1 table

Dipartimento del Museo di Paleobiologia e dell'Orto Botanico (Paleontologia), Università di Modena e Reggio E.

Abstract

For the first time, the Bohemian nautiloid subspecies *Oonoceras acinaces elongatum* (Barrande, 1866) (Nautiloidea, Oncocerida) is described and illustrated from the Upper Silurian (Přídolí) of southwest Sardinia.

Riassunto

Viene descritta e figurata per la prima volta nel Přídolí della Sardegna sud-occidentale la sottospecie boema Oonoceras acinaces elongatum (Barrande, 1866) (Nautiloidea, Oncocerida).

Introduction

Silurian nautiloid cephalopods of Sardinia have first been described and illustrated by Meneghini (1857) in «Paléontologie de l'Île de Sardaigne» as part of the La Marmora's book «Voyage en Sardaigne». About a century later, Serpagli and Gnoli (1977) revised the fossil collection of Meneghini supplemented by further collected material from SW Sardinia. A total of 38 species was described among which oncocerids were represented by *Oocerina abdita* (Barrande, 1877), *Oonoceras plebeium* (Barrande, 1866) and *Galtoceras*? *sardoum* Serpagli and Gnoli, 1977. Such oncocerids were reported from the Mediterranean region for the first time. Further papers on Silurian and early Devonian nautiloids of Sardinia were mostly published by members of the "Palaeozoic Team" of Modena e Reggio E. University and were dealing with the revision of the old collections (Gnoli and Serpagli, 1977), systematics (Gnoli, 1983; 1985; 1987; 1990; 1996; Gnoli and Kiselev, 1994), biostratigraphy (Gnoli and Serpagli, 1991), as well as on nautiloid palaeoecology (Gnoli *et al*., 1980; Histon and Gnoli, 1994). Finally also some Ordovician nautiloids were described (Gnoli and Serventi, 2002; Gnoli and Pillola, 2002). Information on the "state of the art" on Palaeozoic palaeontology and biostratigraphy of southern Sardinia can be found in the two volumes edited by Serpagli (1998; 1999) in connection with the Seventh European Conodont Symposium.

Systematics

We follow the systematics proposed by the Treatise on Invertebrate Paleontology, Part K, Mollusca 3 edited by R. C. Moore, with integrations by Dzik (1984) and Data Retrieval System Nautiloidea available on CD ROM compiled by Dr. T. Engeser (Freie Universität, Berlin). The studied material is part of the Paleontological Collection of the Dipartimento del Museo di Paleobiologia e dell'Orto Botanico (Università di Modena e Reggio E.), Col. No. IPUM 33100.

Subclass Nautiloidea Agassiz, 1847
Order Oncocerida Flower in Flower and Kummel, 1950
Family Oncoceratidae Hyatt, 1884
Genus *Oonoceras* Hyatt, 1884

Type species: By subsequent designation (Bassler, 1915) *Cyrtoceras acinaces* Barrande, 1866.

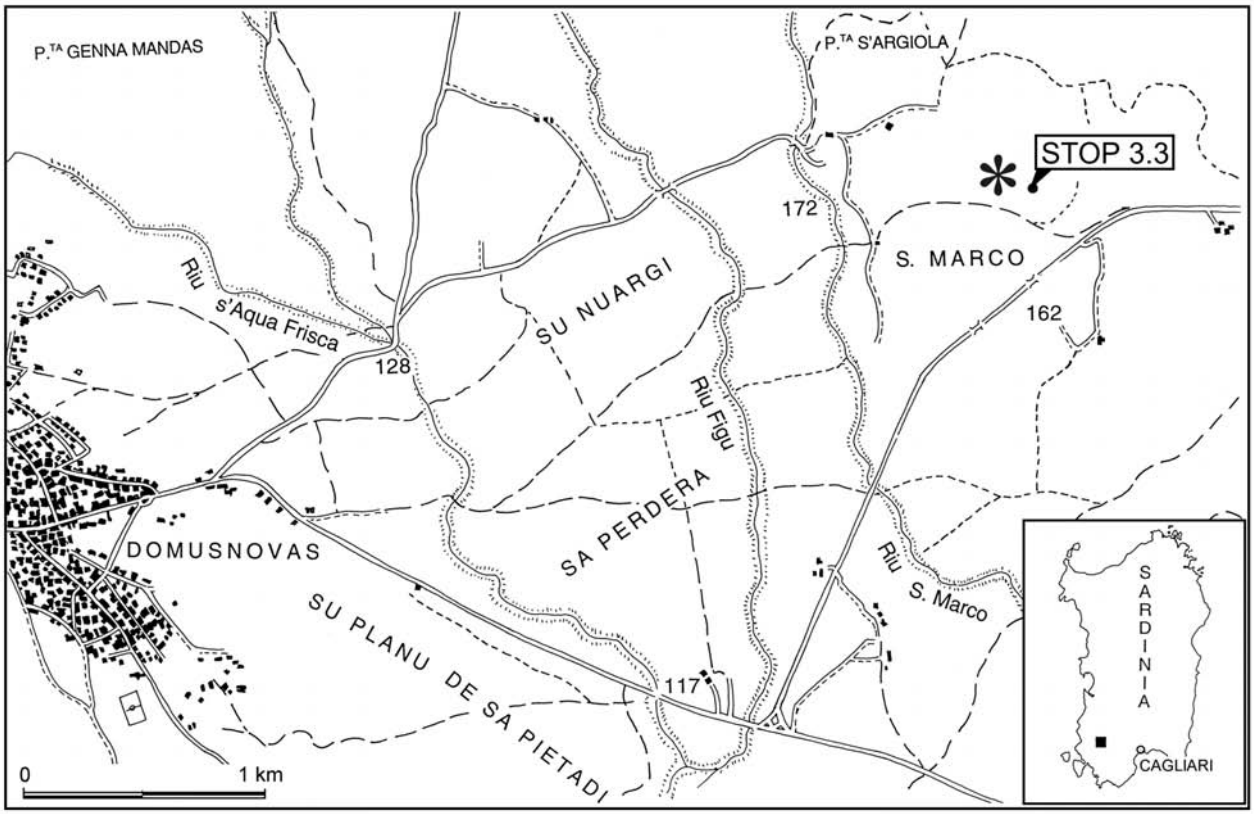

Fig. 1: Map showing the locality (marked with an asterisk*) from which the studied nautiloid was recovered (after Corradini et al., 1998).

Remarks: According to Dzik (1984, p. 55) "... the topotype population of *C. acinaces* recorded from Dlauha Hora includes also *Cyrtoceras sociale*, *C. plebeium*, *C. elongatum* and *C. hoernesi*."

We assume that the differences between these taxa such as different curvatures of the shell, cross-sections and some details like periphracts encircling the basal zone of the body chambers of Oncocerida (e.g. Barrande, 1877, pl. 508, figs. 8, 9, and 11) justify that *C. sociale*, *C. plebeium*, *C. elongatum* and *C. hoernesi* are actually subspecies of *acinaces* (see also http://www.iczn.org/iczn/index.jsp, Article 61.4). Manda (pers. com. 2005-05-05.) also agrees that the Barrande taxa mentioned above are not synonyms at a specific level except *C. acinaces* that could represent a gerontic stage of *C. sociale*. However, in order to verify definitely if the taxa mentioned above are valid at a species or subspecies level it is necessary to know the exact stratigraphic level of each taxon within the Bohemian sequence which seems, at the moment, almost impossible (see tab.1).

Oonoceras acinaces elongatum (Barrande, 1866)
(Text-figs. 2a-d)

1848 *Cyrtoceras elongatum* Barrande - Haidinger, p. 208 (*nomen nudum*).
1852 *Cyrtoceras elongatum* Barrande - Giebel, p. 209 (*nomen nudum*)
1866 *Cyrtoceras elongatum* Barrande, pl. 109, figs. 1-10; pl. 117, figs. 5-11; pl. 157, figs. 50-55; pl. 202, figs. 16-18; pl. 205, figs. 16-18; pl. ?208, figs. ?29-?30.
1874 *Cyrtoceras elongatum* Barrande, pp. 499-500.
1877 *Cyrtoceras elongatum* Barrande, pl. ?508, figs. ?9-?11.
1984 *Oonoceras acinaces* (Barrande, 1866) - Dzik, p. 55.

Description: The available material of this species consists of one incomplete fragment of the conch which is 75 mm long showing ten preserved chambers of the phragmocone and the lower part of the living chamber. It represents an exogastric cyrto-

Tab. 1: Species, localities and ages after Barrande, 1874 compared with available data (Štorch, pers. comm., 2004-3-25).

Barrande species	**Localities after Barrande**	**Horizons/ Age**	**According to Dr. P. Štorch (Czech Academy of Science, Prague) (pers. comm. 2004-3-25) the stratigraphic position of the locations mentioned by Barrande, 1866 reported as at present names could be as follows:**
C. acinaces	Dlauha Hora, Butowitz	E, e2	Dlauha Hora (Kosov-Dlouhá hora u Berouna) - several test pits and small quarries, several stratigraphic levels ranging from middle to uppermost Ludlow (*S. fritschi linearis - M. formosus* graptolite biozones);
C. elongatum	Dvoretz, Vyskocilka, Lochkov, Kozořz, Hinter-Kopanina, Karlstein, Konieprus, Dlauha Hora	E	Butowitz (Butovice) - lowermost Ludlow (*N. nilssoni -L. progenitor* graptolite biozones), Kovářovic Mez nearby corresponds to the upper Ludlow; Karlstein (Karlštejn) - Přídolí and Lochkovian, possibly also uppermost Ludlow. Hinter-Kopanina (Zadní Kopanina) - several levels of Ludlow, Přídolí and lowermost Lochkovian (several scattered outcrops, test-pits and small quarries.
C. hoernesi	Dlauha Hora	E	Dlauha Hora (Kosov-Dlouhá hora u Berouna) - several test-pits and small quarries, several stratigraphic levels ranging from middle to uppermost Ludlow (*S. fritschi linearis - M. formosus* graptolite biozones).
C. plebeium	Dvoretz, Butowitz, Vyskočilka, Lochkov, Kozořz, Karlstein, Dlauha Hora	e1, e2	Dvoretz (Praha 4-Dvorce) - Unclear, probably ranging from Ludlow to upper Přídolí.
C. sociale	Dvoretz, Vyskočilka, Slivenetz, Lochkov, Kozořz, Konieprus, Dlauha Hora	E	Vyskocilka (Malá Chuchle - Vyskočilka), Middle Wenlock, several levels dated as Ludlow and Přídolí (several test pits and small quarries); Lochkov (probably *Orthoceras* quarry) - upper Ludlow and lower Přídolí; Kosorz (if it corresponds with Černá Rokle, it is probably Lochkovian in age). Konieprus (Koněprusy) - once again, this designates several places N and NE of Koněprusy and correspond to several levels within the Ludlow; Slivenetz (Slivenec) – unclear.

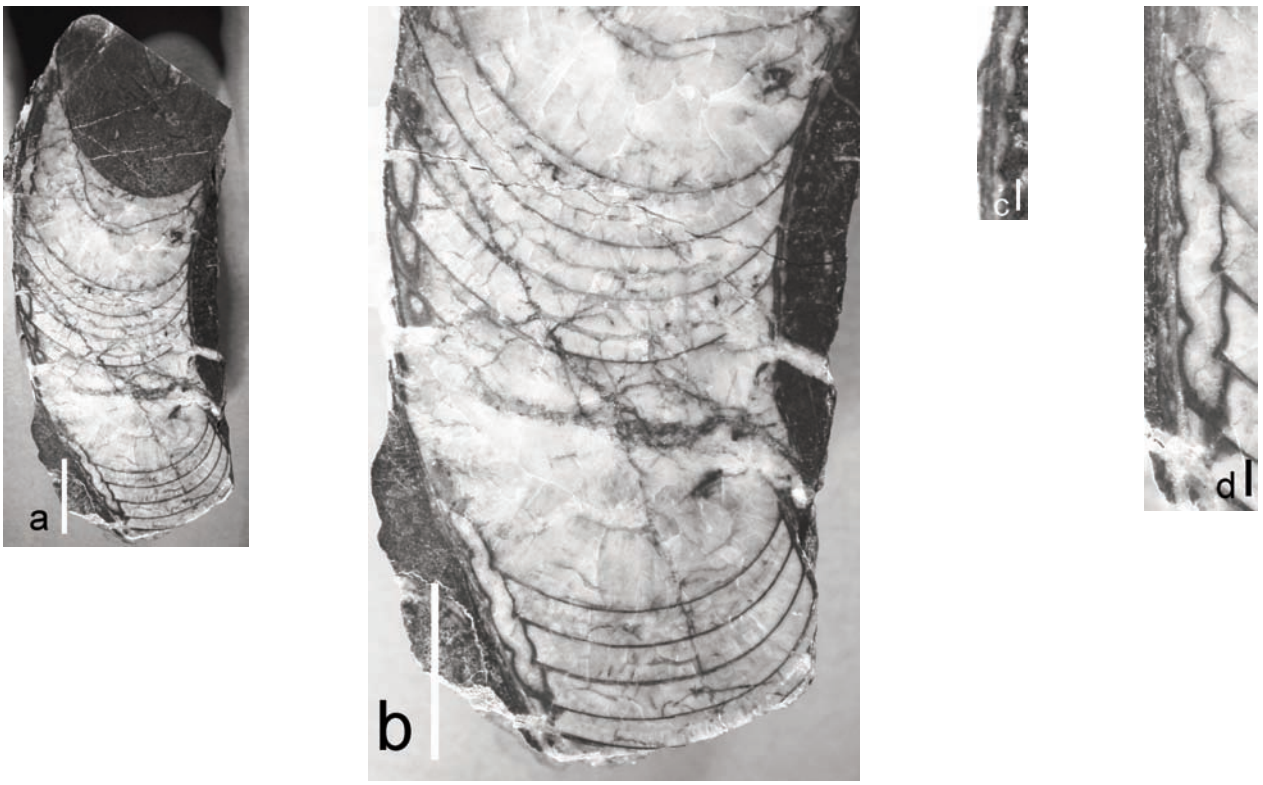

Fig. 2: *Oonoceras acinaces elongatum* (Barrande, 1866)
a) General view of the polished longitudinal middle section of the studied specimen (Coll. No. IPUM 33100);
b) Fig. a enlarged to show the inner features and the preserved chambers of the phragmocone;
c) Enlarged polished longitudinal section showing the pattern of ornamentation in the ventral test of the shell;
d) Detail of the siphuncle in contact to the ventral inner side of the shell showing the very short and recumbent cyrtochoanitic septal necks, the connecting rings slightly expanded inside the chambers and its sigmoidal pattern. Note that all the images do not show any kind of primary deposit either cameral or endosiphuncular. Scale bar in a) and b) = 1cm; in c) and d) = 1mm.

conic depressed, apparently smooth shell of subelliptical cross section. In parts of the ventral test striations in the form of sub-regular oblique, apparently imbricate rounded striae as shown in the enlarged longitudinal polished section of Fig. 2c, are visible. The dorso-ventral diameter near the base of the living chamber measures 26 mm, the lateral one 16 mm, resulting in a ratio of about 3:5 The curvature of the shell is variable due to ontogenesis, the radius of the ventral side of the mature phragmocone measures about 7 cm and that of the dorsal side 5 cm. The chambers are short, the depth measures about 1/4 of their diameter; the distance between the septa varies from 2.5 to 4 mm, corresponding to 1/10 of the dorso-ventral diameter. The siphuncle is very close to the ventral side of the shell. Its elements are cyrtochoanitic in shape resulting in a sigmoid pattern in longitudinal section. The septal neck is very short and recumbent; cyrtochoanitic connecting rings are slightly expanded inside the chambers. Their maximum diameter is 1.5 the septal foramen which in turn is half the septal spacing or 1/12 of the corresponding dorso-ventral diameter of the shell. No primary deposits either cameral or endosiphuncular have been observed.

Remarks: The studied specimen was tectonically deformed and recrystallized during diagenesis. However, despite of that, enough diagnostic features are preserved for a correct identification.

A possible Přídolí age of the studied specimens is supported by the occurrence of the nautiloid species *Orthocycloceras*? *fluminese* in the same iso-

lated block (Meneghini, 1857) (Gnoli and Serpagli, 1991, tab. 1) which up to now is known from limestones of Přídolí age only.

The occurrence of *O. acinaces elongatum* (Barrande) in SW Sardinia allows emphasizing once more the intimate faunistic relationships between the Silurian of Sardinia and Bohemia stressed by fossil cephalopods.

Occurrence: Upper Silurian (Přídolí) of SW Sardinia, Upper Silurian (see tab. 1) of Central Bohemia.

Material studied: One specimen (IPUM 33100) from one isolated block (labelled as BK-ARG 24) composed of micritic limestone poor in fossils collected from the Argiola area near Domusnovas (SW Sardinia, fig. 1).

Acknowledgements

This search was funded by MIUR grants (Responsible Prof. E. Serpagli) and the PRIN 2004 Project "The end and the beginning: loss and recoveries from the end-Ordovician mass extinction in North Gondwana" (Responsible Prof. A. Ferretti, Modena and Reggio E. University). Dr. Š. Manda (Czech Geological Survey) Dr. P. Štorch (Czech Academy of Science) provided invaluable help on the stratigraphy of the Barrandian localities. The authors are deeply indebted to Prof. Serpagli (Modena and Reggio E. University) for useful suggestions and advise. K. Krainer (Innsbruck University) improved the English.

References

Barrande, J. (1866): Système Silurien du Centre de la Bohème - 1re Partie : Rech. Pal. 2, Classe de mollusques, Ordre des Céphalopodes, 2 Sér., pls. 108-244., Prague.

Barrande, J. (1874): Système Silurien du Centre de la Bohème - 1re Partie : Rech. Pal. 2, Classe de mollusques, Ordre des Céphalopodes, Texte 3: 1-804., Prague.

Barrande, J. (1877) : Système Silurien du Centre de la Bohème - 1re Partie : Rech. Pal. 2, Classe de mollusques, Ordre des Céphalopodes, Suppl. et Sér. Tard. Pls. 461-544, Prague.

Corradini, C., Ferretti, A., Serpagli, E. (1998): Wenlock and Pridoli conodonts from Argiola. - Giornale di Geologia, ser. 3°, vol. 60, 1998, Spec. Issue, ECOS VII - Sardinia Guide-book, pp. 194-198, Bologna

Dzik, J. (1984): Phylogeny of the Nautiloidea. - Palaeontologia Polonica, vol. 45: 3-203.

Engeser, T (1999): Data Retrieval System Nautiloidea (available on CD ROM thanks to the courtesy of the Author).

Gnoli M. (1983): A Lower Devonian orthocone cephalopods from Iglesiente and Sulcis regions (south-western Sardinia). - Boll. Soc. Paleont. Ital., 21(1),1982: 73-98.

Gnoli, M. (1985): Paleontological content, constituent analysis and microbiofacies of Early Devonian pelagic limestones from the Fluminimaggiore area. - Boll. Soc. Paleont. Ital., 23(2): 221-228

Gnoli, M. (1987): Revision and autecological remarks of the species *Columenoceras grande* (Meneghini, 1857) (Nautiloidea, Orthocerida). - Boll. Soc. Paleont. Ital., 26(3): 245-250.

Gnoli, M. (1990): New evidence for faunal links between Sardinia and Bohemia in Silurian time on the basis of nautiloids. - Boll. Soc. Paleont. Ital., 29(3): 289-307.

Gnoli, M (1996): Occurrence of a Bohemian type Phragmoceratid (Nautiloidea) from the Silurian of South-western Sardinia. - Accad. Naz. Sci. Lett. Arti di Modena, Collana di Studi, 15: 355-360.

Gnoli, M, Kiselev, G. N. (1994): Revision of the family Sphooceratidae Flower, 1962. - Boll. Soc. Paleont. Ital., 33(3): 415-420.

Gnoli, M, Pillola, G. (2002): The oldest nautiloid cephalopod of Sardinia: *Cameroceras* cf. *vertebrale* (Eichwald, 1860) from the Arenig (Early Ordovician) of Tacconis (South East Sardinia) and remarks on associated biota. - N. Jb. Geol. Paläont. Mh., 2002(1): 19-26, 2 figs., Stuttgart.

Gnoli, M, Serpagli, E. (1977): Silurian cephalopod of the Meneghini collection (1857) with the reproduction of the original plate. - Boll. Soc. Paleont. Ital., 16(2): 137-142.

Gnoli, M., Serpagli, E. (1991): Nautiloid assemblages from Middle-Late Silurian of Southwestern Sardinia: a proposal. - Boll. Soc. Paleont. Ital., 30(2): 187-195.

Gnoli, M, Serventi, P. (2002): Some nautiloid cephalopods from the Ordovician of southern Sardinia. - Boll. Soc. Paleont. Ital., 41(2-3): 109-119.

Gnoli, M., Parea, G. C., Russo, F., Serpagli, E. (1980): Paleoecological remarks on the "*Orthoceras*" limestone of South-western Sardinia (Middle-Upper Silurian). - Mem. Soc. Geol. It., 20(1979): 405-423.

Gnoli, M., Kříž, J., Leone, F., Olivieri, R., Serpagli, E., Štorch, P. (1990): Lithostratigraphic units and biostratigraphy of the Silurian and early Devonian of Southwest Sardinia. - Boll. Soc. Paleont. Ital., 29(1) : 11-23.

Histon, K., Gnoli, M. (1994): Bathymetry of the Silurian nautiloid fauna from the "Orthoceratite Limestone", SW Sardinia. IUGC SSS, Field Meeting 1994, Bibl. Geol. B. - A. 30/94, 131-132.

Kříž, J. (1998): Recurrent Silurian-Lowest Devonian Cephalopod Limestone of Gondwanan Europe and Perunica. In: E. Landing and M. E. Johnson (eds.), Silurian Cycles, Linkage of Dynamic Stratigraphy with Atmospheric, Oceanic, and Tectonic Changes, James Hall Centennial Volume. New York State Museum Bull. 491, pp. 183-198, New York.

Leone, F., Hamman, W., Laske, R., Serpagli, E., Villas, E. (1991): Lithostratigraphic units and biostratigraphy of post sardic Ordovician sequence in South-West Sardinia. - Boll. Soc. Paleont. Ital., 30 (3): 201-235.

Meneghini, G. (1857): Paléontologie de l'Île de Sardaigne in: La Marmora, A. Voyage en Sardaigne, pp. 53-144, Imprimerie Royale, Turin.

Moore, R. C. (Ed.) (1964): Treatise on Invertebrate Paleontology, Part K, Mollusca 3, 219 pp., The Geological Society of America and The University of Kansas Press.

Serpagli, E. (Ed.) (1998): Sardinia Guide-book, ECOS VII. - Giorn. Geologia, 60. Spec. Issue, 212 pp., Bologna.

Serpagli, E. (Ed.) (1999): Studies on conodonts - Proceedings of the Seventh European Conodont Symposium. - Boll. Soc. Paleont. Ital., 37 (2-3) (1998): 420 pp.

Serpagli, E., Gnoli, M. (1977): Upper Silurian cephalopod from South-western Sardinia. - Boll. Soc. Paleont. Ital., 16(2): 153-195.

Geo.Alp, Vol. 3, S. 9–21, 2006

DIE REINGRABENER WENDE IN DER HALLEINER SALZBERGFAZIES (DISTALE HALLSTATTFAZIES) - BIOSTRATIGRAPHISCHE DATEN

Thomas Hornung

Mit 8 Abbildungen

Institut für Geologie und Paläontologie, Innrain 52, A-6020 Innsbruck; e-mail: thomas.hornung@uibk.ac.at

Zusammenfassung

Zwei Profile nahe Bad Dürrnberg (2 km SSW' Hallein, Österreich) ermöglichten erstmals eine durchgehende biostratigraphische Untersuchung der Reingrabener Wende im Bereich des Hallstätter Beckens (Hallstätter Salzbergfazies), welche zeitlich mit dem weitaus bekannteren Raibl-Event im nordalpinen randmarinen Flachwasserbereich vergleich- und vermutlich auch korrelierbar ist. Komplette Profile ohne signifikante stratigraphische Lücken sind jedoch im hochenergetisch-flachmarinen Bereich der nordalpinen Raibler Schichten mehr als fraglich – mangelnde oder fehlende Conodontenfunde lassen dort zudem keine exakte biostratigraphische Einordnung zu. Weitaus besser stehen die Chancen kompletter stratigraphischer Überlieferung im niedrigenergetischen Hallstätter Becken.

Eine detaillierte Bank für Bank-Beprobung beider Profile lieferte eine reichhaltige karnische Condontenfauna, deren charakteristische Vergesellschaftungen eine genaue biostratigraphische Zuordnung der Profile und der in ihnen aufgeschlossenen lithologischen Wenden zuließen. Der Zeitumfang der Reingrabener Wende kann von Jul 1/IIc bis Jul 2/II angegeben werden. Die Bestätigung der Biostratigraphie durch Ammoniten war aufgrund fehlender Funde nicht möglich.

Abstract

For the first time, two outcrops near Bad Dürrnberg (2 km SSW' Hallein / Salzkammergut, Austria) allowed a continuous biostratigraphical investigation of the Reingraben Turnover in the Hallstatt facies belt (epicontinental basin).

Because of rare outcrops of continuous Carnian successions in the Salzkammergut area, this turnover, comparable to the northern Alpine Raibl Event in shallow-marine facies, was treated by a few authors only. The Carnian deposits of the Hallstatt basin should provide more complete sequences as coeval shelf sediments that may be stratigraphically incomplete. The biostratigraphical correlations were assessed by conodont faunas – ammonite findings were completely lacking: several conodont associations were found. They led to a biostratigraphical stratification of the sections and fixed the timespace of the Reingraben Turnover between Julian 1/IIc and Julian 2/II.

Summary

As detailed investigations of complete Carnian sections actually lacked and reworked famous Northern Alpine Raibl-successions obviously provided significant stratigraphical gaps, only basinal sequences, deposited within low energy setting most probably led to complete studies. Two sections in the Salzkammergut region with a nearly complete Carnian succession near Hallein were promising candidates for a Hallstatt "standard section" comparable to other facies belts and, thus, a "hanger" for widespread stratigraphical correlations.

The geology in the vicinity of the Freygutweg section and the Jakobberg gallery near Bad Dürrnberg (Salzburg, Austria) is characterised by a stack of nappes preserved in the western Hallstatt region: First, the Tirolic facies belt was overthrust by the Juvavic (= Hallstatt) nappe (Fig. 1a). Transpression during the latest Jurassic and Cretaceous led to an "out-of-sequence" thrusting of both units (Mandl 1999), resulting in a doubling of the nappe complex. The "lower" stack was, in turn, overthrust by the Berchtesgaden nappe (Fig. 1a, southern Tirolic facies). The overlying (southern) parts were eroded during the late Cretaceous, and subsequently became overlain by the Late Cretaceous and Tertiary Gosau Group (Fig. 1a). For further discussion of paleogeography and regional tectonics see e.g. Neubauer (1994), Schweigl and Neubauer (1997), Gawlick et al. (1999b), Gawlick (2000), Gawlick and Diersche (2000), Gawlick and Lein (1997, 2000), Frisch and Gawlick (2003).

Both sections were combined into a single stratigraphical sequence that starts in the lowermost Julian (questionably topmost Langobardian) and ends in the basal Lacian. The succession contains the "Carnian Terrigenous Event" or the "Reingraben Turnover" (after Schlager and Schöllnberger 1974) which is represented by the Reingraben Shales.

Due to the absence of ammonoids, age-dating of the sections had to be based on conodonts. A detailed Lower Carnian conodont zonation has been proposed by Gallet et al. (1994). This zonation, however, is based on species absent in the investigated Salzkammergut sections (i.e. *Metapolygnathus auriformis*, *M. carnicus*). Therefore, this study accorded mainly to the local studies of Krystyn (1980).

The first occurrence of *Metapolygnathus polygnathiformis* Budurov & Stefanov (Fig. 7, pict. 7) places the Ladinian-Carnian boundary at the base of both Salzkammergut sections (well-bedded grey limestones). Uppermost Langobardian (*regoledanus* ammonite zone) is evidenced by Gawlick et al. (1999a) in the Jakobberg gallery. The presence of the *mostleri* conodont assemblage zone (A. Z.) (lower *aonoides* ammonite zone or Julian 1/I) and of the *tadpole* conodont interval zone (base of the upper *aonoides* Zone or Julian 1/IIa) is uncertain. *Metapolygnathus mostleri* is absent in the Freygutweg section, *Paragondolella. tadpole* occurs only very rarely (two specimens, Fig. 7, pict. 2) present in the middle part of the thick-bedded grey limestones. The *tethydis* conodont assemblage zone (coexistence of *Gladigondolella tethydis* Huckriede with *M. polygnathiformis*), representative of the upper aonoides ammonite zone and the *austriacum* ammonite zone (Julian 1/II to 2/II), includes uppermost thick-bedded grey limestones, ochre-coloured limestones and Reingraben Shales. Because of the absence of *M. auriformis* and the abundance of *Gl. tethydis* (Fig. 7, pict. 3, 4; Fig. 8, pict. 10), the *tethydis* A.Z. is favoured (unlike to Krystyn 1983). As a result, the very depauperate fauna of *M. polygnathiformis* (Fig. 7, pict. 8) and *Gl. tethydis* allows an age assignment of middle to late Lower Carnian (*aonoides* to *austriacum* ammonite zone resp. *tethydis* conodont zone). The abrupt disappearance of *Gl. tethydis* in the nodular red flaser limestones atop the Reingraben Shales proves the exclusive Early Carnian (Julian) age of the Reingraben Turnover in the Hallstatt facies of Berchtesgaden and in other facies regions (Hornung et al. 2005). Two lithological turnovers, **a)** the change of thick-bedded grey limestones to ochre-coloured limestones and **b)**, from ochre-coloured limestones to Reingraben Shales are embedded in the time interval from Julian 1/IIc to Julian 2/II (see Fig. 4).

The boundary between Reingraben Shales and the nodular red flaser limestones is representative for the beginning of the *polygnathiformis* A. Z. (Fig. 7, pics. 12, 14, 17 – *dilleri* ammonite zone and lower *subbullatus* ammonite zone, Tuvalian 1 to 2/I) and a third lithological event ("oxic event"). Rare *Metapolygnathus carpathicus* designed the *carpathicus* A.Z. (Fig. 7, pict. 15; upper *subbullatus* ammonite zone or Tuvalian 2/II). The FAD (first appearance date) of *Metapolygnathus nodosus* (Fig. 7, pict. 16) defines the *nodosus* A. Z. (*spinosus* ammonite zone or Tuvalian 3) at the very base of the bedded light-coloured limestones. The uppermost Carnian conodont assemblage zone identified by the occurrence of *M. communisti* (uppermost spinosus ammonite zone) is evidenced by Gawlick et al. (1999a).

The first occurrence of *Norigondolella navicula* Huckriede (Fig. 8, pict. 1) is representative of the Carnian-Norian boundary. Together with *Epigondolella abneptis* (Fig. 8, pict. 2, 4, 7), *E. spatulata* (Fig. 8, pict. 5) and *E. triangularis* (Fig. 8, pics. 3, 8) these conodonts indicate a condensed fauna of the basal Norian (Lacian 1 to Lacian 3). Therefore, the Carnian / Norian boundary is not equivalent to the litholothical change from nodular red flaser limestones to bedded light-coloured limestones.

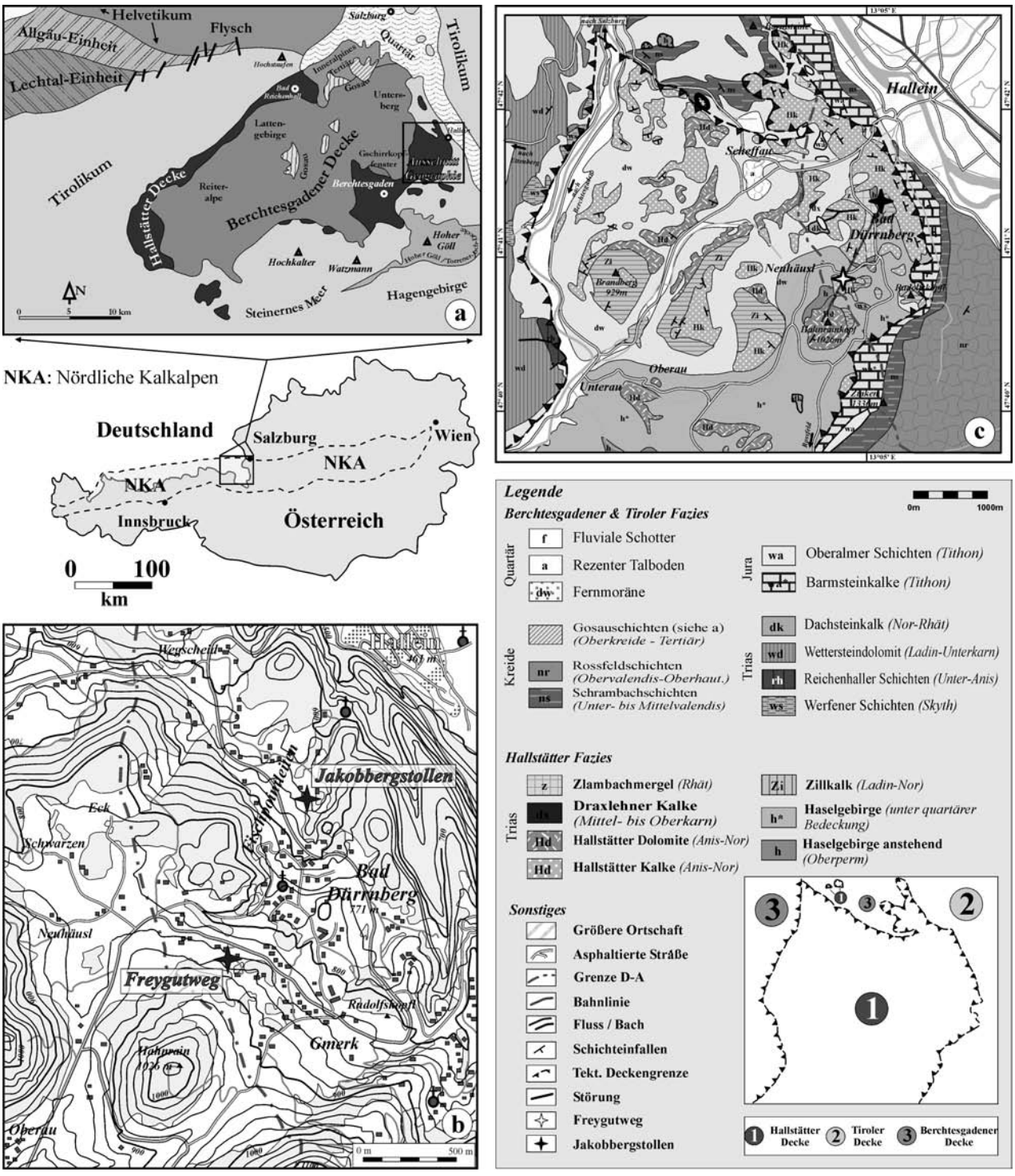

Abb. 1: Geologisch-tektonische Verhältnisse der Hallein Berchtesgadener Schollenregion (a - verändert nach Braun 1998) sowie geographische Lage der untersuchten Profile (b). Vereinfachte geologische Karte der Hallein-Berchtesgadener Schollenregion (c) mit der Lage beider Profile (verändert nach Plöchinger 1955, Prey 1969 und Gawlick 2000).

Fig. 1: Main geological and tectonical setting of the area (a - modified after Braun 1998) and (b) geographic position of the sections. Simplified geological map of the fault-block region of Hallein-Berchtesgaden (c - modified after Plöchinger 1955, Prey 1969 and Gawlick 2000).

At least three distinct lithological changes, **a)** bedded grey limestones to ochre-coloured limestones, **b)** ochre-coloured limestones to the Reingraben Shales, and from **c)** the Reingraben Shales to nodular red flaser limestones can be recognized in the studied succession. They record changes in oxygen, lime and mud supply and might be explained with variations in oceanic circulation. Stagnated and recovered productivity of adjacent carbonate shelves, triggered by different amounts of terrigenous input might have caused nutrient excess and local anoxic setting (Hornung & Brandner 2005).

1. Einleitung

Die Reingrabener Wende sensu Schlager & Schöllnberger (1974) ist in allen Faziesräumen der alpin-mediterranen Tethys sowohl in Lithofazies, Biofazies und Ökofazies nachzuvollziehen. Die Hauptgründe für das Absterben beinahe aller Riffe des westlichen Tethys-Randbereiches dürften der plattentektonische Zerfall Pangaeas und durch drastische Klimaschwankungen ausgelöster verstärkter terrigener Eintrag mit nachfolgendem Nährstoff-Überfluss gewesen sein (z.B. Hallock & Schlager 1986, Riedel 1991, Rüffer & Zamparelli 1997, Keim & Brandner 2001).

Nur wenige Autoren (u.a. Plöchinger 1955, Mandl 1984, Gawlick 2000) schenkten der Reingrabener Wende Beachtung, obgleich die Untersuchung des Hallstätter Faziesbereiches mehr als 150 Jahre währt (Bibliographie siehe u.a. bei Gawlick 2000 sowie Gawlick & Lein 2000). Im Rahmen des FWF-Projektes P 16878-Geo („Das karnische Ereignis im westlichen Tethysraum") bildet die Region des zentralen Salzkammergutes (vgl. Hornung & Brandner 2005) neben Profilen in Niederösterreich, der Türkei und dem indischen Himalaya nur einen Bereich für überregionale hochauflösende stratigraphische Untersuchungen.

2. Geographie und Geologie

Die beiden Lokalitäten liegen unweit der Ortschaft Bad Dürrnberg (ca. 2 km SSW' Hallein, Abb. 1b). Das relativ flache Hochplateau liegt am Fuße eines Höhenzuges, der vom Hohen Göll über das Rossfeld Nord-Süd streicht und sich weiter nördlich kontinuierlich ins die Tiefebene bei Salzburg absenkt. Eine knapp 300 m hohe Steilstufe, die im ausgehenden Pleistozän durch den nach Norden abfließenden Berchtesgadener Gletscher ausgehobelt wurde, trennt die Hochfläche vom weiten Berchtesgadener Talkessel westwärts.

Die Geologie des Untersuchungsgebietes wird von einer ausgeprägte Deckenstapelung bestimmt. Bereits im Jura wurde das Tirolikum von der Hallstätter Decke („Juvavikum") überschoben. Verstärkte Transpression im Oberjura und in der Unterkreide verursachten eine „Out of sequence"-Überschiebung und eine tektonische Verdoppelung beider Decken (Mandl 1999): so kam auf dem zuunterst liegenden Deckenstapel südliche tirolische Fazies („Berchtesgadener Decke") mit auflagernden Reliktschollen von Hallstätter Fazies zum Liegen, die allerdings frühkretazisch weitgehend erodiert und mit spätkretazischer bis tertiärer Gosau plombiert wurden (Abb. 1a).

Exakte Paläopositionen und die zeitlich-tektonische Abfolge sind zurzeit noch Gegenstand der Diskussion (Neubauer 1994, Schweigl & Neubauer 1997, Gawlick et al. 1999b, Gawlick 2000, Gawlick & Diersche 2000, Gawlick & Lein 1997, 2000, Frisch & Gawlick 2003).

3. Stratigraphie

Schlager (1969) etablierte die erste lithostratigraphische Differenzierung der Hallstätter Kalke in einem „Normalprofil", welches von Mandl (1984 & 1999) sowie Gawlick (2000) erweitert wurde (Abb. 2). Dabei fielen zahlreiche lokal unterschiedliche, jedoch isochrone miteinander verzahnende Schichtfolgen auf: ihre unterschiedliche Sedimentationsgeschichte liegt in einer engräumigen, mobilen submarinen Morphologie begründet (synsedimentäre, durch Salzdiapirismus des unterlagernden Haselgebirges angelegte und aufsteigende Tiefschwellen, s.a. Mandl 1999, Gawlick 2000).

Die räumliche Ausdehnung unterschiedlicher Lithologien wie Rotkalke und Schwarzschiefer ist nach neueren Ansichten nicht statisch gewesen, sondern hing von verschiedenen regionalen Faktoren wie mobiler Untergrund, Wasserzirkulation, Sauerstoffangebot und Eintrag terrigenen Materials ab. Auch übergeordnete klimatische und tektonische Prozesse dürften eine entscheidende Rolle gespielt haben (Simms & Ruffell 1989, Mutti & Weissert 1995, Hornung & Brandner 2005). Zudem

wurde der Bereich der Hallstätter Stillwasserzone von benachbarten Karbonatplattformen stärker beeinflusst als bisher angenommen (siehe auch Reijmer & Everaars 1991). So spiegelt sich unterschiedlich hohes Angebot an Kalziumkarbonat in den Beckenbereichen mit tonärmeren oder tonreicheren Ablagerungen wider (s.a. Gawlick 2000).

4. Profile

A) Freygutweg: Das stark kondensierte Profil (Abb. 3 & 6) wurde 1995 im Zuge von Straßenarbeiten neu erschlossen und erstmals von Gawlick et al. (1999a) bearbeitet.

Alle Schichten fallen überkippt mit 25° nach SSE ein. Die sedimentäre Basis bilden ca. 5 Meter mächtige dickbankige Graukalke. Über einer vermutlich tektonisch bedingten Schichtlücke folgen ca. 2,75 m mächtige dunkle Reingrabener Schiefer („Halobienschiefer"), die in wechselnden Abständen von im unteren Abschnitt fossilreichen, komplett entschichteten, im oberen Bereich von feinlaminierten Karbonatbänken durchzogen werden. Die Obergrenze zum Roten Knollenflaserkalk ist über einer sedimentären Schichtlücke (Basalbrekzie) scharf ausgebildet. Die darüber folgenden, im dm-Bereich gebankten Roten Knollenflaserkalke (Mächtigkeit ca. 2,3 m) werden von 3 m mächtigen gebankten Hellkalken überlagert.

B) Jakobbergstollen: Die Schichtenfolge des aufgelassenen Jakobbergstollens (Medwenitsch 1949, 1958, 1962 & 1963, Gawlick et al. 1999a, Gawlick & Lein 1997 & 2000) reicht von dickbankigen Grau-

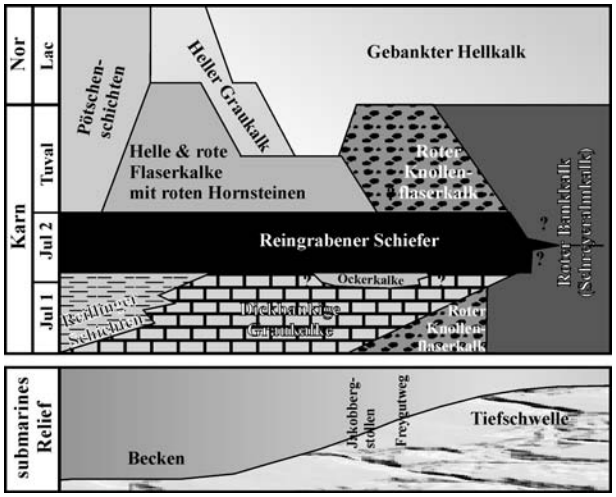

Abb. 2: Stratigraphische Abfolge des Hallstätter Faziesbereichs (verändert aus Mandl 1984 & 1999 sowie Gawlick 2000) in Abhängigkeit zum Paläorelief mit der ungefähren paläogeomorphologischen Lage beider Profile (senkrechte schwarze Pfeile).

Fig. 2: Stratigraphic succession depending on paleomorphological patterns (modified after Mandl 1984, 1999 and Gawlick 2000). The position of the sections might be placed on the upper edge between the top of the "sills" and the basins (black arrows).

kalken des ?Fassan und Langobard bis zu den tiefjurassischen Liasfleckenmergeln. Der für die Untersuchungen interessante Stollenabschnitt liegt zwischen 825 und 835 Metern hinter dem Portal und erschließt in einer geringmächtigen, vermutlich kondensierten Schichtfolge die im Freygutweg tektonisch reduzierte Obergrenze der dickbankigen Graukalke. Diese sind mikrofaziell denen des Freygutweges gleichzusetzen und grenzen scharf an eine dünne grüne Mergellage an, die eine Periode

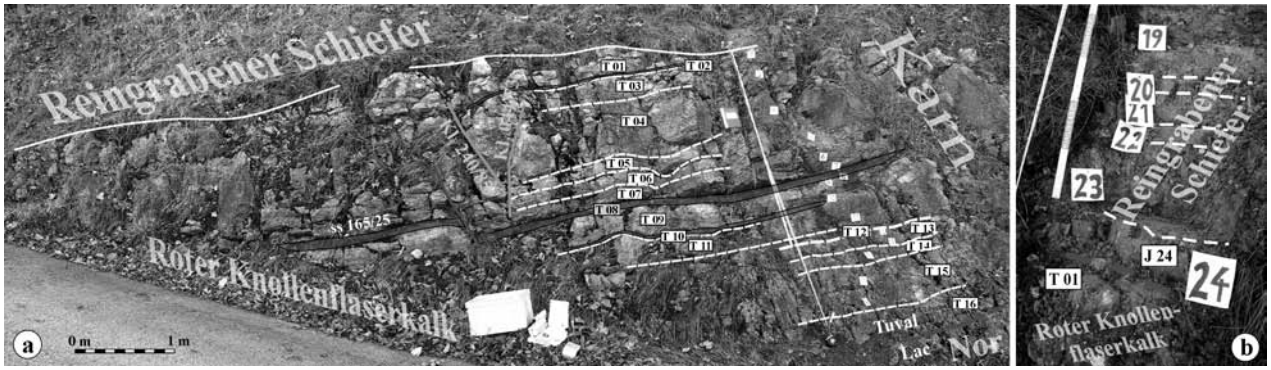

Abb. 3: (a) Aufschluss-Situation am Profil Freygutweg mit durchnummerierten Horizonten des Roten Knollenflaserkalkes. (b) Die tektonisch hangenden Reingrabener Schiefer sind stark verwachsen und wurden im Zuge der Probennahme freigegraben.

Fig. 3: 1) The Freygutweg section (upper part) and 2) the excavated Reingraben Shales and the boundary to the nodular red flaser limestones.

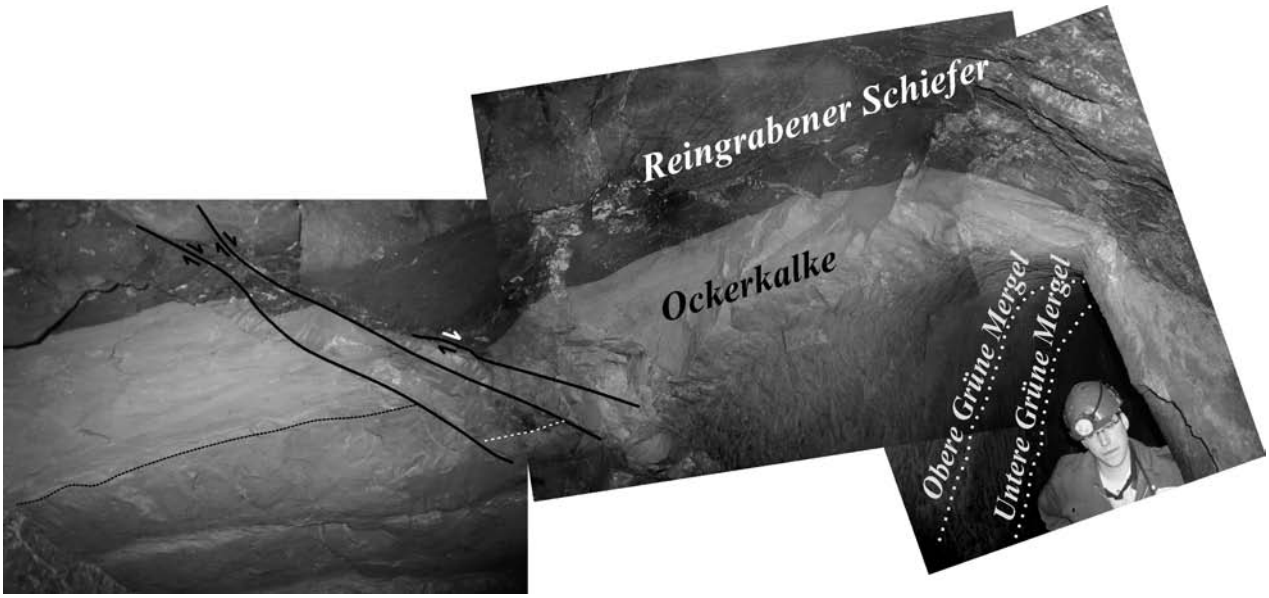

Abb. 4: Aufschluss-Situation des Anschnittes im Jakobbergstollen mit der scharfen Grenze zwischen Ockerkalken und dunklen Reingrabener Schiefern, die von nordgerichteten Abschiebungen gegeneinander versetzt werden.

Fig. 4: The sampled section in the Jakobberg gallery with the distinct boundary between ochre-coloured limestones and Reingraben Shales, disclocated by slight north dipping normal faults.

stagnierender bis ausbleibender Sedimentation bei verminderter Sauerstoffzufuhr anzeigt (Hornung und Brandner 2005). Dieser geringmächtige Horizont wird mit der Untergrenze der Reingrabener Wende gleichgesetzt. Über dieser Fuge folgt eine ca. 1,3 m mächtige Wechselfolge aus ockerfarbenen, limonitreichen Kalken und Mergeln, die ihrerseits in scharfer lithologischer Grenze von schwarzen Reingrabener Schiefern überlagert werden. Noch vor der beginnenden Tunnel-Verschalung konnte eine basale, fossilführende Kalkeinschaltung beprobt werden, die in Habitus ähnlich der biogenreichen Reingrabener Kalkbänke des Freygutweges ist.

Alle Horizonte in diesem Bereich des Stollens fallen steil mit etwa 60° nach SSE ein und werden zudem von mehreren mittelsteilen (45°) nordgerichteten Abschiebungen um wenige Zentimeter gegeneinander versetzt (Abb. 4).

5. Biochronostratigraphie

Trotz der stark kondensierten Abfolge des Freygutweges sowie den conodontenarmen Ockerkalken im Jakobbergstollen sind die aus beiden Profilen kombinierten Conodontendaten zu einer biostratigraphischen Aussage genügend und ermöglichen neben der zeitlichen Aussage eine Korrelation beider Profile (Abb. 6).

Die beschriebenen Definitionen der Conodontenzonen halten sich an die von Krystyn (1980 und 1983) entwickelten lokalen Gliederungen, wenngleich letztere Arbeit mit Conodontenspezies arbeitet (z.B. *Metapolgynathus auriformis* und *Metapolygnathus carnicus*), die in den hier vorgestellten Profilen nicht vorkommen. Neuere detaillierte und globale Gliederungen sind bei Gallet et al. (1994) zu finden.

Das erstmalige Auftreten von *Metapolygnathus polygnathiformis* Stefanov & Budurov (Abb. 7, Fig. 7) bezeichnet die Ladin/Karn-Grenze. Am Freygutweg liegt diese in den unteren Bereichen der dickbankigen Graukalke ("Grauviolette Bankkalke" bei Gawlick et al. 1999a). Hier war aufgrund des Fehlens typisch spätladinischer (langobardischer) Formen der Nachweis der obersten *regoledanus*-Ammonitenzone (Langobard 3) nicht möglich. Gawlick et al. (1999a) wiesen in lithologischen Äquivalenten des Jakobbergstollens Langobard 3 nach.

Unsicher ist die Existenz der von Krystyn (1983) vorgeschlagenen *mostleri* Conodonten-Intervall-Zone (I. Z.) (kein Typus-Exemplar), der *tadpole* I. Z. (zwei Exemplare, Abb. 7, Fig. 2) und der *auriformis* I. Z. (kein Typus-Exemplar). Als gesichert kann die in

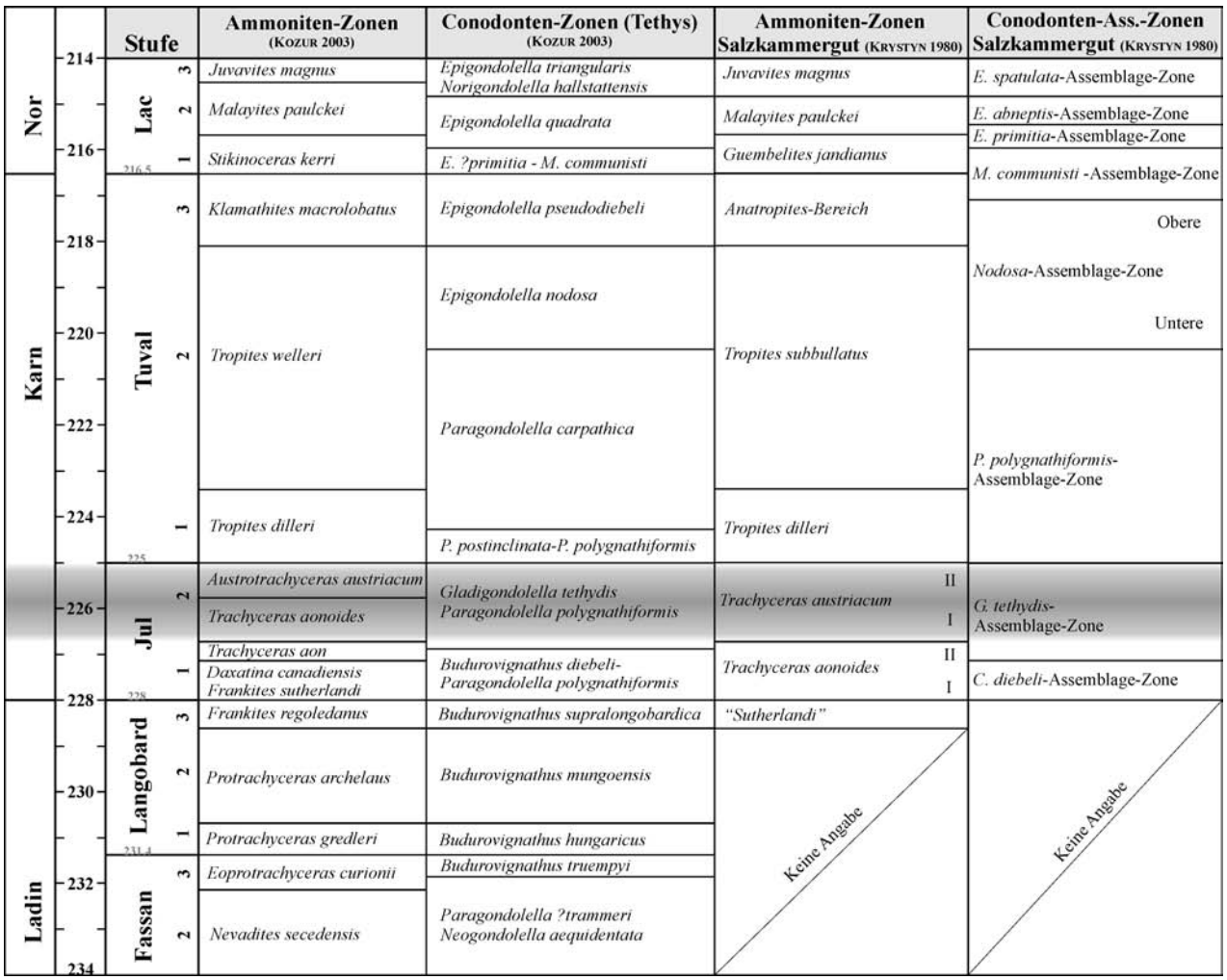

Abb. 5: Vergleich zwischen zwei biostratigraphischen Zonengliederungen: die linken Spalten nach Kozur (2003) beziehen sich auf den Tethys-Faziesbereich, die rechten beiden (nach Krystyn 1980, 1983) speziell auf die Hallstätter Folgen im Salzkammergut. Das Zeitintervall der Reingrabener Wende ist grau eingefärbt.

Fig. 5: Comparison of two biostratigraphic zonations. Left columns according to Kozur (2003), the two right columns after Krystyn (1980, 1983) referring to the Salzkammergut area. The time frame of the Reingraben Turnover is grey-shaded.

den oberen Bereichen der dickbankigen Graukalke, der Ockerkalke und der Reingrabener Schiefer nachgewiesene Koexistenz von *M. polygnathiformis* und *Gladigondolella tethydis* (Abb. 7, Figs. 3, 4; Abb. 8, Fig. 10) gelten, welche nach Krystyn (1980 & 1983) die *tethydis* Conodonten Assemblage-Zone (A. Z.) definiert und die *auriformis* I. Z. vermutlich im Salzkammergut einbezieht. Diese Zone korreliert mit dem Zeitbereich der oberen *aonoides*- bis *austriacum*- Ammonitenzone oder dem Jul 1/II bis Jul 2/II. Wichtig ist der Nachweis von *Gl. tethydis* in den obersten Kalkeinschaltungen der Reingrabener Schiefer am Freygutweg: damit liegt die Zeitspanne des karnischen Terrigen-Intervalls im Berchtesgadener Bereich, im Salzkammergut und vermutlich in den gesamten Nördlichen Kalkalpen ausschließlich im unteren Karn (vgl. Hornung et al. 2005).

Das Aussetzen von *Gl. tethydis* in den Roten Knollenflaserkalken des Freygutweges und das weitergeführte monospezifische Erscheinen von *M. polygnathiformis* (Abb. 7, Figs. 12, 14, 17) definiert die *polygnathiformis* A. Z (Krystyn 1980) und umfasst die *dilleri*-Ammonitenzone (Tuval 1) sowie den unteren Bereich der *subbullatus*-Ammonitenzone (Tuval 2/I). Seltene Exemplare von *Metapolygnathus carpathicus* (Abb. 7, Figs. 15) in den oberen Bereichen des

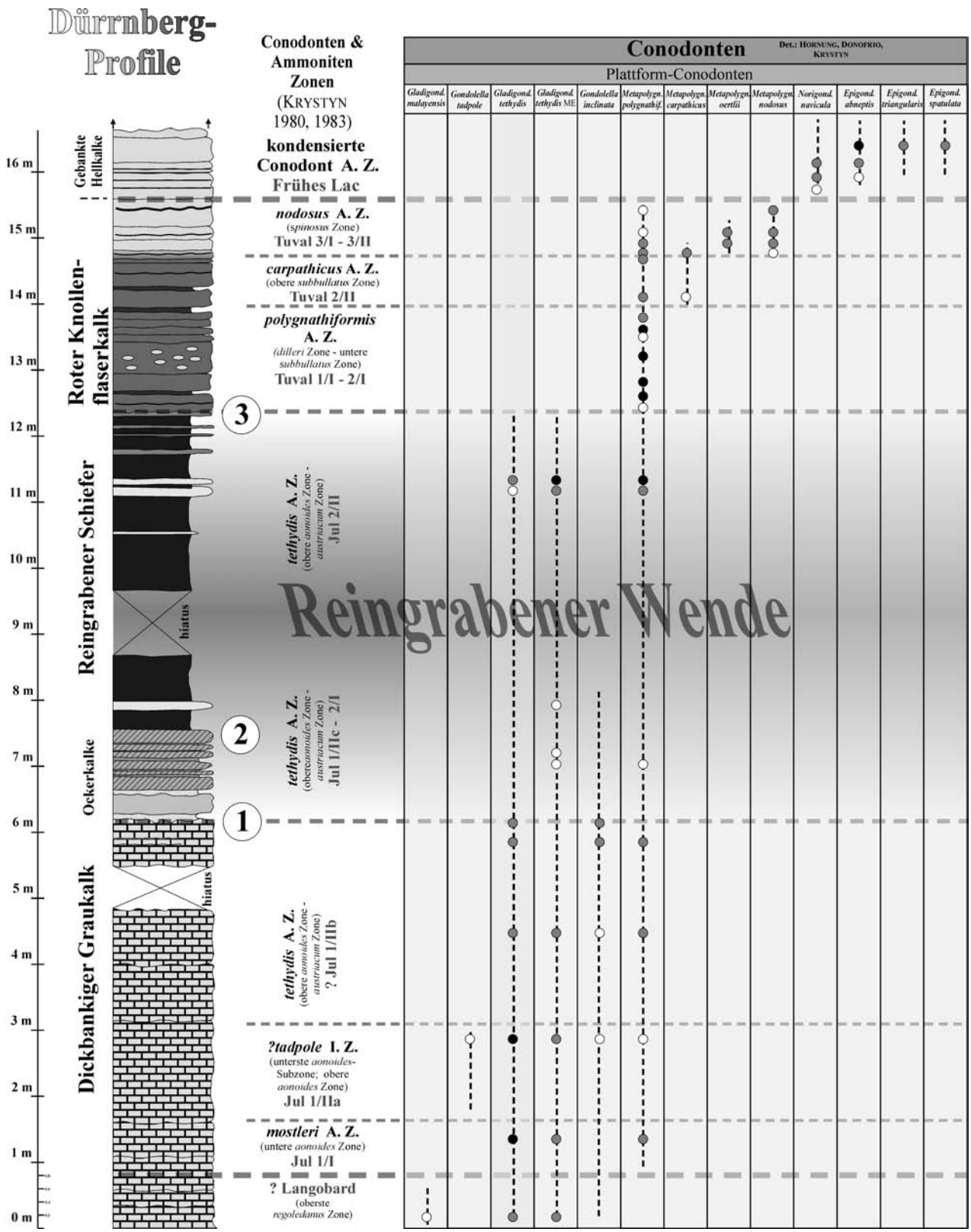
Dürrnberg-Profile
Conodonten & Ammoniten Zonen (KRYSTYN 1980, 1983)
Conodonten
Det.: HORNUNG, DONOFRIO, KRYSTYN
Plattform-Conodonten
Gladigond. malayensis
Gondolella tadpole
Gladigond. tethydis
Gladigond. tethydis ME
Gondolella inclinata
Metapolygn. polygnathif.
Metapolygn. carpathicus
Metapolygn. oertlii
Metapolygn. nodosus
Norigond. navicula
Epigond. abneptis
Epigond. triangularis
Epigond. spatulata
16 m
15 m
14 m
13 m
12 m
11 m
10 m
9 m
8 m
7 m
6 m
5 m
4 m
3 m
2 m
1 m
0 m
Gebankte Hellkalke
Roter Knollen-flaserkalk
Reingrabener Schiefer
Ockerkalke
Dickbankiger Graukalk
hiatus
hiatus
kondensierte Conodont A. Z.
Frühes Lac
nodosus A. Z. (spinosus Zone)
Tuval 3/I - 3/II
carpathicus A. Z. (obere subbullatus Zone)
Tuval 2/II
polygnathiformis A. Z. (dilleri Zone - untere subbullatus Zone)
Tuval 1/I - 2/I
3
tethydis A. Z. (obere aonoides Zone - austriacum Zone)
Jul 2/II
Reingrabener Wende
tethydis A. Z. (obere aonoides Zone - austriacum Zone)
Jul 1/IIc - 2/I
2
1
tethydis A. Z. (obere aonoides Zone - austriacum Zone)
? Jul 1/IIb
?tadpole I. Z. (unterste aonoides-Subzone; obere aonoides Zone)
Jul 1/IIa
mostleri A. Z. (untere aonoides Zone)
Jul 1/I
? Langobard (oberste regoledanus Zone)

Roten Knollenflaserkalkes lassen auf eine stark kondensierte, nur zwei Bänke mächtige *carpathicus* A. Z. schließen (oberer Bereich der *subbullatus*-Ammonitenzone oder Tuval 2/II).

Metapolygnathus nodosus (Abb. 7, Fig. 16), nachgewiesen von Kalkbank 14 bis 16 über dem markanten Wechsel von Schwarzschiefern zu Rotkalken, markiert nach Krystyn (1980) die *nodosus* A. Z., stellvertretend für den Zeitbereich der *spinosus* Ammonitenzone (Tuval 3/IIa). Das Top der *spinosus*-Ammonitenzone wird durch den Fund von *M. communisti* bei Gawlick et al. (1999a) bestätigt.

Mit dem Ersteinsetzen von *Norigondolella navicula* (Abb. 8, Fig. 1), lithologisch bereits in den gebankten Hellkalken, ist die Karn-Nor-Grenze (Krystyn 1980) bestätigt. Das gleichzeitige Auftreten mit *Epigondolella spatulata* (Abb. 8, Fig. 5), *E. abneptis* (Abb. 8, Fig. 2, 4, 7) sowie *E. triangularis* (Abb. 8, Figs. 3, 8) scheint eine stark kondensierte Mischfauna des unteren bis mittleren Lac nachzuzeichnen.

Diskussion

Die hier vorgestellten Conodontendaten lassen die Zeitspanne der Reingrabener Wende im Salzkammergut gut eingrenzen. Die innerhalb der Profilsäule feststellbaren drei lithologischen Grenzen, a) der Übergang von dickbankigen Graukalken zu Ockerkalken, b) von Ockerkalken zu Reingrabener Schiefern und c) von Reingrabener Schiefern zu Rotkalken liegen vermutlich in Änderungen der Wasserzirkulation, des Sauerstoffgehalts, der Produktivität benachbarter Karbonatplattformen, bzw. eines mobilen, salinartektonisch geprägten Untergrundes (Haselgebirge) begründet (Fig. 6, siehe auch Hornung & Brandner 2005).

Die Frage einer möglichen Korrelation in andere Gebiete der Nördlichen Kalkalpen werden weitere Untersuchungen klären. Es scheint sich jedoch aufgrund biostratigraphischer Daten (Hornung et al. 2005) abzuzeichnen, dass die dickbankigen Graukalke mit den Oberen Reiflinger Schichten und die Ockerkalke mit Göstlinger Schichten in Niederösterreich korreliert werden können. Die Reingrabener Schiefer finden sich sowohl im Reiflinger Becken Niederösterreichs als auch im Hallstätter Becken des Salzkammerguts.

Schlußfolgerungen

Aus den oben beschriebenen Daten geht hervor, dass die Reingrabener Wende im des Salzkammergut (und vermutlich auch in anderen Regionen) ausschließlich frühkarnisches Alter besitzt. Dies ist mit den vorliegenden Daten aus Niederösterreich (vgl. Krystyn 1991 und eigene Daten) sowie Südtirol (vgl. Keim & Brandner 2001) konform.

Dank

Mein Dank geht in erster Linie an meinen Betreuer Rainer Brandner (Innsbruck), der mir nicht nur fachlich, sondern auch in tatkräftig behilflich war (Probennahme im Jakobbergstollen). Ferner danke ich Helmut Lindtner (Bad Dürrnberg) für die Erlaubnis, das Profil Freygutweg auf Privatgrund beproben zu dürfen, Hans-Jürgen Gawlick (Leoben) für Unterstützung während des ersten Geländeaufenthaltes. Werner Prochenberger danke ich für die Begehungserlaubnis des stillgelegten Jakobbergstollen, Steiger Thomas Grublacher (beide Saline Bad Dürrnberg) für Unterstützung während der Probennahme.

Leopold Krystyn (Wien) und Antonio Donofrio (Innsbruck) gaben wertvolle Hinweise hinsichtlich der Conodonten-Klassifikation, einem anonymen Reviewer bin ich für Verbesserungsvorschläge Dank schuldig. Dem Fonds zur wissenschaftlichen Förderung (FWF-Projekt P 16878) sei für finanzielle Unterstützung ganz herzlich gedankt.

Abb. 6: Kombinierte Profilsäulen des Freygutweges und des Jakobbergstollens (Profilsäule zwischen den Schichtlücken): links die lithostratigraphischen Einheiten mit Maßstab, rechts neben der Profilsäule horizontiert gefundene Conodonten und dazwischen die daraus abgeleitete Zonierung der Conodontenstufen – daraus leitet sich die entsprechende Ammonitenzonierung ab. Lithologische Events: (1) = initiales Reingraben Event; (2) = Reingraben "Anoxic Event"; (3) = Reingraben „Oxic Event"

Fig. 6: Lithology, conodont biostratigraphy and reconstructed conodont zones in-between (after Krystyn 1980) of the Freygutweg section and the Jakobberg Gallery (in-between the stratigraphical gaps). Due to the lack of ammonite findings, the ammonite zones are construed after the conodont zones (the exact boundaries, thus, are questionable). Lithologic events: (1) = initial Reingraben

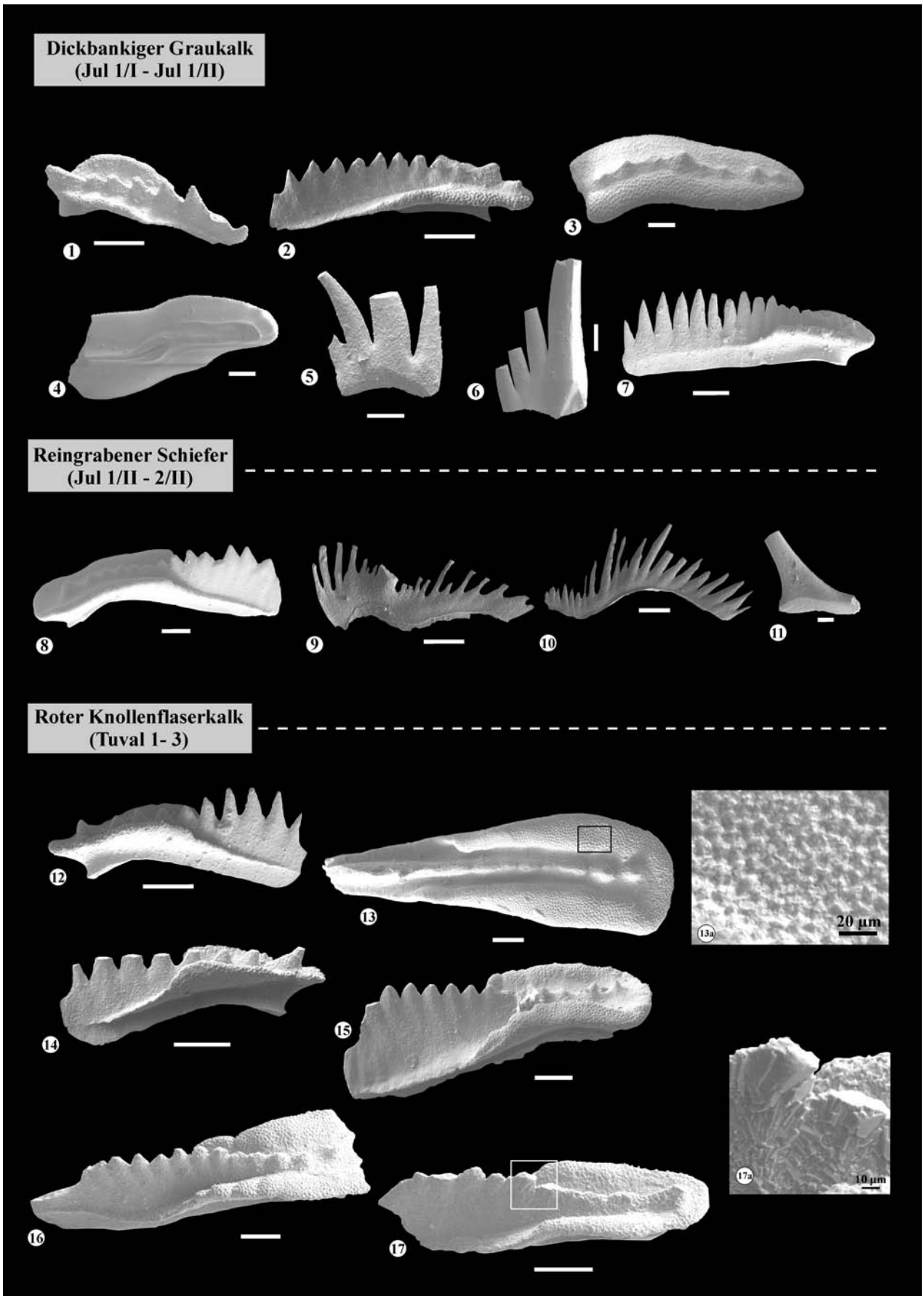
Dickbankiger Graukalk
(Jul 1/I - Jul 1/II)
1
2
3
4
5
6
7
Reingrabener Schiefer
(Jul 1/II - 2/II)
8
9
10
11
Roter Knollenflaserkalk
(Tuval 1- 3)
12
13
13a
20 µm
14
15
16
17
17a
10 µm

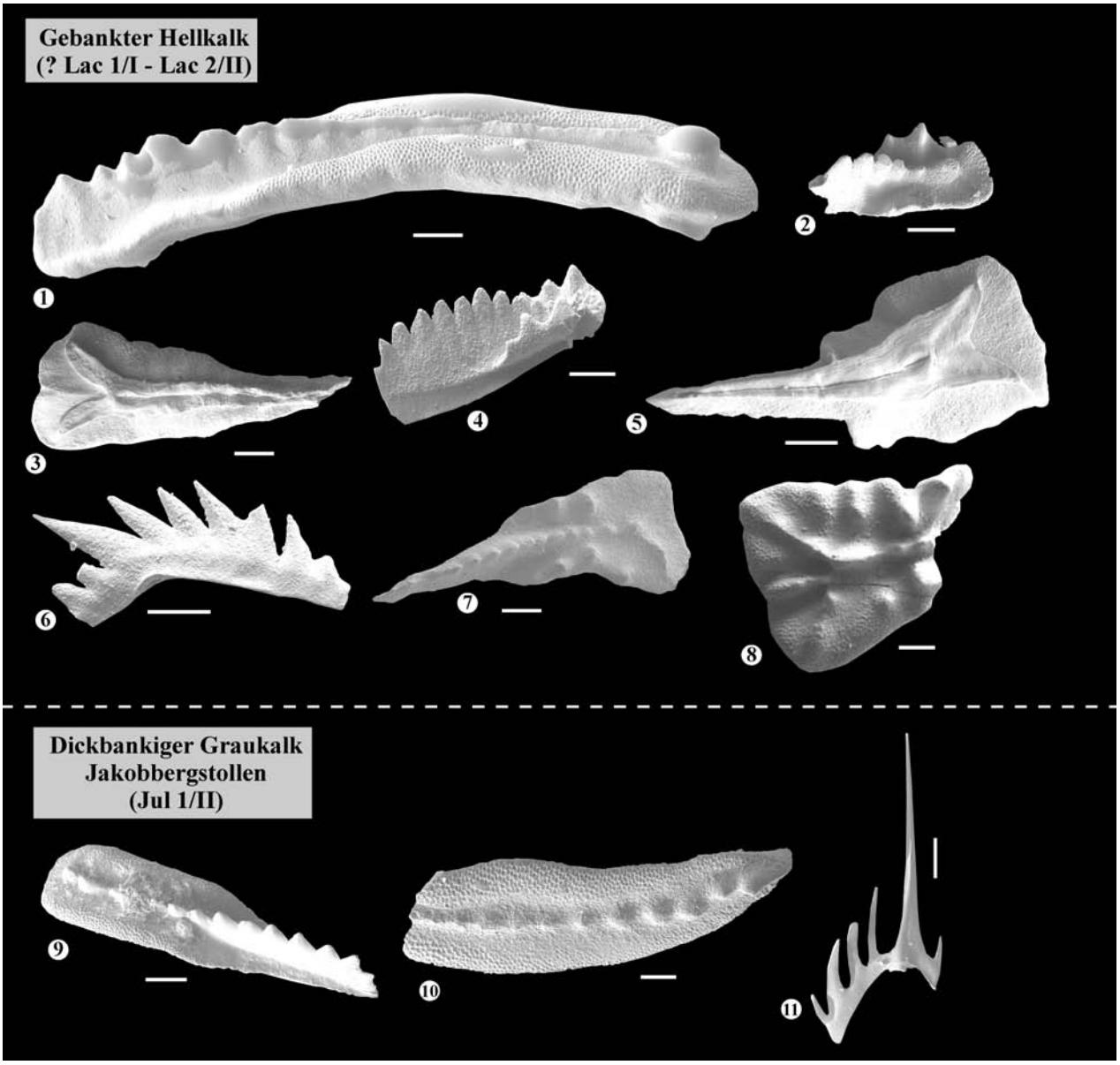

Abb. 7 (links): Conodonten des Freygutweges (Jul 1/I bis Tuval 3/II): Maßstabsbalken = 100 µm / Fig. 7: Conodonts of the Freygutweg section (Julian 1/I to Tuvalian 3/II); scale bar = 100 µm:

1) *Gladigondolella malayensis* Nogami 1968; La 4; CAI = 1,0; 2) *Gondolella tadpole* Hayashi 1968; La 5; CAI = 1,0; 3) *Gladigondolella tethydis* Huckriede; La 4; CAI 1,0; 4) *Gladigondolella tethydis*; La 5; CAI 1,0; 5) *Enantiognathus petraeviridis*, Huckriede; La 4; CAI 1,0-1,5; 6) *Hibbardella lautissima* Huckriede; La 5; CAI 1,0; 7) *Metapolygnathus polygnathiformis*, La 5; CAI = 1,0; 8) *Metapolygnathus polygnathiformis*; J 16a; CAI 1,0; 9) *Hindeodella pectiniformis* Huckriede; J 16a; CAI 1,0; 10) *Hindeodella pectiniformis*; J 16a; CAI 1,0; 11) *Gladigondolella tethydis* ME, Huckriede; J 16b; CAI = 1,0; 12) *Metapolygnathus polygnathiformis*; T 01; CAI = 1,0; 13) *Metapolygnathus oertlii* (Kozur 1980); T 13; CAI = 1,0; 13a) M. oertlii - detail; 14) *Metapolygnathus polygnathiformis*; T 04; CAI = 1,0; 15) *Metapolygnathus carpathicus* (Mock 1979); T 12; CAI = 1,0; 16) *Metapolygnathus nodosus* (Hayashi 1968); T 13, CAI = 1,0; 17) *Metapolygnathus polygnathiformis*; T 13; CAI = 1,0; 17a) *M. polygnathiformis* - detail

Abb. 8 (oben): Conodonten des Freygutweges und des Jakobbergstollens (Jul bis Tuval): Maßstabsbalken = 100 µm / Fig. 8: Conodonts of the Freygutweg section and Jakobberg gallery; scale bar = 100 µm:

Conodonten Freygutweg (frühes Nor); Conodonts of the Freygutweg section (Early Norian): 1) *Norigondolella navicula* Huckriede; L 06; CAI = 1,0; 2) *Epigondolella abneptis* s.l. Huckriede; L 06; CAI = 1,0; 3) *Epigondolella* cf. *triangularis* (Budurov); L 07; CAI = 1,0; 4) *Epigondolella abneptis*; L 07; CAI = 1,0; 5) *Epigondolella spatulata*, Huckriede; L 08; CAI = 1,0; 6) *Ozarkodina* sp.; L 08; CAI = 1,0; 7) *Epigondolella abneptis* s.l.; L 07; CAI = 1,0; 8) *Epigondolella triangularis* (Budurov); L 08; CAI = 1,0

Condonten Jakobbergstollen / Conodonts Jakobberg gallery:
9) *Gondolella inclinata* (Kovács 1983); HB 7; CAI = 1,0; 10) *Gladigondolella tethydis*; HB 7; CAI = 1,0; 11) *Didymodella alternata* Mosher; HB 7; CAI = 1,0

Literatur

Braun, R. (1998): Die Geologie des Hohen Gölls. – Forschungsberichte Nationalpark Berchtesgaden: 192 S., Berchtesgaden.

Frisch, W., Gawlick, H.J. (2003): The nappe structure of the central Northern Calcareous Alps and its disintegration during Miocene tectonic extrusion – a contribution to understanding the orogenic evolution of the Eastern Alps. – Int. J. Earth Sci (Geol. Rundschau), 92: 712–727 (Springer), Berlin.

Gallet, Y., Besse, J., Krystyn, L., Théveniaut, H., Marcoux, J. (1994): Magnetostratigraphy of the Mayerling section (Austria) and Erenkolu Mezarlik (Turkey) section: Improvement of the Carnian (late Triassic) magnetic polarity time scale. – Earth Planet. Sci. Lett. 125: 173–191.

Gawlick, H. (2000): Paläogeographie der Obertrias-Karbonatplattformen in den Nördlichen Kalkalpen. – Exkursionsführer Sediment 2000, Mitt. Ges. Geol. Bergbaustud. Österr., 44: 46–95, Wien.

Gawlick, H.-J., Lein, R., Piros, O., Pytel C. (1999a): Zur Stratigraphie und Tektonik des Hallein – Bad Dürrnberger Salzberges – Neuergebnisse auf der Basis von stratigraphischen und faziellen Daten (Nördliche Kalkalpen, Salzburg). – Abh. Geol., B.-A., 56/2: 69–90, Wien.

Gawlick, H.-J., Frisch, W., Vescei, T., Steiger, F., Böhm, F. (1999b): The Change from rifting to thrusting in the Northern Calcareous Alps as recorded in Jurassic sediments. – Geol. Rundschau 87: 644–657.

Gawlick, H.-J., Lein, R. (1997): Neue stratigraphische und fazielle Daten aus dem Jakobberg- und Wolfdietrichstollen des Hallein- Bad Dürrnberger Salzberges und ihre Bedeutung für die Interpretation der geologischen Verhältnisse im Bereich der Hallein – Berchtesgadener Schollenregion. – Geol. Paläont. Mitt. Innsbruck 22: 199-225.

Gawlick, H.-J., Lein, R. (2000): Die Salzlagerstätte Hallein – Bad Dürrnberg. – Exkursionsführer Sediment 2000, Mitt. Ges. Geol. Bergbaustud. Österr., 44: 263–280, Wien.

Hallock, P., Schlager W. (1986): Nutrient Excess and the Demise of Coral Reefs and Carbonate Platforms. – Palaios 1986: 389–398.

Hornung, T., Brandner, R. (2005): Biochronostratigraphy of the Reingraben Event (Hallstatt Facies Belt): Local black shale events controlled by regional tectonism, climatic change and plate tectonics. – Facies 51: 474-495 (DOI: 10.007/s10347-005-0061-x), Erlangen.

Hornung, T., Brandner, R., Krystyn, L. (2005): Carnian black shale events triggered by Cimmerian-Eurasian collision? – Abstract Book / CD, EGU-Meeting April 2005, Vienna.

Keim, L., Brandner, R. (2001): Facies interfingering and synsedimentary tectonics on late Ladinian-early Carnian carbonate platforms (Dolomites, Italy). – Int. J. Earth Sciences (Geol. Rundsch.), 90: 813–830.

Kozur, H. (2003): Integrated ammonoid, conodont and radiolarian zonation of the Triassic and some remarks to Stage/Substage subdivision and the numeric age of the Triassic stages. – Albertiana 28: 57–74, Wien.

Krystyn, L. (1980): Triassic conodont localities of the Salzkammergut Region (Northern Calcareous Alps). – in: Second European Conodont Symposium-ECOS II, Guidebook and Abstracts. – Abhandlungen der Geologischen Bundesanstalt, Band 35: 61–98.

Krystyn, L. (1983): The Epidauros Section (Greece) – a contribution to the conodont standard zonation of the Ladinian and Lower Carnian of the Tethys Realm. – Schriftenreihe der Erdwissenschaftlichen Komissionen 5: 231–258.

Krystyn, L. (1991): Die Fossillagerstätten der alpinen Trias. – Exkursionsführer, 31 Abb., Wien.

Mandl, G.W. (1984): Zur Trias des Hallstätter Raumes – ein Modell am Beispiel Salzkammergut (NKA, Österreich). – Mitt. Ges. geol. Bergbaustud. Österr., 30/31: 133–176.

Mandl, G.W. (1999): The Alpine sector of the Tethyan Shelf – Examples of Triassic to Jurassic sedimentation and deformation from the Northern Calcareous Alps. – Mitt. Österr. Geol. Ges. 92: 61–79.

Medwenitsch, W. (1949): Fossilfund im Halleiner Salzberg. – Berg- und Hüttenmänn. Mh., 94 (3): 65–66, Leoben.

Medwenitsch, W. (1958): Zur Geologie des Halleiner Salzberges. Die Profile des Jakobberg- und Wolfdietrichstollens. – Mitt. Geol. Ges. Wien, 51: 197–218, Wien.

Medwenitsch, W. (1962): Die Bedeutung der Grubenaufschlüsse des Halleiner Salzberges für die Geologie des Ostrandes der Berchtesgadener Schubmasse. – Z. dt. Geol. Ges., 113: 463–494, Hannover.

Medwenitsch, W. (1963): Zur Geologie des Halleiner und Berchtesgadener Salzberges. – Mitt. Naturwiss. Arbeitsgem. Haus der Natur, 1963: 1–18, Salzburg.

Mutti, M., Weissert, H. (1995): Triassic Monsoonal climate and its signature in Ladinian-Carnian Carbonate Platforms (Southern Alps, Italy). – Journal of Sedimentary Research, 65b (3): 357–367.

Neubauer, F. (1994): Kontinentkollision in den Ostalpen. – Geowissenschaften 12: 136–140

Plöchinger, B. (1955): Zur Geologie des Kalkalpenabschnittes vom Torrener Joch zum Ostfuß des Un-

tersberges; die Göllmasse und die Halleiner Hallstätter Zone. – Jb. Geol. Bundesanst., 95/1: 93–144, Wien.

Prey, S. (1969): Geologische Karte der der Umgebung der Stadt Salzburg 1:50 000. Geol. Bundesanst., Vienna.

Reijmer, J.J.G., Everaas, S.L. (1991): Carbonate Platform Facies reflected in Carbonate Basin Facies (Triassic, Northern Calcareous Alps, Austria). – Facies, 25: 253-278, Erlangen.

Riedel, P. (1991): Korallen in der Trias der Tethys: Stratigraphische Reichweiten, Diversitätsmuster, Entwicklungstrends und Bedeutung als Rifforganismen: Gesellschaft der Geologie- und Bergbaustudenten Österreichs, Mitteilungen, 37: 97–118.

Rüffer, T., Zamparelli, V. (1997): Facies and Biota of Anisian to Carnian Carbonate Platforms in the Northern Calcareous Alps (Tyrol and Bavaria). – Facies 37: 115-136, Erlangen.

Schlager, W. (1969): Das Zusammenwirken von Sedimentation und Bruchtektonik in den triadischen Hallstätterkalken der Ostalpen. – Geol. Rundschau 59: 289-308, 8 Abb., Stuttgart.

Schlager, W., Schöllnberger, W. (1974): Das Prinzip stratigraphischer Wenden in der Schichtenfolge der Nördlichen Kalkalpen. – Mitt. Geol. Ges. Wien, 66/67: 165-193; Wien.

Schweigl, J., Neubauer, F. (1997): Structural evolution of the central Northern Calcareous Alps: Significance fort he Jurassic to Tertiary geodynamics in the Alps. – Eclogae geol. Helv. 90: 303–323, Zürich.

Simms M.J., Ruffel A.H. (1989): Synchroneity of climate change and extinctions in the Late Triassic – Geology 17: 265–268

Geo.Alp, Vol. 3, S. 23–31, 2006

CONODONT BIOSTRATIGRAPHY OF THE LERCHECK / KÖNIGSLEITEN SECTION NEAR BERCHTESGADEN (LATE LADINIAN – HALLSTATT LIMESTONES)

Thomas Hornung

With 3 figures and 1 plate

Institut für Geologie und Paläontologie, Innrain 52, A-6020 Innsbruck; e-mail: thomas.hornung@uibk.ac.at

Abstract

Grey to faintly red-coloured, well-bedded limestones in the south-western part of the Lercheck-Hallstatt Limestone succession near Berchtesgaden, Southern Germany, were age-dated by conodonts into the Longobardian 1-2. This disagrees with earlier studies, which assigned the succession to the "Carnian and Norian" limestones. These investigations, however, did not provide detailed biostratigraphical data. A monospecific presence of *Gladigondolella tethydis* (Huckriede) found within reddish-coloured limestones of the lower (Königsleiten) part of the section defines the *Budurovignathus truempyi* to *B. hungaricus* conodont assemblage zone (A.Z.) representing Fassanian 2 to Longobardian 1. The assemblage of five species (*Budurovignathus mungoensis*, *Gladigondolella malayensis*, *Gl. tethydis*, *Paragondolella inclinata* and *P. trammeri*), occurring in bedded grey limestones in the upper (Lercheck) part of the section, indicates the *B. mungoensis* A.Z. (Longobardian 2).

The Limestones can be compared to the thick-bedded grey limestones of the uppermost Longobardian to lower Julian. As exposed at the adjacent Freygutweg section and in the Jakobberg gallery, the Lercheck and Königsleiten section can be interpreted as their downward continuation (Hornung and Brandner 2005, Hornung 2006, this volume).

Zusammenfassung

Im Rahmen des FWF-Projektes P16878-N10 ("Das Reingraben-Event im westlichen Tethysraum") wurde die Südwestecke des Lercheck-Blocks (Berchtesgadener Hallstätter Kalke) einer eingehenden Beprobung unterzogen, insbesondere, um Daten aus dem Liegenden der tuvalischen Roten Knollenflaserkalke zu erhalten, welche im nahen Draxllehen-Steinbruch aufgeschlossen sind. Die gefundenen Conodonten-Assoziationen erlauben eine genaue Zuordnung der gut gebankten, unten rötlichgrau, nach oben hellgrau gefärbten Hallstätter Kalke in den Bereich des obersten Fassans bis Longobard 2. Das widerspricht Literaturdaten, die diesen Bereich des Lerchecks zu „Karnisch-Norischen Hallstätterkalken" stellen, jedoch ohne einen genaueren biostratigraphischen Nachweis durch entsprechende Leitfossilien zu liefern.

Nahezu monospezifisches Auftreten der Gattung *Gladigondolella tethydis* mit sehr seltenen *Gl. malayensis* im unteren Abschnitt lässt auf die *Budurovignathus truempyi*- bzw. *B. hungaricus* Condonten Zone (Oberstes Fassan bzw. Longobard 1) schließen. Die Vergesellschaftung von fünf Conodonten-Arten (*Budurovignathus mungoensis*, *Gladigondolella malayensis*, *Gl. tethydis*, *Paragondolella inclinata* und *P. trammeri*) im oberen Abschnitt deutet auf die *B. mungoensis* Conodonten-Zone (Langobard 2) hin.

Die untersuchte Abfolge gleicht lithologisch den dickbankigen Graukalken des nahen Freygutweges und Jakobbergstollens. Die neu gewonnenen biostratigraphischen Daten deuten darauf hin, dass sich das südwestliche Lercheck, vermutlich mit Schichtlücken, sehr wahrscheinlich als die untere Fortsetzung der Dürrnberger Profile (Hornung und Brandner 2005, Hornung 2006, dieser Band) ansehen lässt.

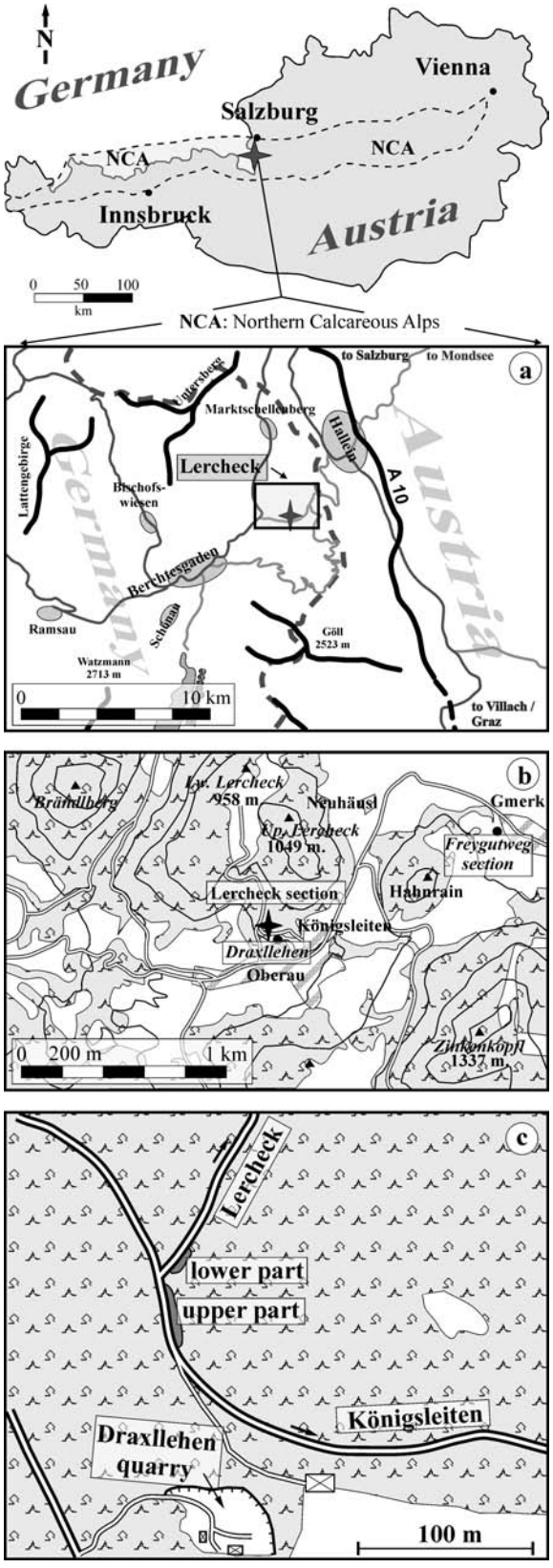

Fig. 1: a) Geographic overview and detailed geographic maps from the outcrops (b and c); Lercheck section UTM: WGS84, Zone 33; E 354767; N 5279689).

Introduction – Previous studies

The lithologic successions of the Lercheck mountain range have been known since the nineteenth century. Descriptions can be found in Gümbel (1861) and Schlosser (1898). Detailed mapping was carried out by Plöchinger (1955) and Pichler (1963). The exposed limestones were classified to Middle and Upper Triassic (Anisian to Norian), but age-dating was based on rare macrofossils (Plöchinger 1955). As high-resolution conodont-microbiostratigraphy remained underdeveloped during that time, reliable chronostratigraphic data did not exist in this region. Both Plöchinger (1955) and Pichler (1963) mapped the south-western part of the Upper Lercheck as "Carnian and Norian Hallstatt limestones". Rieche (1971) described a composed cross-section from Königsleiten to the Upper Lercheck as questionably Late Anisian to Norian. His short outcrop description, however, does neither provide geographic position, nor tectonic and stratigraphic information and macro- and microfossil descriptions. At this time, first proposals about conodont zonation in the Hallstatt succession were established by Krystyn (1970).

Due to the adjacent Draxllehen Quarry (Fig. 1b) exposing a Tuvalian sequence of nodular red flaser limestones, and its obvious lithological similarities to Early Carnian thick-bedded grey limestone successions exposed in the Dürrnberg sections (Hornung and Brandner 2005 and Hornung 2006, this volume), the studied section was sampled in order to obtain conodont data in high-resolution. The question, whether the Lercheck section might be the temporal equivalent or a possible downward continuation of the Early Carnian thick-bedded grey limestones exposed at the Dürrnberg sections (Hornung and Brandner, 2005; Hornung, 2006, this volume), may be solved only by this biostratigraphic statement.

Geological setting

The studied section is located near Oberau circa 5.4km ENE of Berchtesgaden on a private driveway from Lercheck (lower part) to Königsleiten (upper part), close to the Draxllehen Quarry (Figs. 1b, c). The succession is part of the Lercheck Block which consists of Anisian to lowermost Norian limestone successions.

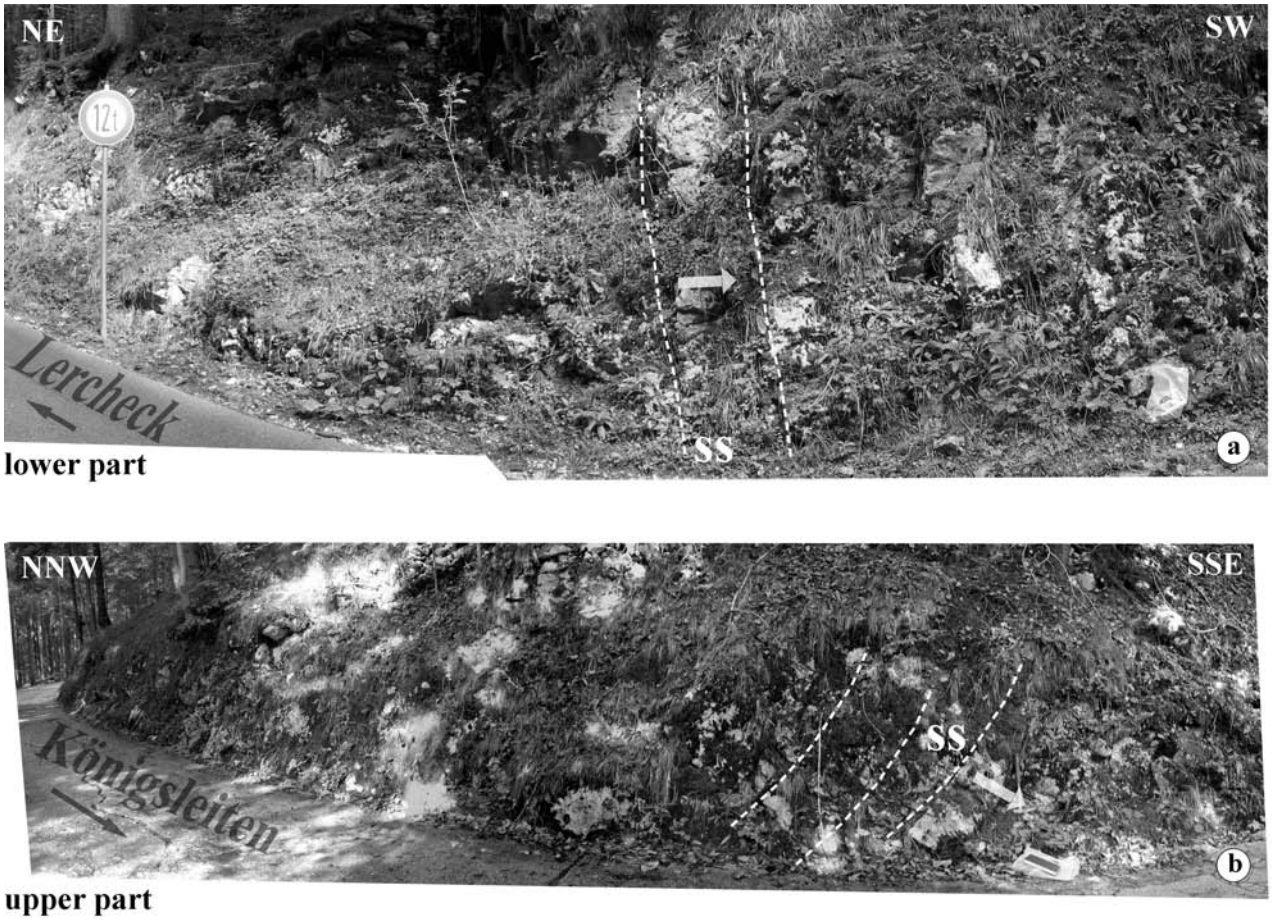

Fig. 2: Lower (a) and upper part (b) of the Lercheck section. The dashed lines show the bedding planes, the white arrow the direction of sedimentation.

The lower part of the Lercheck section consists of medium to thick-bedded light grey coloured limestones (per bed max. 1.25 m), whereas its upper part is made up of a medium-bedded limestone succession (per bed max. 0.5 m) of faintly red tints (Figs. 2, 3). The red colouring is primarily due to the presence of finely dispersed hematite and dark red pressure solution seams of argillaceous lime mudstones. All layers dip uniformly and steeply NNW at 70°. The section is overturned. Due to the obvious difference in stratification relative to the upright and steeply southern dipping succession of red Draxllehen limestone, a normal fault and a block-rotation between the units can be assumed. The complete Lercheck Block exhibits complicated and narrow-spaced imbrication faults, which subsequently became steepened. All layers show – along intensive pressure solution caused by compaction – common vertical tension joints cemented by radial-fibrous calcites and, subsequently, by coarse blocky calcite spar.

Results

All samples (max. 1 kg per layer) were digested in acetic acid, the insoluble residue was washed and fractioned by sieving (coarse: 250 µm; fine: 100 µm). All selected material is archived at the Institute of Geology and Paleontology in Innsbruck (archive Hornung, "Lercheck").

Conodont-Parataxonomy

As ammonite findings lacked completely, the biostratigraphy had to be based on conodonts. All conodonts found within the Lercheck succession show a CAI (Conodont Alteration Index) of 1.0 representing an average thermal overprint of 65°C. The following description is restricted to platform conodonts. The different species being found are shortly described, in order of their first stratigraphical appearance.

A) *Gladigondolella tethydis* Huckriede, 1958

* 1958 *Gladigondolella tethydis* n. sp.; in Huckriede (1958); pl. 12, figs. 38a-b; pl. 13, figs. 2-5
* 1980 *Gladigondolella tethydis*, Huckriede (1958): in Kovács and Kozur (1980); pl. 3, figs. 5-6
* 1983 *Gladigondolella tethydis*, Huckriede (1958); in Kolar-Jurkovsek (1983); pl. 3, figs. 1a-b, 2a-c
* 1995 *Gladigondolella tethydis*, Huckriede (1958); in Neri et al. (1995); pl. 2, fig. 1
* 1995 *Gladigondolella tethydis*, Huckriede (1958); in Mastandrea (1995); pl. 2, figs. 1-2
Pl. 1, figs. 3, 4, 5, 6

Material:
Common appearance in the section. Two nearly complete specimens in the lower part, ten broken specimens in the upper part.

Description:
Large and asymmetrical units showing thick-bulged reticular brims. Flat scupltureless troughs laterally of the reduced carina are characterised by discrete, roundish to oval-shaped denticles. The big and robust keel includes a small oval basal pit, situated between the midlength and the posterior third, often producing a laterally or downwards directed torsion of the platform as described by Vrielynck (1987) and Mastandrea (1995). This was observed only on some specimen.

Remarks:
The most important difference between *Gl. tethydis* and *Gl. malayensis* is the different position of the basal pit: *Gl. malayensis* has a posterior position of an eye-shaped basal pit.

B) *Gladigondolella malayensis* Nogami, 1968

* 1968 *Gladigondolella malayensis* n. sp.; in Nogami (1968); pl. 9, figs. 11-18; pl. 11, fig. 7
* 1995 *Gladigondolella malayensis malayensis* Nogami (1968); in Mastandrea (1995); pl. 1, figs. 1-3.
Pl. 1, fig. 2, 8

Material:
Rare occurrence in the complete section. Three fragmented specimens.

Description:
Large-sized robust and broken units showing a low posterior carina, which consists of four low and stepped denticles descending into a very low ridge of fused, oval-shapes nodules at midlength. All specimens show very flat, indistinct and scupltureless troughs along the nodules. The central keel contains a terminal, eye-shaped basal pit.

Remarks:
Gl. malayensis differs from *Gl. tethydis* in that it has a larger and more thickened platform and stepped distinct roundish nodules and a posterior basal pit. *Gl. tethydis* is more oblong, the nodules are oval-shaped and fused to a low carinal ridge. The example pictured in plate 1, no. 1 is classified as *Gl.* cf. *malayensis* representing most probably a "super - adult" growth-stage of this species (pers. comm. L. Krystyn, Vienna, and H. Kozur, Budapest).

C) *Paragondolella trammeri* (Kovács 1983)

* 1980 *Gondolella trammeri* (Kozur 1971); in Kovács and Kozur (1980); pl. 6, figs. 6-8
Pl. 1, fig. 14

Material:
Rare occurrence. Two specimens in Le 10.

Description:
Almost flat, very slightly arched, robust, but slender units. The platform comprises thickened margins embraces the whole unit without a free blade; the marginal rims have the same height as the low posterior carina with deep scupltureless furrows in-between. The terminal oval-shaped and node-like tooth is stepped, robust and inclined posteriorly. Only the anterior carina shows three to four distinct and high teeth, developed as a saw-blade. The carinal ridge tends to be straight, subsequently descending to the very anterior part. Unfortunately, the anterior part is broken on both specimens. A broad posterior keel with a narrow basal pit is also noted.

D) *Budurovignathus* cf. *mungoensis* (Diebel)

* 1972 *Metapolygnathus mungoensis* (Diebel); in Kozur (1972): pl. 2, figs. 1-4

* 1980 *Metapolygnathus mungoensis* (Diebel); in Kovács and Kozur (1980); pl. 7, fig. 3
* 1995 *Budurovignathus mungoensis* (Diebel); in Neri et al. (1995); pl. 2, figs. 7-9

Pl. 1, fig. 11

Material:
Rare occurrence. One broken specimen.

Description:
Small-sized unit with abrupt incipient platform and characteristic marginal teeth. Short free blade with a high carina of six denticles, whose height decreases slowly towards the posterior part. Unfortunately, the posterior platform third and some of the carinal teeth are broken. This is why this specimen can be assigned to *B. mungoensis* only under reserve.

Remarks:
According to Kovács (1983), *B. mungoensis* coexists with the similar shaped species *B. longobardicus*: due to the fragmentary preservation, a firm assignment to *B. mungoensis* thus cannot be assured.

E) *Paragondolella inclinata* (Kovács 1983)

* 1983 *Gondolella foliata inclinata*, n. subsp.; in Kovács (1983); pl. 11, figs. 1-4
* 1983 *Gondolella inclinata* (Kovács 1983); in Krystyn (1983); pl. 3, fig. 5; pl. 4, figs. 1-2; pl. 5, figs. 1-2
* 1995 *Neogondolella foliata inclinata* (Kovács 1983); in Neri et al. (1995); pl. 2, figs. 10, 14, 20

Pl. 1, figs. 7, 9, 10, 12, 13

Material:
Frequent within the complete section. Circa 20 complete specimens.

Description:
Longish and slender, drop-shaped and slightly arched specimens in lateral view. The platform extends the whole length of the unit embracing a denticled carina of moderate height. In its anterior half to two-thirds, the carina tends to be straight but descending slightly at the very anterior part. Towards the posterior half the carina descends gradually, forming a low ridge of fused older teeth (especially in adult growth stages). All carinal denticles are inclined posteriorly defining an angle of less than 90° with respect to the basal edge. The most terminal tooth is stepped and stronger inclined than the others. From the lower view, the keel is slightly elevated widening posteriorly and comprising an oval-shaped to rounded terminal basal pit. The honeycomb structure covers about one to two thirds of the posterior thickened platform margins. The anterior third and the adcarinal troughs are *unsculptured.*

Remarks:
According to Kovács (1983), *P. inclinata* developed from the similar *P. excelsa*: the main differences are the slight arching and the absent downward bending of the posterior end.

Discussion - Biostratigraphy

According to Kozur (1980), the monospecific but rare presence of *Gl. tethydis* within the grey- to reddish-coloured limestones (lower part) is typical for the time interval of the *Budurovignathus truempyi* to the *B. hungaricus* conodont assemblage zone. In general, uppermost Fassanian to lowermost Longobardian successions of the Austroalpine Facies yield only rare conodonts and often provide solely gladigondolellids without the type species *B. truempyi* and *B. hungaricus*. Thus, only a general assignment to these two conodont assemblage zones seems to be reasonable, even because parts of the section are overgrown.

The co-existence of at least five conodont species within the bedded grey limestones (upper part section) points to a range within the *Budurovignathus mungoensis* A. Z. representing the *Protrachyceras archelaus* ammonite zone or the Longobardian 2 (Kozur, 1980 and 2003). In the revision of the Austroalpine conodont zonation of Kozur (1980), this assemblage zone is characterised by the co-occurrence of rare *B. mungoensis* and *Paragondolella trammeri*, common *Gladigondolella tethydis* and *Gl. malayensis* as well as *P. inclinata*, but without *M. diebeli*, *M. polygnathiformis* and *M. tadpole*. The rare appearance of *M. noah* (see Kozur 1980 – synonymous for *M. polygnathiformis noah*) in the uppermost part of this assemblage zone could not be evidenced.

Because of the presence of a typical Longobardian conodont assemblage in the SW' Lercheck suc-

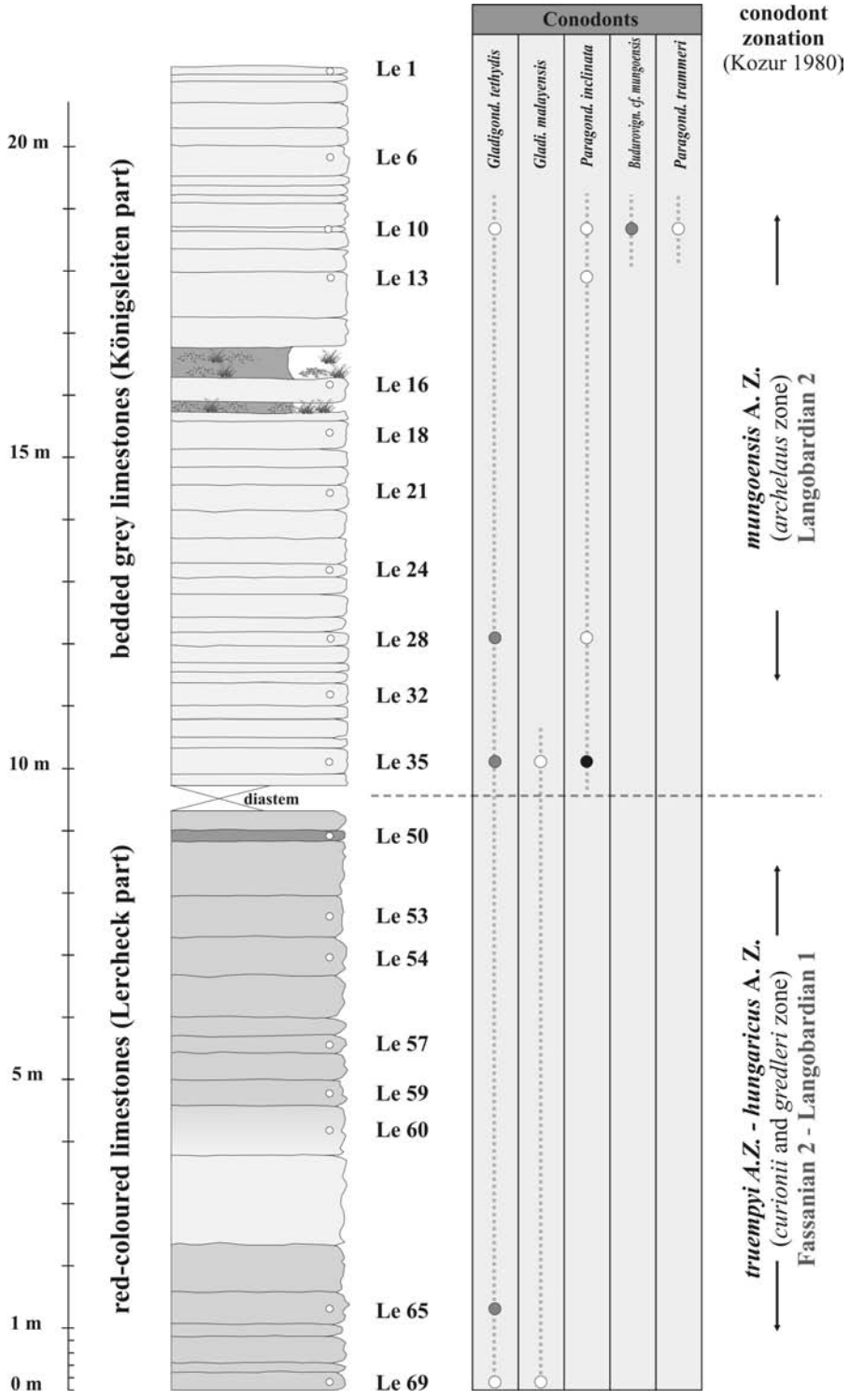

Fig. 3: Lithology, conodont biostratigraphy and reconstructed conodont zones (after Kozur 1980) of the Lercheck section including possible stratigraphical gaps and non-outcropping parts of the sequence. Due to the lack of ammonite findings, the ammonite zones are constructed after the conodont zones. The exact boundaries, thus, are questionable.

cession, Rieche (1971) must be disagreed as he mapped "Carnian and Norian Limestones" in this location. The bedded grey to light-reddish coloured limestones studied herein can be compared to a sequence which he described similarly as the "Late Anisian": in its base white-coloured, the limestones are getting subsequently grey, light-reddish and finally dark reddish-coloured. With regards to Rieche's work in 1971, there is no exact proof about the age-dating, e.g. evidenced or confirmed by biomarkers of stratigraphical importance. The overturning of the section, thus, remained unperceived to him.

Conclusions

Despite of lithological similarities to the Early Carnian part of the adjacent Dürrnberg sections, the biostratigraphical data gained from the Lercheck / Königsleiten section show evidently uppermost Fassanian to Longobardian age. Thus it is most likely that the presented succession can be seen as their downward continuation.

The obvious stratigraphical hiatus between the Longobardian Lercheck limestones and Tuvalian red limestones outcropped in the adjacent Draxllehen quarry (ca. 100 metres in SE direction) can be explained by the occurrence of a steeply dipping normal fault between the two sections. The complete lacking of the Reingraben Shales (found at Freygutweg) as a corresponding stratigraphical unit between the Lercheck and the adjacent Draxllehen section, maybe due to the following two reasons: a) the formation was not deposited primarily, b) during orogenetic faulting, the Reingraben Shales, as the ductile and mobile member, were sheared off from their underlying part.

Acknowledgements

I am sincerely grateful to Leo Krystyn (Vienna), Manuel Rigo (Padua) and Heinz Kozur (Budapest) for some suggestions about conodont classifications and Bernard Millen (Innsbruck) for a helpful review of the manuscript. Thanks to an anonymous reviewer who aided to refine the data presented herein. At least, the financial support by the Austrian Scientific Found (FWF) is appreciated (Project P 16878).

References

Gümbel, C.W. (1861). Geognostische Beschreibung des Bayrischen Alpengebirges und seines Vorlandes. Perthes-Verlag, Gotha, 940 pp.

Hornung, T. (2006): Die Reingrabener Wende in der Halleiner Salzbergfazies (distale Hallstatt Fazies) - biostratigraphische Daten. – Geo.Alp 3: 7–19, Innsbruck.

Hornung, T., Brandner, R. (2005): Biochronostratigraphy of the Reingraben Turnover (Hallstatt Facies Belt): Local black shale events controlled by regional tectonics, climatic change and plate tectonics. – Facies 51: 460–479, online: DOI: 10.1007/s10347-005-0061-x, Erlangen.

Huckriede, R. (1958): Die Conodonten der mediterranen Trias und ihr stratigraphischer Wert. – Paläont. Z., 32/3-4: 141-175.

Kolar-Jurkovsek, T. (1983): Srednjetriasni konodonti Slovenije. – Rud.-met. Zbor. 30/4: 323-364

Kovács, S. (1983). On the evolution of *excelsa*-stock in the Upper Ladinian-Carnian (Conodonta, genus *Gondolella*, Triassic). – Schriftenr. Erdwiss. Komm. Österr. Akad. Wiss., **5**: 107-119.

Kovács, S., Kozur, H. (1980). Stratigraphische Reichweite der wichtigsten Conodonten (ohne Zahnreihen-Conodonten) der Mittel- und Obertrias. – Geol. Paläont. Mitt. Innsbruck, 10/2: 42-78, Innsbruck.

Kozur, H. (1972). Die Gattung *Metapolygnathus* Hayashi 1968 und ihr stratigraphischer Wert. – Geol. Paläont. Mitt. Innsbruck, 2/11: 1-39, Innsbruck.

Kozur, H. (1980): Revision der Conodontenzonierung der Mitte- und Obertrias des tethyalen Faunenreichs. – Geol. Paläont. Mitt. Innsbruck, Bd. 10, 3/4: 79-172, Innsbruck.

Kozur, H. (2003). Integrated ammonoid, conodont and radiolarian zonation of the Triassic and some remarks to Stage/Substage subdivision and the numeric age of the Triassic stages. Albertiana 28, 57-74.

Krystyn, L. (1970): Zur Conodonten-Stratigraphie in den Hallstätter Kalken des Salzkammergutes (Österreich). – Verh. Geol. B.-A.: 497-502, Wien.

Krystyn, L. (1983). The Epidauros Section (Greece) – a contribution to the conodont standard zonation of the Ladinian and Lower Carnian of the Tethys Realm. – Schriftenr. Erdwiss. Komi. Österr. Akad. Wiss., **5**: 231-258.

Mastandrea, A. (1995): Carnian Conodonts from upper Triassic strata of Tamarin section (San Cassiano Fm., Dolomites, Italy). – Riv. It. P

Neri, C., Russo, F., Mastandrea, A., Baracca, A. (1995): Lithostratigrafia, ammonoidi e conodonti della Formazione di S. Cassiano: la sezione dei Prati di

Sturoes (Stuores-Wiesen, Dolomiti). – Ann. Univ. Ferrara, 5 (Suppl.): 59-74.
Nogami, Y. (1968): Trias-Conodonten von Timor, Malaysien und Japan (Paleontological study of Portugese Timor, 5). – Mem. Fac. Science, Kvoto University, Geol. And Min., Vol. 35 (2): 115-136.
Pichler, H. (1963). Geologische Untersuchungen im Gebiet zwischen Rossfeld und Markt Schellenberg im Berchtesgadener Land. Beih. Geol. Jb., 48, 129-204.
Plöchinger, B. (1955): Zur Geologie des Kalkalpenabschnittes vom Torrener Joch zum Ostfuß des Untersberges; die Göllmasse und die Halleiner Hallstätter Zone. – Jb. Geol. Bundesanst., **95/1**: 93-144, Wien.
Rieche, J. (1971): Die Hallstätter Kalke der Berchtesgadener Alpen. – Unpubl. Diss. Univ. Berlin, 173 pp.
Schlosser, M. (1898). Das Triasgebiet von Hallein. Z. deutsch. Geol. Ges. 50, 333-384.
Vrielynck, B. (1987): Conodontes du Trias périméditerrannéen. Systematique, Stratigraphie. – Docum. Lab. Géol. Lyon, 97: 301 pp.

Plate 1: Conodonts of the Lercheck section: for all specimens CAI = 1.0; scale bar = 100 µm:

1: *Gladigondolella* cf. *malayensis* Nogami, 1968; very robust, superadult and pathological specimen, anteriorly broken; very big terminal, keel-like tooth; Lercheck section (Le 69).
2: *Gladigondolella malayensis* Nogami, 1968; angular view; anteriorly broken; Lercheck section (Le 65)
3: *Gladigondolella tethydis* Huckriede, 1958; lower view; anterior part broken; Lercheck section (Le 65)
4: *Gladigondolella tethydis* Huckriede, 1958; upper view; nearly complete specimen; Lercheck section (Le 65)
5: *Gladigondolella tethydis* Huckriede, 1958; lower view, posterior half with the basal pit, characteristically situated in midlength of the unit; Lercheck section (Le 35)
6: *Gladigondolella tethydis* Huckriede, 1958; upper view, adult growth stage, anterior part as well as the posterior third are broken off; Lercheck section (Le 35)
7: *Paragondolella inclinata* (Kovács 1983); angular view, adult growth stage, anteriorly fragmented carina; Lercheck section (Le 35)
8: *Gladigondolella malayensis* Nogami 1968; angular view, broken anterior half with robust isolated nodules; Lercheck section (Le 28)
9: *Paragondolella inclinata* (Kovács 1983); angular view, adult growth stage; note the melted low posterior carinal ridge (also Plate 1, fig. 2); Lercheck section (Le 10)
10: *Paragondolella inclinata* (Kovács 1983); angular view, adult growth stage; Lercheck section (Le 10)
11: *Budurovignathus cf. mungoensis* (Diebel); angular view, posterior platform third is broken off; Lercheck section (Le 10).
12: *Paragondolella inclinata* (Kovács 1983); upper view, adult growth stage; note the posterior restriction of the honeycomb structure of platform rims (also fig. 5); Lercheck section (Le 10)
13: *Paragondolella inclinata* (Kovács 1983); angular view, mid-age growth stage (denticled posterior carina), broken anterior carinal denticle; Lercheck section (Le 10)
13: *Gondolella trammeri* Kozur, 1971; angular view, adult growth stage, broken anterior carina and platform rims; Lercheck section (Le 10)
14: *Paragondolella trammeri* Kozur, 1971; angular view, adult growth stage, broken anterior carina and platform rims; Lercheck section (Le 10)

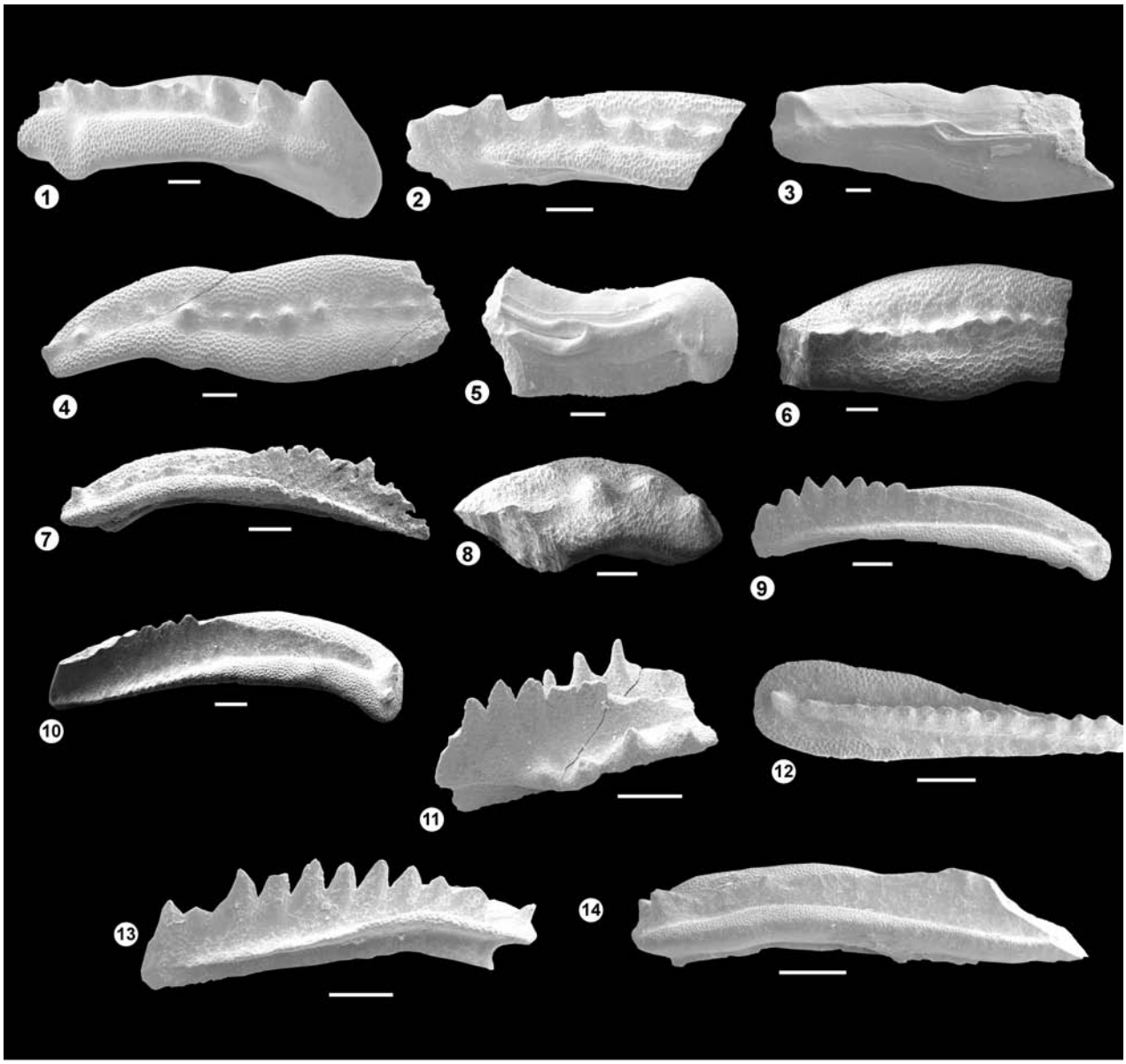
1
2
3
4
5
6
7
8
9
10
11
12
13
14

Geo.Alp, Vol. 3, S. 33–45, 2006

EINE ROTLIEGENDFLORA AUS SEESEDIMENTEN DES BOZNER VULKANITKOMPLEXES BEI SINNICH (SÜDTIROL)

Adolf Fritz[1] & Karl Krainer[2]

Mit 3 Abbildungen und 3 Tafeln

[1] Koschatstraße 99, A-9020 Klagenfurt

[2] Institut für Geologie und Paläontologie der Universität Innsbruck, Innrain 52, 6020 Innsbruck
e-mail: Karl.Krainer@uibk.ac.at

Abstract

In the Sinnichbach gorge near Meran (South Tyrol/Alto Adige; Northern Italy) alluvial and lacustrine sediments are intercalated in the Lower Permian Bolzano Volcanic Complex (Athesian Volcanic Group). Theses sediments accumulated in a small basin which formed by block faulting during a phase of volcanic quiescence. The lacustrine sediments contain a macroflora composed of species of *Cordaites*, conifers, seedplants with fernlike leaves and rare fragments of tree ferns. The abundance of conifers (Lebachiaceans), the occurrence of *Cordaites* and fragments of „voltzoid" branches indicate that the sediments accumulated during the Saxonian (Late Artinskian).

Zusammenfassung

Im Sinnichbach-Graben bei Meran (Südtirol) sind innerhalb des unterpermischen Bozner Vulkanitkomplexes alluviale und lakustrine Sedimente eingeschaltet, die in einem lokalen, durch Bruchtektonik herausgeformten Sedimentbecken während einer vulkanischen Ruhephase abgelagert wurden. Die Seesedimente enthalten eine Makroflora, die sich aus Cordaiten, Koniferen und farnlaubigen Samenpflanzen sowie vereinzelt Resten von Baumfarnen zusammensetzt. Das zahlreiche Auftreten von Koniferen (Lebachiaceen), sowie das Vorkommen von Cordaiten und „voltzoiden" Zweigresten erlauben eine Einstufung der Sedimentabfolge in das Saxon (jüngeres Artinsk).

1 Einleitung

Innerhalb des unterpermischen Bozener Vulkanitkomplexes sind in verschiedenen stratigraphischen Niveaus bis zu über 200 m mächtige alluviale und lakustrine Sedimente eingeschaltet. Aus dem Etschtal, zwischen Bozen und Meran, sind solche Einschaltungen aus dem Grissianer Graben, oberhalb vom Gehöft Gorl nordöstlich von Terlan, aus der Umgebung von Vöran und aus dem Sinnichbach bei Meran bekannt (Fels & Paul-Koch 1985, Hartkopf-Fröder & Krainer 1990, Krainer & Spötl 1998, Aspmair & Krainer 1998).

Diese eingeschalteten Sedimente weisen auf längere Ruhephasen der vulkanischen Aktivität. Während dieser vulkanischen Ruhephasen wurde der Verwitterungsschutt in relativ kleinräumigen, durch Bruchtektonik (? Vulkanotektonik) herausgeformten Becken in Form von alluvialen und lakustrinen Sedimenten abgelagert (Aspmair & Krainer 1998).

Aus feinkörnigen Seesedimenten dieser Einschaltungen konnte eine reichhaltige und außerordentlich gut erhaltene Mikroflora nachgewiesen werden (Hartkopf-Fröder & Krainer 1990, Hartkopf-Fröder et al. 2001). Im Sinnichbach konn-

te in Seesedimenten auch eine interessante Makroflora in Form von Abdrücken und verkieselten Stammresten gefunden werden. In der vorliegenden Arbeit werden die Sedimentabfolge und die darin aufgefundenen fossilen Pflanzenreste beschrieben und dokumentiert sowie deren stratigraphische und palökologische Bedeutung kurz diskutiert.

2 Fundstelle und Geologischer Rahmen

Das Profil durch die alluvialen und lakustrinen Sedimente liegt im Sinnichbach südöstlich von Meran, und zwar oberhalb vom Silizium-Werk im Bereich der Wasserfassung (Abb. 1). Die Sedimentabfolge ist ca. 40 m mächtig, wobei aber nur die obersten 20 m entlang der Ostseite des Sinnichbaches gut aufgeschlossen sind. Die Sedimente werden von mächtigen Vulkaniten überlagert, sie gehören im Vergleich zu den Sedimenteinschaltungen oberhalb Gorl oder bei Vöran einem deutlich tieferen (älteren) Niveau an, und zwar der Monte Luco (Laugen) Formation im Sinne von Bargossi et al. (2004).

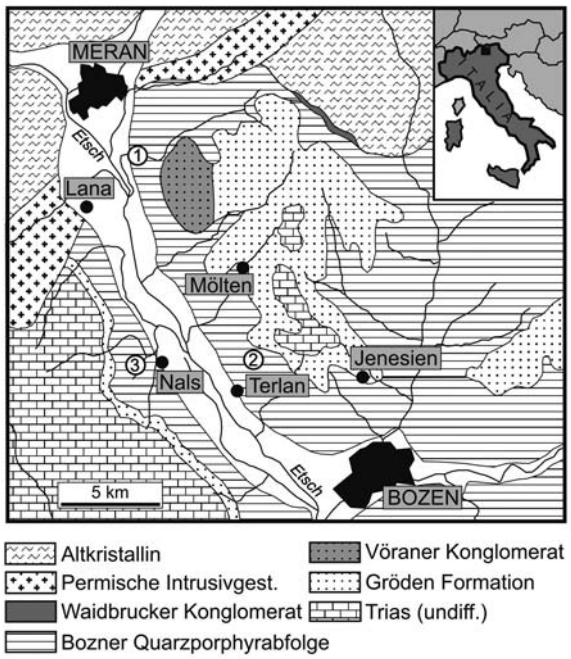

Abb. 1: Übersichtskarte mit Lage des untersuchten Profiles im Sinnichbachgraben bei Meran (1). Auf der Karte sind auch die Lokalitäten der Sedimenteinschaltungen oberhalb Gorl (2) und im Grissianer Graben (3) markiert.

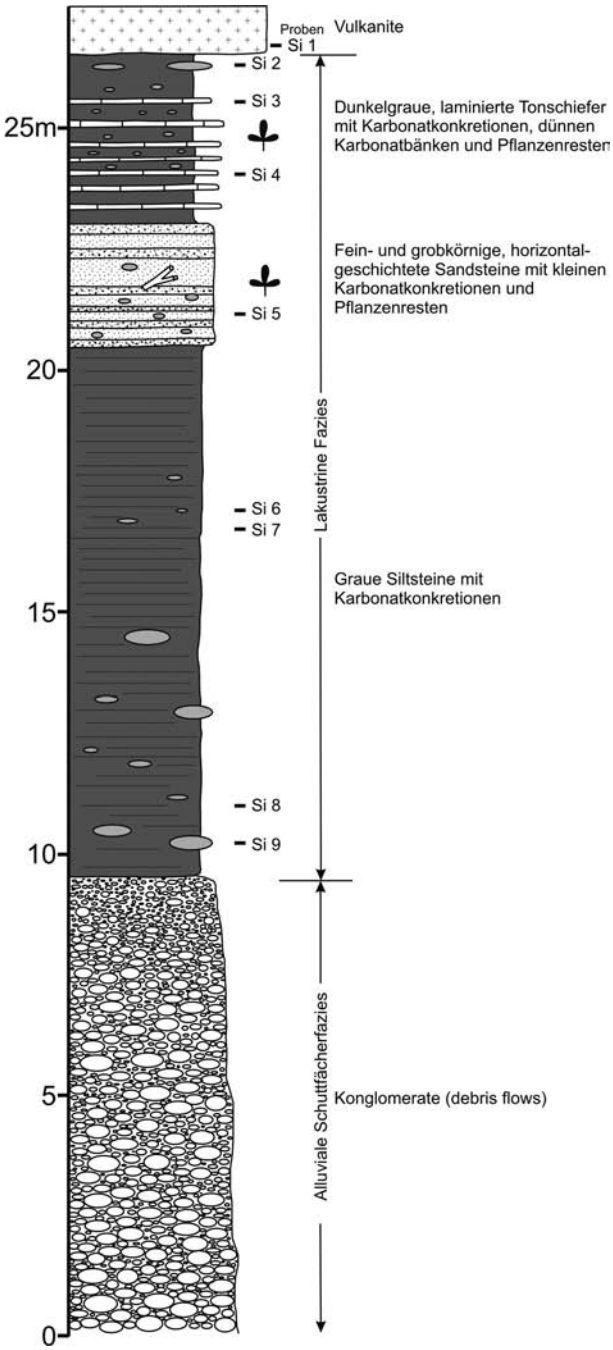

Abb. 2: Profil durch die Sedimentabfolge im Sinnichbach-Graben.

3 Die Sedimentabfolge im Sinnichbach-Graben

Die ca. 40 m mächtige Sedimentabfolge (Abb. 2) besteht im unteren Teil aus schlecht aufgeschlossenen Konglomeraten. Diese zeigen keine Schichtung, sind schlecht sortiert und besitzen eine sandige Matrix. Das Gefüge ist meist korngestützt. Im obers-

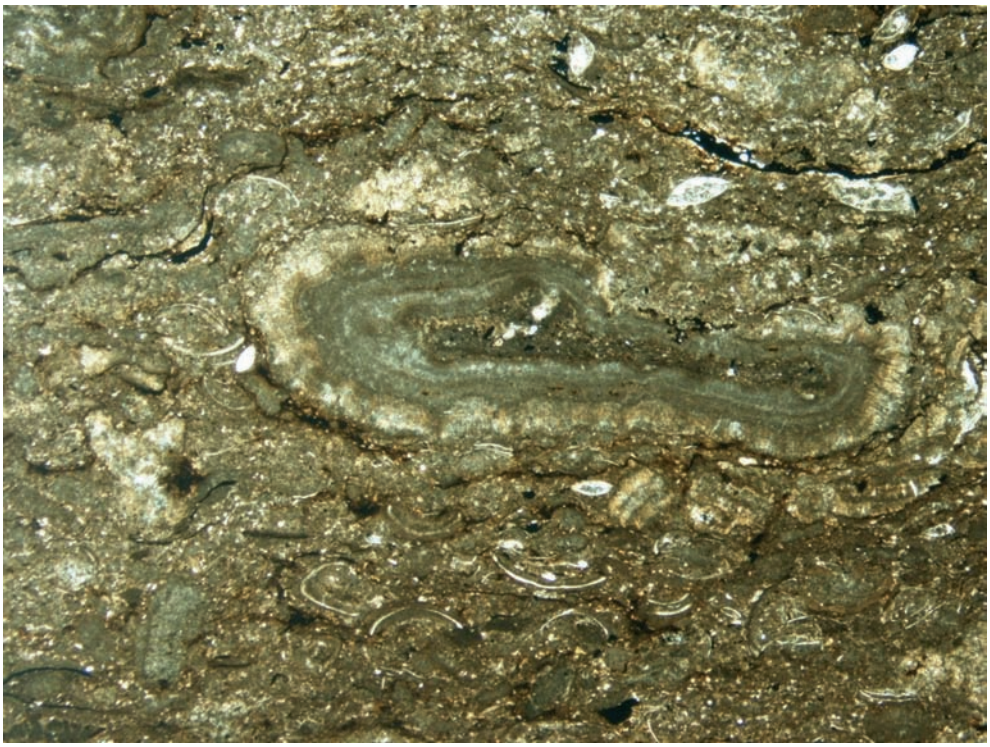

Abb. 3: Dünnschliffaufnahme einer dünnen Kalklage mit Onkoiden und zahlreichen Ostrakodenschalen. Bildbreite 15 mm.

ten Abschnitt ist die Konglomeratabfolge stellenweise stärker sandig entwickelt.

Über den Konglomeraten folgen ca. 11 m graue, siltige, geschichtete Sedimente, die vor allem im unteren Abschnitt bis zu über 40 cm große Karbonatkonkretionen enthalten. Die Siltsteine enthalten Quarz, Feldspat, Glimmer (Muskovit), selten Chlorit, opake Komponenten, inkohlte kleine Pflanzenreste und tonige Matrix.

Darüber folgt eine 2.5 m mächtige Abfolge aus abwechselnd fein- und grobkörnigen Sandsteinlagen. Die Sandsteine zeigen undeutliche Horizontalschichtung und enthalten cm-große rundliche Konkretionen und Pflanzenreste (Stammreste).

Die Sandsteine sind durchwegs schlecht sortiert, die Komponenten sind meist angular bis subangular. Sie bestehen aus Quarz (Porphyrquarz), Feldspat, diversen vulkanischen Gesteinsbruchstücken, einzelnen Glimmern und vielen opaken Komponenten. Feldspäte sind häufig stark zersetzt oder von Karbonat verdrängt. Die Matrix ist tonig bis feinsiltig, lokal tritt Karbonatzement auf. Vereinzelt sind in den Sandsteinen bis zu mehrere cm große Siltstein-Intraklaste enthalten. In den Sandsteinen finden sich auch bis zu mehrere cm große onkoidartige Algenkrusten und Algenlaminite.

Über dem Sandsteinhorizont folgen 3 m dunkelgraue, laminierte tonige Sedimenten, die kleine (~ 1cm) rundliche und größere ovale Karbonatkonkretionen enthalten. Eingeschaltet sind mehrere, bis zu etwa 3cm dicke Karbonatbänke. Diese bestehen aus zahlreichen, meist < 1cm großen, selten größeren, stark umkristallisierten Algenonkoiden (Abb. 3). Den Kern der Onkoide bilden häufig Ostrakodenschalen, selten auch größere Schalenreste. Die Matrix ist karbonatisch, überwiegend siltig, teilweise auch feinsandig mit einzelnen angularen bis subangularen Quarzkörnern. Die Matrix enthält zum Teil zahlreiche Ostrakodenschalen (Abb. 3). Selten sind die Ostrakoden doppelklappig erhalten, häufig sind die Schalen infolge Kompaktion verbogen oder zerbrochen. Vereinzelt sind auch größere und etwas dickere Schalenreste, vermutlich von Bivalven, enthalten.

Den Abschluss der Sedimentabfolge bildet ein 0.5 m mächtiger siltig-toniger Horizont mit bis zu 20 cm großen, brotlaibförmigen Karbonatkonkretionen. Die Sedimente werden von Vulkaniten überlagert, der Kontakt ist leicht tektonisch überprägt.

Die Pflanzenreste stammen aus den tonigen Sedimenten des obersten Profilabschnittes.

4 Die Rotliegend-Flora aus dem Sinnichbach-Graben

Die Rotliegend-Flora aus dem Sinnichbach-Graben schließt sich in gewisser Weise an jene aus dem Grödener Sandstein bei Mölten (Fritz & Krainer 1999: 637-650) an, erweist sich aber nach dem gegenwärtig bekannten Florenbestand durch das Fehlen mesophytischer Elemente als älter, auch wenn beide Floren, wie für den Sinnichbach-Graben noch begründet werden wird, dem Rotliegenden angehören. Das steht in guter Übereinstimmung mit der Einstufung der Möltener Flora in das höchste Saxon (= oberstes Kungur), eine Einstufung, die bereits 1999 von den Autoren als für sehr wahrscheinlich gehalten wurde (Fritz & Krainer 1999: 649).

Versteinertes Achsenstück eines Cordaitenbaumes (*Cordaixylon* sp. ?)

Das in Taf. 1, Abb. 1 dargestellte versteinerte Achsenstück eines Cordaitenbaumes besitzt eine Länge von 38 cm, einen Durchmesser von17 cm und gabelt sich in drei Astabgängen mit den Querschnitten 5x7 cm, 6x6 cm und 6x9 cm (Tafel 1, Abb. 2) auf. Es liegt offensichtlich ein Stammfragment aus dem Kronenbereich vor. Die Stärke des Stammstückes und die Art der Stammverzweigung entsprechen den Verhältnissen wie sie für Cordaiten bekannt sind.

Ähnliche Funde liegen auch aus dem Sandsteinbruch am Möltener Joch vor (Fritz & Krainer 1999: 641, Abb. 7), von dort sogar in der Länge von 150 cm bei einer Stammstärke von 50 cm.

Cordaites principalis (Germar)

Taf. 1, Abb. 3 zeigt ein basisnahes Blattfragment eines Cordaitenbaumes, das sich bei einer Länge von 47 mm divergierend von ca.15 mm auf 30 mm verbreitert. Die Aderung ist sehr kräftig ausgeprägt, die dünnen Baststränge dagegen sind nur unter dem Stereomikroskop und dann auch nur an kleinen, besser erhaltenen Stellen des Blattes erkennbar. Die Zahl der Baststränge entspricht der für *Cordaites principalis* angegebenen Norm (Josten 1991: 349). Das Blattfossil weist einige zerstreut liegende, bis knapp 1 mm große Abbruchstellen von vermutlich haarartigen Anhängen auf, in deren Vertiefungen sich kohlige Reste erhalten haben. Das Vorkommen derartige Blattanhänge scheint für Cordatienblätter etwas sehr seltenes zu sein und wurde vom Erstautor bisher noch an keinem Cordaitenblatt beobachtet. Es dürfte sich um eine Anpassung (Verdunstungsschutz) an geänderte Klimaverhältnisse im Rotliegenden handeln.

Querschnitt eines versteinerten Gymnospermenholzes ohne Zuwachsstreifen (*Cordaixylon* ?)

Der in Taf. 1, Abb. 4 dargestellte Ausschnitt eines strukturzeigenden Gesteinsschliffes entspricht typisch quergeschliffenem Sekundärholz. Das heißt, die Tracheiden-Querschnitte sind nach Art des Gymnospermenholzes in radialen Reihen angeordnet, enthalten aber im vorliegenden Fall keine Zuwachsstreifen. Die grundsätzlich isodiametrisch geformten Zellen sind radial mehr oder weniger leicht abgeplattet und schwanken in den Abmessungen etwa zwischen 70 µ bis 90 µ, bei einem Abstand der Markstrahlen von ca. 120 µ.

In Anbetracht dessen, dass im Sinne von Gothan& Weyland (1973: 375) Cordaitenholz keine Zuwachszonen aufweist und weiters in den fossilführenden Schichten des Sinnichbach-Grabens versteinertes Holz von Cordaiten nachweislich vorhanden ist, dürfte der in Taf. 1, Abb. 4, vorliegende Gesteinsschliff fossilem Cordaitenholz zuzuordnen sein.

Querschnitt eines versteinerten Gymnospermenholzes mit Zuwachszonen (*Dadoxylon*)

Im Gegensatz zum versteinerten Cordaitenholz in Taf. 1 Abb. 4 zeigt der Gesteinsschliff in Taf. 1, Abb. 5 ein Koniferenholz mit deutlich ausgebildeten Zuwachsstreifen. Das Frühholz besteht aus mehr oder weniger isodiametrisch geformten Zellen, die radial leicht gestreckt sein können. Der Zuwachsstreifen an Frühholz umfasst im Allgemeinen etwa 6 bis 7 Zellen bei einer Zellgröße von durchschnittlich 60 µ. Die Zellen des Spätholzes sind dagegen radial abgeflacht und dadurch im Querschnitt rechteckig geformt. Sie treten in Schüben von ca. fünf Zellen je Spätholzstreifen mit einer durchschnittlichen Zellgröße von ca. 20 x 37 µ auf. Der Abstand zwischen den Markstreifen schwankt etwa zwischen 110 µ und 300 µ.

Der Fund von zahlreichen Zweigresten und Zapfen von Koniferen legt nahe, dass es sich um Koniferenholz handelt. Nach Florin (1940: 293) sind Zuwachsstreifen bei Koniferenhölzern des Oberkarbons und Unterperms bisweilen zu erwarten, auch wenn diese zumeist nur sehr undeutlich ausgeprägt sind.

Walchianthus sp.

Die Fossilaufsammlungen im Sinnichbach-Graben lieferten einige Stücke eines zapfenartigen Fossils in unterschiedlicher fragmentarischer Erhaltung, die sich als männliche Koniferenzapfen (Mikrosporophyllstand) erweisen. Taf. 1, Abb. 6 zeigt einen nur 12 mm langen und 5 mm breiten Mikrostrobolus, welcher der Gestalt nach am vollkommensten erhalten ist. Die übergreifenden proximalen Abschnitte der Mikrosporophylle sind gut erkennbar. Ein etwas größerer Zapfen (Taf. 1, Abb. 7), dessen Spitze abgebrochen ist, besitzt als Bruchsstück eine Länge von 28 mm und eine Breite von 15 mm. Die Bruchstelle gibt den Blick auf die Zapfenachse mit einem Durchmesser von etwa 3 mm frei, deren Gewebe bereits zerstört ist.

Drei isolierte Querbrüche von männlichen Zapfen (Taf. 1, Abb. 8) lassen vermuten, dass noch weitere derartige Funde von Mikrostrobili in den fossilführenden Schichten des Sinnichbach-Grabens zu erwarten sind.

Die Oberfläche des Zapfens in Taf. 1, Abb. 7, ist relativ gut erhalten. Der Bildausschnitt in Taf. 2, Abb. 1 vermittelt eine konkrete Vorstellung des oberflächlich sichtbaren Teiles eines 6 mm breiten Mikrosporophylls, welcher mit einem schildförmigen Anhang versehen ist. Schuppen dieser Art nennt man hypopeltat und sind im Sinne von Florin (1940: 435) offenbar typisch für den Formenkreis der künstlichen Gattung *Walchia* (*Walchia, Lebachia*, *Ernestiodendron*), Familie Lebachiaceen. Die Mikrosporophylle der Walchiaceen bestehen grundsätzlich aus zwei Abschnitten, einem proximalen stielartigen Teil, welcher der Zapfenachse entspringt, die Mikrosporangien trägt, und aus einem distalen, flächenförmig ausgebreiteten Abschnitt, welcher gegenüber dem Stiel etwa um 90° abgewinkelt ist. Andeutungen der stielartigen Abschnitte lassen sich an dem Querbruch des Zapfens in Taf. 1, Abb. 8 erkennen.

Der isolierte, distal verbreiterte Abschnitt des Mikrosporophylls in Taf. 2, Abb. 2, zeigt die der Zapfenachse zugekehrte Seite mit der Anheftungsstelle des Stiels.

Walchiostrobus sp. (*Otovicia hypnoides* (Brongniart) Kerp et al., 1990)

Aus den fossilführenden Schichten des Sinnichbach-Grabens liegt ein Fund vor (Taf. 2, Abb. 3), der im Sinne von Florin (1940: 261/262) als Samenschuppenkomplex (*Walchiostrobus*) eines weiblichen Koniferenzapfens aus der Familie der Walchiaceen aufzufassen ist. Der Kurztrieb misst maximal 7 mm in der Höhe und 8,5 mm in der Breite und besteht aus einem divergierenden Büschel von Schuppen. Drei dieser Schuppen lassen terminal knotenartige Verdickungen erkennen, welche als Samenanlagen gedeutet werden.

Walchiostrobus-Zapfen treten nach Florin (1944: 432) mit zwei Haupttypen, dem *Lebachia*- und dem *Ernestiodentron*-Typ auf. Diese unterschieden sich (im Sinne von Florin) unter anderem dadurch, dass der *Lebachia*-Typ nur eine einzige Samenschuppe (ausnahmsweise zwei), der *Ernestiodendron*-Typ hingegen drei bis mehrere Samenschuppen aufweist.

Nach Untersuchungen von Kerp & Clement-Westerhof (1991: 257-268) besitzt jedoch die Typusart *Walchiostrobus gothanii* Florin offensichtlich drei Samenschuppen, *Ernestiodendron filiciforme* als Vertreter des *Ernestiodendron*-Typs hingegen nur eine einzige. Demzufolge wäre der Fossilfund aus dem Sinnichbach-Graben der *Walchiostrobus gothanii*-Form im Sinne von Kerp & Westerhof zuzurechnen.

Samenschuppe (Voltziaceae?)
(*Pseudovoltzia*, Majoniaceae)

Taf. 2, Abb. 4, zeigt eine dreilappige, leicht längs gestreifte Schuppe mit einer Länge von 7 mm und einer maximalen Breite von 6 mm. Die beiden seitlichen Lappen lassen unter dem Stereomikroskop je eine Verdickung erkennen, die als Samenanlage angesprochen werden könnte. Das würde bedeuten, dass die zur Zapfenachse gerichtete (adaxiale) Fläche der Schuppe vorliegt. Die Einfachheit des Schuppenbaus spricht für die Zugehörigkeit zu den Voltziaceen. Voltziaceen verkörpern gegenüber den Walchiaceen eine bereits höhere Entwicklungsstufe der Nadelhölzer, was zu einer Reduktion des Schuppenkomplexes in Fruchtschuppe und Deckschuppe führte (Mägdefrau 1956: 189). Letztere wäre vermutlich nur von der abaxialen Seite des Schuppenkomplexes her zu sehen. Die Interpretation der abgebildeten Schuppe als isolierter Schuppenkomplex einer Voltziaceae erfährt durch das Auftreten von heterophyllen Zweigresten, wie sie bei Voltziaccen vorkommen (Taf. 3, Abb. 4), eine gewisse Bestätigung. In Abb. 4 auf Taf. 2 scheinen zwischen den drei großen Samenschuppen noch zwei weitere kleine vorhanden zu sein (ev. *Pseudovoltzia liebeana*).

Isolierte Zweigreste von Koniferen (*Walchia* sp. ?, *Ernestiodendron filiciforme*?)

Die fossilführenden Schichten enthalten zahlreiche isolierte Zweigreste permischer Koniferen. Eine Auswahl der recht unterschiedlich gestalteten Zweigfragmente ist in Taf. 3, Abb. 1 bis 8 zusammengestellt. Die meisten Zweigfossilien stammen von den Walchiaceen. Die lateralen Sprosssysteme dieses Koniferen-Typs bestanden aus kräftigen Seitenästen mit zweireihig in einer Ebene angeordneten, Laubblätter (Nadeln) tragenden Seitenzweigen.

Die Laubblätter der Seitenzweige treten in zwei Gruppen auf. Die für die Gattung *Otovicia* typischen Laubblätter sind z.T. durch kleine bis sehr kleine Blattachselwinkel gekennzeichnet (wie in Taf. 3, Abb. 6 und 8), sodass deren Oberseiten mehr oder weniger eng dem Spross anliegen.

Walchia-Arten (Taf. 3, Abb. 3 und 5) besitzen eine Benadelung, bei denen die Blattorgane nicht unmittelbar dem Seitenzweig anliegen, aber in der Weise aufwärts gekrümmt sind, dass deren Spitzen den Zweigachsen etwa parallel verlaufen.

Noch andere Astfragmente haben abstehende bis fast gespreizte und adaxial mehr oder weniger stark gekrümmte Nadeln, die zum Blatttyp der Gattung *Ernestiodendron* (Taf. 3, Abb. 7) mit gespreizten bis hängenden Laubblättern überleiten.

Einen gänzlich anderen Zweigtypus, wie die bisher beschriebenen, zeigt das Zweigfragment auf Taf. 3, Abb. 4. Die Benadelung ist in diesem Fall typisch heterophyll (unterschiedlich lang) und entspricht den Verhältnissen, wie man sie in der Familie der Voltziaceen (*Pseudovoltzia liebeana*, siehe oben) antrifft.

Diverse Fruktifkationen

Samaropsis sp.

Bilateralsymmetrischer breit-ovaler Same, der von einem in der größeren Symmetrieebene umlaufenden Flügel umgeben ist (Taf. 2, Abb. 5). Der Flügel ist am Apex geteilt. Größte Länge 10 mm, größte Breite 8 mm. *Samaropsis*-Samen gehören zu verschiedenen systematischen Gruppen (Pteridospermen, Cordaiten, Coniferen). Eine Zuordnung des *Samaropsis*-Fundes zu den Koniferen ist allerdings aufgrund der zahlreichen Lebachiaceen-Reste durchaus möglich.

Trigonocarpus sp.

25 mm großer, längsovaler Same einer farnlaubigen Samenpflanze (Pteridospermae) aus der *Trigonocarpus*-Gruppe (Taf. 2, Abb. 7). Die fleischige Hülle des Samenkerns ist nicht mehr vorhanden, eine der drei Längsrippen der hartschaligen Skerotesta ist erkennbar. Dieser Samentyp gehört innerhalb der Farnsamer zu den Vertretern aus der Familie der Medullosaceae oder Trigonocarpaceae.

Radiärsymmetrischer Same einer Pteridospermae (?)

Scheibenförmiger, leicht kuppelförmig aufgewölbter, radiärsymmetrischer Same mit einem Durchmesser von etwa 17 mm (Taf. 2, Abb. 6).

Thuringia Remy ?

Männliche Pteridospermen-Fruktifikation der *Callipteris*-Gruppe (Haubold et al. 1983: 115). Die Sporen (Pollenkörner) produzierenden Organe (Pollangien) sind zylinderförmig zu einem schlauchförmigen Mikrosporangium (Synangium) verschmolzen. Das in Taf. 2, Abb. 8 abgebildete Synangium-Fragment besitzt eine Länge von 2,5 mm und eine Breite von 1 mm.

Pecopteris sp.

Isoliertes Einzelfiederchen eines Farns, 5 mm lang und 3 mm breit (Taf. 2, Abb. 9). Die Fiederchenränder verlaufen parallel, die Fiederchenspitze ist gerundet. Die Seitenadern, deren mögliche Verzweigung nicht eindeutig erkennbar ist, bilden zur eingesenkten Mittelader einen Winkel von etwa 45°.

5 Diskussion

Ähnlich wie bei den Vorkommen im Grissianer Graben und oberhalb Gorl (Aspmair & Krainer 1998; Krainer & Spötl 1998) zeigen auch die Sedimenteinschaltungen im Sinnichbach-Graben einen „fining-upward"-Trend. Die Ablagerung der Sedimente erfolgte in einem lokalen, durch Bruchtektonik herausgeformten, abflusslosen Becken. Die Sedimente lassen sich lateral nicht verfolgen, daher können über die Dimensionen dieses Sedimentbeckens keine Angaben gemacht werden. Bei den Sedimentationsprozessen spielte auch das Klima eine maßgebliche Rolle. Die Abfolge beginnt mit einer grobkörnigen, proximalen alluvialen Schuttfächerfazies bestehend aus Konglomeraten, die als debris flows gedeutet werden. Diese werden von einer Abfolge aus feinkörnigen Schichtflutsedimenten und siltig-tonigen Seesedimenten überlagert. Die dünnen Karbonatlagen entstanden durch Cyanobakterientätigkeit im See in Form von

dünnen „Algenmatten" und Onkoiden. Ostrakodenschalen belegen, dass der See zumindest zeitweise von zahlreichen Ostrakoden besiedelt war. Die in den lakustrinen Sedimentabfolgen der Lokalitäten Grissianer Graben und Gorl typischen kieseligen Sedimentlagen (Aspmair & Krainer 1998, Krainer & Spötl 1998) fehlen im Sinnichbach-Graben. Die recht zahlreichen Pflanzenreste deuten darauf hin, dass die Uferbereiche zumindest stellenweise von einer recht üppigen Vegetation bewachsen waren. Die Mikrofloren in den Seesedimenten weisen auch darauf hin, dass die Sedimente bereits unter deutlich trockeneren klimatischen Verhältnissen entstanden sind als im Oberkarbon. Die alluvialen Schuttfächer- und Schichtflutsedimente weisen ebenfalls auf ephemerale Bedingungen hin.

Die pflanzlichen Großfossilien aus dem Sinnichbach-Graben belegen die Existenz von Cordaiten, Koniferen und Samenfarne sowie mit einem einzigen isolierten Fiederchen auch das Vorkommen von Farnen. Reste von schachtelhalmartigen Pflanzen (Equisetophyta) und von Schuppenbaumgewächsen (Lepidophyten) sind bis jetzt nicht aufgefunden worden, obwohl deren Anwesenheit, hinsichtlich der Lepidophyten zumindest in Form von Subsigillarien, zu erwarten wäre. Gemessen an den zahlreich auftretenden Zweigfragmenten und Fruktifikationen von Koniferen scheinen diese eine sehr maßgebende Rolle in der Vegetation gespielt zu haben, insbesondere vertreten durch die Walchiaceen, deren Habitus an gewisse rezente Araukarien südhemisphärischer Verbreitung erinnert.

Die hohe Beteiligung der Walchiaceen an der Vegetation und zwar sowohl in Form der Gattung *Walchia* als auch der Gattung *Ernestiodendron* spricht für ein Rotliegend-Alter der fossilen Flora. Diese Alterseinstufung bei Ausschluss eines jüngeren, oberpermischen Alters (Thuring) ergibt sich auch aus der Anwesenheit der Cordaiten, die mit dem Rotliegenden aussterben und nicht mehr in das Ober-Perm (Thuring) aufsteigen. Die Anwesenheit „voltzioider" Zweigreste steht nicht unbedingt im Widerspruch mit der Einordnung der fossilen Flora in das Rotliegende (Saxon= höheres Artinsk/ Kungur). Mit dem Saxon-Alter der Flora hängt es vermutlich auch zusammen, dass die Lepidophyten gänzlich zurücktreten, deren Gattung *Lepidodendron* bereits im älteren Autun erlischt. Das offensichtliche Fehlen typisch mesophytischer Formen, wie *Sphenobaiera* und *Pterophyllum*, die, wie bereits erwähnt, im Oberrotliegenden des Grödener Sandsteins am Möltener Joch aufgefunden wurden, lässt die Flora vom Sinnichbach-Graben als etwas älter erscheinen.

Die ersten radiometrischen Datierungen ergaben für den Bozner Vulkanitkomplex ein Alter von ca. 270 Ma (Borsi et al. 1974, D´Amico 1986). Die von Barth & Mohr (1994) veröffentlichten radiometrischen Altersdaten von 276 Ma stimmen gut mit den neuesten Daten von Bargossi et al. (2004) überein, während die von Hess (1990) angegebenen Gesamtalter von 298 und 286 Ma, gemessen an Biotiten aus Ignimbriten im mittleren und höheren Abschnitt des Bozner Vulkanitkomplexes zu alt sind.

Die jüngst veröffentlichten radiometrischen Altersdaten (Zirkonalter) belegen für das Basiskonglomerat ein Alter von 284.9 $\pm$1.6 Ma (Grenze Sakmar/Artinsk), für die Vulkanite der Monte Luco Formation 279.6 $\pm$1.1 Ma (Artinsk) und für die Ora Formation am Top der Vulkanitabfolge 274.1 $\pm$1.6 Ma (ältestes Kungur) (Bargossi et al. 2004).

Entsprechend können die der Monte Luco (Laugen) Formation angehörenden pflanzenfossilführenden Seeablagerungen im Sinnichbach in das Artinsk (vermutlich jüngeres Artinsk) eingestuft werden.

Dank

Die fossilen pflanzlichen Großreste aus dem Sinnichbach-Graben bei Meran hat Herr Florian Mair (Meran) aufgesammelt und für eine Bearbeitung zur Verfügung gestellt. Die Autoren möchten sich für dieses Entgegenkommen herzlichst bedanken, zumal nach unserer Kenntnis aus den entsprechenden fossilführenden Schichten bis jetzt noch keine pflanzlichen Großrestfossilen bekannt gemacht wurden. Weiters möchten wir uns bei Evelyn Kustatscher und Volkmar Mair für die kritische Durchsicht des Manuskripts und wertvolle Hinweise bedanken.

Literatur

Bargossi, G.M., Klötzli, U.S., Mair, V., Marocchi, M. & Morelli, C. (2004): The Lower Permian Athesian Volcanic Group (AVG) in the Adige Valley between Merano and Bolzano: A stratigraphic, petrographic and geochronological outline. 32nd Int. Geol. Congr. Abstracts, Vol. I. 35-15, p. 187.

Barth, S. & Mohr, B.A.R (1994): Palynostratigraphically determined age of the Tregiovo sedimentary complex in relation to radiometric emplacement ages of the Atesina volcanic complex (Permian, Southern Alps, N Italy). – N. Jb. Geol. Paläont. Abh. 192: 273-292.

Borsi, S., D´Amico, C & Del Moro, A. (1974): Studio radiometrico delle rocce intrusive del massiccio di Cima d´Asta (Trentino). – Mem. Soc. Geol. It. 13: 145-159.

Aspmair, C. & Krainer, K. (1998): Fossile Pflanzenreste in Seeablagerungen der Bozner Quarzporphyrabfolge des mittleren Etschtales (Südtirol) und ihre Bedeutung für das Klima im Perm der Südalpen. – Der Schlern 72, Heft 4: 245-260.

D´Amico, C. (1986): Volcanic sequence in Trentino – Alto Adige. – In: Field Conference on Permian and Permian-Triassic Boundary in the South Alpine Segment of the Western Tethys, Field Guide-Book, Soc. Geol. It., 16-22.

Fels, H. & Paul-Koch, G. (1985): Alluviale Schuttfächer innerhalb der unterpermischen Vulkanite Südtirols (Italien). – Z. dt. Geol. Ges. 136: 167-179.

Florin, R. (1940): Die Koniferen des Oberkarbons und des Unteren Perms. - Palaeontographica, Heft 5: 244- 363.

Florin, R. (1944): Die Koniferen des Oberkarbons und des Unteren Perms.- Palaeontographica, Heft 6: 364: 456.

Fritz, A. & Krainer, K. (1999): Eine Rotliegend-Flora aus dem Grödnener Sandstein bei Mölten, Südtirol. - Der Schlern, Heft 10: 637-650.

Gothan, W. & Weyland, H. (1973): Lehrbuch der Paläobotanik. - BLV Verlagsgesellschaft München Bern Wien.

Hartkopf-Fröder, C. & Krainer, K. (1990): Fluviatile und lakustrine Sedimente innerhalb der permischen Bozner Quarzporphyrabfolge (Südtirol/ Italien): Ihre Biostratigraphische und palökologische Bedeutung. – Abstract Sediment ´90, Bonn, 3 Seiten.

Hartkopf-Fröder, C., Wood, G.D. & Krainer, K. (2001): Palynology of the Permian Bolzano Volcanic Complex, southern Alps, Italy, Part 1: Miospore preservation, quantitative spore color and quantitative fluorescence microscopy. – In: Goodman, D.K. & Clarke, R.T. (eds.), Proceedings of the IX International Palynological Congress, Houston, Texas, USA, 1996; American Association of Stratigraphic Palynologists Foundation, p. 79-97.

Haubold, H., Barthel, M, Katzung, G. & Schneider, J. (1983): Die Lebewelt des Rotliegenden. - Die Neue Brehm Bücherei, A. Ziemsen Verlag, Wittenberg Lutherstadt.

Hess, J.C. (1990): Numerische Stratigraphie permokarbonischer Vulkanite Zentraleuropas. Allgemeine Einführung und Teil I: Südtirol. – Z. dt. Geol. Ges. 141: 1-11.

Josten, K.H. (1991): Die Steinkohlen-Floren Nordwestdeutschlands. – Geologisches Landesamt Nordrhein-Westfalen, Krefeld.

Josten, K.H. & Van Amerom, H.W.J. (1999): Die Pflanzenfossilien im Westfal D, Stefan und Rotliegend Norddeutschlands. - Fortschr. Geol. Rheinld u. Westf., 39, 1–168, Krefeld.

Kerp, H. & Clement-Westerhof, J.A. (1991): Aspects of Permian palaeobotany and Palynology XII. The form-genus *Walchiostrobus* FLORIN reconsidered.- N. Jb. Geol. Paläont. Abh., 183 (1-3):257-268.

Krainer, K. & Spötl, C. (1998): Abiogenic silica layers within a fluvio-lacustrine succession, Bolzano Volcanic Complex, northern Italy: a Permian analogue for Magadi-type cherts? – Sedimentology 45: 489-505.

Mägdefrau, K. (1956): Paläobiologie der Pflanzen- Gustav Fischer Verlag, Jena.

Tafel 1

1: Versteinertes Achsenstück eines Cordaitenbaumes aus dem Kronenbereich mit drei Astabgängen. Das Stammfragment ist 38 cm lang und 17 cm stark.
2: Querschnitte der Astabgänge mit den Maßen 5x7, 6x6 und 6x9 cm.
3: Basisnahes Blattfragment eines Cordaitenbaumes in der Länge von 47 mm und einer maximalen Breite von 30 mm mit Abbruchstellen vermutlich haarartiger Blattanhänge.
4: Querschnitt eines versteinerten Holzes (*Cordaixylon* ?), vermutlich ein versteinertes Cordaitenholz. Mikroskopische Aufnahme, Bildbreite 2mm.
5: Strukturzeigendes Koniferenholz (*Dadoxylon* sp.) mit Zuwachsstreifen. Mikroskopische Aufnahme, Bildbreite 1,5 mm.
6: *Walchianthus* sp. mit Zapfen, 12 mm lang und 5 mm breit. Die übergreifenden proximalen Abschnitte der Mikrosporophylle sind deutlich erkennbar.
7: *Walchianthus* sp., 28 mm lang und 15 mm breit. Die Zapfenspitze ist abgebrochen und gibt den Blick auf die Zapfenachse frei, deren Gewebe zerstört ist.
8: *Walchianthus* sp., isolierter Querbruch mit Andeutungen der distalen stielartigen Abschnitte, die radial der Zapfenachse entspringen. Der Durchmesser des Zapfens beträgt 12 mm.

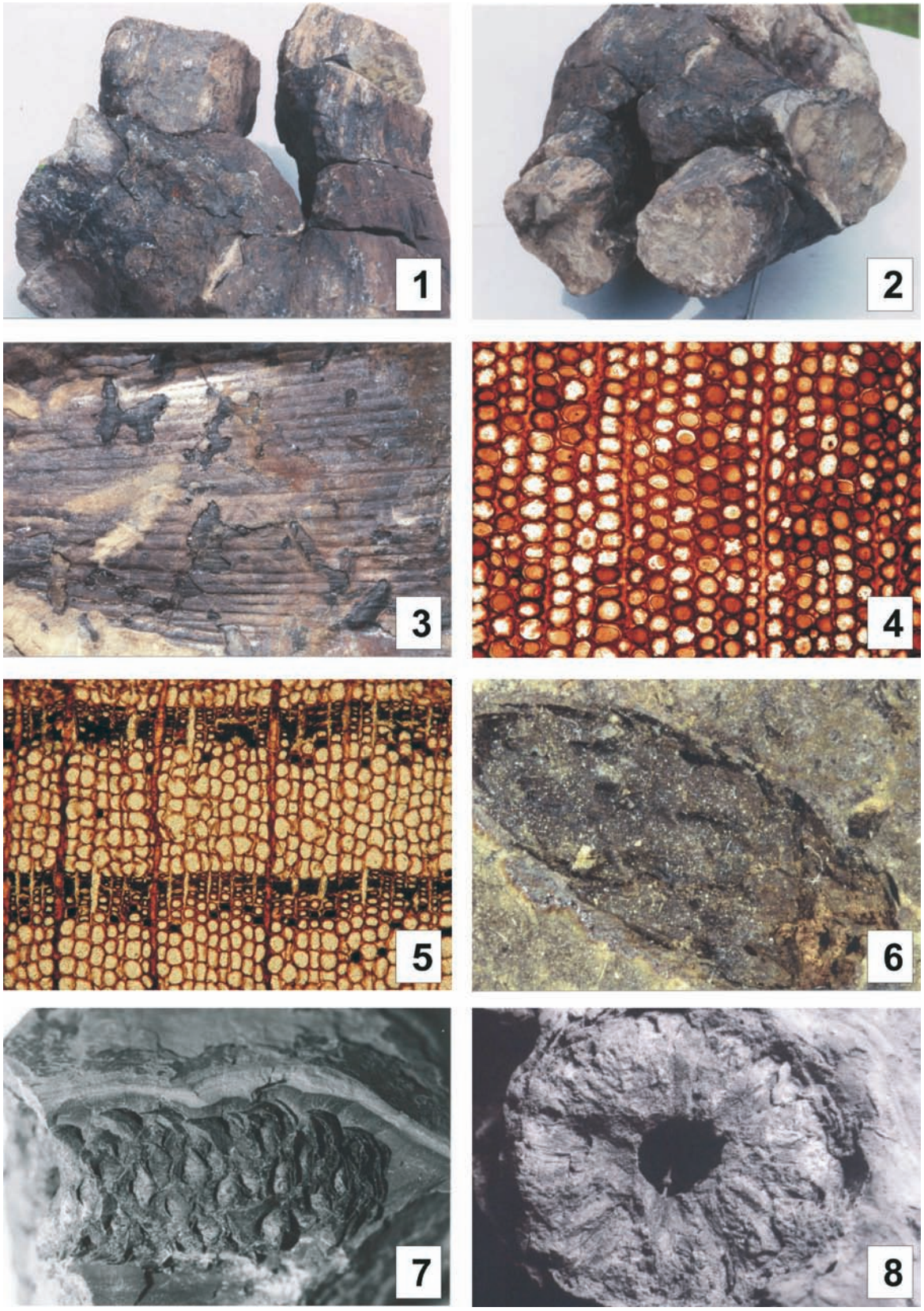
1
2
3
4
5
6
7
8

Tafel 2

1: Distaler, flächig ausgebreiteter Abschnitt eines Mikrosporophylls. Detailaufnahme aus dem Zapfen in Taf. 1, Abb. 7. Schuppenhöhe 6 mm, Schuppenbreite 5 mm.
2: Isolierter distaler Schuppenabschnitt eines Mikrosporophylls von der der Zapfenachse zugewendeten Seite (abaxial) mit der Anheftungsstelle des proximalen Stiels gesehen.
3: Isolierter Kurztrieb (Samenschuppenkomplex) einer Konifere (*Walchiostrobus*), etwa 7 x 8,5 mm groß mit knotenartigen Verdickungen an drei der erkennbaren Schuppen.
4: Isolierter Schuppenkomplex eines weiblichen Koniferenzapfens in adaxialer Ansicht, der vermutlich den Voltziaceen (*Pseudovoltzia liebeana* sp. ?) angehört.
5: *Samaropsis* sp. Bilateralsymmetrischer, breitovaler Same, geflügelter Same, der in der Fossilüberlieferung des Sinnichbach-Grabens vermutlich von Koniferen stammt.
6: Radiärsymmetrischer Same mit einem Durchmesser von 17 mm (Pteridospermae ?).
7: *Trigonocarpus* sp. 25 mm großer, längsovaler Samenkern einer Pteridospermae.
8: *Thuringia* sp. ? Fragment einer männlichen Pteridospermen-Fruktifikation der *Callipteris*-Gruppe. 2,5 mm lang, 1 mm breit (vergleiche Mägdefrau 1956, Abb. 163, Seite 176).
9: *Pecopteris* sp., isoliertes Einzelfiederchen eines Farns.


1


2

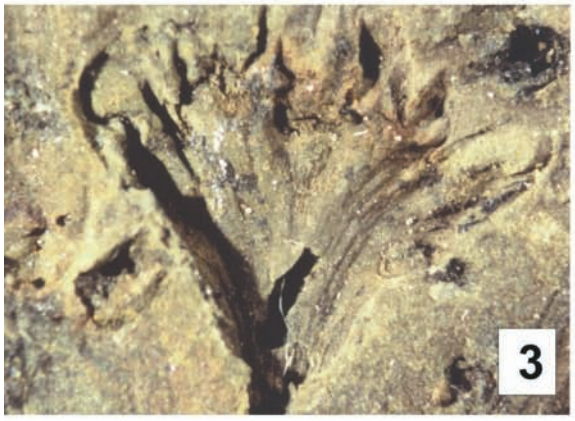
3


4

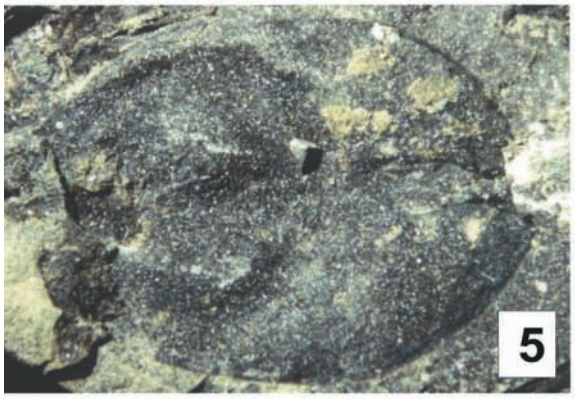
5


6

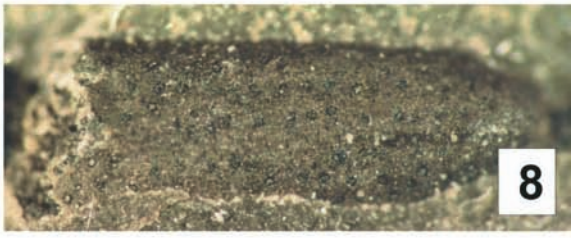
8


7


9

Tafel 3

1: *Walchia*, Seitenzweig letzter Ordnung. Nadeln bis 4 mm lang, parallelrandig, locker gestellt und stark gespreizt.
2: *Walchia*, dreidimensional erhaltene, längsgestreifte Koniferennadel, 9 mm lang, 2 mm breit, mit deutlich ausgebildeter Gratbildung.
3: *Walchia,* Seitenzweig letzter Ordnung. Nadeln aufwärts gekrümmt, nicht am Zweig anliegend.
4: Heterophylles, „voltzoides" Zweigfragment einer Konifere mit ca. 25 mm Länge.
5: *Walchia*, Seitenzweig letzter Ordnung mit nicht anliegenden, aufwärts gekrümmten Nadeln. Die Nadelspitzen verlaufen parallel zur Zweigachse.
6: *Walchia*, Seitenzweig letzter Ordnung. Nadeln eng der Achse anliegend.
7: *Ernestiodendron filiciforme* ? Seitenzweig letzter Ordnung. Nadeln gespreizt bis waagrecht der Zweigachse angeheftet. Nadelenden aufwärts gekrümmt (vergleiche Abb. 2a auf Taf. 24 in Josten & Van Amerom, 1999, Seite 149).
8: *Walchia*, Seitenzweig letzter Ordnung. Nadeln linealisch und eng der Zweigachse anliegend.

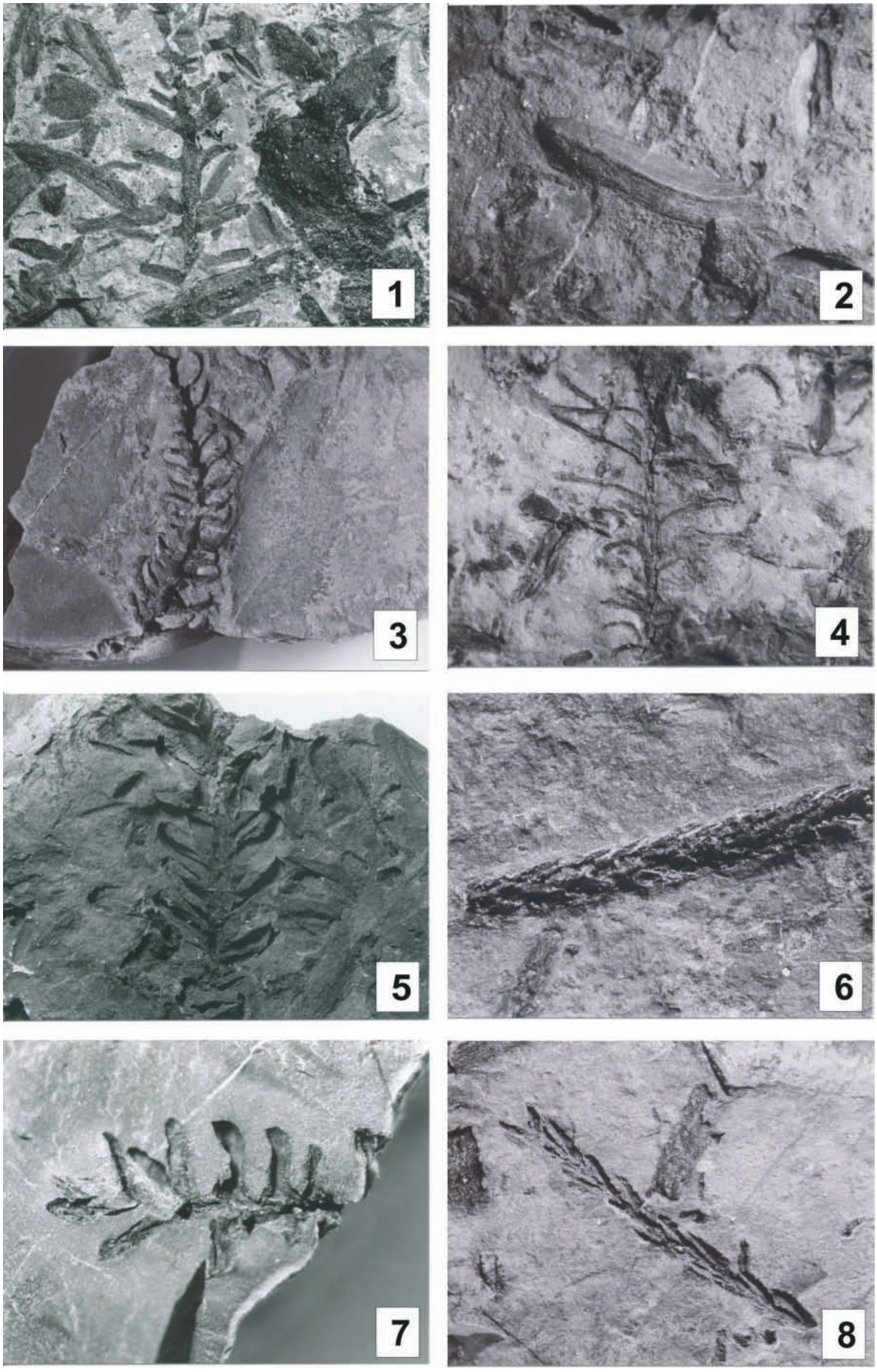
1
2
3
4
5
6
7
8

Geo.Alp, Vol. 3, S. 47–53, 2006

OLD TREASURES NEWLY DISCOVERED: *SCYTOPHYLLUM BERGERI* FROM THE LADINIAN OF THE DOLOMITES IN THE HISTORICAL COLLECTIONS OF THE GEOLOGISCHE BUNDESANSTALT WIEN

Evelyn Kustatscher[1], Barbara Meller[2] & Johanna H.A. van Konijnenburg-van Cittert[3]

With 1 figure and 2 plates

[1] Naturmuseum Südtirol, Bindergasse 1, 39100 Bozen, Südtirol, Italy. e-mail Evelyn.Kustatscher@naturmuseum.it

[2] Geologische Bundesanstalt, Neulinggasse 38, 1030 Wien, Austria, e-mail: melbar@geologie.ac.at

[3] Laboratory of Palaeobotany and Palynology, Budapestlaan 4, 3584 CD Utrecht, The Netherlands, e-mail: j.h.a.vankonijnenburg@bio.uu.nl and National Natural History Museum 'Naturalis', PO Box 9517, 2300 RA Leiden, The Netherlands. e-mail: Konijnenburg@naturalis.nl

Abstract

A specimen of *Scytophyllum bergeri* Bornemann from Corvara, that was mentioned in literature from the 19th century under various names but has never been described and figured, has been rediscovered in the collections of the Geological Survey in Vienna. It is the first specimen of this species from Ladinian sediments in the Dolomites and is described, figured and discussed here.

Zusammenfassung

Aus dem Ladinium von Corvara wird erstmals *Scytophyllum bergeri* Bornemann beschrieben, abgebildet und diskutiert. Dieses Exemplar, welches in wenigen Publikationen aus dem 19. Jahrhundert unter verschiedenen Namen erwähnt, jedoch niemals beschrieben und abgebildet worden ist, konnte in der Sammlung der Geologischen Bundesanstalt in Wien wieder entdeckt werden.

1. Introduction

Fossil plants of Ladinian age (referred to the "Buchensteiner Schichten" or "Wengener Schichten") from the Dolomites have been known for over 120 years. The first fragment of a fern frond from the Ladinian of the Dolomites has been figured by Wissmann & Münster (1841); for a detailed historical overview see also Wachtler & Van Konijnenburg – Van Cittert (2000a, b), Kustatscher (2004) and Kustatscher & van Konijnenburg – van Cittert (2005). In the latter also a detailed list of both inedited and revised material stored at several local and international museums and universities has been published.

During an extended research on the plant fossils mentioned by Mojsisovics (1879, pp. 57-8, 244) the first author detected at the Austrian Geological Survey, a frond fragment originating from the "Halobienschichten" of "Corfara". This specimen and its various entries in the historical literature are the topic of this article.

2. History of the specimen in the literature

The specimen stored at the Austrian Geological Survey has two different labels: The original label indicates that the "*Zamites* n. sp." has been collected by "v. Richthofen" in 1856 from the "Halobienschichten" of "Corfara". The second one, dated probably from the period around 1938-1945, says *Thinnfeldia richthofeni* Stur from the Upper Triassic (Carnian) of the same locality.

As far as the authors could detect, the specimen is mentioned only a few times in literature, but has never been figured or described in detail.

For the first time it has been cited by Richthofen in 1860 (p. 69). The article suggests that it has been collected, together with a shoot of "*Araucarites*", in

the "Schichten von Wengen (Halobienschichten)" of "Corfara". Constantin R. von Ettingshausen (probably by personal communication; there was never any publication) attributed the specimen to a new species of *Zamites*, characterized by particularly wide pinnae (see Richthofen 1860).

The same specimen was mentioned also by Stur (1868a, p. 113) as a frond fragment collected by "Ferdinand Freiherr von Richthofen" in the "Wengerschiefer" arround St. Kassian. He disagreed with Richthofen's (1860, p. 69) attribution of the specimen to the genus *Zamites* and assigned the frond fragment instead to the genus *Thinnfeldia*, considered by him as a fern genus.

Later in the same year, Stur (1868b, p. 550, 563), however, cited the same specimen as "*Thinnfeldia richthofeni* n. sp.", without figuring or giving a diagnosis. He mentioned also two newly found plant remains from the "Wenger Schiefer" near Corvara, *Neuropteris* cf. *ruetimeyeri* Heer and *Pterophyllum giganteum* Schenk (Stur, 1868b, p. 551, 563).

Mojsisovics (1879), too, cited plant remains from the "Wengener Schichten" of 'Corvara in Enneberg', including *Thinnfeldia richthofeni* Stur (on his p. 244). In a list composed of 19 taxa (on his p. 56-7), however, he mixed *Th. richthofeni* Stur and *Neuropteris* cf. *ruetimeyeri* Heer collected at 'Corvara in Enneberg' with others from 'Idria in Krain', just referring to Stur as the person who made the classification.

On the basis of the labels and the information in the literature, we assume that this plant fossil originated from the surroundings of Corvara (Fig. 1). Regarding the age of the specimen, the "Schichten von Wengen (Halobienschiefer)" of Richthofen (1860) as well as the "Wengerschiefer" of Stur (1868a, b) and the "Wenger Schichten" of Mojsisovics (1879) correspond today to the "Gruppo di Wengen" as introduced by Assereto *et al.* (1977). The Wengen Group is characterised at its base by the start of the basic volcanic activity and comprises today several different formations of Ladinian age (comm. pers. Piero Gianolla, 2005).

The specimen has been studied macroscopically and a small sample has been analysed using Schulze's method for cuticular analysis. The specimen lies on the surface of a dark brown and thin sediment block which is finely parallel bedded. On the backside the sediment has a gray colour. The frond is accompanied by some *Trachyceras*-like ammonoids and an imprint of the bivalve of the genus *Daonella* (comm. pers. Alexander Lukeneder) (Plate 2, Fig. 1, 4). The gross morphology of the specimen is well preserved, but the secondary venation is missing.

The specimen yielded, due to its preservation, just small pieces of a well-preserved cuticle. Notable are the numbers next to the apical end of the pinnae on the right half of the frond, counting the numbers of pinnae. It is not known, who has written this numbers and when it has been done.

3. Systematic descriptions and discussion

Order Peltaspermales Taylor, 1981
Family Peltaspermaceae Pilger & Melchior, 1954
(In: Melchior and Werdermann, 1954)

Genus *Scytophyllum* Bornemann, 1856
***Scytophyllum bergeri* Bornemann, 1856**
Plate 1, Fig. 1; Plate 2, Fig. 1-4

Description:
The specimen represents an (almost) entire frond of *Scytophyllum bergeri* of c. 27 cm length and 14 cm width (Plate 1, Fig. 1). The slightly curved rachis is 7 mm wide at the base and reduces just slightly apically. Nineteen partially to entirely preserved pinnae arise (sub)alternately from the rachis, at an angle of c. 45 degrees. The distance between single pinnae decreases from 23-30 mm at the base to 13 mm at the top (Plate 2, Fig. 1, 3), with the last two pinnae oppositely inserted (paripinnate). The pinnae are lanceolate with an acute apex (Plate 2, Fig. 2, 4); the margin is always entire, sometimes slightly undulate. The basal pinnae are small, 55 mm long and 12 mm wide. The length of the pinnae increases upwards reaching a length of 102 mm and a width of 15 mm at 2/3 of the frond. Then they decrease again apically, the last entire pinna measuring 75 mm in length and 12 mm in width, while the two apical pinnae are not preserved entirely (Plate 2, Fig. 1). The lamina of the pinnae is always broadly attached at the basal side, while it is usually slightly constricted at the apical side (Plate 2, Fig. 3). The midrib of the pinnae is distinct and up to 2.5 mm wide, secondary venation is not visible.

Due to the preservation of the cuticle just small fragments were obtained. The epidermal cells are isodiametric to hexagonal, covered by strong papillae. The stomata are scarce and scattered on the surface, without visible order but probably situated

between veins. The sunken guard cells are surrounded by 6-7 subsidiary cells. This cuticle differs from usual *S. bergeri* cuticles only in the presence of the papillae on the normal epidermal cells (Linnell, 1933) but the presence of papillae is often caused by environmental circumstances only and is not a diagnostic feature.

Discussion

We disagree with Richthofen (1860) about attributing the specimen to the genus *Zamites*, since the latter is a bennettitalean genus with symmetrical pinnae, with a slightly constricted base on both sides.

Additionally, the cuticle of our specimen is totally different from the bennettitalean cuticle of *Zamites* or the corystosperm one of *Thinnfeldia*, as considered by Stur (1868a, b). Moreover, the new species, proposed by Stur (1868b) and mentioned by Mojsisovics (1879) is not validly published, as no diagnosis or description was given.

Remarks: According to ICBN Art. 32 a taxon is not validly published when no diagnosis or description is given (see Greuter et al., 2000).

We attribute, therefore, this specimen due to its macromorphological (pinna shape, margin and attachment, strong midrib) and cuticular features to *Scytophyllum bergeri.*

Scytophyllum bergeri has been described for the first time from the Lettenkohle (late Ladinian) of Germany by Bornemann (1856) and was later discussed in detail by Linnell (1933). It has, however, never been described from the Ladinian of the Alpine area. On the other hand, abundant plant remains attributed to this species have been found in Anisian sediments of the Dolomites. The latter material, already mentioned as *Scytophyllum* sp. in Broglio Loriga *et al*. (2002) and Kustatscher (2004) will be discussed in detail with all its taxonomical and morphological problems in another article (Kustatscher *et al*., submitted).

Other species have been studied from Ladinian sediments from the surroundings of Corvara. At the Museum of Natural History at Vienna a frond fragment of *Cladophlebis leuthardtii* Leonardi, 1953 (2005B0004/0001) is stored (Plate 2, Fig. 5). A leaf fragment attributed as cf. to the cycad genus *Bjuvia* (AS XIII 18) and a leaf fragment of *Taeniopteris* sp.

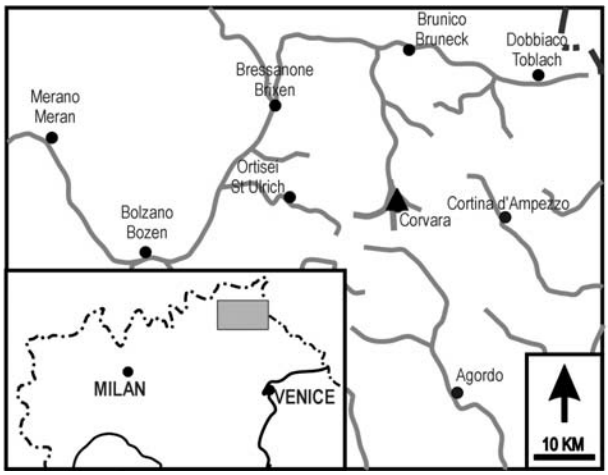

Fig. 1: Map of the fossil plant locality of the discussed specimen.

(1912 III 7) are stored at the Palaeontological Museum of Munich. Both specimens have been already discussed and figured by Ogilvie–Gordon (1927, pl. 8, figs. 2, 6).

Acknowledgements

We want to thank Irene Zorn (Austrian Geological Survey) for the help in discover the wherabouts of the material discussed by Mojsisovics, Piero Gianolla (University of Ferrara) for stratigraphic discussions, Helga Schmitz at the Naturhistorisches Museum Wien for help in the research of the old bibliography, Alice Schuhmacher from the Naturhistorisches Museum Wien for taking the pictures. Alexander Lukeneder classified the invertebrate imprints on the rock sample and Andreas Kroh helped to find and photography other historical specimens stored at the Naturhistorisches Museum Wien. The latter has been possible due to the financial support of the Synthesys project (AT-TAF-1125).

The manuscript was greatly improved by the constructive remarks and considerations from Prof. Dr. Hans Kerp.

References:

Assereto R., Brusca A., Gaetani M., Jadoul F. (1977): Le mineralizzazioni Pb-Zn nel Triassico delle Dolomiti: quadro geologico ed interpretazione genetica. – L'Industria Mineraria, 28: 367-402.

Bornemann, J. G. (1856): Über organische Reste der Lettenkohlegruppe Thüringens. Ein Beitrag zur Fauna und Flora dieser Formation. - 85 pp., Verlag Wilhelm Engelmann, Leipzig.

Broglio Loriga C., Fugagnoli A., van Konijnenburg-van Cittert J. H. A., Kustatscher E., Posenato R., Wachtler M. (2002): The Anisian macroflora from the Northern Dolomites (Monte Prà della Vacca/Kühwiesenkopf, Braies): a first report. – Riv. Ital. Paleont. Strat., 108: 381-390, 1 pl.

Greuter, W., McNeill, J., Barrie, F.R., Burdet, H. M., Demoulin, V., Filgueiras, T. S., Nicolson, D. H., Silva, P.C., Skog. J. E., Trehane, P., Turland, N. J. and Hawksworth, D. L. 2000. *International Code of Botanical Nomenclature (Saint Louis Code).* Koeltz Scientific Books, Königstein, Germany, 474 pp.

Kustatscher, E. (2004): Macroflore terrestri del Triassico Medio delle Dolomiti e loro inquadramento bio-cronostratigrafico e paleoclimatico mediante palinomorfi. – PhD thesis, Dept. of Earth Sciences, Uni. Ferrara, Italy. 220 pp.

Kustatscher, E., van Konijnenburg-van Cittert, J.H.A. (2005): The Ladinian Flora (Middle Triassic) of the Dolomites: palaeoenvironmental reconstructions and palaeoclimatic considerations. - Geo.Alp, 2: 31-51.

Kustatscher, E., Wachtler, M., van Konijnenburg-van Cittert, J.H.A. Horsetails and seed ferns from the Middle Triassic (Anisian) locality Kühwiesenkopf (Monte Prà della Vacca) in the Dolomites (Northern Italy) – Palaeontology (submitted).

Linnell, T. (1933): Zur Morphologie und Systematik Triassischer Cycadophyten, II. Über *Scytophyllum* Bornemann, eine wenig bekannte Cycadophytengattung aus dem Keuper. - Svensk Bot. Tidskrift, 27: 310-331.

Melchior, H., Werdermann, E. (1954): *A. Engler's Syllabus der Pflanzenfamilien*. Vol. 1. 567 pp., Gebrüder Bornträger, Berlin.

Mojsisovics, E. (1879): Die Dolomit-Riffe von Südtirol und Venetien: Beiträge zur Bildungsgeschichte der Alpen. - 551 pp., A. Hölder Verlag, Wien.

Ogilvie-Gordon, M.M. (1927): Das Grödner-, Fassa- und Enneberggebiet in den Südtiroler Dolomiten. – Abh. Geol. Bundesanst., 24 (2): 1-376.

Richthofen, F., Freiherr von (1860): Geognostische Beschreibung der Umgebung von Predazzo, Sanct Cassian und der Seisser Alpe. - 327 pp., J. Perthes Verlag, Gotha.

Stur, D. (1868a): Beiträge zur Kenntnis der geologischen Verhältnisse der Umgebung von Raibl und Kaltwasser. – Jahrb. geol. Reichsanst., 18 (1): 71-122.

Stur, D. (1868b): III. Eine Exkursion in die Umgebung von St. Cassian – Jahrb. geol. Reichsanst., 18(3): 529-568.

Taylor, T. N. (1981): Paleobotany: An Introduction to Fossil Plant Biology. - 589 pp., McGraw Hill, New York.

Wachtler, M., van Konijnenburg-van Cittert, J.H.A. (2000a): The fossil flora of the Wengen Formation (Ladinian) in the Dolomites (Italy). - Beitr. Paläont., 25: 105-141.

Wachtler, M., van Konijnenburg-van Cittert, J.H.A. (2000b): La flora fossile della Formazione di La Valle - Wengen (Ladinico) nelle Dolomiti (Italia). - Studi Trent. Sci. Nat., Acta Geol., 75: 113-146.

Wissmann, H.L., Münster, Graf von, G. (1841): Beiträge zur Geognosie und Petrefactenkunde des südöstlichen Tirol's vorzüglich der Schichten von St. Cassian. - 152 pp., Buchner'sche Buchhandlung, Bayreuth.

Plate 1

Scytophyllum bergeri Bornemann, 1856 (Nr. 2005/7/1, Austrian Geological Survey, Wien), x 0.9.

Plate 2

1. *Scytophyllum bergeri* Bornemann, 1856, detail of the apical part with imprint of trachiceratide ammonoid (same specimen as on plate 1), x 1.5.
2. *Scytophyllum bergeri* Bornemann, 1856, detail of the pinnae apex (same specimen), x 2.
3. *Scytophyllum bergeri* Bornemann, 1856, detail of the rachis and the pinnae base (same specimen), x 1.5.
4. *Scytophyllum bergeri* Bornemann, 1856, detail of the pinnae apex with imprint of Daonella (same specimen), x 1.5.
5. *Cladophlebis leuthardtii* Leonardi, 1953, frond fragment (Nr. 2005B0004/0001, Natural History Museum Wien), x 2.5.

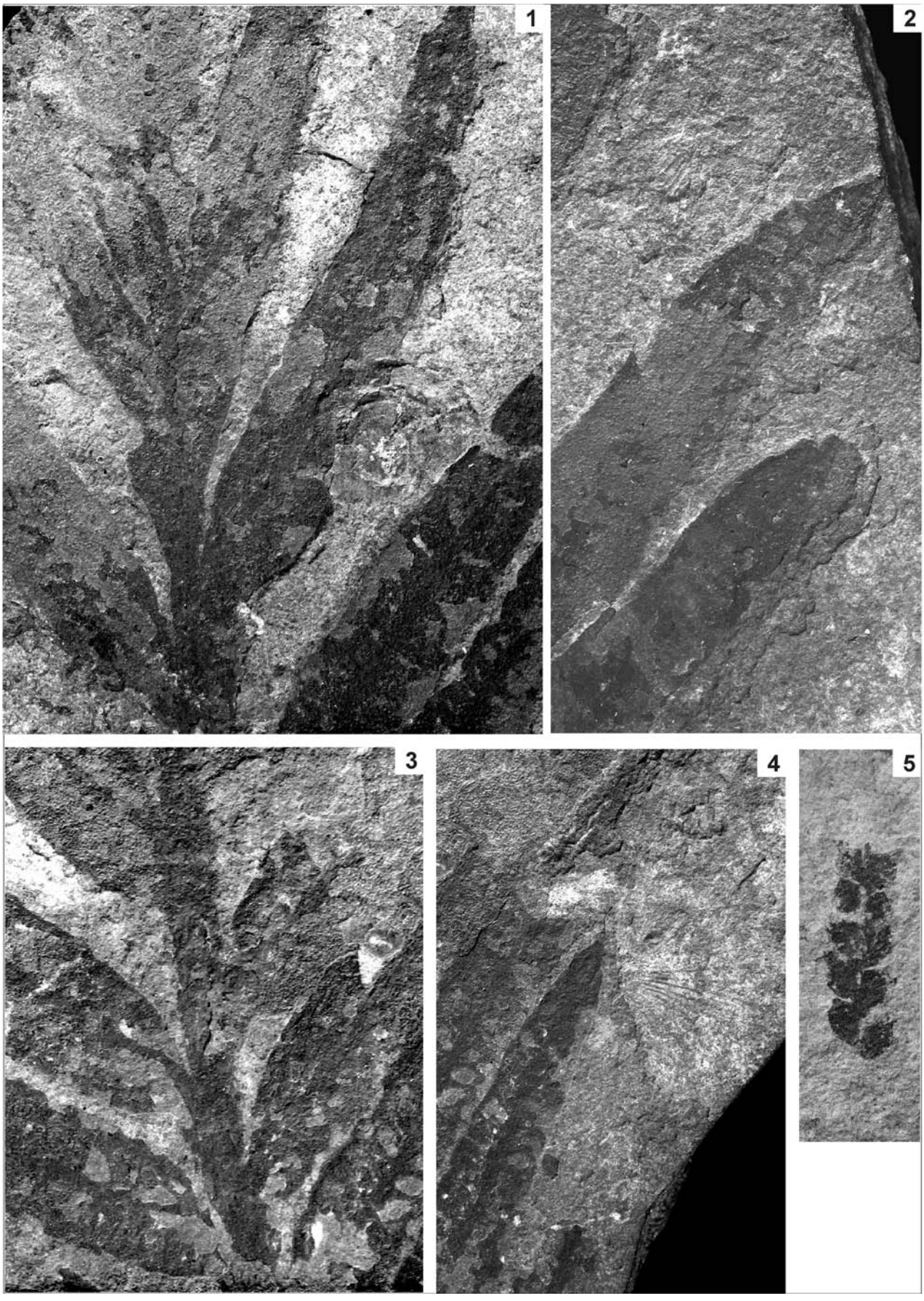
1
2
3
4
5

Geo.Alp, Vol. 3, S. 55–83, 2006

STRATIGRAPHIC IMPLICATIONS OF A NEW LOWER CRETACEOUS AMMONOID FAUNA FROM THE PUEZ AREA (VALANGINIAN – APTIAN, DOLOMITES, SOUTHERN ALPS, ITALY)

Alexander Lukeneder[1] & Christian Aspmair[2]

With 6 figures and 8 plates

[1] Natural History Museum, Geological-Palaeontological Department, Burgring 7, A-1010 Wien, Austria, e-mail: alexander.lukeneder@nhm-wien.ac.at

[2] Prissian 102, I – 39010 Tisens (BZ), Italy

Abstract

Lower Cretaceous ammonoids (n = 424) were collected at the Puez locality in the Dolomites of Southern Tyrol. The cephalopod fauna from the marly limestones to marls here indicates Late Valanginian to Early Aptian age. The deposition of the marly limestones and marls of this interval occurred during depositionally unstable conditions. The underlying Biancone Formation (Maiolica Formation) is of Early Valanginian, whereas the lowermost Rosso Ammonitico is of Jurassic to Berriasian age.

The ammonoid fauna consists of 27 different genera, each represented by 1-2 species. The assemblage at the Puez section is dominated by the Phylloceratina (30%) and the Ammonitina (34%). *Phyllopachyceras* (17%) and *Phylloceras* (13%) (both Phylloceratina) are the most frequent components, followed by *Lytoceras* (12%) (Lytoceratina), and *Barremites* (10%) and *Melchiorites* (8%) (both Ammonitina). The cephalopod fauna is purely of Mediterranean origin.

Zusammenfassung

Unterkreide Ammonoideen (424 Exemplare) der Puez Lokalität in den Dolomiten Süd-Tirols wurden untersucht. Die Fauna der mergeligen Kalke und Mergel von Puez zeigen ein Alter von Ober-Valanginium bis Unter-Aptium an. Die mergeligen Kalke und Mergel dieses Abschnitts lagerten sich unter instabiler Bedingungen ab. Die unterlagernde Biancone Formation (Maiolica Formation) zeigt Unter-Valanginium an, wogegen die tiefste Formation des Rosso Ammonitico auf Ober-Jura bis Berriasium hindeutet.

Die Ammonoideen Fauna besteht aus 27 unterschiedliche Gattungen, von denen jede durch 1-2 Arten vertreten ist. Das Vorkommen vom Puez Gebiet wird von den Phylloceratina (30%) und den Ammonitina (34%) dominiert. *Phyllopachyceras* (17%) und *Phylloceras* (13%) (beide Phylloceratina) sind die häufigsten Komponenten, gefolgt von *Lytoceras* (12%) (Lytoceratina), und *Barremites* (10%) und *Melchiorites* (8%) (beide Ammonitina). Die Cephalopodenfauna setzt sich ausschließlich aus Mediterranen Elementen zusammen.

1. Introduction

Cretaceous pelagic sediments cover wide areas in various European areas (e.g., NCA - Northern Calcareous Alps, Vocontian Trough, Southern Alps/Dolomites, Umbria-Apennines, Western Carpathians, Gerecse and Mecsek Mountains and others).

Lower Cretaceous deposits form a major element of the Southern Alps and especially of the Dolomites (Baccelle and Lucchi-Garavello 1967a, b; Costamoling and Costamoling 1994; Haug, 1887, 1889; Hoernes, 1876; Uhlig, 1887; Rodighiero, 1919; Stöhr, 1993, 1994). The geology of the Dolomites and adjacent areas has been described and summarized in detail by Bosellini (1998),

Bosellini *et al.* (2003), Geyer (1993), Heissel (1982) and Pozzi (1993).

In the Dolomites, Lower Cretaceous cephalopod-bearing deposits are mainly recorded from two different facies, the Biancone Formation (calcareous limestones, = Maiolica Formation) and the overlying Puez Formation (marls-marly limestones).

The Lower Cretaceous relics are situated on the Triassic carbonates of the Dolomites (Hauptdolomit, up to 1000 m thick). At most of the localities where we found Lower Cretaceous sediments in the Dolomites, we also observed a relatively thin red nodular limestone of the Rosso Ammonitico Formation (10–20 m) between the Triassic and Lower Cretaceous. The Triassic-Jurassic succession is overlain by relic areas formed of Lower Cretaceous sediments. This "volcanic-conus"-like formation is especially evident on the Puez-Odle-Gardenaccia plateau (= Gherdenacia). Well known are the Col de la Soné (2633 m) and Muntejela (2666 m). The Piz de Puez (Puez Spitzen, 2846 m) together with the Col Puez (Puezkofel, 2725 m) form the major Lower Cretaceous wall starting at about 2400 m above sea level. Other well-known Lower Cretaceous localities in this area are Piz Boè (Sella Group), the plateaus of the area around Ampezzo (Rote Wand, Fosses, Fanes) and near Cortina d'Ampezzo at Ra Stua (= La Stua) and Antruilles.

The section studied is located in the Southern Alps (Dolomites) of northern Italy. The stratigraphy of the Lower Cretaceous sediments here is based on ammonoids. During the late 19th and early 20th century, a rich fauna of cephalopods was collected from Lower Cretaceous sediments from this area and determined by Haug (1887, 1889), Hoernes (1876), Uhlig (1887) and Rodighiero (1919). After this phase of stagnancy in Lower Cretaceous papers, small scaled ammonoid faunas were described from different localities near the Puez area, e.g. from Ra Stua (La Stua) by Baccelle and Lucchi-Garavello (1967a, b) and Stöhr (1993, 1994). No paper, however, dealt with the fauna from the Puez locality itself. Faraoni *et al.* (1996) reviewed the papers published on Cretaceous ammonoids of the Maiolica Formation from the Venetian Alps (Venetia), which directly adjoin to the south. An additional paper was published the following year by Baudin *et al.* (1997) dealing with a comparable ammonoid fauna (Hauterivian) of the Lessini Mountains and the southern Trento Plateau.

The cephalopod fauna presented herein was collected in marly limestones and marls of the Puez Formation. The main goal is to present a more appropriate and modern stratigraphy of Lower Cretaceous sequences from the Puez area referring to the ammonoid fauna. We update the ammonoid drawings in the scarce and old literature from the Puez area with new and better illustrations (photographs) combined with an improved stratigraphy of the well-preserved ammonoid fauna from this locality.

2. Geographical setting

The ammonoids described herein were collected from huge outcrops located at the southern margin of the Puez Plateau. They are located within the area of the Puez-Odle-Geisler natural park in the northern part of the Dolomites (Trentino – Alto Adige; South Tyrol). The Dolomites (Permian to Cretaceous) are an internal part of the Southern Alps. The exact position is about 30 km northeast of Bolzano (Bozen) (Fig. 1). The locality is accessible from the village Wolkenstein (1560 m) in the Val Gardena (Grödner Tal) by following the Val Lunga (Langental) to its eastern end and then hiking on path 16 up the steep dolomite wall. The outcrops are located near the Rifugia Puez (Puez Hütte, 2475 m). The Lower Cretaceous crops out running between the Col da la Pieres 2747 m) at the west flank and the Col de Puez (2725 m) at the eastern border (Fig. 2).

The grey, green to red succession, comprising the ammonoid-bearing beds, is located on the southern side of the Piz de Puez (2846, 1:25 000, sheet 05 Val Gardena). The section is well exposed on the steep flanks. 2700 m high mountains and steep terrain made sampling very difficult.

3. Geological setting

The Southern Alps are a Northern Italian chain that emerged during the deformation of the passive continental margin of the Adriatic (Bosselini *et al.*, 2002). The geological landscape of the Puez region is dominated by the giant Triassic carbonate plat-

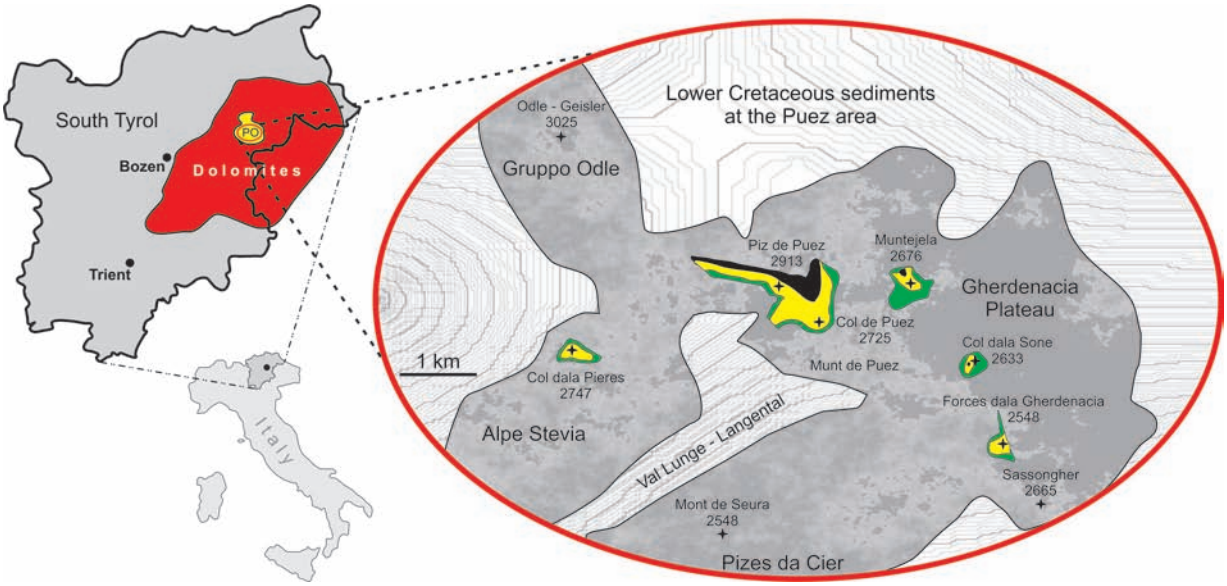

Fig. 1: Map of Italy with included locality map of South Tyrol showing the outcrop of Lower Cretaceous sediments (ellipse: grey shaded - carbonate platforms (plateaus), yellow - Puez Formation; green – Biancone Formation) around the Puez section investigated within the Dolomites. PO Puez-Odle natural park.

forms. The top of these carbonates bears relics of Lower Cretaceous sediments which were formerly much more widespread but have been eroded through time. The Lower Cretaceous sediments here are overthrusted ("Gipfelüberschiebung") by older Triassic Haupdolomit. This phenomenon can only be observed at the Puez-Gardenazza and Sella areas located directly to the south (Heissel, 1982). The thickness of the overthrusting Dolomite differs markedly at different localities (Col Pieres 0 m; Col Puez 120-150 m, Muntejela 0-10 m). Upper Jurassic (Kimmeridgian-Tithonian) to lowermost Cretaceous (Berriasian) Rosso Ammonitico (A.R. Superiore) limestone is overlain by the Lower Cretaceous Biancone Formation and Puez Formation (Valanginian-Aptian). Due to the bad outcrop situation of the lowermost part of the Puez section, Rosso Ammonitico is not observable there, but most probably present (Fig. 3, log idealized).

Biancone is the local name for the more broadly known Italian Maiolica Formation (Faraoni *et al.*, 1996; Wieczorek, 1988). The succession at the Puez area is very similar to the one of La Stua, which also shows Rosso Ammonitico, Biancone, "Ammonitenmergel", grey marls and Aptian marls (Stöhr, 1993). This sequence shows the evolution of the northernmost part of the Trento Plateau at this time. The Trento Plateau reaches from the south (around Trento) up to the Puez region and was formerly sur-

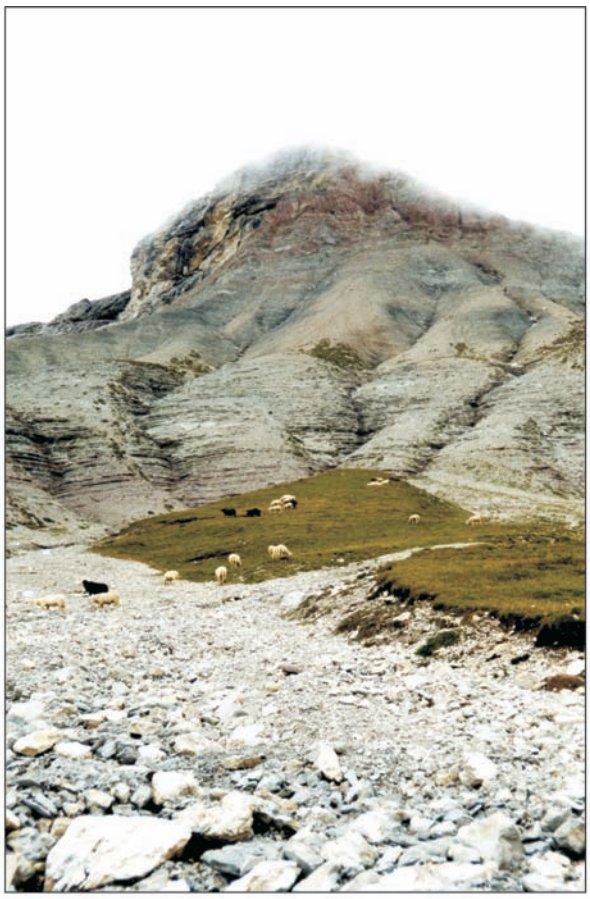

Fig. 2: Exposure of the Puez Formation and outcrop situation around the Piz de Puez and Col de Puez.

rounded by two basins: the Lombardian Basin to the west and the Belluno Basin to the east (Bosselini *et al.*, 1981). The reason for the Upper Jurassic to Lower Cretaceous separation into a basin-plateau-basin succession lies in the rifting history of the Piemonte-Ligurian Tethys Ocean (Penninic Ocean) (Mayer and Appel, 1999).

4. Lithology

The Puez section consists essentially of red to grey calcareous marls and grey, silty marlstones of the Puez Formation (150–200 m) accompanied by "real" green-grey calcareous limestones of the Biancone Formation and red nodular limestones of the Rosso Ammonitico. A very unique feature of the middle section of the Puez Formation is the numerous cherty and calcareous concretions (Fig. 3). They appear in different shapes but pear-shaped forms up to 20 centimetres in height dominate. Here, we refer to the whole sequence of Lower Cretaceous marly limestones and marls as the Puez Formation (Puez marls plus limestones) and not Biancone Formation. The Biancone Formation as traditionally defined (pelagic nannofossil limestone) occurs only at the lowermost part of the section. The outcrops are generally exposed on steep walls up to the Piz de Puez (Puezspitzen) and Col de Puez (Puezkofel). $CaCO_3$ (calcium carbonate contents, equivalents calculated from total inorganic carbon) displays values between 30 and 85 %.

The following microfacies types occur: radiolarian-wackestone (lowermost part), biogenic-rich mudstone and radiolarian wackestone (lower middle part), biogenic-rich radiolarian mudstone and radiolarian wackestone (upper middle part), mudstones (uppermost marly part).

Radiolarians, ostracods, echinoderms, sponge spiculae, brachiopods, and foraminifera are the most prominent constituents of the microfauna.

5. Material and methods

The material (Plates 1-8) originates from the Puez locality (Dolomites). Localities Puez, Col de Puez and Piz de Puez are considered to be the same locality complex. Most of the material was collected by Christian Aspmair for a project on the "Puez marls" for the South Tyrol Museum of Natural Sciences (from 1999-2003), by different collectors (A. Heinrich and others) for the Natural History Museum in Vienna (from 1883-1915) and by Alexander Lukeneder (2003).

Unfortunately, the specimens collected by private collectors or scientists (one hundred years ago) are from rock samples and not from bed by bed sampling. The authors can therefore only summarize the species now in the collections and cannot provide details on which bed the single specimens are from.

Conventions: NHMW Natural History Museum Vienna (Naturhistorisches Museum Wien; 2005 numbers), NMB South Tyrol Museum of Natural Sciences (Natur-Museum Bozen; PZO numbers). All specimens are stored either at the NHMW (n = 201) or in the collections of the NMB (n = 223). All specimens in Plates 1 - 8 were coated with ammonium chloride before photographing. The brachiopod systematics is in accordance with Sulser (1999). The authors follow the basic classification of Cretaceous Ammonoidea by Wright *et al.* (1996). The detailed ammonoid systematics was adopted and correlated with papers of Autran (1993), Avram (1994), Baudin *et al.* (1997), Bogdanova and Hoedaemaeker (2004), Cecca and Pallini (1994), Cecca *et al.* (1998), Company (1987), Company *et al.* (2003), Delanoy (1992, 1994, 1997), Dimitrova (1967), Fülöp (1964), Faraoni *et al.* (1995, 1996), Hoedemaeker (1994), Immel (1979, 1987), Kakabadze and Hoedemaeker (2004), Houša and Vašíček (2004), Klein (2005), Baccele and Lucchi-Garavello (1967a, 1967b), Lukeneder (2003a, b, 2004a, b, c), Reboulet (1995), Stöhr (1993), Thieuloy (1964), Uhlig (1883), Vašíček (2005), Vašíček *et al.* (1994), Vermeulen (2002), and Wippich (2001, 2003). Only papers with photographed specimens were taken into account to ensure correct determination of the ammonoid species.

Ammonoids represent almost the totality of the macrofauna (85%); they are well preserved (mostly in concretions) and appear as steinkerns without shell. Some specimens show suture lines.

During the course of this study, 424 ammonoid specimens, 6 nautiloids,10 lamellaptychi, 6 belemnites, 26 sea urchins (Disasteroida – Collyritidae), 12 bivalves, 21 brachiopods (*Pygope* and *Triangope*) and a huge number of encrusting

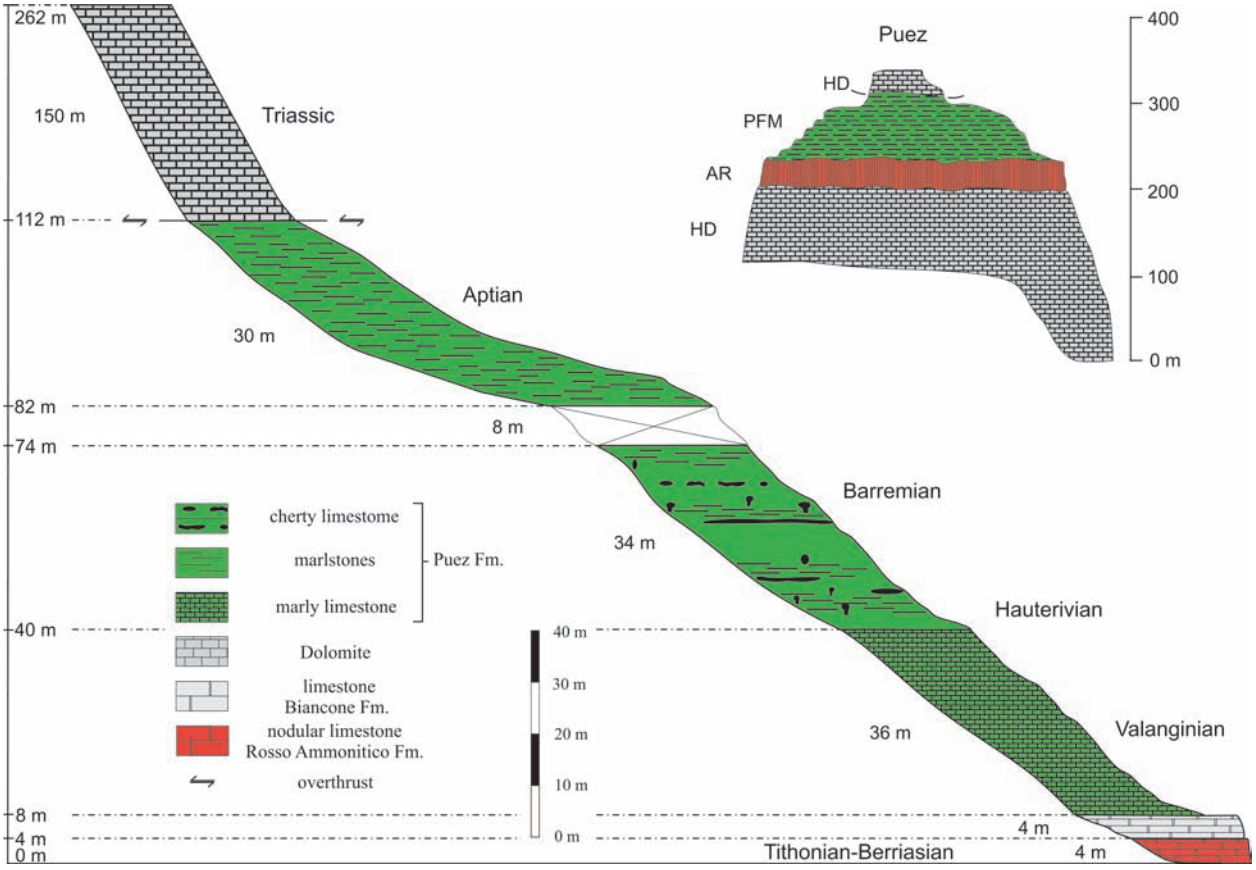

Fig. 3: Log of the Puez section with indicated age and thickness of the different members. In the right upper corner the overthrusting by Triassic Hauptdolomit is indicated. HD Haupdolomit, PFM Puez Formation, AR Ammonitico Rosso. Lower part (Ammonitico Rosso) is idealized because of bad outcrop situation.

species (serpulids and corals, Lukeneder in prep.) were examined.

The very abundant and generally well-preserved Lower Valanginian to Lower Aptian assemblage consists of 27 genera: from phylloceratids *Phylloceras*, *Phyllopachyceras*, from lytoceratids *Lytoceras*, *Eulytoceras*, *Protetragonites*, *Leptotetragonites*; from ammonitids *Neolissoceras*, *Barremites*, *Melchiorites*, *Abrytusites*, *Neocomites*, *Criosarasinella*, *Kilianella*, *Olcostephanus*, *Silesites*, *Jeanthieuloyites*, *Heinzia*, *Discoidellia*, *Acanthodiscus* and from the ancyloceratids *Pseudothurmannia*, *Macroscaphites*, *Dissimilites*, *Acrioceras*, *Crioceratites*, *Anahamulina*, *Hamulina*, *Ancyloceras*.

Calcium carbonate contents ($CaCO_3$) were determined using the carbonate bomb technique. Total carbon content was determined using a LECO WR-12 analyser. All the chemical analyses were carried out in the laboratories of the Department of Geology and the Department of Forest Ecology at the University of Vienna. Thin sections (37) were made to show the microfacies changes in the log.

6. Fauna

The extraordinarily rich invertebrate fauna consists of ammonoids, ammonoid jaws (aptychi), coleoids, bivalves, brachiopods, serpulids, sea urchins, ophiurids, corals, benthic/planktonic foraminifera and radiolarians. The benthic macrofossils observed in the ammonoid beds comprise bivalves, brachiopods and, surprisingly, corals (Lukeneder, in prep.). As far as genera are concerned, abundant and generally well-preserved cephalopods are dominated by *Phyllopachyceras* (17 %) (Fig. 4). The fairly fossiliferous parts of the section show remarkable abundances, contrasting with parts that are almost barren of macrofossils.

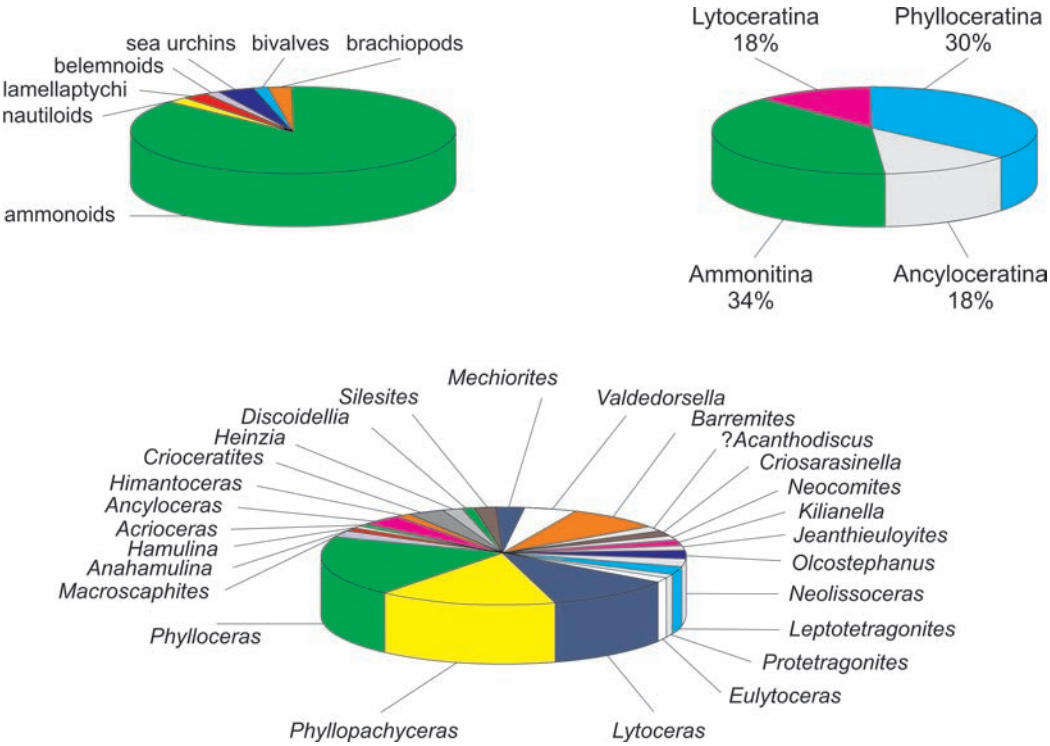

Fig. 4: Ammonoid spectrum from the Puez locality. Note the dominance of the Phyllopachiceratidae.

7. Biostratigraphy

The association indicates that the cephalopod-bearing beds of the Puez Formation comprise Valanginian, Hauterivian, Barremian and Aptian ammonoid assemblages. More specifically, ammonoid zones from the Early Valanginian up to the Early Aptian are represented (Hoedemaeker *et al.*, 2003) (Fig. 5).

Following new (unpublished) results of the IUGS Lower Cretaceous Ammonite Working Group (Kilian Group) from the 7th International Cretaceous Symposium in Neuchatel (2005), *Heinzia sayni* will be erected as the new index fossil for the *H. sayni* Subzone, which is considered to be the lower Subzone of the new *Toxancyloceras vandenheckii* Zone (former *Ancyloceras vandenheckii* Zone) in the lowermost part of the Upper Barremian (Reboulet and Hoedemaeker (reporters) *et al.*, submitted for Cretaceous Research).

The following ammonoids were determined: *Phylloceras thetys* (d'Orbigny), *Phyllopachyceras infundibulum* (d'Orbigny), *Phyllopachyceras winkleri* (Uhlig), *Lytoceras subfimbriatum* (d'Orbigny), *Eulytoceras phestum* (Matheron), *Leptotetragonites* cf. *honnoratianus* (d'Orbigny), *Protetragonites crebrisulcatus* (Uhlig), *Protetragonites quadrisulcatus* (d'Orbigny), *Neolissoceras grasianum* (d'Orbigny), *Olcostephanus densicostatus* (Wegner), *Olcostephanus (Jeannoticeras) jeannoti* (d'Orbigny), *Jeanthieuloyites* cf. *quinquestriatus* (Besairie), *Kilianella* cf. *roubaudiana* (d'Orbigny), *Neocomites* sp., *Criosarasinella furcillata* Thieuloy, *?Acanthodiscus* sp., *Barremites psilotatus* (Uhlig), *Abrytusites neumayri* (Haug), *Melchiorites cassioides* (Uhlig), *Silesites vulpes* (Coquand), *Discoidellia vermeuleni* (Cecca, Faraoni, Marini), *Heinzia sayni* (Hyatt), *Psilotissotia* sp., *Crioceratites nolani* (Kilian), *Crioceratites krenkeli* (Sarkar), *Crioceratites thiollierei* (Astier), *Discoidellia vermeuleni* (Cecca, Faraoni, Marini), *Himantoceras* sp., *Ancyloceras matheronianum* (d'Orbigny), *Ancyloceras* sp., *Acrioceras (Acrioceras) pulcherrimum* (d'Orbigny), *Acrioceras (Dissimilites) dissimilis* (d'Orbigny), *Acrioceras (Dissimilites) trinodosum* (d'Orbigny), *Anahamulina subcincta* (Uhlig), *Hamulina lorioli*

Uhlig, *Macroscaphites nodosostriatum* (Uhlig), and *Macroscaphites yvani* (Puzos) (Fig. 4).

The following index fossils were examined within the collections of the NHMW (Austria) and the NMB (Italy): for the latest Valanginian *Criosarasinella furcillata* (*C. furcillata* Zone and Subzone), for the middle Early Hauterivian *Olcostephanus (Jeannoticeras) jeannoti* (*O. (J.) jeannoti* Subzone) and *Heinzia sayni* for the earliest Late Barremian (*H. sayni* Subzone; Reboulet and Hoedemaeker (reporters) *et al.*, submitted).

Typical Valanginian species are: *Lytoceras subfimbriatum*, *Haploceras grasianum*, *Kilianella* sp., *Neocomites* sp., *Criosarasinella furcillata, Himantoceras* sp., *Jeanthieuloyites* cf. *quinquestriatus*, *Olcostephanus guebhardi*, *Leptotetragonites* cf. *honnoratianus*, *Protetragonites quadrisulcatus, Phylloceras thetys*.

Typical Hauterivian species are: *Phyllopachyceras infundibulum*, *Phyllopachyceras winkleri*, *Lytoceras subfimbriatum*, *Haploceras grasianum*, *Olcostephanus (Jeannoticeras) jeannoti*, *Neocomites* sp., *Discoidellia vermeuleni*, *Crioceratites nolani*, *Crioceratites krenkeli.*

Typical Barremian species are: *Phyllopachyceras infundibulum*, *Eulytoceras phestum, Protetragonites crebrisulcatus*, *Barremites psilotatus*, *Abrytusites*, *Melchiorites cassioides*, *Anahamulina subcincta*, *Hamulina lorioli*, *Heinzia sayni*, *Crioceratites thiollierei*, *Acrioceras (Acrioceras) pulcherrimum*, *Acrioceras (Dissimilites) dissimilis*, *Acrioceras (Dissimilites) trinodosum*, *Macroscaphites yvani*, *Macroscaphites nodosostriatum*.

A typical Lower Aptian species is: *Ancyloceras matheronianum*.

Note that some of the species can pass over two stages but are mostly found in the emphasized stage of the Early Cretaceous.

8. Discussion

Since Uhlig's (1887) and Haug's (1887, 1889) description of Lower Cretaceous ("Neocomian") ammonoid faunas from the Puez locality, we know that the fauna of this area is one of the most important in the whole Alps. The well-preserved fauna is, compared to other Lower Cretaceous out-

Stages		Zones	Subzones
APTIAN	Lower	*D. furcata*	
		D. deshayesi	
		D. weissi	
		D. oglanlensis	
BARREMIAN	Upper	*P. waagenoides*	
		C. sarasini	
		I. giraudi	
		H. feraudianus	
		G. sartousiana	*C. provincialis*
			C. sartousiana
		A. vandenheckii	
	Lower	*C. darsi*	
		K. compressissima	
		N. pulchella	
		K. nicklesi	
		T.hugii auct.	
HAUTERIVIAN	Upper	*P. angulicostata* auctorum	*P. catulloi*
			P. angulicostata auct.
		B. balearis	
		P. ligatus	
		S. sayni	
	Lower	*L. nodosoplicatum*	
		C. loryi	*O. (J.) jeannoti*
			C. loryi
		A. radiatus	
VALANGINIAN	Upper	*T. callidiscus*	
		H. trinodosum	*C. furcillata*
			O. (O.) nicklesi
		S. verrucosum	*V. peregrinus*
			K. pronecostatum
			S. verrucosum
	Lower	*B. campylotoxus*	
		T. pertransiens	
		T. otopeta	
BERRIASIAN	Upper	*F. boissieri*	*T. alpillensis*
			B. picteti
			M. paramimounum
	Middle	*T. occitanica*	*D. dalmasi*
			B. privasensis
			T. subalpina
	Lower	*B. jacobi*	

Fig. 5: The stratigraphic position of the Puez-fauna (in grey) of the Puez Group within the Lower Cretaceous biostratigraphic scale (Early Valanginian to Early Aptian). Table after Hoedemaeker *et al.* (2003).

crops, extremely rich in species and numbers. 61 species were summarized by Haug (1889). The authors recently observed 30 species in the collections of the Natural History Museum (Vienna) and the South Tyrol Museum of Natural Sciences (Bozen). Most of the herein reported species have been observed in the older literature.

The ammonoid assemblage is very similar to ammonoid faunas of the Northern Calcareous Alps (Lukeneder, 2004c). This mainly reflects the palaeogeographic position of the Southern Alps in Lower Cretaceous time. The Southern Alps were located near to the south of the Northern Calcareous Alps (see Cecca, 1998; Lukeneder, 2004a; Vašíček *et al.*, 1994) (Fig. 6). During the Early Cretaceous the Mediterranean palaeogeographic domain was characterized by the presence of microplates located in the middle of the Tethyan oceanic corridor between the African and European landmasses (Stampfli *et al.*, 2002).

The region (Southern Alps) in which the investigated area was situated during the Early Cretaceous was formed on the Apulian block (Dercouret *et al.*, 1979) to the south-east of the Alpine-Carpathian Block, which was located at the western margin of the Tethys (Cecca, 1997, 1998; Vašíček and Michalík, 1999; Stampfli and Mosar, 1999; Zharkov *et al.*, 1998) (Fig 4). The fact that most depositional areas of the Mediterranean had some form of contact led to similar distribution patterns of Lower Cretaceous ammonoids. This explains the clear similarities in the respective regions and countries of Europe.

Large similarities in the faunal assemblage can also be observed with faunas from the Early Cretaceous of Hungary. As reported by Fülöp (1964), in the Bakony mountains *Olcostephanus* and *Holcodiscus* are missing. *Holcodiscus* is missing in the fauna of the Puez locality and *Olcostephanus* is only represented by a single specimen. *Holcodiscus* and *Olcostephanus* are also very common in the Northern Calcareous Alps.

Bochianites is totally absent at the Puez locality, but common in Lower Cretaceous sediments of various regions like the Northern Calcareous Alps (Lukeneder, 2003b) and Western Carpathians (Vašíček *et al.*, 1994). Note also that extensive accordances exist between the whole cephalopod fauna from the Puez and reported faunas from comparable sediments from the Northern Calcareous Alps (Lukeneder, 2003b), the Vocontian Trough (Bulot and Thieuloy, 1994), the Swiss Alps (Ooster, 1861), the Betic Cordillera (Hoedemaeker, 1994; Company *et al.* 1994), the Southern Carpathians (Avram, 1994) and the Western Carpathians (Vašíček, 1994; Vašíček *et al.*, 1994).

It is still unclear why certain ammonoid species are present in the Northern Calcareous Alps but absent in the Southern Alps (situated to the south at the Early Cretaceous). One explanation is current and drifting features combined with depth parameters. Some authors (Cecca, 1998; Reboulet, 1995) also suggested that reproductive strategies (r- or K-strategy) could have had some effect on the distribution of different ammonoid species from the Valanginian to the Barremian. An opportunistic behaviour of the eurytopic genus *Bochianites* was proposed by (Cecca, 1998). Cecca (1998) correlated the distribution of Valanginian and Barremian ammonoid species with their suggested living mode, related to their facies and combined with the faunal spectra.

Cecca (1998) reported no Boreal elements from various Italian localities of the Trento Plateau and the Umbria-Marche region in the Valanginian and Barremian stage. Hence it is not surprising that no Boreal ammonoids were observed at the Puez locality.

Most recently, Kakabadze *et al.* (2004) introduced a very valuable source for ideas on Early Cretaceous biogeography (Barremian-Albian) based on ammonoids. The latter authors explained the distribution of different ammonoid genera and the history of provincialism from the Barremian to Albian starting from the Colombian ammonoid fauna, correlating it with faunas from around the world.

Unsurprisingly, the biggest accordance in ammonoid assemblage exists with described faunaspectra from the La Stua locality (Belluno). La Stua is located approximately 10 kilometres to the east of the Puez area in the "Dolomites d'Ampezzo" (Stöhr, 1993). Both localities are assigned to the northern Trento Plateau. Small ammonoid faunas from the same locality were also reported by Baccele and Lucchi-Garavello (1967a, 1967b) and Stöhr (1994). The cephalopod faunas reported by the latter authors confirm the affinity of both faunas. The fauna (43 species) investigated by Stöhr (1993) also comprises cephalopods from Lower

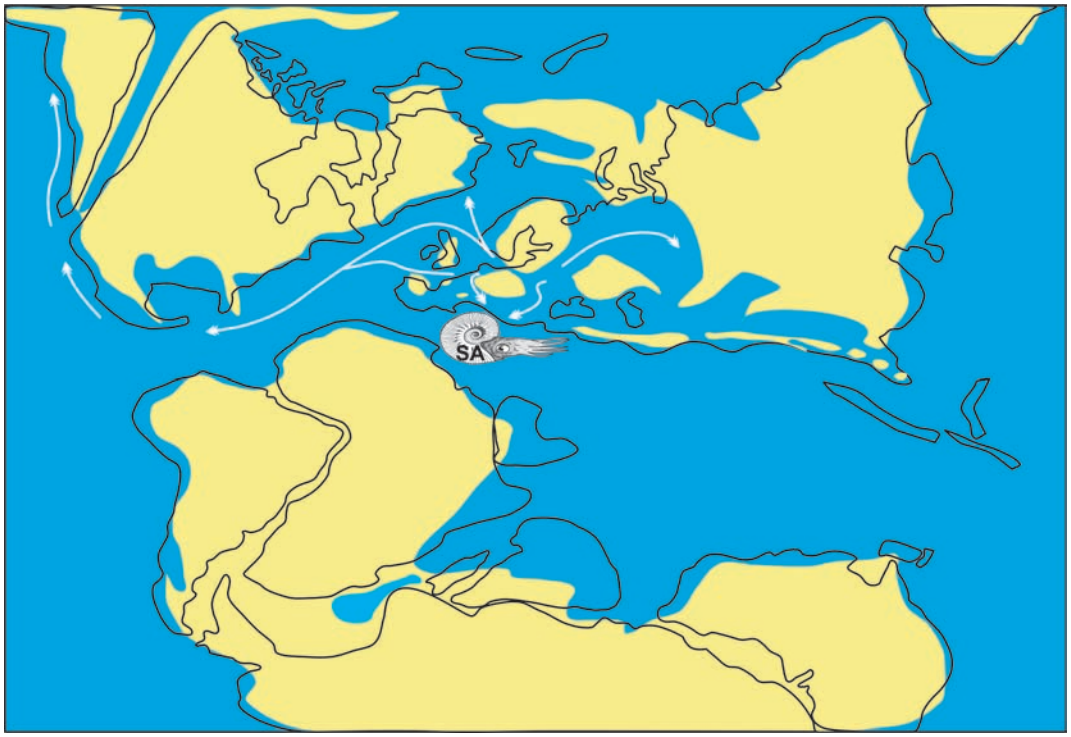

Fig. 6: Lower Cretaceous palaeogeography with indicated ammonoid migration-routes modified after Caracuel *et al.* (1998), Kiessling *et al.* (2003), Kotetichvili (1988), Lukeneder (2004), Scotese (2001), Wiedmann (1988) and Zharkov *et al.* (1998) with indicated position of the Southern Alps (marked by ammonoid).

Cretaceous sediments (Valanginian to Early Aptian, 191 m thick). He summarized the similarities between the fauna from La Stua and other localities of the West-Tethyan Realm, but noted the major similarities of faunas from the western Dolomites (Puez) with assemblages from the eastern Dolomites (La Stua). Most similarities can be observed in the abundance of Phylloceratidae and Desmoceratidae in both regions.

Stöhr (1993) proposed a migration route for the northern marginal faunas of the southern border of the European Plate (e.g., SE France - Vocontian Trough, Spain, Switzerland) down to the Southern Alps directly over the Carpathians. The latter author failed to mention that a huge area – the Northern Calcareous Alps – was situated between the Carpathians and the terrain of the Dolomites (Southern Alps). The migration had to pass the NCA before reaching the more southern Dolomites (Fig. 6). Stöhr (1993) missed Immel's (1987) paper on Lower Cretaceous ammonoid faunas from the NCA.

As noted by Uhlig (1887) and Haug (1887, 1889), the ammonoid fauna from the Puez area is of Valanginian to Aptian age. The latter authors also recognized that no Berriasian element (concerning the ammonoid fauna) could be detected. The present paper supports this conclusion, although the ammonoid zonation and most of the generic names of ammonoids have been changed and therefore the parameters are quite different today. The frequency of the ammonoids and the richness of the fauna have allowed the recognition of several Valanginian, Hauterivian, Barremian and Aptian ammonoid zones or at least time intervals which can be correlated with the Mediterranean standard zonation by Hoedemaeker *et al.* (2003).

A noticeable feature of the middle section (Hauterivian) of the Puez Formation is the numerous cherty and calcareous concretions. Most of these concretions bear ammonoids of all morphologies and sizes. This phenomenon was for example also reported by Fülöp (1964) for the Bakony mountains (Hungary) and by Lukeneder (2004c) for the Hauterivian limestones of the Northern Calcareous Alps (Austria). It is therefore apparently possible to correlate Hauterivian radiolarian-rich (cherty) sediments comprising chert-nodules, -layers and -concretions over wider distances or even countries.

9. Conclusions and perspectives

The macrofauna is represented especially by ammonoids, ammonoid jaws (aptychi), nautiloids, belemnoids, sea urchins, brachiopods and bivalves. The latter assemblage shows typical affinities to other Lower Cretaceous fossil communities in Europe (e.g., Northern Calcareous Alps, Carpathian mountains, Bakony mountains). The whole section yielded about 424 ammonoids. Good preservation within calcareous and cherty concretions (radiolarians) of the ammonoids allow precise determinations.

Some ammonoid zones defined by Hoedemaeker *et al.* (2003) can be recognized. The following index fossils were examined within the collections of the NHMW (Austria) and the NMB (Italy): for the latest Valanginian *Criosarasinella furcillata* (*C. furcillata* Zone and Subzone), for the middle Early Hauterivian *Olcostephanus (Jeannoticeras) jeannoti* (*O.(J.) jeannoti* Subzone) and *Heinzia sayni* for the earliest Late Barremian (*H. sayni* Subzone; Reboulet and Hoedemaeker (reporters) *et al*., submitted).

The frequency of the ammonoids and the richness of the fauna make this section especially suited to accurately study the vertical ammonoid distribution. The main focus in the future will be to investigate in detail the stratigraphic framework of the Puez section. Bed-by-bed collecting is required to obtain crucial data on the ammonoid distribution and occurrence (range). A cooperative project with this aim is being planned by the South Tyrol Museum of Natural Sciences Bozen and the Natural History Museum Vienna.

A further study on the the palaeoecology and synecology of the cephalopod fauna of the Puez section is currently under preparation by Lukeneder. It focuses on the autecological features exhibited by different fossil groups (annelids, bryozoans, foraminifera, corals) on ammonoid shells, which act as cryptic habitats for different encrusters in the Lower Cretaceous biota of the Puez locality.

Hauterivian limestone intervals from the Puez area, containing cherty ammonoid bearing concretions, can be correlated with similar occurrences of different other areas of Europe as for example the Northern Calcareous Alps in Austria or the Bakony mountains of Hungary. This requires further attention and will be the focus of future work.

10. Results

The ammonoid fauna (27 genera) at the Puez section is dominated by *Phyllopachyceras* (17%) and *Phylloceras* (13%) from the Phylloceratina and *Barremites* (10%) and *Melchiorites* (8%) from the Ammonitina. The ammonoid families Phylloceatidae and Desmoceratidae are dominating the cephalopod-fauna.

The stratigraphic investigation of the cephalopods revealed that the Puez section (Pizes de Puez, Col de Puez, Puez) comprises Lower Valanginian to Aptian sediments.

The ammonoid fauna from the Puez locality contains only descendants of the Mediterranean Province (Tethyan Realm). Most affinities of the cephalopod fauna are observed with faunas from the adjacent areas of Italy (Lessini Mountains, Belluno, southern Trento Plateau), the Northern Calcareous Alps (Austria) and the Bakony, Gerecse and Mecsek Mountains of Hungary. This is explained by the neighbouring position of the latter areas during the Early Cretaceous on the Apulian/Adria block and the Alpine-Carpathian microplate.

11 ammonoid families were recorded by the following species: **Phylloceratidae**: *Phylloceras thetys*, *Phyllopachyceras infundibulum*, *Phyllopachyceras winkleri*; **Lytoceratidae**: *Lytoceras* subfimbriatum, *Eulytoceras phestum, Leptotetragonites* cf. *honnoratianus*, *Leptotetragonites crebrisulcatus*, *Protetragonites quadrisulcatus*; **Haploceratidae**: *Haploceras grasianum*; **Olcostephanidae**: *Olcostephanus guebhardi*, *Jeanthieuloyites* sp.; **Neocomitidae**: *Kilianella* cf. *roubaudiana*, *Neocomites* sp., *Criosarasinella furcillata*, *?Acanthodiscus* sp.; **Desmoceratidae**: *Barremites psilotatus*, *Abrytusites neumayri*, *Melchiorites cassioides*; **Silesitidae**: *Silesites vulpes*; **Pulchelliidae**: *Heinzia sayni, Discoidellia vermeuleni*; **Ancyloceratidae**: *Crioceratites nolani*, *Crioceratites krenkeli*, *Crioceratites thiollierei*, *Himantoceras sp.*, *Pseudothurmannia*, *Ancyloceras matheronianum*, *Ancyloceras* sp. *Acrioceras (Dissimilites) dissimilis*, *Acrioceras (Acrioceras) pulcherrimum*; **Hamulinidae**: *Hamulina lorioli*, *Anahamulina subcincta*; **Macro-**

scaphitidae*: Macroscaphites yvani*, *Macroscaphites nodosostriatum*.

Acknowledgements

Thanks are due to the Austrian Science Fund (FWF) for financial support (project P16100-N06). I am particularly grateful to Miguel Company (Granada) for important discussions on some of the ammonoid specimens. Special thanks go to Jörg Mutterlose (Bochum) and Jozef Michalík (Bratislava) for their thoughtful and valuable comments on this paper. Many thanks go to Evelyn Kustatscher (Bozen) for providing access to the collection of the South Tyrol Museum of Natural Sciences. Sea urchins were determined by Andreas Kroh (Vienna). Photographs were taken by Alice Schumacher (NHMW).

References

Avram, E. (1994): Lower Cretaceous (Valanginian – Early Aptian) ammonite succession in the Svinita region (SW Romania). In: Bulot L.G., Argot M., Arnaud H. (eds.): Lower Cretaceous Cephalopod biostratigraphy of the Western Tethys. – Géol. Alp., Mém. H.S., 20: 113–167.

Autran, G. (1993): L'evolution de la marge nord-est provencale (Arc de Castellane) du Valanginien moyen à l'Hauterivien à travers l'analyse biostratigraphique des séries de la région de Peyroules: Séries condensées, discontunuites et indices d'une tectogenese distensive. – Ann. Mus. Hist. Nat. Nice, 10: 239 p.

Baccelle, L., Lucchi Garavello, A. (1967a): Prima segnalazione di Ammoniti Aptiane e Albiane nelle Dolomiti. – Ann. Univ. Ferrara, 4/7: 91–101.

Baccelle, L., Lucchi Garavello, A. (1967b): Ammonite dei livelli cretacici di La Stua (Cortina d' Ampezzo). – Ann. Univ. Ferrara, 4/9: 117–166.

Baudin, F., Faraoni, F., Marini, A., Pallini, G. (1997): Organic matter characterization of the "Faraoni level" from Northern Italy (Lessini Mountains and Trento Plateau): comparison with that from Umbria-Marche Apennines. – Palaeopelagos, 7: 41-51.

Bogdanova, T.N., Hoedemaeker, Ph.J. (2004): Barremian-Early Albian Deshayesitidae, Oppeliidae, Desmoceratidae and Silesitidae of Colombia. – Scripta Geol., 128: 183-312.

Bosellini, A. (1998): Die Geologie der Dolomiten. 192 pp. Verlagsanstalt Athesia, Bozen/Bolzano.

Bosellini, A., Masetti, D., Sarti, M. (1981): A Jurassic "Tongue of the Ocean" infilled witth oolitic sands: The Belluno Trough, Venetian, Alps, Italy: Marine Geol., 44: 59-95.

Bosellini, A., Gianolla, P. and Stefani, M. 2003. Geology of the Dolomites. – Episodes 26/3: 181-185.

Bulot, L.G., Thieuloy, J.-P. (1994): The Valanginian biohorizon succession of Se France: a key tool for heigh resolution correlations in the Western Tethys. In: Bulot L.G., Argot M., Arnaud H. (eds.): Lower Cretaceous Cephalopod biostratigraphy of the Western Tethys. – Géol. Alp., Mém. H.S., 20: 15-41.

Caracuel, J., Oloriz, F., Sarti, C. (1998): Updated biostratigraphy of the Kimmeridgian and Lower Tithonian at Lavaraone (Trento Plateau). Correlation for epioceanic western Tethys. – Geol. et Palaeont., 32: 235-251.

Cecca, F. (1998): Early Cretaceous (pre-Aptian) ammonites of the Mediterranean Tethys: palaeoecology and palaeobiography. Palaeogeogr. Palaeoclim. Palaeoecol., 138: 305-323.

Cecca, F., Pallini, G. (1994): Latest Hauterivian – Barremian Ammonite biostratigraphy in the Umbria – Marche Apennines (Central Italy). In: Bulot L.G., Argot M. & Arnaud H. (eds.): Lower Cretaceous Cephalopod biostratigraphy of the Western Tethys. – Géol. Alp., Mém. H.S., 20: 205-217.

Cecca, F., Faraoni, P., Marini, A. (1998): Latest Hauterivian (Early Cretaceous) ammonites from Umbria-Marche Apennines (Central Italy). – Palaeo. Italica, 85, 61-110.

Company, M. (1987): Los Ammonites del Valanginiense del sector oriental de las Cordilleras Béticas (SE de España). Departemento de Estratigrafía y Paleontología, Universidad de Granada. Tesis doctoral). 294 p.

Company, M., Hoedemaeker, Ph.J. Sandoval, .J., Tavera J.M. (1994): Lower Cretaceous of the Subbetic and Prebetic ranges (Mula, SE Spain). In Bulot L.G., Argot M., Arnaud H. (eds.): Lower Cretaceous Cephalopod biostratigraphy of the Western Tethys. – Géol. Alp., Mém. H.S., 20: 401-420.

Company, M., Sandoval, J., Tavera J.M. (2003): Ammonite biostratigraphy of the uppermost Hauterivian in the Betic Cordillere (SE Spain). – Geobios, 36: 685-694.

Costamoling, H., Costamoling W. (1994): Fossilien des Gardertales. 111 pp., Verlagsanstalt Athesia Ges. m.b.H., Bozen/Bolzano.

Delanoy, G. (1992): Les Ammonites du Barremien supérieur de Saint-Laurent de l'Escarène. – Ann. Mus. Hist. Nat. Nice, 9: 148 p.

Delanoy, G. (1994): Les zones à Feraudianus, Giraudi et Sarasini du Barrémian supérieur de la région strato-

typique d'Angles-Berrême-Castellane (Sud-Est de la France). In: Bulot L.G., Argot M., Arnaud H. (eds.): Lower Cretaceous Cephalopod biostratigraphy of the Western Tethys. – Géol. Alp., Mém. H.S., 20: 279-319.

Delanoy, G. (1997): Biostratigaphie des faunas d'Ammonites à la limite Barrémien-Aptien dans la région d'Angles-Barrême-Castellane. Etude particulière de la famille des Heteroceratina Spath, 1922 (Ancyloceratina, Ammonoidea). – Ann. Mus. Hist. Nat. Nice, 12: 270 p.

Dercouret, J., Zonensheim, L.P., Ricou, L.E., Katmin, V.G., Le Pichon, X., Knipper, A.M., Grandjacquet, C., Sborshchikov, I.M., Boulin, J., Sorokhtin, O., Geyssant, J., Lepvrier, C., Biju Duval, B., Sibuet, J.C., Savostin, L.A., Westphal, M., Lauer, J.P. (1985): Présentation de 9 cartes paléogeographiques au 1/20,000.000e s'étendant de l'Atlantique au Pamir pour la période du Lias à l'actuel. – Bull. Soc. Géol. Fr., 8 Vol. 1 (5), 635-652.

Dimitrova, N. (1967): Les fossiles de Bulgarie IV. Crétacé inférieur - Cephalopoda (Ammonoidea and Nautiloidea). – Sofia, Academie Bulgare des Sciences. 424 p.

Faraoni, P., Marini, A., Pallini, G. (1995): The Hauterivian ammonite succession in the central Apennines, Maiolica formation (Petrano Mt., Cagli -PS) Preliminary results. – Palaeopelagos, 5: 227-236.

Faraoni, P., Marini, A., Pallini, G., Pezzoni, N. (1996): The Maiolica Fm. of the Lessini Mts and central Apennines (North eastern and Central Italy): a correlation based on new bio-lithostratigraphical data from the uppermost Hauterivian. – Palaeopelagos, 6: 249-259.

Faraoni, P., Flore, D., Marini, A., Pallini, G., Pezzoni, N. (1997): Valanginian and early Hauterivian ammonite successions in the Mt Catria group (Central Apennines) and in the Lessini Mts (Southern Alsp), Italy. – Palaeopelagos 7, 59-100.

Fülöp, J. (1964): Unterkreide-Bildungen (Berrias - Apt) des Bakony-Gebirges. – Geol. Hung., Ser. Geol., 13: 1-194.

Geyer, O.F. 1993. Die Südalpen zwischen Friaul und Gardasee. – Sammlung Geologischer Führer, 86: 576 p. Bornträger, Berlin-Stuttgart.

Haug, E. (1887): Die geologischen Verhältnisse der Neocomablagerungen der Puezalpe bei Corvara in Südtirol. – Jb. K. -K. Geol. R. -A., 37/2: 245-280.

Haug, E. (1889): Beitrag zur Kenntniss der oberneocomen Ammonitenfauna der Puezalpe bei Corvara (Südtirol). – Beitr. Paläont. Geol. Österr. -Ung., 7/3:193-229.

Heissel, W. (1982): Südtiroler Dolomiten. Sammlung Geologischer Führer, 71, 172 pp, Gebrüder Borntraeger, Berlin-Stuttgart.

Hoedemaeker, P.J. (1994): Ammonite distribution around the Hauterivian – Barremian boundary along the Río Argos (Caravaca, SE Spain). In: Bulot L.G., Argot M., Arnaud H. (eds.): Lower Cretaceous Cephalopod biostratigraphy of the Western Tethys. – Géol. Alp., Mém. H.S., 20: 219-277.

Hoedemaeker, P.J., Reboulet, St., Aguirre-Urreta, M., Alsen, P., Aoutem, M. Atrops, F., Barrangua R., Company, M., Gonzales, C., Klein, J., Lukeneder, A., Ploch, I., Raisossadat, N., Rawson, P., Ropolo, P., Vašíček, Z., Vermeulen, J., Wippich, M. (2003): Report on the 1st International Workshop of the IUGS Lower Cretaceous Ammonite Working Group, the 'Kilian Group' (Lyon, 11 September 2002). – Cret. Research, 24: 89-94.

Hoernes, R. (1876): Neocomfundorte in der Gegend von Ampezzo und Enneberg in Südtirol. – Verh. K. -K. Geol. B. -A., 7: 140-141.

Houša, V., Vašíček, Z. (2004): Ammonoidea of Lower Cretaceous deposits (Late Berriasian, Valanginian, early Hauterivian) from ?tramberk, Czech Republic. – Geolines 18: 7-57.

Immel, H. (1987): Die Kreideammoniten der Nördlichen Kalkalpen. – Zitteliana 15: 3-163.

Immel, H., (1979): Die Crioceratiten (Ancyloceratina, Ammonoidea) des mediterranen und borealen Hauterive-Barreme (Unterkreide). – Palaeontographica A, 163: 1-85.

Kakabadze, M.V., Hoedemaeker, P.J. (2004): Heteromorphic ammonites from the Barremian and Aptian strata of Colombia. – Scripta Geologica, 128: 39-182.

Kakabadze, M.V., Hoedaemaeker Ph.J, Bogdanova, T.N., Sharikadze M.Z. (2004): On the Barremian-Early Albian biogeography (by ammonites) of Colombia. – Scripta Geologica, 128: 183-312.

Kiessling, W., Flügel, E., Golonka, J. (2003): Patterns of Phanerozoic carbonate platform sedimentation. – Lethaia, 36: 195-226.

Klein, J. (2005). Lower Cretaceous Ammonites I. Perisphinctaceae 1. In: Riegraf, W. (ed.): Fossilium Catalogus I: Animalia. 139, 484 pp. Backhuys, Leiden.

Kotetichvili, E.V., (1988): Distribution globale des Ammonites éocrétacés du Caucase. In: Wiedmann J., Kullman J. (eds): Cephalopods – Present and Past, pp. 453-468.

Lukeneder, A. (2003a): Ammonoid stratigraphy of Lower Cretaceous successions within the Vienna Woods (Kaltenleutgeben section, Lunz Nappe, Northern Calcareous Alps, Lower Austria). In: W.E. Piller (Ed.): Stratigraphia Austriaca. Österr. Akad. Wiss., Schrift. Erdwiss. Komm., 16: 165-191.

Lukeneder, A. (2003b): Ammonoid stratigraphy of Lower Cretaceous successions within the Vienna Woods (Kaltenleutgeben section, Lunz Nappe, Northern Calcareous Alps, Lower Austria). In: Piller W.E. (Ed.): Stratigraphia Austriaca. Österr. Akad. Wiss., Schrift. Erdwiss. Komm., 16: 165-191.

Lukeneder, A. (2004a): Late Valanginian ammonoids: Mediterranean and Boreal elements - implications on sea-level controlled migration (Ebenforst Syncline; Northern Calcareous Alps; Upper Austria). – Austrian J. Earth Sci., 95/96, 46-59.

Lukeneder, A. (2004b): A Barremian ammonoid association from the Schneeberg Syncline (Early Cretaceus, Northern Calcareous Alps, Upper Austria). Ann. Naturhist. Mus. Wien, 106A: 213-225.

Lukeneder, A. (2004c) Stratigrafische Erkenntnisse aus einem neuen Vorkommmen von Unterkreide-Ammonoideen in der Losensteiner Mulde (Ternberger Decke, Nördliche Kalkalpen). – Jb. Geol. B. -A., 144/2: 173-189.

Mayer, H., Appel, E. (1999) Milankovitch cyclicity and rock-magnetic signatures of palaeoclimatic change in the Early Cretaceous Biancone Formation of the Southern Alps, Italy. – Cret. Research, 20: 189-214.

Ooster, W.A. (1860): Catalogue des Céphalopodes fossiles des Alpes Suisses avec la description et les figures des espéces remarquables. Part 4: Céphalopodes Tentaculifères, Ammonitides. – Nouv. Mém. Soc. Helv. Sci, Nat., 18: 152 p, pls. 13-27, Zürich.

Pozzi, E. (1993): Die Fossilien der Dolomiten. 176 pp. Tappeiner Verlag, Lana.

Reboulet, S. (1995): L'evolution des ammonites du Valanginien-Hauterinien inférieur du bassin Vocontien et de la plate-forme provencale (sud-est de la France): Relations avec la stratigraphie séquentielle et implications biostratigraphiques. – Doc. Lab. Géol. Fac. Sci. Lyon, 137: 1-371.

Rodighiero, A. (1919): Il sistema Cretaceo del Veneto Occidentale compreso fra l'Adige e il Piave con speziale reguardo al Neocomiano die Sette Comuni. – Palaeontogr. Ital., 25: 39-125.

Scotese, C.R. (2001): Atlas of Earth History. Paleomap project, Arlington, 52 pp., Texas.

Stampfli, G., Mosar, J. (1999): The making and becoming of Apulia. – Mem. Scié. Géol. (University of Padova). Special volume, 3rd Workshop on Alpine Geology 51/1, Padova.

Stampfli, G.M., Borel, G.D., Marchant, R, Mosar J. (2002): Western Alps geological constraints on western Tethyan reconstructions. In: Rosenbaum, G. and Lister, G.S. 2002. Reconstruction of the evolution of the Alpine-Himalayan Orogen. – J. Virt. Expl., 8: 77-106.

Stöhr. D. (1993): Die Ammoniten der Kreide von La Stua (Dolomiten, Norditalien). – Unveröffentlichte Dissertation, Universität Giessen, 1-173, 4 plates, & tables, 6 figures.

Stöhr. D. (1994): Ammonoidea aus Schwarzschiefern von La Stua (Norditalien, Provinz Belluno). – Giess. Geol. Schrift., 51: 291-311.

Sulser, H. (1999): Die fossilen Brachiopoden der Schweiz und der angrenzenden Gebiete. Juragebirge und Alpen. 315 p. H. Tschudy & Co AG., St. Gallen.

Thieuloy, J.P. (1964): Un Céphalopode remarquable de l'Hauterivien basal da la Dr?me: *Himantoceras* nov. gen., Bull. Soc. Géol. Fr., 6: 205-213.

Uhlig, V. (1883): Die Cephalopodenfauna der Wernsdorfer Schichten. – Denkschr. Akad. Wiss., math. -nat. Kl., 46: 127-290.

Uhlig, V. (1887): Ueber neocome Fossilien von Gardenazza in Südtirol nebst einem Anhang über das Neocom von Ischl. – Jb. Geol. R. -A., 37/1: 69-108.

Uhlig, V. (1902): Über die Cephalopodenfauna der Teschener und Grodischter Schichten. – Denkschr. Akad. Wiss., math. -nat. Kl., 72: 1-88.

Vašíček, Z. (1994): Lower Cretaceous ammonite biostratigraphy in the Western Carpathians (The Czech and Slovak Republics). In: Bulot L.G., Argot M., Arnaud H. (eds.): Lower Cretaceous Cephalopod biostratigraphy of the Western Tethys. – Géol. Alp., Mém. H.S., 20: 169-189.

Vašíček, Z. (2005): The oldest (Late Valanginian) Crioceratinae (heteromorphic ammonoids) from the central Western Carpathians (Slovakia). – Geol. Carpath., 56: 245-254.

Vašíček, Z., Michalík, J. (1999): Early Cretaceous ammonoid paleobiogeography of the west Carpathian part of the Paleoeuropean shelf margin. – N. Jb. Geol. Paläont., Abh., 212: 241-262.

Vašíček, Z., Michalík, J., Reháková, D. (1994): Early Cretaceous stratigraphy, palaeogeography and life in Western Carpathians. – Beringeria, 10: 3-169.

Vermeulen, J. (2002): Etude stratigraphique et paléontologique de la famille des Pulchelliidae (Ammonoidea, Ammonitina, Endemoceratacеae). – Géol. Alp., Mém. H.S., 42: 333p.

Wieczorek, J. (1988): Maiolica – a unique facies of the western Tethys. – Ann. Soc. Geol. Pol., 58: 255-276.

Wiedmann, J. (1988): Plate tectonics, sea level changes, climate - and the relationship to ammonite evolution, provincialism, and mode of life. In: Wiedmann J.,

Kullmann J. (eds): Cephalopods – Present and past, pp. 735-765.

Wippich, M.G.E. (2001): Die tiefe Unter-Kreide (Berrias bis Unter-Hauterive) im Südwestmarokkaniscen Becken: Ammonitenfauna, Bio- und Sequenzstratigraphie. – PhD Thesis, Ruhr-University of Bochum, Bochum, 142 pp.

Wippich, M.G.E. (2003): Valanginian (Early Cretaceous) ammonite faunas from the western High Atlas, Morocco, and the recognition of western Mediterranean 'standard' zones. – Cret. Research, 24: 257-374.

Wright C.W., Calloman J.H., Howarth M.K. (1996): Treatise on invertebrate paleontology, Part L, Mollusca 4 revised (Cretaceous Ammonoidea), Geological Society of America, Boulder and University of Kansas Press, Lawrence, 362 pp.

Zharkov, M.A., Murdmaa, I.O. and Filatova, N.I. (1998): Peleogeography of the Berriasian-Barremian Ages of the Early Cretaceous. – Stratigr. Geol. Correl., 6: 47-69.

Plate 1

Fig. 1: *Protetragonites crebrisulcatus* (Uhlig), Puez section, x 1, 2005z0245/0053
Fig. 2: *Protetragonites quadrisulcatus* (d'Orbigny), Puez section, x 1, 2005z0245/0054
Fig. 3: *Protetragonites crebrisulcatus* (Uhlig), Puez section, x 1, 2005z0245/0055
Fig. 4: *Leptotetragonites honnoratianus* (d'Orbigny), Puez section, x 1, 2005z0245/0030
Fig. 5: *Lytoceras subfimbriatum var. B* (d'Orbigny), Puez section, x 0.5, 2005z0245/0044
Fig. 6: *Lytoceras subfimbriatum var. A* (d'Orbigny), Puez section, x 1, 2005z0245/0040
Fig. 7: *Eulytoceras phestum* (Matheron), Puez section, x 1, 2005z0245/0042
Fig. 8: *Phylloceras thetys* (d'Orbigny), Puez section, x 1, 2005z0245/0014
Fig. 9: *Phyllopachyceras winkleri* (Uhlig), Puez section, x 1, 2005z0245/00038


1
2
3
5
4
6
7
8
9

Plate 2

Fig. 1: *Phyllopachyceras infundibulum* (d'Orbigny), Puez section, x 1, 2005z0245/0015
Fig. 2: *Phyllopachyceras infundibulum* (d'Orbigny), Puez section, x 1, 2005z0245/0016
Fig. 3: *Neolissoceras grasianum* (d'Orbigny), Puez section, x 1, 2005z0245/002
Fig. 4: *Neocomites* sp., Puez section, x 1, 2005z0245/0010
Fig. 5: *Olcostephanus densicostatus* (Wegner), Puez section, x 1, 2005z0245/0039
Fig. 6: *Olcostephanus jeannoti* (d'Orbigny), Puez section, x 1, 1884/0026/0570
Fig. 7: Neocomites sp., Puez section, x 1, 2005z0245/0021
Fig. 8: *Kilianella* aff. *roubaudiana* (d'Orbigny), Puez section, x 1, 2005z0245/0032
Fig. 9: *Jeanthieuloyites* cf. *quinquestriatus* (Besairie), Puez section, x 1, 2005z0245/009
Fig. 10: *Criosarasinella furcillata* Thieuloy, Puez section, x 1, 2005z0245/0013

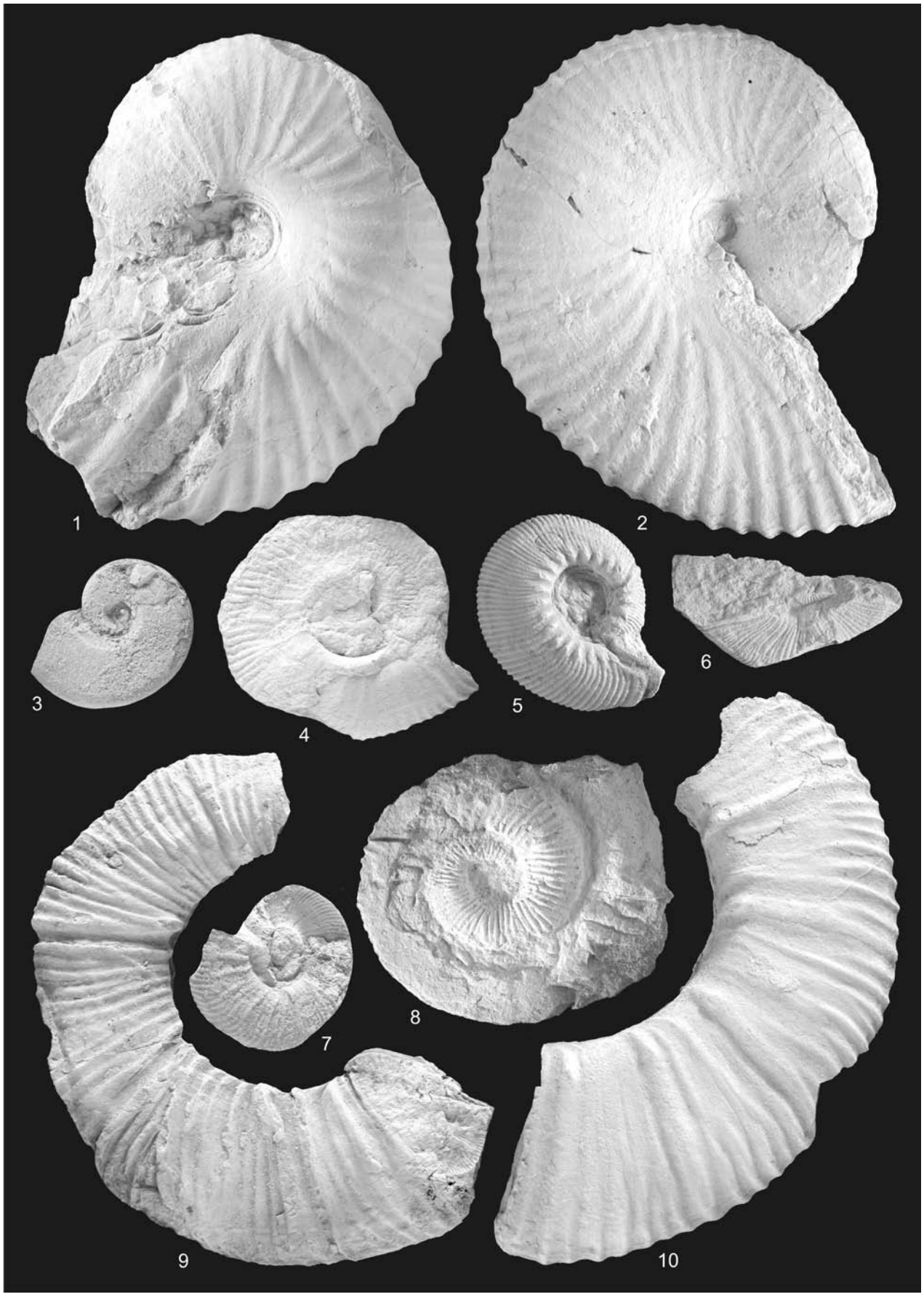
1
2
3
4
5
6
7
8
9
10

Plate 3

Fig. 1: ?*Acanthodiscus*, Puez section, x 1, 1884/0026/0567
Fig. 2: *Barremites psilotatus* (Uhlig), Puez section, x 1, 1962/0002/2223
Fig. 3: *Barremites psilotatus* (Uhlig), Puez section, x 1, 2005z0245/0001
Fig. 4: *Melchiorites cassioides* (Uhlig), Puez section, x 0.5, 2005z0245/0017
Fig. 5: *Abrytusites neumayri* (Haug), Puez section, x 1, 2005z0245/0056
Fig. 6: *Abrytusites neumayri* (Haug), Puez section, x 1, 2005z0245/0057
Fig. 7: *Abrytusites neumayri* (Haug), Puez section, x 1, 2005z0245/0058
Fig. 8: *Melchiorites cassioides* (Uhlig), Puez section, x 0.5, 2005z0245/0045

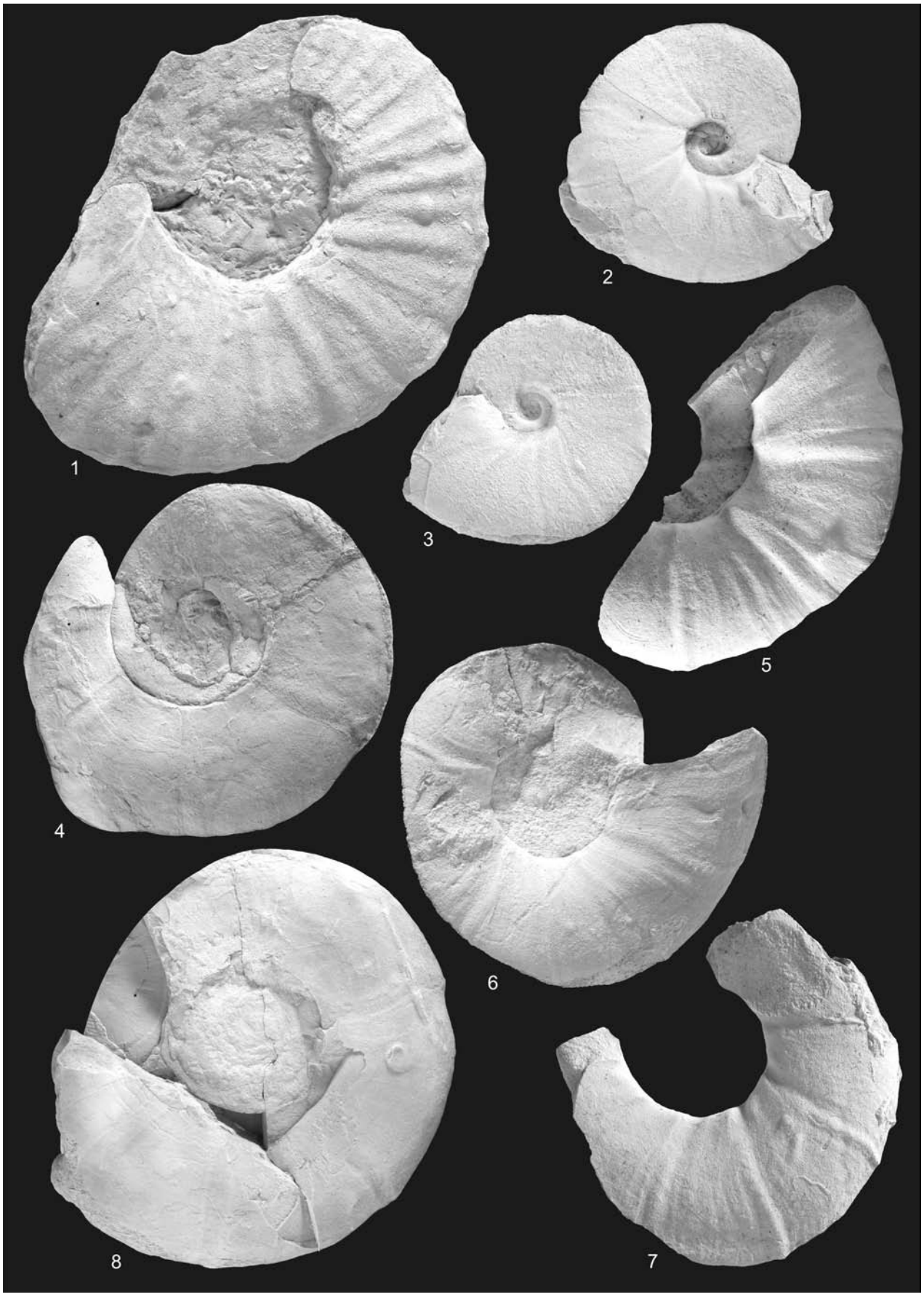
1
2
3
4
5
6
7
8

Plate 4

Fig. 1: *Silesites vulpes* (Coquand), Puez section, x 1, 2005z0245/0029
Fig. 2: *Silesites vulpes* (Coquand), Puez section, x 1, 2005z0245/0037
Fig. 3: *Silesites vulpes* (Coquand), Puez section, x 1, 2005z0245/0041
Fig. 4: *Silesites vulpes* (Coquand), Puez section, x 1, 2005z0245/0043
Fig. 5: *Silesites vulpes* in concretion (Coquand) , Puez section, x 1, 2005z0245/0046

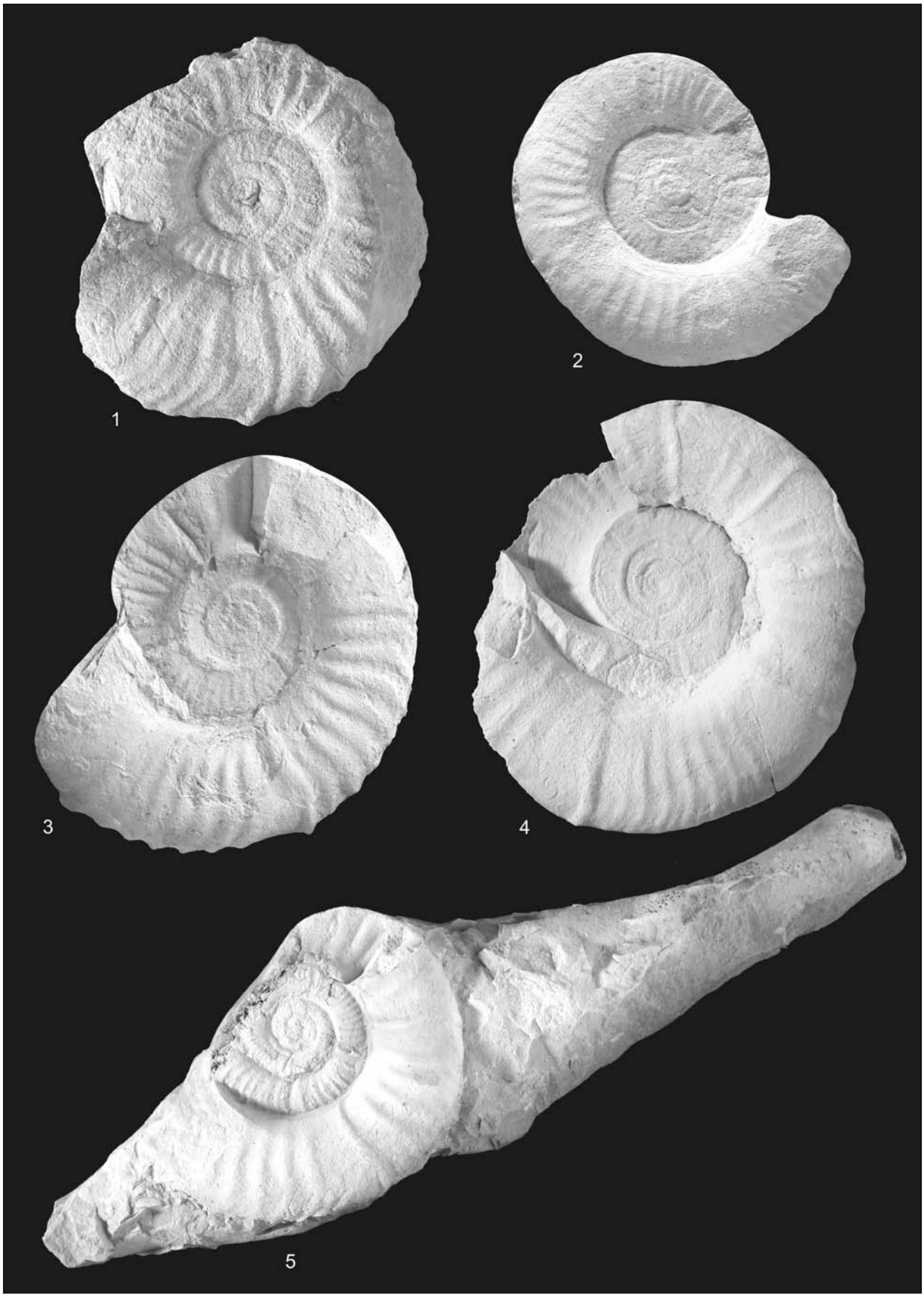
1
2
3
4
5

Plate 5

Fig. 1: *Abrytusites neumayri* (Haug), Puez section, x 0.5, 1886/0008/0014
Fig. 2: *Heinzia sayni* (Hyatt) , Puez section, x 1, 2005z0245/0003
Fig. 3: *Heinzia sayni* (Hyatt) , Puez section, x 1, 2005z0245/0022
Fig. 4: *Heinzia sayni* (Hyatt) , Puez section, x 1, 1886/0008/0019
Fig. 5: *Crioceratites krenkeli* (Sarkar), Puez section, x 1, 2005z0245/0035
Fig. 6: *Crioceratites krenkeli* (Sarkar), Puez section, x 1, 2005z0245/0033
Fig. 7: *Crioceratites krenkeli* (Sarkar), Puez section, x 1, 2005z0245/0028
Fig. 8: *Crioceratites krenkeli* (Sarkar), Puez section, x 1, 2005z0245/0034
Fig. 9: *Crioceratites* sp., Puez section, x 1, 2005z0245/0050
Fig. 10: *Crioceratites nolani* (Kilian), fron view, Puez section, x 0.5, 2005z0245/0008
Fig. 11: *Crioceratites nolani* (Kilian), back view of Fig. 10, Puez section, x 0.5, 2005z0245/0008


1
2
3
4
5
6
7
8
9
10
11

Plate 6

Fig. 1: *Himantoceras* sp., Puez section, x 1, PZO-P21
Fig. 2: *Ancyloceras matheronianum* (d'Orbigny), Puez section, x 0.5, 2005z0245/0012
Fig. 3: *Ancyloceras matheronianum* (d'Orbigny), Puez section, x 0.5, 2005z0245/0049
Fig. 4: *Ancyloceras matheronianum* (d'Orbigny), Puez section, x 0.5, 2005z0245/0048
Fig. 5: *Ancyloceras* sp., Puez section, x 0.5, 2005z0245/0011
Fig. 6: *Ancyloceras* sp., Puez section, x 0.5, 2005z0245/0047
Fig. 7: Acrioceras *(Dissimilites) dissimilis* (d'Orbigny), Puez section, x 1, PZO-CP56
Fig. 8: Acrioceras *(Dissimilites) trinodosum* (d'Orbigny), Puez section, x 1, PZO-CP68
Fig. 9: *Dissimilites (Dissimilites) trinodosum* (d'Orbigny), Puez section, x 1, 2005z0245/0036
Fig. 10: *Acrioceras (Acrioceras) pulcherrimum* (d'Orbigny), Puez section, x 1, 1926/0002/2221
Fig. 11: *Crioceratites thiollierei* (Astier), Puez section, x 1, PZO-P21


1
2
3
4
5
6
7
8
9
10
11

Plate 7

Fig. 1: *Dissimilites (Dissimilites) trinodosum* (d'Orbigny), Puez section, x 1, 1886/0008/0017
Fig. 2: *Hamulina lorioli* Uhlig, Puez section, x 1, 2005z0245/0019
Fig. 3: *Anahamulina subcincta* (Uhlig), Puez section, x 1, 2005z0245/0005
Fig. 4: *Anahamulina subcincta* (Uhlig), Puez section, x 1, 2005z0245/0006
Fig. 5: *Macroscaphites nodosostriatum* (Uhlig), Puez section, x 1, 2005z0245/0020
Fig. 6: *Macroscaphites nodosostriatum* (Uhlig), Puez section, x 1, 2005z0245/0031
Fig. 7: Ammonites indet, Puez section, x 0.5, 2005z0245/0051
Fig. 8: Ammonites indet, Puez section, x 0.5, 2005z0245/0052
Fig. 9: *Macroscaphites yvani* (Puzos), Puez section, x 1, PZO-P17
Fig. 10: *Discoidellia vermeuleni* (Cecca, Faraoni, Marini), Puez section, x 1, 1926/0002/2222

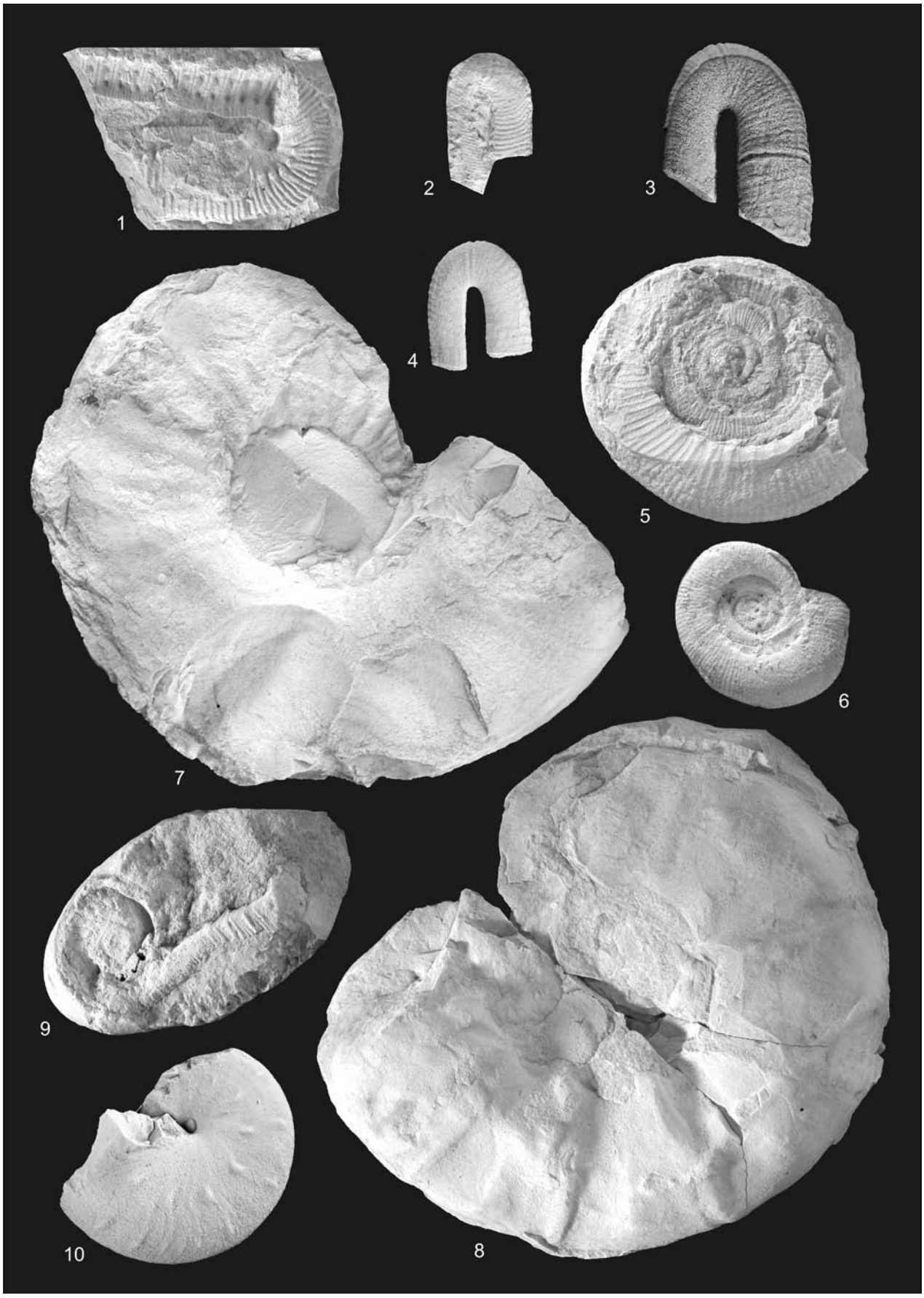
1
2
3
4
5
6
7
8
9
10

Plate 8

Fig. 1: *Cymatoceras* sp., Puez section, x 1, 2005z0245/0018
Fig. 2*:* *Lamellaptychus* sp., Puez section, x 1, 1886/0026/0576
Fig. 3: *Pygope* sp., Puez section, x 1, 1884/0026/0578
Fig. 4: *Pygope* sp., Puez section, x 1, 1886/0008/0001
Fig. 5*:* Belemnites indet with *Acrothoracica* borrows, Puez section, x 1, 1886/0026/0577
Fig. 6*:* *Propaeamussium* sp., Puez section, x 1, 2005z0245/0004
Fig. 7: Brachiopod indet, Puez section, x 1, 2005z0245/0026
Fig. 8: Belemnites indet, Puez section, x 1, 2005z0245/0025
Fig. 9: *Propaeamussium* sp., Puez section, x 1, 2005z0245/0027
Fig. 10: *Inoceramus* sp., Puez section, x 1, 2005z0245/0007
Fig. 11: Sea urchin (Disasteroida), Puez section, x 1, 2005z0245/0023
Fig. 12: Sea urchin (Disasteroida), Puez section, x 1, 1886/0008/0016
Fig. 13: Sea urchin (Disasteroida), Puez section, x 1, 1884/0026/0574
Fig. 14: Sea urchin (Disasteroida), Puez section, x 1, 2005z0245/0024

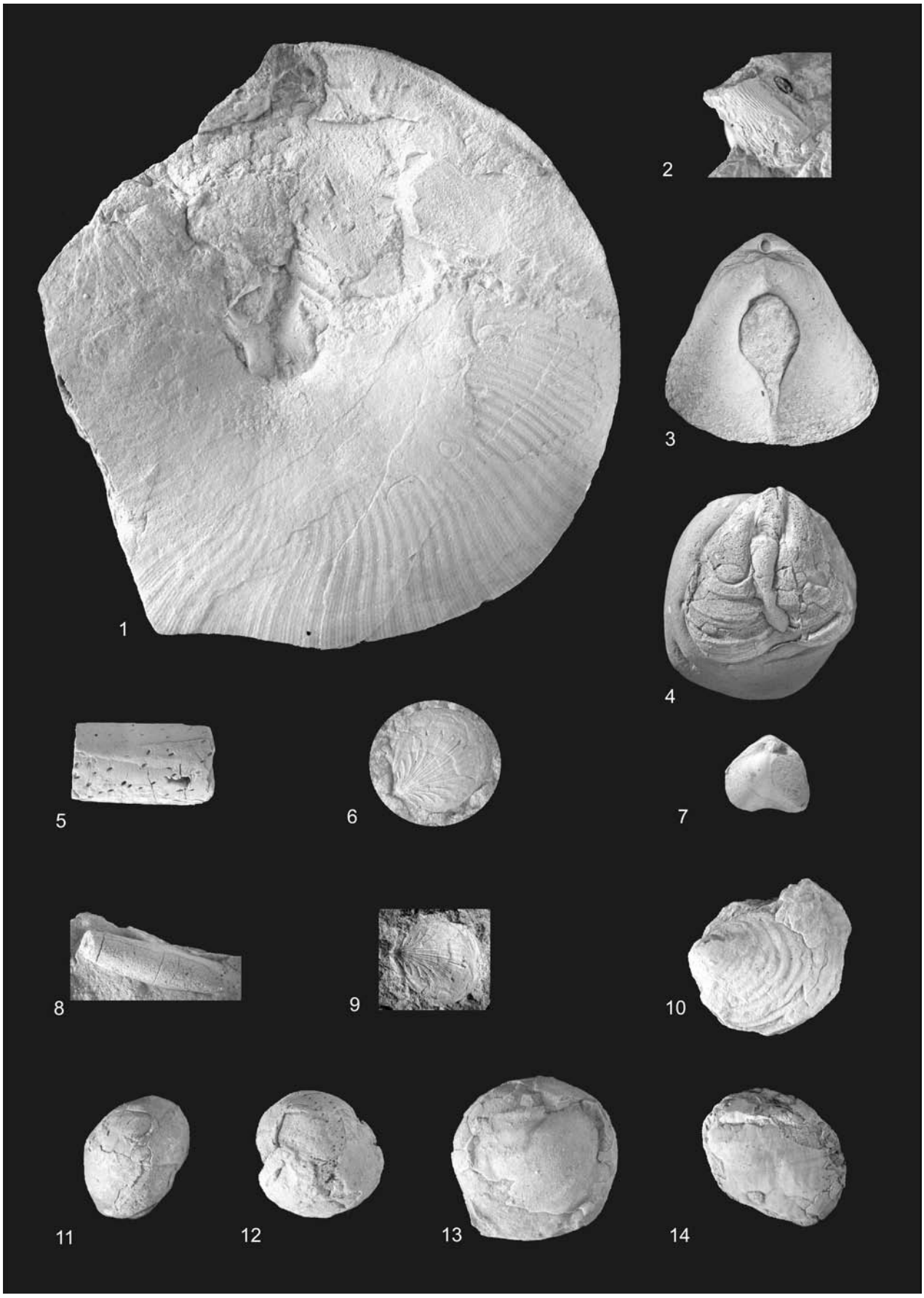
1
2
3
4
5
6
7
8
9
10
11
12
13
14

Geo.Alp, Vol. 3, S. 85–91, 2006

IRANOKIRKBYA BRANDNERI N. GEN. N. SP., A NEW KIRKBYID OSTRACOD FROM THE LATE PERMIAN (DORASHAMIAN) OF ZAL, NW IRAN

Heinz W. Kozur[1] & Wolfgang Mette[2]

With 6 figures

[1] Rézsü u. 83, Hungary, e-mail: kozurh@helka.iif.hu

[2] Institut für Geologie und Paläontologie, Innrain 52, A-6020 Innsbruck, Österreich, e-mail: Wolfgang.Mette@uibk.ac.at

Abstract

The new genus *Iranokirkbya* with the new species *I. brandneri* n. sp. is described from the basal Dorashamian of Zal, NW Iran. The earliest Dorashamian age of the stratum typicum is determined by conodont faunas from immediately under- and overlying beds.

Introduction

Upper Permian ostracods are mostly dominated by Bairdiacea (Belousova, 1965, Chen De-qiong & Shi Cong-guang, 1982, Crasquin-Soleau & Baud, 1998, Crasquin-Soleau et al. (2004a, b), Gerry et al., 1987,Hao Weicheng, 1994, 1996, Jordan, 1968, Kirkby, 1858, Kozur, 1984, 1985, Krömmelbein, 1958, Reuss, 1854, Richter, 1855, 1867, Shi Cong-Guang & Chen De-Qiong, 1985, 1987, Wang, Shang-qi, 1978, Zalányi, 1974). Kirkbyacea (and Kloedenellacea) are characteristic components of Upper Permian ostracod faunas but are less dominant, and mainly confined to shallow water deposits (Crasquin-Soleau et al. 2004a, Gerry & Honigstein, 1984, Gerry et al., 1987, Hao Weicheng, 1994, 1996, Kirkby, 1858, Knüpfer, 1967, Kozur, 1984, 1985, 1993, Olempska & Błaszyk, 1996). In Upper Permian pelagic Tethyan deposits of NW and Central Iran, Transcaucasia and Sicily, Kirkbyacea are rare (Belousova, 1965), but maintain the considerable diversity that characterised this group in the Late Palaeozoic (Kozur, 1991). In this paper, *Iranokirkbya* n. gen. n. sp. from pelagic Upper Permian sediments is described from Zal (NW Iran), and the age of the stratum typicum is discussed.

Geological setting and age of the investigated sample

The Zal sections are situated about 22 km SSW of Jolfa, 2-2.5 km NNW of Zal village (Fig. 1). Sections Zal I and II were sampled by Kozur in 1998 and 2002. Section Zal I is situated at the base of a westward facing slope and exposes the upper Dzhulfian to lowermost Triassic interval. Only the upper Dorashamian to lowermost Triassic beds were sampled in detail. Section Zal II exposes the upper 2 m of the *Codonofusiella* beds, the *Araxilevis* Beds and the lower part of the *Araxoceras* Beds, all of Lower Dzhulfian age. Only the upper 2 m of the *Codonofusiella* beds and the lowermost *Araxilevis* Beds were investigated. The conodonts and stratigraphy of these sections are described in Kozur (2004, 2005), the carbon isotope trends around the Permian-Triassic boundary by Korte et al. (2004).
The section Zal III (Figs. 1, 2) was sampled by Mette and Mohtat-Aghai in 2002. Foraminifers were studied by Mohtat-Aghai. This section exposes the Dzhulfian, Dorashamian and lowermost Triassic. For the present paper the Dzhulfian-Dorashamian boundary interval was studied. A new ostracod species, Iranokirkbya brandneri n. gen. n. sp. is descri-

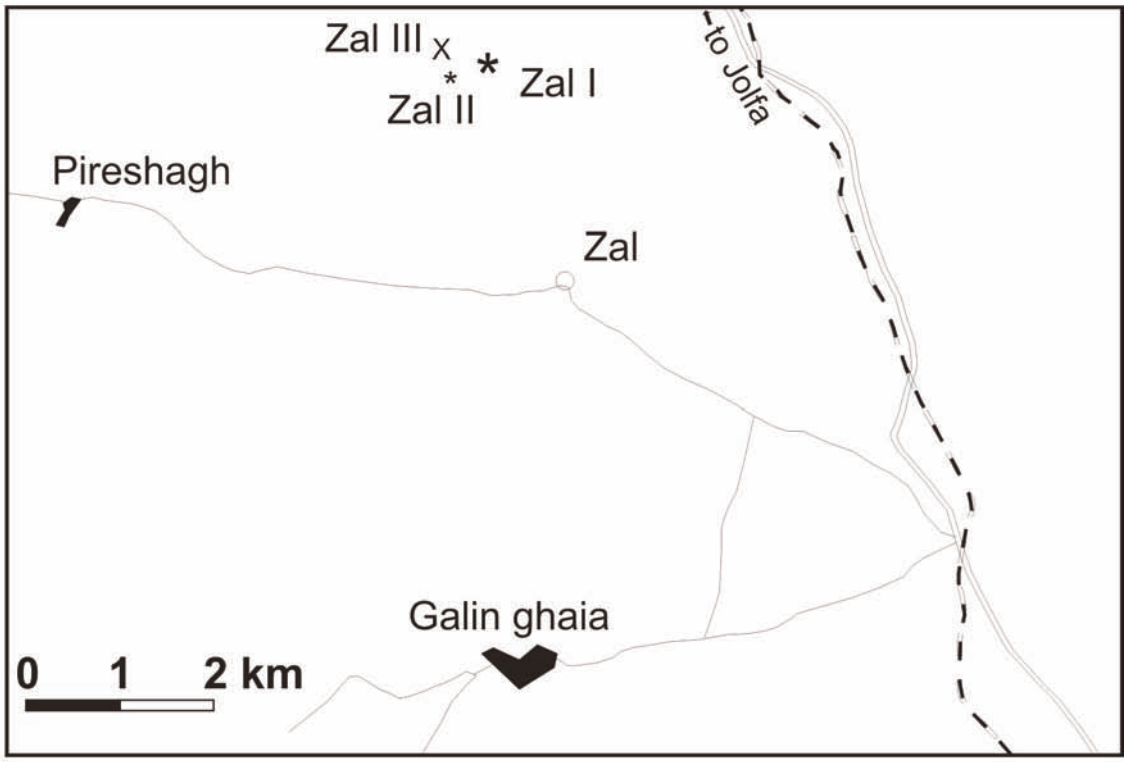

Fig. 1: Location map. 1a: Studied area 22 km SSW of Jolfa, 2.2 to 2.5 km NNW of Zal village. A) position of the studied area within NW Iran. B) detail of the studied area with position of the Zal I and II section investigated by Kozur (2004, 2005), section Zal I also by Korte et al. (2004), and section Zal III studied in the present paper.

Figure 1

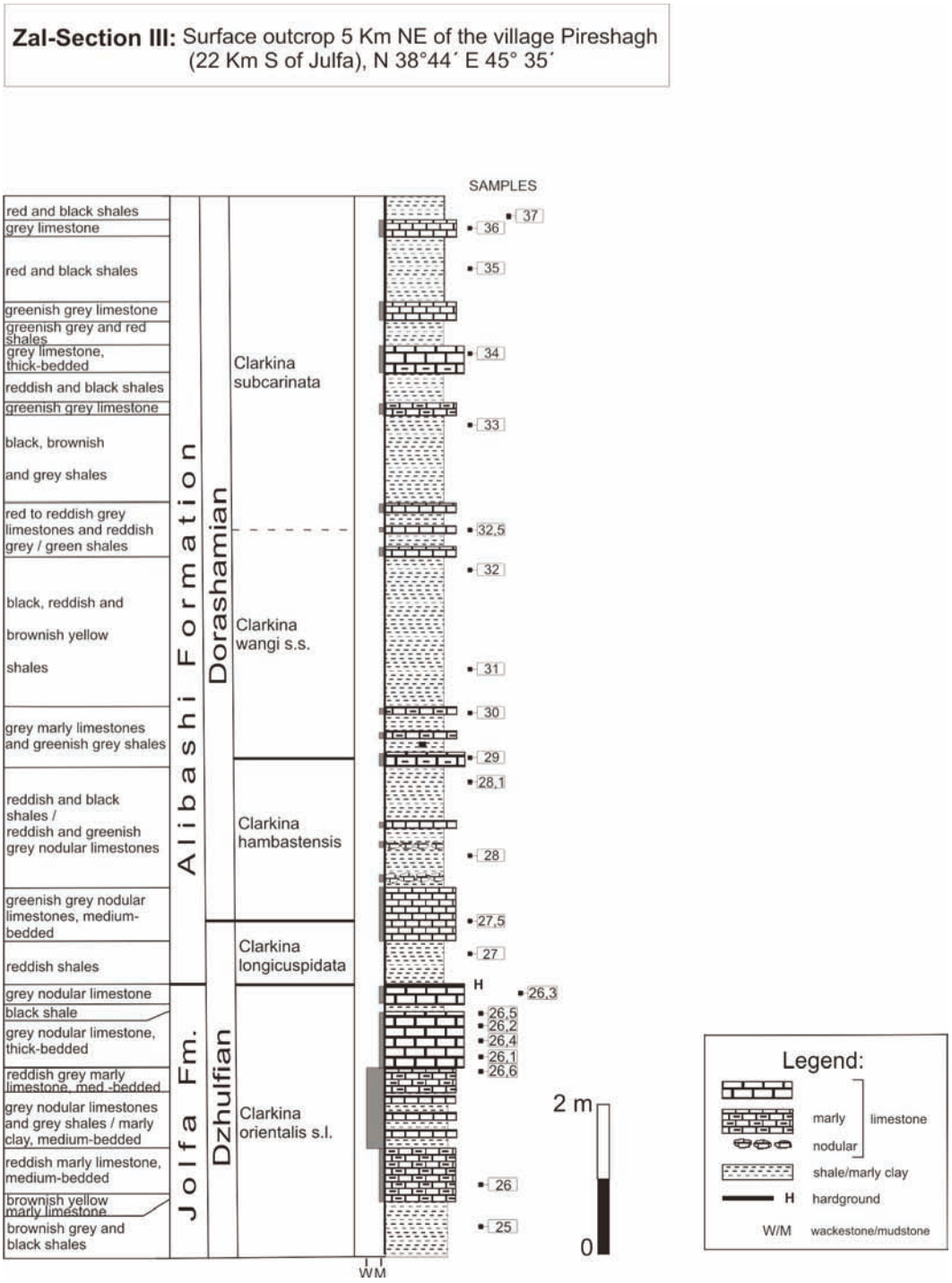

Fig. 2: Uppermost Dzhulfian and lower Dorashamian of section Zal III.

bed from sample 28 from the lowermost Dorashamian lower Alibashi Formation, 1.70 m above a distinct hardground which marks the boundary between the Jolfa Formation and the Alibashi Formation (Fig. 2).

Sample 26; situated about 4.5 m below sample 28 yielded a rich pelagic conodont fauna with numerous *Clarkina orientalis* (Barskov & Koroleva) and some transition forms between *C. orientalis* and *C. inflecta* Mei & Wardlaw. This sample about 2.5 m

below the hardground (Fig. 2) belongs to the upper *C. orientalis* Zone s.l. which can be also discriminated as *C. inflecta* Zone. The reddish shales immediately above the hardground did not yield conodonts, but in section Zal I conodonts of the *C. longicuspidata* Zone are present in that level.

An especially interesting conodont fauna occurs in sample 27.5, situated 0.8 m below sample 28. The conodont fauna of sample 27.5 consists of *C. longicuspidata* Mei & Wardlaw and a new species or new subspecies of *C. hambastensis* Kozur. The latter species was assigned by Jin Yugan et al. (2004a, b) to *C. wangi* (Dai & Zhang), but is clearly distinguished by the carina which does not continue beyond the posterior margin in form of a long protrusion as typical for *C. wangi* pointed out both in the original diagnosis by Wang, Chengyuan & Wang, Zhihao (1981) and in the nearly identical emended diagnosis by Jin et al. (2004a, b). In Iran, *C. hambastensis* begins much earlier than true *C. wangi*. Jin Yugan et al. (2004a, b) illustrated assumed transitional forms between *C. longicuspidata* and *C. wangi* (including *C. hambastensis*), but these forms are *C. longicuspidata* with a small gap between the cusp and the carina, which occur in a longer interval beside *C. longicuspidata* with big gap between the cusp and the carina. They are regarded as intraspecific variants of *C. longicuspidata*. Among *C. longicuspidata* there occur forms, in which the anterior edge of the cusp is prolonged across the gap until the end of the carina. Such forms are also present in the type material, illustrated by Mei Shilong et al. (1994) from South China. In the uppermost *C. longicuspidata* Zone 2 or 3 highly fused denticles evolved on this edge and fill up a large part of the gap between the cusp and the end of the carina. However, a small gap remains between these denticles and the end of the carina. By disappearance of this gap typical *C. hambastensis* evolved from these transition forms, which will be described in another paper. The occurrence of these transition forms indicates a position close to the base of the *C. hambastensis* Zone for sample 27.5.

Sample 29 (Fig. 2), 1.30 m above sample 28 contains numerous transition forms between *C. hambastensis* and *C. wangi* and a single specimen of typical *C. wangi*. This fauna is characteristic for the upper *C. hambastensis* Zone s.l. which can be also discriminated as *C. wangi* Zone s.s. (without the *C. hambastensis* Zone), but typical *C. wangi* were found in Iran only in Zal. As sample Zal 28 with ostracods, but without conodonts lies in the middle part of the interval between samples 27.5 (close to the base of the *C. hambastensis* Zone) and sample 29 (immediately above the *C. hambastensis* Zone s.s.), sample 28 belongs surely to the *C. hambastensis* Zone and therefore to the lowermost Dorashamian. As the base of the Changhsingian stage at Meishan was defined (Jin Yugan et al., 204a, b) by the FAD of *C. wangi*, in which *C. hambastensis* was included (and from the lowermost Changhsingian only *C. hambastensis* was illustrated under *C. wangi*), sample 28 can be correlated with the basal Changhsingian.

Samples 32.5 and 36 (Fig. 2) yielded conodonts of the *C. subcarinata* Zone. As the interval between samples 29 and 32.5 has not yielded conodonts, the lower boundary of the *C. subcarinata* Zone may be situated somewhat lower than indicated in Fig. 2, but this is irrelevant for the dating of sample 28, the stratum typicum of the *Iranokirkbya brandneri*.

Systematics

Order Reticulocopida Kozur, 1993
Suborder Punciocopina Schallreuter, 1968
Superfamily Kirkbyacea Ulrich & Bassler, 1906
Family inc.

Genus *Iranokirkbya* n. gen.

Type species:
Iranokirkbya brandneri n. gen. n. sp.

Diagnosis:
Carapace large, equivalved, subrectangular, flat (low convexity). Lateral surface reticulated, with distinct adductorial pit (kirkbyan pit). A distinct straight or indistinctly curved oblique ridge is present above the adductorial pit, which runs from the lower anteromedial field to the upper posteromedial field. A low rib runs parallel and with small distance to the free margin. A second, very distinct and high rib is present parallel to the low rib and join it at the anterodorsal corner. It ends in the posterodorsal corner in a posteriorly-upward directed short spine. The dorsal rib overreaches slightly the dorsal margin. It ends before the anterior and posterior ends

Figs 3-6: *Iranokirkbya brandneri* n. gen. n. sp., section Zal III (NW Iran), sample 28, lower Alibashi Formation, *Clarkina hambastensis* Zone, lowermost Dorashamian, scale 200 µm, collection of Institute of Geology and Palaeontology, Innsbruck University; Fig. 3: RV; Fig. 4: carapace, view from left, holotype (repository number Kozur/Mette 1-2005); Fig. 5: carapace, upper view; Fig. 6: other carapace, lower view.

of the dorsal margin. The ventral surface is flat and throughout of the same width. The dorsal surface is slightly concave, narrowest at the end of the anterior fourth of the carapace and widest at the beginning of the posterior fourth of the carapace. The muscle scars in the adductorial pit consist of at least 6 small spots.

Assigned species: *Iranokirkbya brandneri* n. gen. n. sp.

Distribution: Lower Dorashamian of Iran.

Remarks: *Kirkbya* Jones, 1859 is similar in outline and sculpture but is more convex, has a posterior shoulder and no lateral rib. It does not appear to be closely related to the proposed new genus.

The forerunner of *Iranokirkbya* is not known. There are two possibilities, either *Tubulikirkbya* Kozur, 1985 (family Kirkbyidae Ulrich & Bassler, 1906, subfamily Coronakirkbyinae Kozur, 1985) or "*Kirkbya*" sp. n. Olempska & Błaszyk, 1996 (n. gen., Amphissitidae Knight, 1928).

In *Tubulikirkbya* the marginal ridge along the free margin consists of fused tubules, which are difficult to recognise in advanced forms, and are apparently absent in the new genus. Otherwise *Tubulikirkbya* is very similar in outline and sculpture, also a lateral rib may be present but it is not straight. It is possible that *Iranokirkbya* evolved from *Tubulikirkbya* by disappearance of the marginal tubules. However, it cannot be excluded that both genera are unrelated.

"*Kirkbya*" sp. n. from the Permian of Spitsbergen is a representative (new genus) of the Amphissitidae. It is similar to *Amphissites* Girty, 1910 in outline and sculpture, especially in the two vertical carinae in similar position as in *Amphissites*, but the characteristic subcentral node is absent. There are 1-3 lateral ribs below or above the adductorial kirkbyan pit, which are, however, mostly not straight. By disappearance of the vertical carinae *Iranokirkbya* may have evolved from this amphissitid new genus. The absence of transition forms means we cannot determine the phylomorphogenetic lineage to which

Iranokirkbya belongs, and cannot assign this genus to a family within the superfamily Kirkbyacea.

Iranokirkbya brandneri n. gen. n. sp.
(Figs. 3-6)

Derivatio nominis: In honour of Univ. Prof. Dr. R. Brandner, Innsbruck
Holotypus: Carapace (repository number Kozur/Mette 1-2005), illustrated on Fig. 4

Locus typicus: Section Zal III, NW Iran

Stratum typicum: Shales of lower Alibashi Formation, sample 28 (see Fig. 2). *C. hambastensis* Zone of lowermost Dorashamian

Material: 5 specimens.

Diagnosis: Carapace large, up to 1000 µm long, equivalved, subrectangular, flat (low convexity). Dorsal margin straight, ventral margin straight to slightly concave; ventral outline in lateral view straight. Anterior margin strongly and symmetrically rounded, a little higher than the slightly obliquely rounded posterior margin. Lateral surface reticulated, with distinct adductorial pit. A distinct straight or indistinctly curved oblique ridge is present above the adductorial pit, which runs from the lower anteromedial field to the upper posteromedial field. A low rib runs parallel and with small distance to the free margin. This rib is not to seen in lateral view, if the carapace is not tilted, but well recognisable in lower view (Fig. 6). A second, very distinct and high rib is present parallel to the low rib and join it in the antrodorsal corner (Fig. 5). It ends in the posterodorsal corner in a posteriorly-upward directed short spine. The dorsal rib overreaches slightly the dorsal margin. It ends before the anterior and posterior ends of the dorsal margin. Below the dorsal rib the reticulation may be arranged in an indistinct rib. The muscle scars in the adductorial n pit consist of at least 6 small spots.

Dimensions. l = 756-1000 µm, h = 366-457 µm, l/h = 2.15-2.19, maximum width: 311-356 µm

Distribution and remarks as for the genus.

Acknowledgement:

The studies were supported by the Austrian FWF project no. P 14490-GEO. We thank very much Dr. P. J. Jones (The Australian National University, Canberra) for his suggestions which have greatly improved the final manuscript.

References

Belousova, Z.D. (1965): Tip Arthropoda, Klass Crustacea, Podklass Ostracoda. In: Ruzhentsev, V.I. & Sarytcheva, T.G.: Razvitie i smena morskich organismov na rubezhe paleozoja i mezozoja. – Trudy Pal. Inst. AN SSSR, **108**, 254–265, 404–413.

Chen, De-Qiong & Shi, Cong-Guang (1982): Latest Permian Ostracoda from Nantong, Jiangsu and from Mianyang, Hubei. – Bull. Nanjing Inst. Geol. & Palaeont., Acad Sinica, **4**, 105–152.

Crasquin-Soleau, S. & Baud, A. (1998): New Permian ostracods from Greece (Hydra Island). – J. Micropalaeont., **17**, 131–152.

Crasquin-Soleau, S., Marcoux, J., Angiolini, L. & Nicora, A. (2004a): Palaeocopida (Ostracoda) across the Permian-Triassic events: new data from southwestern Taurus (Turkey). – J. Micropalaeont., **23**, 67–76.

Crasquin-Soleau, S., Marcoux, J., Angiolini, L., Richoz, S., Nicora, A., Baud, A. & Bertho, J. (2004b): A new ostracod fauna from the Permian-Triassic boundary in Turkey (Taurus, Antalya Nappes). – Micropaleontology, **50** (3), 281–295.

Gerry, E. & Honigstein, A. (1984): Permian ostracodes of Israel.-The Israel Institute of Petroleum and Energy, Report **3/84**, 1–14.

Gerry, E., Honigstein, A., Derin, B. & Flexer, A. (1987): Late Permian ostracodes of Israel. Taxonomy, distribution, and palaeogeographical implications. – Senckenbergiana lethaea, **68** (1/4), 197–223.

Hao, Weicheng (1994): The development of the Late Permian-Early Triassic ostracod fauna in Guizhou province. – Geol. Rev., **40** (1), 87–92.

Hao, Weicheng (1996): Ostracods for the Upper Permian and Lower Triassic of the Zhenfeng section, South China. – J. Geosci., Osaka City Univ., **39** (2), 19–27.

Jin, Yugan, Henderson, C., Wardlaw, B., Shen Shouzhong, Wang Xiangdong, Wang Yue, Cao Changqun & Chen Lide (2004 a): Proposal for the Global Stratotype Section and Point (GSSP) for the Wuchiapingian-Changhsingian Stage boundary (Upper Permian

Lopingian Series). – Base Changhsingian Stage GSSP Proposal, 1–17.

Jin, Yugan, Henderson, C., Wardlaw, B., Shen, Shouzhong, Wang, Xiangdong, Wang, Yue, Cao, Changqun & Chen, Lide (2004 b): Proposal for the Global Stratotype Section and Point (GSSP) for the Wuchiapingian-Changhsingian Stage boundary (Upper Permian Lopingian Series). – Permophiles, **43**, 8–23.

Jordan, H. (1968): Neue taxionomische und biostratigraphische Ergebnisse mikropaläontologischer Untersuchungen im germanischen Zechsteinbecken unter besonderer Berücksichtigung der Ostracoden. – Ber. deutsch. Ges. geol. Wiss., A, Geol. Paläont., **13** (2), 199–213.

Kirkby, J.W. (1858): On Permian Entomostraca from the fossiliferous limestone of Durham. – Ann. Mag. Nat. hist., (3) **2**, 317–330, 432–438.

Knüpfer, J. (1967): Zur Mikrofauna aus dem utneren Teil deas Zechsteins von Rügen. – Freiberger Forsch.-H., **C 213**, 73-99.

Korte, C., Kozur, H. W. & Partoazar, H. (2004): Negative carbon isotope excursion at the Permian/Triassic boundary section at Zal, NW-Iran. – Hallesches Jahrb. Geowiss., Reihe B, Beiheft, **18**, 69–71.

Kozur, H. (1985a): Neue Ostracoden-Arten aus dem oberen Mittelkarbon (höheres Moskovian), Mittel- und Oberperm des Bükk-Gebirges (N-Ungarn).- Geol. Paläont. Mitt. Innsbruck, Sonderband, **2**(1), 1-145.

Kozur, H. (1985b): Biostratigraphic evaluation of the Upper Paleozoic conodonts, ostracods, and holothurian sclerites of the Bükk Mts., Part II: Upper Paleozoic ostracods.- Acta Geol. Hungar., **28**(3-4), 225-256.

Kozur, H. (1991): Permian deep-water ostracods from Sicily (Italy). Part 1: Taxonomy.- Geol. Paläont. Mitt. Innsbruck, Sonderbd., **3**, 1-24.

Kozur, H. (1993): Relation between Late Paleozoic Kirkbyacea and Cretaceous-Recent Punciacea (Ostracoda). – In: Mckenzie, K. G. & Jones, P. J. (eds.): Ostracoda in Earth and Life Sciences, 91–106, Rotterdam-Brookfield (A. A. Balkema).

Kozur, H. W. (2004): Pelagic uppermost Permian and the Permian- Triassic boundary conodonts of Iran. Part 1: Taxonomy. – Hallesches Jahrb. Geowiss., Reihe B, Beiheft, **18**, 39–68.

Kozur, H. W. (2005): Pelagic uppermost Permian and the Permian-Triassic boundary conodonts of Iran. Part 2: Investigated sections and evaluation of the conodont faunas - Hallesches Jahrb. Geowiss., B, Beiheft, **19**, 1-36.

Krömmelbein, K. (1958): Ostracoden aus dem Unteren Zechstein der Bohrung Leba in Pommern. – Geol. Jb., **75**, 115-134.

Mei, Shi-long, Jin, Yugan & Wardlaw, B.R. (1994): Succession of Wuchiapingian conodonts from north-eastern Sichuan and its worldwide correlation.- Acta Micropaleont. Sinica, **11** (2), 121–139.

Mette, W. & Mohtat-Agai, P. (2004): Late Permian and Early Triassic microfossil assemblages of Iran. – Ber. Inst. Erdwiss. K.-F. Univ. Graz, **9**, 263-265.

Olempska, E. & Błaszyk, J. (1996): Ostracods from the Permian of Spitsbergen. – Polish Polar Research, **17** (1-2), 3-20.

Reuss, A.E. (1854): Über Entomostraceen und Foraminiferen im Zechstein der Wetterau. – Jahresber. Wetterau. Ges. Naturk., **5**, 59–77.

Richter, R. (1855): Aus dem thüringischen Zechstein. – Z. deutsch. Geol. Ges., **7**, 526–533

Richter, R. (1867): Aus dem thüringischen Zechstein. – Z. deutsch. Geol. Ges., **19**, 216–236.

Shi, Cong-Guang & Chen, De-Qiong (1985): South China (Permian marine Ostraoda). – International Symposium on Ostracoda July 29 - August 2,1985, Guidebook of excursions. Exc. 2: South China, 1–12, Shizuoka.

Shi, Cong-Guang & Chen, De-Qiong (1987): The Changhsingian ostracodes from Meishan, Changxing, Zhejiang. – In: Stratigraphy and Palaeontology of systemic boundaries in China, Permian and Triassic boundary, 23–80 (Nanjing University Press).

Wang, Chengyuan & Wang, Zhihao (1981): Conodonts. In: Zhao Jin-ke, Sheng Jin-zhang, Yao Zhao-qi, Liang Xi-luo, Chen Chu-zhen, Rui Lin, Liao Zhuo-ting: The Changhsingian Stage and Permian-Triassic boundary of South China. – Bull. Nanjing Inst. Geol. Palaeont. Acad. Sinica, 2, 79–81, 3 pls., Nanjing.

Wang, Shang-qi (1978): Late Permian and Early Triassic ostracods of western Guizhou and northeastern Yunnan. – Acta Palaeont. Sinica, **17** (3), 277-308.

Zalányi, B. (1974): Die oberpermischen Ostracoden des Bükk-Gebirges. – In: Sidó, M. (ed.): Neue paläontologische Ergebnisse aus dem Oberpaläozoikum des Bükk-Gebirges. 95–251, Budapest (Akademia Kiadó).

Geo.Alp, Vol. 3, S. 93–145, 2006

BEITRAGE ZUR STRATIGRAPHIE UND MIKROPALAONTOLOGIE DER MITTELTRIAS DER INNSBRUCKER NORDKETTE (NORDLICHE KALKALPEN, AUSTRIA)

Petra Nittel

Mit 18 Abbildungen und 12 Tafeln

With 18 figures and 12 plates

Institut für Geologie und Paläontologie Innsbruck, Innrain 52, 6020 Innsbruck; e-mail: petra.nittel@uibk.ac.at

Zusammenfassung

Nördlich von Innsbruck im Gebiet der Nordkette (Karwendelgebirge, Nördliche Kalkalpen NKA) wurde eine vielfältige Schichtfolge erfasst, die zeitlich in die Mitteltrias bis frühe Obertrias (Cordevolium) zu stellen ist. Die mitteltriassischen Steinalm-, Reifling- und Wettersteinkalk-Formationen werden in dieser Arbeit in Bezug auf deren Stratigraphie und Mikropaläontologie näher beschrieben.

Die Karbonate der Steinalm-Formation wurden bei günstigen Lebensbedingungen in überwiegend flachem Wasser abgelagert und bilden die erste triassische Karbonatplattform der NKA. Sie weisen kleinräumig stark schwankende Mächtigkeiten auf, hervorgerufen durch unterschiedliche Sedimentationsraten und -bedingungen. Der Mikrofossilgehalt ist geprägt durch eine Vielzahl an Dasycladaceen, Foraminiferen und Brachiopoden.

Eine Transgression führte zum Ertrinken der Plattform und leitete damit die Ablagerung der Reifling-Formation als mit der frühen Wettersteinkalk-Formation verzahnende Beckenfazies ein. Die zum Wetterstein-Riff distalen Knollenkalke des Knollenkalk-Members und die proximalen Bankkalke der „Seegrube-Einheit" zeigen in ihrem Mikrofossilgehalt neben häufig auftretenden Radiolarien und Filamenten nur wenige Foraminiferen. Ein weiteres Charakteristikum stellen die umgelagerten Tuffe von drei „pietra verde"- Horizonten dar.

Die Karbonatplattform der Wettersteinkalk-Formation zeigt eine deutliche Abgrenzung von Vorriff, Riff und Lagune. Durch eine steigende regressive Tendenz wird das Riff schließlich von der Lagune überlagert. Der Mikrofossilgehalt variiert stark je nach Ablagerungsraum. Das Riff ist charakterisiert durch das Vorkommen von Sphinctozoen (*Solenolmia manon*, *Vesicocaulis carinthiacus*, *Colospongia catenulata*), inkrustierenden Organismen (*Tubiphytes, Ladinella porata*) und Mikroproblematika (*Tubiphytes*, *Baccanella floriformis*, *Ladinella porata*). Foraminiferen sind in der gesamten Wettersteinkalk-Formation zu finden, treten aber vermehrt in der Lagune auf. Dasycladaceen kommen ausschließlich in der Lagune vor und geben Aufschlüsse über das Alter und die Entfernung zum Riff. In der Lagunenfazies der Wettersteinkalk-Formation konnten zwei neue Arten bestimmt werden, die Foraminifere *Austrocolomia carinata* und die Dasycladacee *Probolocuspis aculeata*.

Abstract

North of Innsbruck, in the area of Nordkette (Karwendel range, Northern Calcareous Alps, NCA) a variegated Middle to lower Upper Triassic (Cordevolian) sucession of shallow-water carbonates is preserved, and includes the Steinalm-, Reifling- and Wettersteinkalk-Formations, respectively.

The Steinalm-Formation accumulated under favourable ecological conditions, from prevalently shallow waters, and comprises the first Triassic carbonate platform of the NCA. The thickness is laterally variable, because of different rates of sedimentation. The bioclast spectrum is characterized by abundant dasycladaceans, foraminifera and brachiopods.

Following a rise of sea-level, the Reifling-Formation accumulated as the basinal equivalent to and that interfingered with the Wettersteinkalk-Formation.

In the Reifling Formation, the nodular limestones of the Knollenkalk-Member and the bedded limestones of the "Seegrube-unit" are relatively poor in foraminifera and radiolaria, whereas "filament" shells are common. In addition, three thin intervals of "pietra verde" interpreted as volcanic tuffitic deposits are present.

The succession of the Wettersteinkalk-Formation shows a differentiation into reef slope, reef, backreef and lagoon. Because of platform progradation, the slope to reef facies belt is overlain by limestones that accumulated from backreef to lagoonal environments. The reef limestones are characterized by sphinctozoans (*Solenolmia manon*, *Vesicocaulis carinthiacus*, *Colospongia catenulata*), encrusting organisms (*Tubiphytes, Ladinella porata*) and microproblematica (*Tubiphytes*, *Baccanella floriformis*, *Ladinella porata*). Whereas benthic foraminifera are most common within the lagoonal sucession, dasycladaceans are present only in the lagoonal limestones, and can be used as biostratigraphic index fossils and as proxy indicators for the distance to the reef belt.

Two new species are described from lagoonal limestones of the Wettersteinkalk-formation, the foraminifer *Austrocolomia carinata* and the dasycladacean *Probolocuspis aculeata*.

Abridged Version

This paper is based on part of the author's M. S. thesis, dealing with stratigraphical, structural and micropaleontological aspects of the Steinalm-Reifling- and Wettersteinkalk Formations. With respect to the Middle to Upper Triassic stratigraphy and micropaleontology of the investigated area, most papers are from Ampferer & Hammer (1899), Ampferer (1903, 1911), Sarnthein (1968), Ott (1967, 1972), Kubanek (1969), Mostler (1972), Bechstädt & Mostler (1974,1976), Frisch (1975), Resch (1977, 1979), Donofrio et.al (1979), Heissel (1978, 1989), Brandner & Resch (1981), Eisbacher & Brandner (1995) , Rüffer (1995), Brandner & Poleschinski (1996), und Rüffer & Zamparelli (1997).

The investigated area is located on the southern slope of the Nordkette range north of Innsbruck. There, within the Upper Austroalpine (Tirolic) Inntal nappe, Middle Triassic formations that consist mainly of limestones of neritic environment are well-exposed.

Steinalm-Formation

The base of the Steinalm platform is characterized by a thick carbonate bed above an interval of ocre-coloured, thin-bedded nodular limestones. Upsection, within the Steinalmkalk, a former shallow-water-area in the west was separated by a swell from a a shelf sector that gently dipped towards the east. Farther east, within the Steinalmkalk, biostromal accumulations composed of abundant dasycladalean fragments, and calcareous sponges, corals, hydrozoans, bryozoans, molluscs and crinoids are common. For the western, shallow-water area abundant dolostones and stromatolithically laminated limestones indicate sedimentation in a protected, normal-saline to hypersaline area with tidal flats. In the investigated area, dark grey to black coloured neritic limestones with brachiopods and crinoid fragments are most common. This indicates deeper water and a flat slope submerging towards the west- southwest. The top of the Steinalm Formation is represented by an interval of glauconite-bearing encrinite which heralds incipient drowning of the platform.

Microfacies

Facies type 1 is characterized by Anisian dasycladacean fragments (*Physoporella-Oligoporella*) in pack-wackestones, *Stromatactis*, and by the Pelsonian to Illyrian foraminifer *Meandrospira dinarica*. Facies type 2 is dominated by fragments of crinoids and echinids, within mud-packstones and oncoid-packstones. The presence of *Ophtalmidium abriolense* indicates "deeper" neritic habitats. Facies type 3 is characterized by pack-grainstones and oncoid grainstones. Anisian brachiopods such as *Tetractinella trigonella* and *Decurtella decurtata* are common. Facies type 4 is dominated by peloidal wacke-grainstones with fragments of crinoids, gastropods and foraminifera (e. g. *Turriglomina mesotriassica*) again indicating "deeper" neritic habitats. Facies type 5 is confined to a thin interval marking the boundary between the Steinalm Formation and the overlying Reifling Formation; this facies is characterized by glauconite, "filament" shells, and few radiolarians.

Reifling-Formation

Above the encrinite interval atop the Steinalm Formation, the lower part of the Reifling Formation consists of nodular lime mudstones to radiolarian-"filament" wackestones. Three horizons of Pietra Verde tuffs can be intercalated in both members. Within the Reifling Formation, the lower stratigraphic unit ("Knollenkalk Member") consists of nodular limestones with chert nodules. The upper, as yet informal stratigraphic unit ("Seegrube unit") of the Reifling Formation consists of well-bedded radiolarian-"filament"limestones. Up-section within the unit, bedding becomes thicker, and event beds rich in bioclasts derived from reefal to peri-reefal settings are present. Closely east of the working area, ammonites near the base of the Seegrube unit indicate a late Illyrian age (Avisianus Zone).

Microfacies

The Reifling Formation was subdivided into three facies types, which are (1) Pakstones mainly of "filament" shells, (2) bioturbated radiolarian-"filament" lime mudstones to packstones, and (3) bioturbated bioclastic packstones devoid of radiolarians. In each of these facies foraminifera such as *Turriglomina mesotriassica*, *Ophtalmidium abriolense* and *Ophtal - midium ubeyliense* suggest, deeper subtidal open-marine conditions. In calciclastic event beds of the Seegrube unit, *Tubiphytes* is common.

Wettersteinkalk Formation

In the considered area, the Wettersteinkalk could be subdivided into a forereef, reef, and backreef (lagoonal) belt.

In its basal part, the interval corresponding to the forereef facies belt is dominated by dark-coloured limestones with small-sized fragments of reef builders. Higher up, light-grey coloured calcirudites consisting of bioclasts ranging in size from about 2 mm to 3 dm are present.

The central reef is dominated by encrusters and frame builders such as *Tubiphytes*, sphinctozoans and microproblematica such as *Ladinella porata;* corals are subordinate in abundance. In addition, cavities up to a few meters in width filled by interlaminated microdolomite and radiaxial calcite are common.

The lagoonal succession is characterized by well-bedded, light-grey coloured limestones. Within this succession, vertically repetitive intervals rich in tepee structures, sheet cracks, pisolite layers, loferites and stromatolithically laminated limestones record episodic establishment of tidal flats in a hot, arid to semi-arid environment. The limestones corresponding to shallow subtidal, lagoonal deposition are rich in dasycladaceans such as *Teutloporella herculea*, *Teutloporella nodosa*, *Poikiloporella duplicata*, *Clypeina besici*, amoing others.

Microfacies

(1) Within distal calciturbidites, skeletal grains and microproblematica such as *Baccanella florifomis*, *Tubiphytes obscurus* and *Ladinella porata* are common. Typical foraminifera include *Palaeolituonella meridionalis, Planiivoluta carinata, Turriglomina mesotriassica* and *Ophtalmidium tricki*; the latter two foraminifera, together with radiolarians and "filament" shells suggest deeper, open-marine conditions.

(2) Grainstones of proximal calciturbidites are characterized by sphinctozoans (*Solenolmia manon*, *Solenolmia manon minor*, *Colospongia catenulat*a), and a few fragments of corals and crinoids. (3) Forereef breccias are characterized by fragments of both calciturbidites and reef fossils such as *Folicatena cautica, Vesicocaulus carinthiacus, Colospongia catenulata* and *Solenolmia manon manon*. Typical foraminifera include *Palaeolituonella meridionalis, Frondicularia* sp.*, Aulotortus friedli and* Astrorhizacea. The central part of the reef belt is represented by two facies types. (4) Bind-bafflestones mainly of encrusting *Tubiphytes* and porostromate algae, and of abundant fragments of bryozoans and corals. (5) Baffle-boundstones with corals, solenporaceans and encrusters such as *Tubiphytes obscurus, Ladinella porata* and sphinctozoans.

From the wide range of different lagoonal facies types (see Sarnthein 1965), only a few could be identified within the working area. Facies type C1 is represented by dasycladacean rud-grainstones rich in fragments of *Teutloporella herculea*, *Diplopora annulata*, *Teutloporella nodosa*, *Clypeina besici* and *Aciculella bacillum*. Additionally, porostromate algae (e.g. *Cayeuxia*, *Ortonella*) are present. Typical foraminifera include *Lamelliconus* sp, *Glomospirella*, *Aulotortus tenuis*, *Aulotortus sinuosus*, *Glomospira* sp., *Trochammina* sp. and *Aulotortus friedli*. This facies accumulated on and between bioclastic sand bodies situated in the backreef belt. Facies type C2 is dominated by peloidal-bioclastic grainstones with

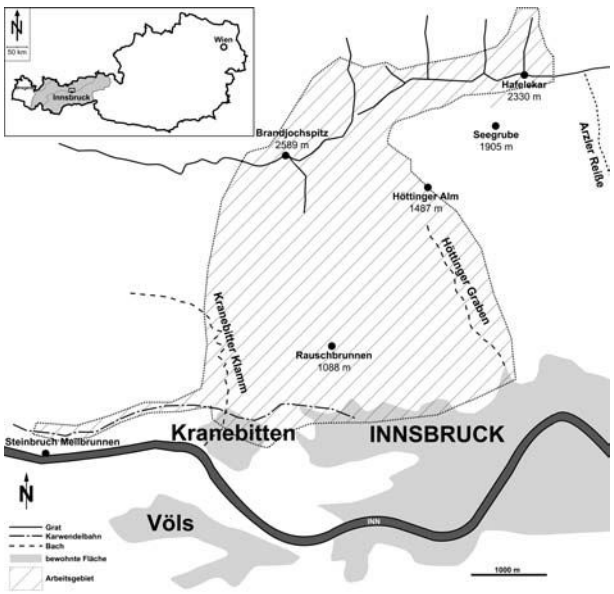

Abb. 1: Lage des Arbeitsgebietes.

Fig. 1: Locality of area of investigation.

dasycladaceans (*Clypeina besici*, *Poikiloporella duplicata*, *Physoporella jomdaensis* and *Teutloporella herculea*) and foraminifera (*Gaudryina* sp., *Glomospirella* sp., *Trochammina* sp., *Aulotortus friedli* and *Agathammina austroalpina*). The dasycladaleans *Clypeina besici*, *Poikiloporella duplicata*, *Physoporella jomdaensis* indicate a Cordevolian age (Jul1/l).

Whereas very shallow subtidal deposition is indicated by peloidal grapestones, stromatolitic bindstones and loferites indicate inter- to supratidal conditions. Within thrse facies, fragments of porostromate algae are fairly common. The foraminifer *Turriglomina mesotriassic*a, characteristic for these limestones, may have thrived in shallow depressions within the lagoon.

1. Einleitung

Trotz zahlreicher Untersuchungen triassischer Sedimente und speziell der Karbonatplattformen gibt es nur wenig neuere Literatur, die sich mit der Stratigraphie und Mikropaläontologie der Mitteltrias der NKA beschäftigt.

Eine erste umfassende Kartierung im Karwendelgebirge erfolgte bereits von Ampferer & Hammer (1899), und Ampferer (1903). Von Ampferer wurde zum ersten Mal der Deckenbau angesprochen, in dem er 1911 bereits Inntaldecke und Lechtaldecke beschrieb. Weitere Bearbeitungen im Karwendelgebirge erfolgten unter anderem von Ott (1967, 1972), Sarnthein (1968), Kubanek (1969), Mostler (1972), Bechstädt & Mostler (1974,1976), Frisch (1975), Resch (1977,1979), Donofrio et.al (1979), Heissel (1978, 1989), Brandner & Resch (1981), Eisbacher & Brandner (1995), Brandner & Poleschinski (1996), Rüffer (1995) und Rüffer & Zamparelli (1997).

Die vorliegende Arbeit stellt einen Teil der Ergebnisse der Diplomarbeit der Autorin vor. Zielsetzungen der Diplomarbeit waren eine Untersuchung des unmittelbar nördlich von Innsbruck gelegenen Teils des Karwendelgebirges nach modernen stratigraphischen, strukturgeologischen und mikropaläontologischen Methoden sowie eine Einteilung in lithostratigraphische Formationen. In der Lagunenfazies der Wettersteinkalk-Formation konnten zwei neue Arten bestimmt werden, die Foraminifere *Austrocolomia carinata* und die Dasycladacee *Probolocuspis aculeata*.

Methoden

Kartiert wurde im Zeitraum von 2000-2004 im Maßstab 1:10000 und 1:5000. Als Kartengrundlage dienten die vergrößerten ÖK- Karten (Blatt 118-Raum Innsbruck und Blatt 117, 1:25000) und die Alpenvereinskarte Karwendelgebirge (Westliches Blatt 1:25000). Lokalitätsnamen beziehen sich auf ÖK und Alpenvereinskarte.

Im Gelände wurden ~ 190 Proben gesammelt, davon 41 Proben aus den Profilen. Die daraus resultierenden 211 Karbonatschliffe wurden mit einem Durchlichtmikroskop der Marke Wild (M5-47895) untersucht. Zusätzlich wurden einige der Proben (Reifling- und Steinalm-Formation) mit Essigsäure angesetzt um Conodonten und Foraminiferen aus den Säurerückständen zu gewinnen.

Die Differenzierung der Faziestypen erfolgte hauptsächlich aus eigenen Daten und in Anlehnung an Brandner & Resch (1981), Rüffer & Zamparelli (1997) und Wilson (1975). Die Faziestypen C1-C3 der Wettersteinkalk-Formation beziehen sich ausschließlich auf die im Zuge der Diplomarbeit gemachten Dünnschliffe. Auf weitere, in der Wettersteinkalk-Formation vorkommende Faziestypen wird hier nicht eingegangen.

2. Geographisch-geologische Übersicht

Das Arbeitsgebiet befindet sich direkt nördlich von Innsbruck an den Hängen der Nordkette. Der Gebirgszug der Nordkette gehört geographisch gesehen zum Karwendelgebierge, welches die größte Gebirgsgruppe der Nördlichen Kalkalpen darstellt. Die Inntalkette (auch Nordkette wegen ihrer Lage nördlich von Innsbruck) ist die kürzeste von vier Hauptketten des Karwendelgebirges und bildet dessen Südrand. Sie stellt auch die Südgrenze der NKA dar und ist im Süden zum Innsbrucker Quarzphyllit der Grauwackenzone, der die ursprüngliche geologische Unterlage bildete, durch das jungtertiäre, sinistrale Inntalscherungssystem begrenzt. Die im Rahmen der Diplomarbeit untersuchte Abfolge ist Teil des permomesozoischen Sedimentstapels der oberostalpinen Inntaldecke (Tirolikum), mit Ausbildung der Mittel-Trias, insbesondere den Reichenhaller Schichten, der Virgloria-Fm., Steinalm-Fm., Reifling-Fm. und der Wettersteinkalk-Fm.

3. Stratigraphie und Mikropaläontologie

3.1. Steinalm-Formation

3.1.1. Lithologie

Die basale Grenze des Steinalmkalkes lässt sich über einer 3-4 m mächtigen, ockerfarbenen Wurstelkalkabfolge der Virgloria-Formation (Markerhorizont), bzw. mit dem ersten Einsetzen einer ca. 1-2 m mächtigen Kalkbank der Steinalm-Formation ziehen.

Die darüber folgenden Gesteine der Steinalm-Formation weichen von ihrer herkömmlichen lithologischen Beschrei - bung in der Literatur ab (unter anderem Tollmann, 1976) und zeigen sich weitaus vielfältiger. Neben den typischen hell- bis mittelgrauen, z.T. dolomitischen, dasycladaceen-führenden Kalken treten im Arbeitsgebiet überwiegend dunkle Gesteinstypen mit unterschiedlichem Fossilgehalt auf.

Die Entstehung dieser Fazies hängt primär mit der Geometrie des Sedimentationsraumes, bzw. mit der Ablagerungstiefe zusammen. Es handelt sich im Westen um einen Flachwasserbereich, der, vermutlich durch eine kleine Hochzone getrennt, entlang einer flachen Rampe in eine Depression im Osten übergeht (Abb. 3).

Aus dem Gebiet Reutte und Mieminger Gebirge ist dieser Faziesübergang bekannt (Mostler, 1972). Algenreiche Flachstwassergebiete (Mieminger Gebirge) wechseln lateral mit Ablagerungsbereichen mit einer Wassertiefe bis zu etwa 80 m (Reutte) (Mostler, 1972). Diese unterschiedlichen faziellen Bereiche spiegeln sich auch in den stark schwankenden Mächtigkeiten der einzelnen Profile wider (Abb. 4).

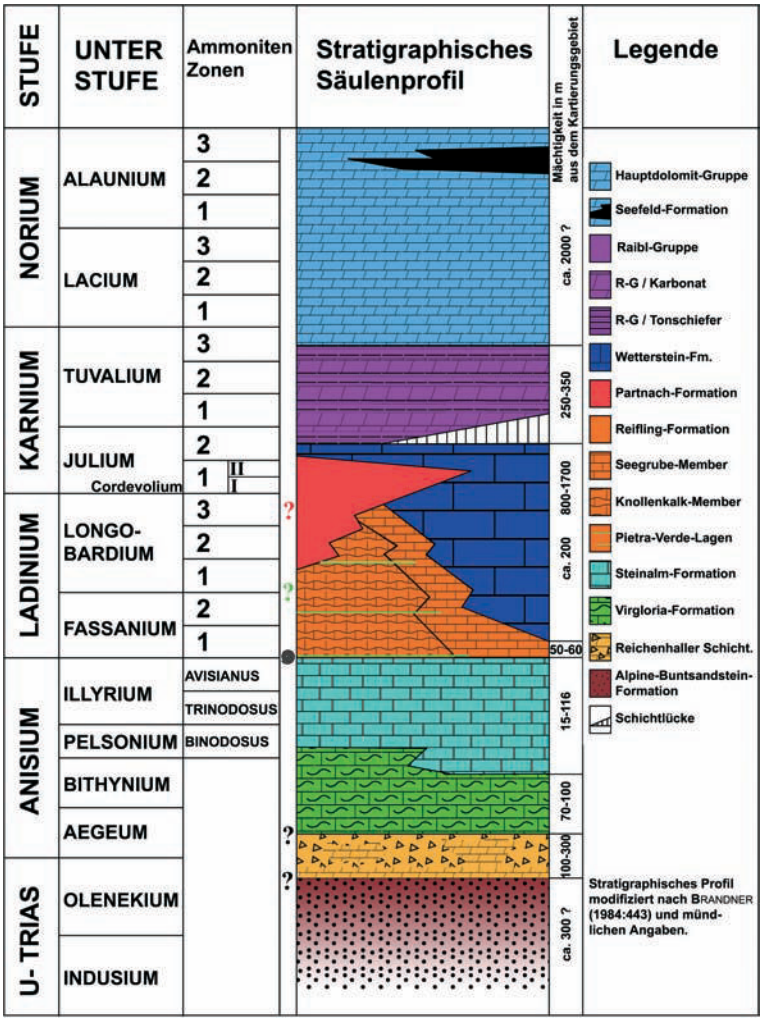

Abb. 2: Stratigraphisches Säulenprofil. Lithostratigraphische Übersicht der mitteltriassischen Formationen. aus Nittel 2004

Fig. 2: Stratigraphic column. Lithostratigraphical overview of the middle Triassic formations.

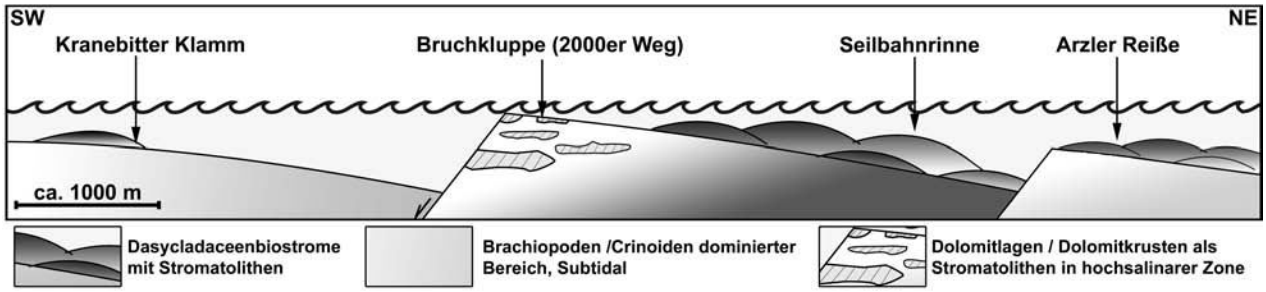

Abb.3 : Schematische, geomorphologische Darstellung des Ablagerungsraumes der Steinalm-Formation vor der Ablagerung des ersten Encrinithorizontes.

Fig. 3: Schematical, geomorphological display of the deposition area of the Steinalm formation.

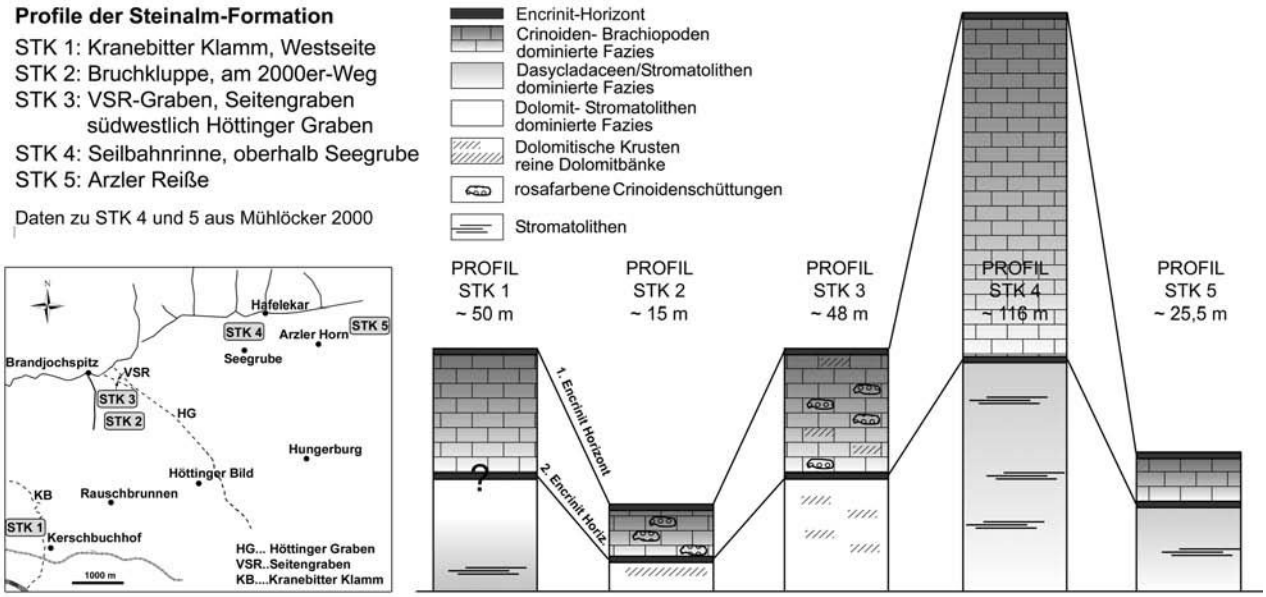

Abb. 4: Profile STK1-5, Steinalm-Formation. Lage der Profile STK1-5. Der Korrelationshorizont an der Basis der Profile ist mit der Überlagerung der Virgloria-Formation definiert.

Fig. 4: Section STK1-5, Steinalm-formation. Location of section STK1-5. Correlation-horizon at the base is definated by the overlap of the Virgloria-formation.

So kann man die Gesteine der Steinalm-Formation in eine von Stromatolithen dominierte Flachwasserfazies, eine Fazies aus Dasycladaceen - biostromen und in eine Brachiopoden- Crinoiden-dominierte neritische Fazies unterteilen, wie es auch schon von Sarnthein (1965) erwähnt wird.

Durch eine rasche Zunahme der Wassertiefe kommt es in allen Faziesbereichen zur Ablagerung des ersten Encrinithorizontes. Darüber folgen im Gebiet Arzl bis Zirl nur noch Crinoiden-Brachiopoden- dominierte Ablagerungen. Diese Entwicklung hält solange an, bis durch einen erneuten Meeresspiegelanstieg die Steinalmplattform endgültig ertrinkt und mit einem zweiten Encrinithorizont die Reiflinger Knollenkalke bzw. Bankkalke einleitet.

Dolomite/Flachwasserbereich

Die Flachwassergebiete sind vor allem durch das Auftreten von Dolomitbänken die teilweise Stromatolithen führen gekennzeichnet. Die Dolomit-reichen Partien treten im Arbeitsgebiet vor allem in Form von eingeschalteten Dolomitbänken und dolomitischen Kalken mit dolomitischen Krusten und auswitternden Dolomitknollen auf, wie sie auch schon von Frisch (1975) und Sarnthein (1965) beschrieben wurden. Die dolomitischen, teilweise sekundär auftretenden Krusten, Knollen und „Knauern" zeigen meist eine mausgraue bis leicht rosarote Verwitterungsfarbe. Sie sind im Arbeitsgebiet stets unterhalb des ersten Encrinithorizontes zu finden. Dies zeichnet sich auch in den Profilen von Frisch (1975), aufgenommen in der Lechtaldecke und Inntaldecke westlich von Innsbruck (zwischen Ehrwald und Garmisch, zwischen Scharnitz und Mittenwald, und Reutte) ab. Stromatolithen mit deutlichen LF-Strukturen waren im Arbeitsgebiet nur in der Kranebitter Klamm an der Basis der Steinalm-Formation aufgeschlossen. Dominierend sind aber Stromatolithen in Form von käsig, kavernösen, dolomitischen Krusten. Auch Sarnthein (1965) interpretiert diese Formen, nach der Arbeit von Logan et al. (1964), als Stromatolithenrasen, die in einem sehr geschützten, hochsalinen Ablagerungsraum, mit periodischer Trockenlegung und Bewässerung durch Gezeitenfluten gewachsen sind. Die durch das Milieu bedingte verringerte Sedimentation erklärt auch die geringe Mächtigkeit in diesem Abschnitt (Minimum mit ca. 5m, siehe Abb.4, Profil STK 2)

Dasycladaceen-Biostrome

Die Dasycladaceen-Biostrome treten nur im östlich ans Untersuchungsgebiet angrenzenden Gebiet auf, wo sie im Profil Seilbahnrinne (Mühlöcker, 2000) mit einer Mächtigkeit von 45 m ihr Maximum (im Bezug auf das Gebiet Zirl bis Arzl) erreicht haben. Bereits in der östlicher gelegenen „Arzler Reiße" beträgt ihre Mächtigkeit nur noch ca. 17 m. Im Arbeitsgebiet westlich davon sind nur noch aufgearbeitete und eingeschwemmte Reste dieser Biostrome in Form von Dasycladaceenbruchstücken zu finden. Es handelt sich bei den Biostromen um wechselnde Faunengemeinschaften von kalkabscheidenden Grünalgen, Schwämmen, Korallen,

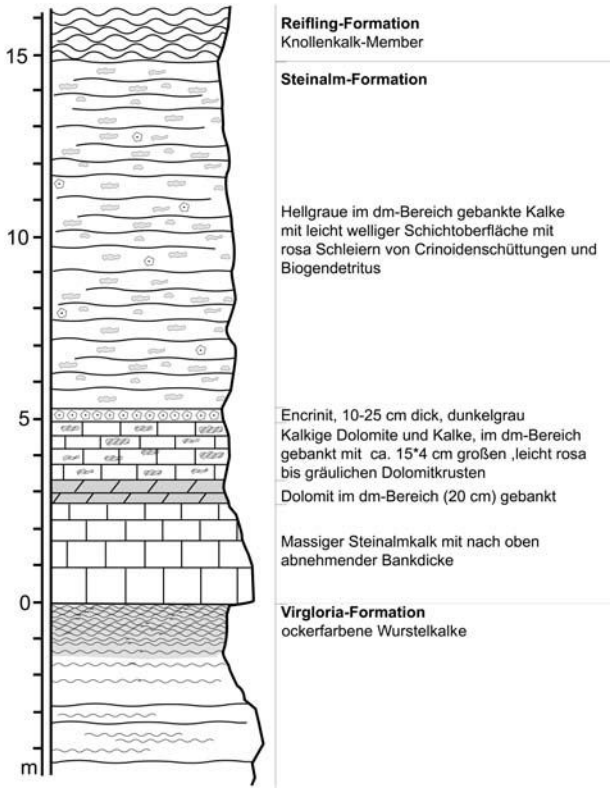

Abb. 5: Profil STK2, Steinalm-Formation, in der Bruchkluppe am 2000er Weg (südöstlich des Höttinger Grabens).

Fig. 5: Section STK2, Steinalm-formation, at Bruchkluppe on "2000er Way" (southeast of Höttinger Graben).

Hydrozoen, Bryozoen, Mollusken und Crinoiden, die alle ein gut durchlüftetes und durchlichtetes Wasser benötigen (Sarnthein,1966).

In den dasycladaceenreichen Gesteinen (Abb. 4, Profil STK 4) sind des öfteren Stromatolithen eingeschaltet, die im Arbeitsgebiet aber nur spärlich vertreten sind. Die Stromatolithen weisen auf eine intertidale Ablagerung hin.

Fazies mit Crinoiden und Brachiopoden

Im Arbeitsgebiet westlich des Höttinger Grabens sind bereits unterhalb des ersten Encrinithorizontes Crinoiden-Brachiopoden-dominierte Faziestypen zu finden, die auf etwas tieferes Wasser, also einen leichten Abhang Richtung Westen bzw. Südwesten hinweisen. Vor allem im oberen Bereich der Steinalm-Formation (oberhalb des ersten Encrinithorizontes) treten diese Lithotypen über den gesamten Faziesraum verbreitet auf. Auch hier zei-

gen sie wieder mit 70 m die größte Mächtigkeit im Profil Seilbahnrinne (Abb. 4, Profil STK 4). Im Profil Arzler Reiße im Osten (Abb. 4, Profil STK 5) beträgt ihre Mächtigkeit nur noch 8m. Auch nach Westen zeigt sich eine kontinuierliche Abnahme der Mächtigkeit, die ihr Minimum im Profil STK 2 (Abb. 4) mit ca. 5-7 m erreicht. Weiter nach Westen, in Richtung Kranebitter Klamm scheint die Mächtigkeit wieder anzusteigen (genaue Angaben sind aufgrund der unsicheren Lage des ersten Encrinithorizontes im Profil Kranebitter Klamm nicht möglich). Auch das Aussehen der Gesteine ändert sich Richtung Westen. Die im Bereich der Profile STK 2-3 so typischen dm-gebankten Kalke mit den rosafarbenen Crinoidenschüttungen an den Schichtoberflächen fehlen im Westen, im Gebiet der Kranebitter Klamm völlig, wobei sich aber der Fossilinhalt nicht ändert. Die Mächtigkeitsunterschiede sind vermutlich auch durch den Ausfall der Kalkalgen-Karbonatproduktion bedingt.

Am Top der Steinalm-Formation, in den höchsten Teilen der Brachiopoden-Crinoiden dominierten Kalke, vollzieht sich innerhalb der letzten Bank ein markanter Fazieswechsel, wie er schon von Bechstädt & Mostler (1974) beschrieben wurde. Charakteristisch ist das vermehrte Auftreten von Glaukonit und Filamenten gegenüber den zuvor massenhaft vorhandenen Crinoiden des Encrinithorizontes. Glaukonit tritt in Form von einzelnen Körnern und Foraminiferen-Steinkernen im Säurerückstand, im Dünnschliff in Form von gerundeten Komponenten, und als authigene Bildung fein verteilt in der schlammigen Matrix auf (Tafel I, Fig. 2), was auf eine marine Ablagerung in eher geringer Wassertiefe bei stark verminderter Sedimentationsrate schließen lässt (Amorosi 1993). Da Glaukonit sowohl am Top der Steinalm-Formation als auch an der Basis der Reifling-Formation auftritt, bildet dieser Transgressionshorizont die Basis der folgenden Reifling-Formation.

3.1.2. Lithotypen und Fossilführung

Faziestyp 1: Dasycladaceenkalke

Auch Tollmann (1976) erwähnt die für den Steinalmkalk typischen anisischen Dasycladaceen, die als Fragmente im Profil Kranebitter Klamm-West und oberhalb der Klamm, am Bockgufel auftreten. Es handelt sich dabei überwiegend um *Physoporella-Oligoporella* Arten. Diese Dasycladaceen-Arten zeigen eine Verbreitung von Unteranis bis Ende Unterillyr, wobei die Untergrenze faziesbedingt und nicht altersbedingt ist (Tollmann, 1976).

Über 70% der Komponenten in den Pack-Wackestones werden aus Dasycladaceenschutt von *Physoporella dissita, Physoporella pauciforata pauciforata, Physoporella pauciforata sulcata, Physoporella minutula, Oligoporella* sp., *Aciculella bacillum* und *Favoporella annulata* gebildet. Weiters treten neben kurzen Filamenten vereinzelt dickschalige Ostracoden, sowie vereinzelte Foraminiferen wie *Frondicularia woodwardi, Glomospirella* sp. und *Meandrospira dinarica*, selten Gastropoden, Schwammspiculae und Muschelbruchstücke auf. Charakteristisch sind auch die mit Blockzement verfüllten stromatactoiden Hohlräume.

Faziestyp 2: Crinoiden-Echiniden dominierte Kalke

Zur Ablagerung reiner „Encrinite" und von Crinoiden-dominierter Faziestypen kommt es vor allem bei Transgression rasch absinkender Schelfzonen. Frisch (1975) deutet die Anhäufung von Crinoidendetritus am Top der Steinalm-Formation (mittlere Gesteinsserie) als möglichen Spülsaum.

2a: Crinoiden-dominierte Mud-bis Packstones

Vorwiegend handelt es sich um bioklastische Wacke-bis Packstones, die teilweise bioturbat sein können. Der Großteil der Komponenten wird von Crinoiden wie *Encrinus liliformis* neben Echinidenstacheln, Ophiurenwirbeln und anderem Echinodermendetritus gebildet. Die teilweise auftretenden Anbohrungen der Crinoidenstielglieder deuten auf ein längeres Freiliegen an der Sedimentoberfläche hin. Seltener treten Ostracoden, Gastropoden, Brachiopoden wie *Decurtella decurtata* und *Tetractinella trigonella*, Schalenreste, Foraminiferen und vereinzelt Filamente auf. Häufige Foraminiferen sind Lageniden, *Frondicularia* sp., *Glomospirella* sp., *Austrocolomia* sp., *Trochammina* sp., *Gaudryina* sp. und *Ophtalmidium abriolense*, die auf tieferes Wasser hinweist.

2b: Crinoiden-dominierte Onkoid-Packstones

Der Kern der Onkoide wird fast ausschließlich von Crinoiden und Echinidenresten, darunter überwiegend Echinidenstacheln und Ophiurenreste

gebildet. Die größten der Crinoidenfragmente, *Encrinus liliformis*, sind nicht immer onkoidisch umkrustet und zeigen häufig eine randliche Anlösung. Vereinzelt treten als Kern auch Spirorbis, Ostracoden, Brachiopoden wie *Coenotyris* sp. und Foraminiferen wie *Austrocolomia* sp., *Dentalina* sp., *Meandrospira dinarica* und *Frondicularia* sp. auf. Die Matrix ist ausgewaschen, was auf Ablagerung in einem mäßig hochenergetischen Bereich hindeutet.

Faziestyp 3: gemischt bioklastische Fazies

3a: Bioklastische Pack-bis Grainstones

In den teilweise ausgewaschenen Packstones findet man als Hauptkomponenten Brachiopoden, wie *Decurtella decurtata* und *Tetractinella trigonella*, die hierin häufiger auftreten als in den anderen brachiopodenführenden Faziestypen (2a, 2b). Ebenso kommen Gastropoden, Spirorbiden und Ostracoden häufiger vor. Auch ein vermehrtes Auftreten von Foraminiferen ist festzustellen: *Ophtalmidium abriolense, Ophtalmidium ubeyliense, Turriglomina mesotriassica,* die alle für tieferes Wasser sprechen, *Frondicularia* sp. und *Tolypam - mina* sp.. Seltener findet man *Tubiphytes* sp., Filamente und Dasycladaceenfragmente. Crinoiden, wie *Encrinus liliformis* und Echinidenreste treten an Häufigkeit stark zurück, Onkoide und Ooide treten nur sehr vereinzelt auf.

Charakteristisch sind auch die mit spätdiagenetischen Blockzementen verfüllten stromatactoiden Hohlräume.

3b: Bioklastisch dominierte Onkoid-Pack-bis Grainstones

Fast alle Komponenten der Pack- bis Grainstones sind onkoidisch umkrustet. Als Kerne dienen Brachiopoden, Spirorbiden, Crinoiden, Echinidenstacheln, Gastropoden, Ostracoden und selten Bryozoen in wechselnder Häufigkeit. Generell gilt, dass keine der Gattungen eine vorherrschende Rolle spielt. Auch Foraminiferen sind relativ stark vertreten, mit: *Frondicularia sp., Meandrospira dinarica,* als Leitfossil fürs Untere Anis und die Steinalm-Formation, weiters *Meandrospiranella* sp., *Gaudryina* sp., *Ophtalmidium abriolense, Dentalina* sp., *Tolypammina* sp., Duostominidae und Lageniden. Vereinzelt sind auch Ooide zu finden. Die Matrix ist häufig dolomitisiert, während die Intrapartikelporen in den ausgewaschenen Bereichen durch spätdiagenetischen Blockzement charakterisiert sind, der gegenüber frühen, isopachen, radiaxialen Zementen dominiert.

Faziestyp 4: Pelsparite

In den von Peloiden dominierten Wacke-bis Grainstones treten vereinzelt Crinoiden, Gastropoden, Dasycladaceenfragmente, Ostracoden, Ooide und folgende Foraminiferen auf: *Pilammina semiplana, Glomospirella* sp., *Glomospira* sp., *Turriglomina mesotriassica,* die ein Hinweis für tieferes Wasser ist, und *Scherochorella* sp.. Die Pelsparite zeigen keine Gradierung oder Sortierung und sind meist stark umkristallisiert und dolomitisiert. Vereinzelt tritt Glaukonit auf.

Dieser eher selten als Einschaltung in den Karbonaten der Steinalm-Formation auftretende Faziestyp spricht für offenere marine Bedingungen. (Rüffer & Zamparelli, 1997).

Faziestyp 5: Filament-Peloidpackstones

Dieser Faziestyp ist durch das vorherrschende Auftreten von Schalenbruchstücken, Peloiden und untergeordnet Radiolarien und Filamenten charakterisiert. Vereinzelt kommen Crinoiden, *Girvanella* sp., Ostracoden und die Foraminiferen *Turriglomina mesotriassica* und *Dentalina* sp. vor. Dieser Faziestyp findet sich im Grenzbereich Steinalm-Formation/ Reifling-Formation und weist fast immer Glaukonit auf.

3.1.3. Ablagerungsraum

Der Steinalmkalk stellt insgesamt die erste Karbonatplattform der Trias der NKA dar. Die gesamte Fauna weist auf Lebensbedingungen in einem sauerstoffreichen, warmen, gut durchlüfteten Wasser hin. Die rasche Zunahme der Bankmächtigkeit bis hin zur Massigkeit über den Wurstelkalken der Virgloria-Formation dürfte die Folge einer zunehmenden Absenkungsgeschwindigkeit des Meeresbodens sein, verbunden mit einer erhöhten Sedimentbildung und Anlieferung (Frisch, 1975).

Im flachen Rampenbereich sind stellenweise auch „Shallowing upward"-Sequenzen zu finden (Nittel, 2004).

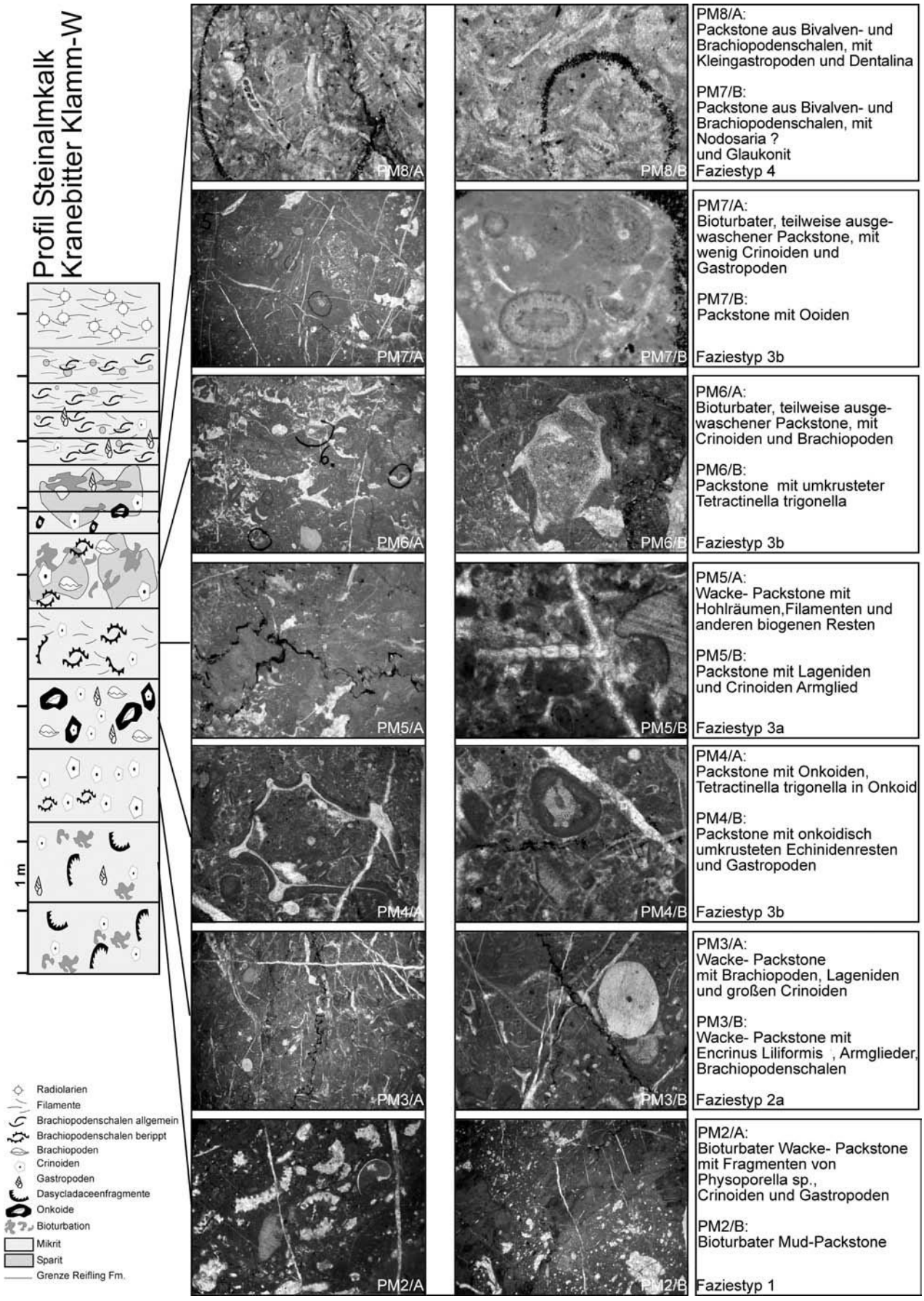
Profil Steinalmkalk
Kranebitter Klamm-W
1 m
PM8/A
PM8/B
PM8/A:
Packstone aus Bivalven- und Brachiopodenschalen, mit Kleingastropoden und Dentalina
PM7/B:
Packstone aus Bivalven- und Brachiopodenschalen, mit Nodosaria ?
und Glaukonit
Faziestyp 4
PM7/A
PM7/B
PM7/A:
Bioturbater, teilweise ausgewaschener Packstone, mit wenig Crinoiden und Gastropoden
PM7/B:
Packstone mit Ooiden
Faziestyp 3b
PM6/A
PM6/B
PM6/A:
Bioturbater, teilweise ausgewaschener Packstone, mit Crinoiden und Brachiopoden
PM6/B:
Packstone mit umkrusteter Tetractinella trigonella
Faziestyp 3b
PM5/A
PM5/B
PM5/A:
Wacke- Packstone mit Hohlräumen,Filamenten und anderen biogenen Resten
PM5/B:
Packstone mit Lageniden und Crinoiden Armglied
Faziestyp 3a
PM4/A
PM4/B
PM4/A:
Packstone mit Onkoiden, Tetractinella trigonella in Onkoid
PM4/B:
Packstone mit onkoidisch umkrusteten Echinidenresten und Gastropoden
Faziestyp 3b
PM3/A
PM3/B
PM3/A:
Wacke- Packstone mit Brachiopoden, Lageniden und großen Crinoiden
PM3/B:
Wacke- Packstone mit Encrinus Liliformis , Armglieder, Brachiopodenschalen
Faziestyp 2a
PM2/A
PM2/B
PM2/A:
Bioturbater Wacke- Packstone mit Fragmenten von Physoporella sp., Crinoiden und Gastropoden
PM2/B:
Bioturbater Mud-Packstone
Faziestyp 1
Radiolarien
Filamente
Brachiopodenschalen allgemein
Brachiopodenschalen berippt
Brachiopoden
Crinoiden
Gastropoden
Dasycladaceenfragmente
Onkoide
Bioturbation
Mikrit
Sparit
Grenze Reifling Fm.

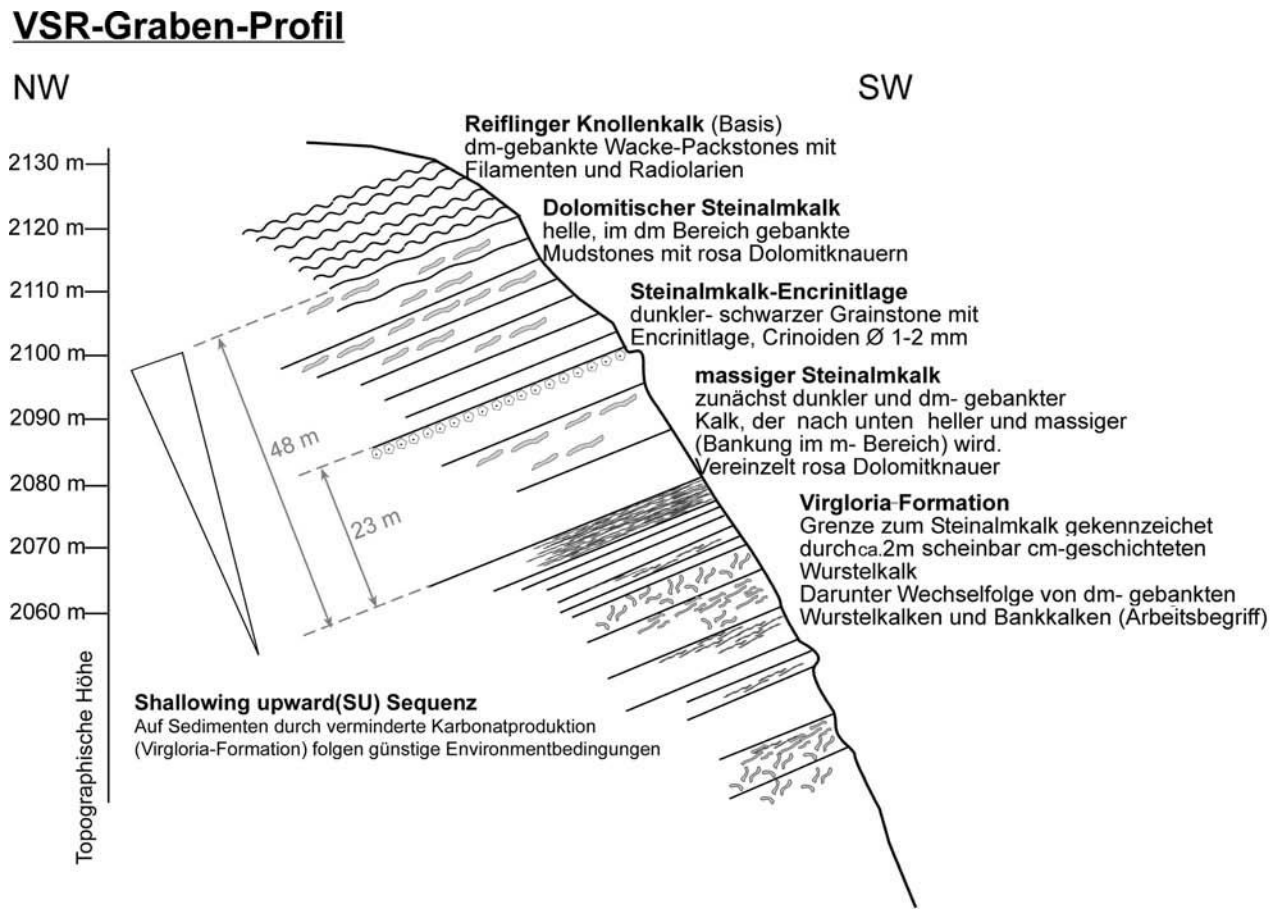

Abb. 7: Profil durch den VSR-Graben, westlich des Höttinger Grabens mit „Shallowing Upward"Sequenz.

Fig. 7: Section of "VSR-Graben", west of "Höttinger Graben" with shallowing upward sequence.

3.2. Reifling-Formation

3.2.1. Lithologie

Die Reiflinger Kalke im Typusprofil Großreifling umfassen Illyr (Trinodous-Zone) bis Cordevol (Tollmann, 1976).

Die Reifling-Formation setzt mit dem ersten Auftreten von filament- und radiolarienführenden Knollenkalken über den obersten Encriniten bzw. dem Crinoidenhorizont der Steinalm-Formation ein.

Im allgemeinen kann man die Gesteine der Reifling-Formation in ein Knollenkalk-Member und in ein Bankkalk-Member, welches der Seegrube-Einheit entspricht, unterteilen, die miteinander verzahnen und sich gegenseitig vollständig vertreten können (Mühlöcker 2000). Weiters ist die Reifling-Formation durch centimeter-dezimeter mächtigen Einschaltungen von grünen bis grün-rot-gelblichen Tuffen und Tuffiten, den sogenannten "pietra verde" Lagen, die in drei Horizonte unterteilt werden können, charakterisiert. Eine Besonderheit stellt ein lokal auftretender Ammonitenhorizont, der meist mit unterlagernden, auffallend großen Exemplaren von *Encrinus liliformis,* vergesellschaftet ist, dar.

3.2.1.1. Knollenkalk-Member

Die durchschnittlich 10-30 cm dicken Bänke der Knollenkalke zeigen meist eine mittel- bis braun-

Abb. 6: Profil STK1, Steinalm-Formation. Dargestellt sind die obersten 11 Profilmeter bis zur Grenze Reifling-Formation aus dem Profil STK1 (Kranebitter Klamm-West) mit Abbildungen zu den Faziestypen.

Fig. 6: Section STK1, Steinalm-formation. The first 11 profile meters are plotted with picutres of the facies types.

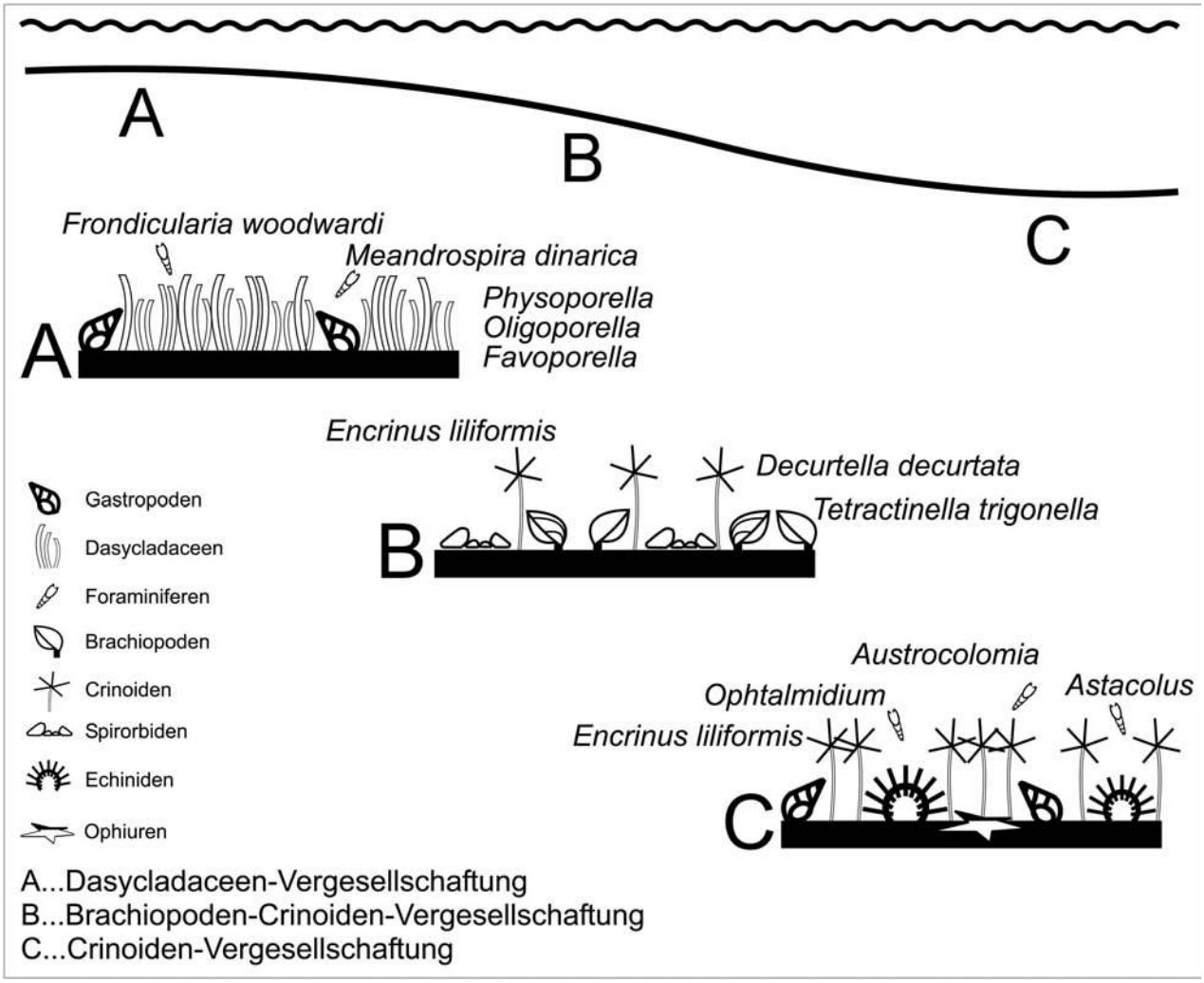

Abb. 8: Schematisches Ablagerungsmodell der Steinalm-Formation mit den wichtigsten Fossilvergesellschaftungen. (Alle dargestellten Foraminiferen sind benthische Formen).

Fig. 8: Schematical deposition modell of Steinalm-formation with the most important fossile associations.Abb. 8: Schematisches Ablagerungsmodell der Steinalm-Formation mit den wichtigsten Fossilvergesellschaftungen. (Alle dargestellten Foraminiferen sind benthische Formen).

graue Farbe, können aber vereinzelt auch grünlich bis rötlich (siehe „Schusterbergkalk") sein. Sie weisen wellige bis knollige, höckerige Schichtoberflächen und Unterseiten auf, die meist von gelblichen, rötlichen oder vereinzelt grünlichen Tonbelägen überzogen sind. Teilweise kann man eine Fortsetzung der Knollen auch innerhalb der einzelnen Bänke beobachten. Typisch für die Knollenkalke ist ein wechselnder Hornsteingehalt, der in Form von Knauern, die sich aber auch zu ganzen Bändern verbinden können, auftritt.

Knollenkalkbildung

Zur Knollenkalkbildung der Reiflinger Kalke gibt es unterschiedliche Theorien. In Anlehnung an Hollmann (1962, 1964) sieht Sarnthein (1965,1966) die Knollenkalkbildung in engem Zusammenhang mit Subsolution und Omission, die durch die CO_2-Zufuhr des „pietra verde Vulkanismus" begünstigt wird. Kubanek (1968/69) weist darauf hin, daß die Gesteine als „Flaser- Knollenkalke" (nach Definition Gründel & Rössner 1963) anzusprechen sind und

nicht als Subsolutionsgefüge. Weiters führt er einige Hinweise an, die eindeutig die Drucklösung und Flaserung zeigen (Kubanek, 1969). Auch in den Dünnschliffen aus dem Untersuchungsgebiet konnte die Autorin eine Begrenzung der einzelnen Knollen durch Stylolithen und eine zur Flaserung parallele Einregelung der Fossilien feststellen, was Kubaneks Theorien unterstützt.

Weiters führt Kubanek (1969) für die Entstehung der Flaser-Knollenkalke Sedimentinhomogenitäten an, unter anderem bedingt durch Durchwühlung (unterschiedliche Porenzementation). Wühlgefüge treten in den Knollen–kalken in Form von unscharf begrenzten Nestern und fleckenartigen Unterschieden in Biogenzusammensetzung und Packungsdichte auf, was ein Hinweis für Bioturbation in noch weichem Sediment ist. Da die Bioturbation auch in nicht-knolligen Bereichen, ohne Drucklösungsstrukturen auftritt kann sie nur eine untergeordnete Rolle bei der Entstehung der Knollengefüge spielen (Bechstädt & Mostler 1974).

Hornsteinentstehung

Miller (1962) sieht die Herkunft der Kieselsäure als fraglich, haltet aber eine Anlieferung durch den Vulkanismus als wahrscheinlich. Dieser Meinung schließen sich auch Sarnthein (1965), Frisch (1968), Kobel (1969) und Kubanek (1969) an. Mostler (1976) hingegen sieht eine Verbindung zu den radiolarienreichen Filamentmikriten, an die die Hornsteinknauern gebunden sind. Auch im untersuchten Gebiet sind fast alle, der teilweise stark angehäuften Radiolarien vollständig in Calcit umgewandelt. Dies führt zu einem relativ großen Kieselsäureangebot, das durchaus zur Bildung der Hornsteinknauern ausgereicht haben könnte.

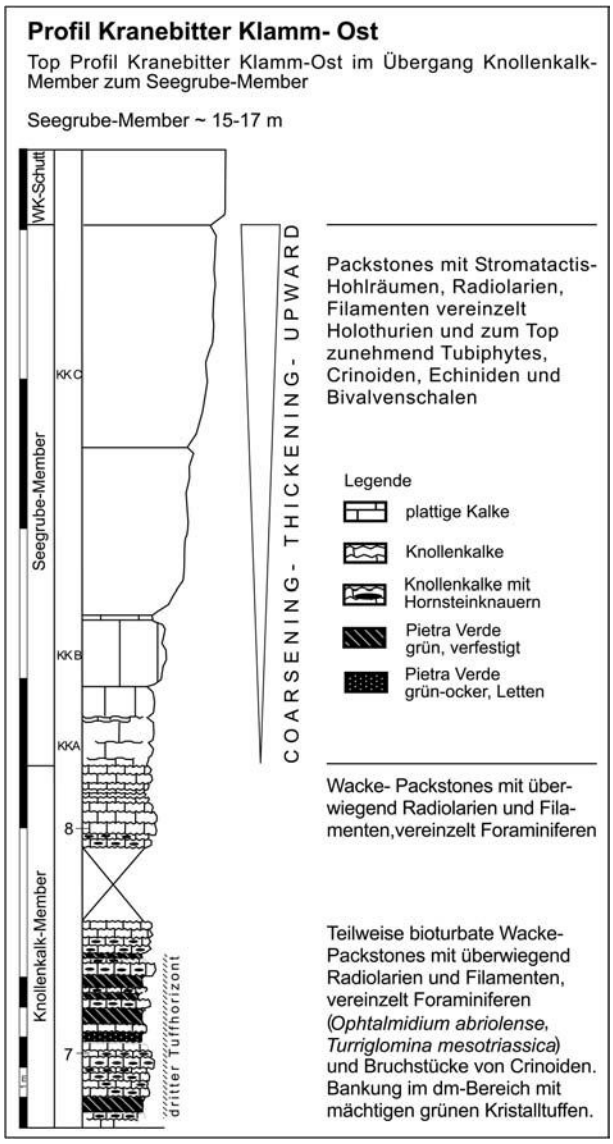

Abb. 9: Top Profil Kranebitter Klamm Ost im Übergang Knollenkalk- Seegrube-Einheit.

Fig. 9: Top section "Kranebitter Klamm East" in the passage Knollenkalk- Seegrube unit.

3.2.1.2. Seegrube-Einheit (= Reiflinger Bankkalke)

Der Begriff „Seegrube-Einheit" wurde eingeführt (erstmals in Mühlöcker 2000) um Verwechslungen mit den Reiflinger Bankkalken des Typusprofils in Großreifling zu vermeiden. Fälschlicherweise wurde letzterer Begriff auf die gebankte Abfolge der Reifling-Formation mit Riffdetritusschüttungen übertragen. Der untere Bereich der Seegrube-Einheit ist - mikrofaziell gesehen - mit Filament-Radiolarien-Mikriten dem Knollenkalk-Member noch sehr ähnlich. Nach oben immer häufiger einsetzende Calciturbidite verzahnen mit der Hintergrundsedimentation. Der Übergangsbereich vom ersten Auftreten der Rifforganismen und dem letzten Auftreten von Filamenten beträgt im Profil Seegrube 35 m (Mühlöcker, 2000) und kann laut Meischner (1964) bis zu 100 m mächtig werden.

Die Bankkalke der Seegrube-Einheit zeigen gegenüber dem Knollenkalk-Member nur noch eine leicht wellige Schichtoberseite bzw. vollkommen planare Flächen aufgrund der Sedimentation des Riffdetritus als Calciturbidite. Ihre Bankmächtigkeit

reicht von 10-50 cm, wobei die mächtigeren Bänke mit einer durchschnittlichen Dicke von 30-50 cm überwiegen. Im Profil Kranebitter Klamm und Karwendelbahn erreicht die Mächtigkeit der einzelnen Bänke ihr Maximum mit ca. 7 m. Die maximale Mächtigkeit erreicht das Seegrube-Einheit mit 80 m in der Seilbahnrinne, wobei das erste Einsetzen von gröberem Riffdetritus nach 35 m erfolgt (Mühlöcker, 2000). Nach Westen hin nimmt die Mächtigkeit ab bis zum Profil Karwendelbahn, wo die im m-Bereich gebankte Seegrube-Einheit nur noch eine Mächtigkeit von ca. 15 m hat.

Aufgrund der Ammonitenfunde im Seegrube-Einheit im Gebiet östlich des Höttinger Grabens konnte ein Einsetzen der Sedimentation im Oberillyr (Avisianuszone) festgestellt werden.

Die zunehmende Bankmächtigkeit und die zunehmende Größe der Komponenten zum Top des Members bzw. der Reifling-Formation hin spricht für eine „coarsening upward"(CU)- bzw. eine „thickening upward"-Abfolge (Abb. 7). Die Wassertiefe nimmt hierbei nach oben hin ab, da das Riff ins Becken progradiert.

Zum Ammonitenhorizont

Der Ammonitenhorizont, der teilweise die Basis der Reifling-Formation bildet, tritt nur lokal und vermehrt östlich des Höttinger Grabens auf. Im Arbeitsgebiet weisen nur überlieferte Funde auf das Vorhandensein des Ammoniten-Horizontes hin: im ehemaligen Steinbruch beim Kerschbuchhof, die Ammonitenbank beim Eingang zur Kranebitter Klamm (mündliche Mitteilung Brandner 2004), und ein großer Block aus der Brandjochrinne, in dem R. Oberhauser *Paraceratites trinodosus* und *Flexoptychites flexuosus* gefunden hat (mündlicher Mitteilung Mostler). Detaillierte Angaben dazu siehe Mühlöcker, 2000.

„Schusterbergkalk"

Die sogenannten Schusterbergkalke, Rotkalke in der Reifling-Formation, sind im Arbeitsgebiet nur spärlich aufgeschlossen. Im Gebiet östlich des Höttinger Grabens bis zur Arzler Reiße treten sie vermehrt auf. Mühlöcker (2000) beschreibt einerseits eine direkte Überlagerung des Steinalmkalkes, andererseits eine Überlagerung des Ammonitenhorizontes, der gegen Osten teilweise die Basis der Reiflinger Knollenkalke bildet. Lithologisch gesehen handelt es sich dabei um rötlich gefärbte Knollenkalke, die von dunkelroten Mergelschlieren über- und durchzogen sind und die teilweise eine Anhäufung an Radiolarien aufweisen. Ansonsten entsprechen die Schusterbergkalke in der Fossilführung dem herkömmlichen Knollenkalk-Member. In der Arzler Reiße erreichen sie eine max. Mächtigkeit von 4 m (Mühlöcker, 2000). Die Rotfärbung die durch das enthaltene Fe^{3+} hervorgerufen wird, dürfte auf eine verminderte Sedimentationsrate hindeuten. Zur Bildung von marinen Rotsedimenten ist ein geringer Gehalt an organischer Substanz im Sediment und das Fehlen von sulfatreduzierenden Bakterien nötig, damit das vorhandene Fe^{3+} nicht reduziert und als Pyrit gebunden werden kann. Deshalb werden von verschiedenen Autoren eine geringe Sedimentationsrate und O_2-haltiges Wasser am Meeresboden gefordert (Hinze & Meischner, 1968).

Pietra-Verde-Lagen

Die pietra verde lässt sich von ihrer Verteilung her grob in drei Horizonte einteilen. Der erste befindet sich ca. 1m über der Grenze zum Steinalmkalk und ist nur sehr geringmächtig (1-2 cm). Der zweite Horizont an der Basis des oberen Drittels der Formation besteht aus mehreren dünnen Lagen, die aus grünlichem bis ockerfarbenem Letten bestehen. Der dritte Horizont, im oberen Drittel der Formation besteht ebenfalls aus mehreren Lagen, wobei einzelne eine Mächtigkeit bis zu 50 cm zeigen können wie im Profil Kranebitter Klamm und im Profil Karwendelbahn.

Ehemals als vulkanoklastische Sand- Silt und Tonsteine abgelagert, treten die Pietra Verde Lagen heute als Tuffite und Kristalltuffe, auf. Sie sind Produkte eines sauren, rhyolithischen bis rhyodacitischen Vulkanismus. Aufgrund ihres Zirkongehaltes konnten diese Lagen, die ebenfalls in den Buchensteiner Schichten im Südalpin auftreten, datiert werden. Brack et.al (1996) konnte mit U/Pb Messungen an Einzelzirkonen die absolute Sedimentationsraten bzw. Progradationsrate des Schlernriffwachstums errechnen:

- Tc-Tuffit (drei Tufflagen im untersten Bereich der Knollenkalke)

(Basis Scedensis Zone): $241{,}2^{+0{,}8}/_{-0{,}6}$ Ma

- Basis mittleres Tuffitintervall (Basis Gredleri Zone): $238{,}8^{+0{,}5}/_{-0{,}2}$ Ma
- Oberes Tuffitniveau (Basis Archelaus Zone): $238{,}0^{+0{,}4}/_{-0{,}7}$ Ma

Diese drei Alter wurden durch die Datierung der in der Archelaus Zone folgenden Predazzo Granit-Intrusion mit einem Alter von $237.3^{+0}.4/_{-1.0}$ Ma zusätzlich korreliert (Brack et al., 1997)

Aufgrund ihrer Untersuchungen kommen Bechstädt & Mostler (1974) zum Schluß, dass die intermediären bis basischen Tuffe in den Südalpen, Gailtaler Alpen und in den Nördlichen Kalkalpen zeitgleich abgelagert wurden und zeitgleich im Illyr einsetzen, aber der mit der ladinischen Grabenbruchtektonik auftretende Vulkanismus wesentlich schwächer als jener in den Südtiroler Dolomiten ist (Brandner & Poleschinski, 1986). Der Nachweis für die Zeitgleichheit der Reiflinger Knollenkalke (NKA) und den dazu äquivalenten Buchensteiner Knollenkalken (Südalpen) erfolgte erst 1998 durch Gallet et al., mittels Paläomagnetismus.

3.2.2. Lithotypen und Fossilführung

A. Filament/Schill Packstones

Dieser an der Grenze zur Steinalm-Formation auftretende Faziestyp ist durch das Vorkommen von kurzen Filamenten in großer Dichte charakterisiert. Neben vereinzelt auftretenden Bivalvenschalen, Brachiopodenschalen und dickschaligen Ostracoden tritt hier der erste Glaukonit der Reifling-Formation auf. Weiters sind vereinzelt Foraminiferen wie *Pseudonodosaria* sp. und Echinidenreste und erste Radiolarien vertreten.

B. Bioturbate Mud- Packstones, Grainstones mit Radiolarien und Filamenten

Hauptkomponenten sind Radiolarien, Filamente, Brachiopodenschalen und dickschalige Ostracoden, mit einem maximalen Durchmesser von 1 mm. Sie kommen in unterschiedlicher Häufigkeit vor. Unter den eher spärlich auftretenden Foraminiferen sind *Turriglomina mesotriassica* und *Ophtalmidium abriolense* die häufigsten, seltener sind *Earlandia* sp., *Ichtyolaria* sp. und *Ophtalmidium ubeyliense*, die fast alle für tieferes Wasser sprechen.

Vereinzelt sind Intraklasten und Resedimente zu finden. Die knolligen Gefüge, die sich auch innerhalb der Dünnschliffe abbilden, zeigen zwischen den einzelnen Knollen Anlagerungen und Anhäufungen von Schill bzw. Filamenten, die meist auch eingeregelt sind.

Ein weiteres Charakteristikum ist die Schirm - porosität, die in diesem Fall immer eine aufrechte Lagerung anzeigt, ebenso wie die geopetal verfüllten Radiolarien.

C. Bioturbate Wacke-bis Packstones (ohne Radiolarien)

Neben den dominierenden Filamenten kommen Echinidenstacheln, Peloide, Ostracoden und vereinzelt *Tubiphytes* vor. Letzteres kann als erster Hinweis für die Nähe zum Riff gesehen werden. Häufige Foraminiferen sind *Ophtalmidium abriolense*, *Turriglomina mesotriassica*, *Nodosaria* sp. und selten *Turriglomina magna*.

Zusätzlich zu den fossilen Komponenten sind vereinzelt stromatactoide Hohlräume zu finden.

Fossilführung

Neben den typischen pelagischen Organismen wie Radiolarien und Filamenten findet man auch noch Foraminiferen, Conodonten, Holothurien-sklerite und bereichsweise Crinoiden.

In der Reifling-Formation treten Echinidenreste und Crinoiden gegenüber der Steinalm-Formation stark zurück. Sie kommen nur noch vereinzelt im Bereich über der Steinalmkalkgrenze und in den obersten Knollenkalken an der Grenze zur Seegrube-Einheit und zum Wettersteinkalk vor. Bei letzteren Vorkommen könnte sich um erste allodapische Schüttungen handeln, die Henrich (1983) mit besonders hohen Gehalten an Echinodermenschutt beschreibt. In den oberen Bereichen des Knollenkalk-Members treten auch häufiger wellige Filamente von Daonellen auf. Unter den nach oben hin zunehmenden Rifforganismen der Seegrube-Einheit tritt im Arbeitsgebiet überwiegend *Tubiphytes* auf. Die in der Reifling-Formation häufig vorkommende Foraminifere *Turriglomina mesotriassica* und das Vorkommen von Radiolarien weisen auf offen-marine (pelagische) Ablagerungsbedingungen hin.

3.2.3. Ablagerungsraum

Die meisten Autoren sehen die Bildungsbedingungen für die Reifling-Formation als hemipelagisch-epibathyal bis subeuxinisch (Tollmann, 1976). Die Sedimente der Seegrube-Einheit hingegen zei-

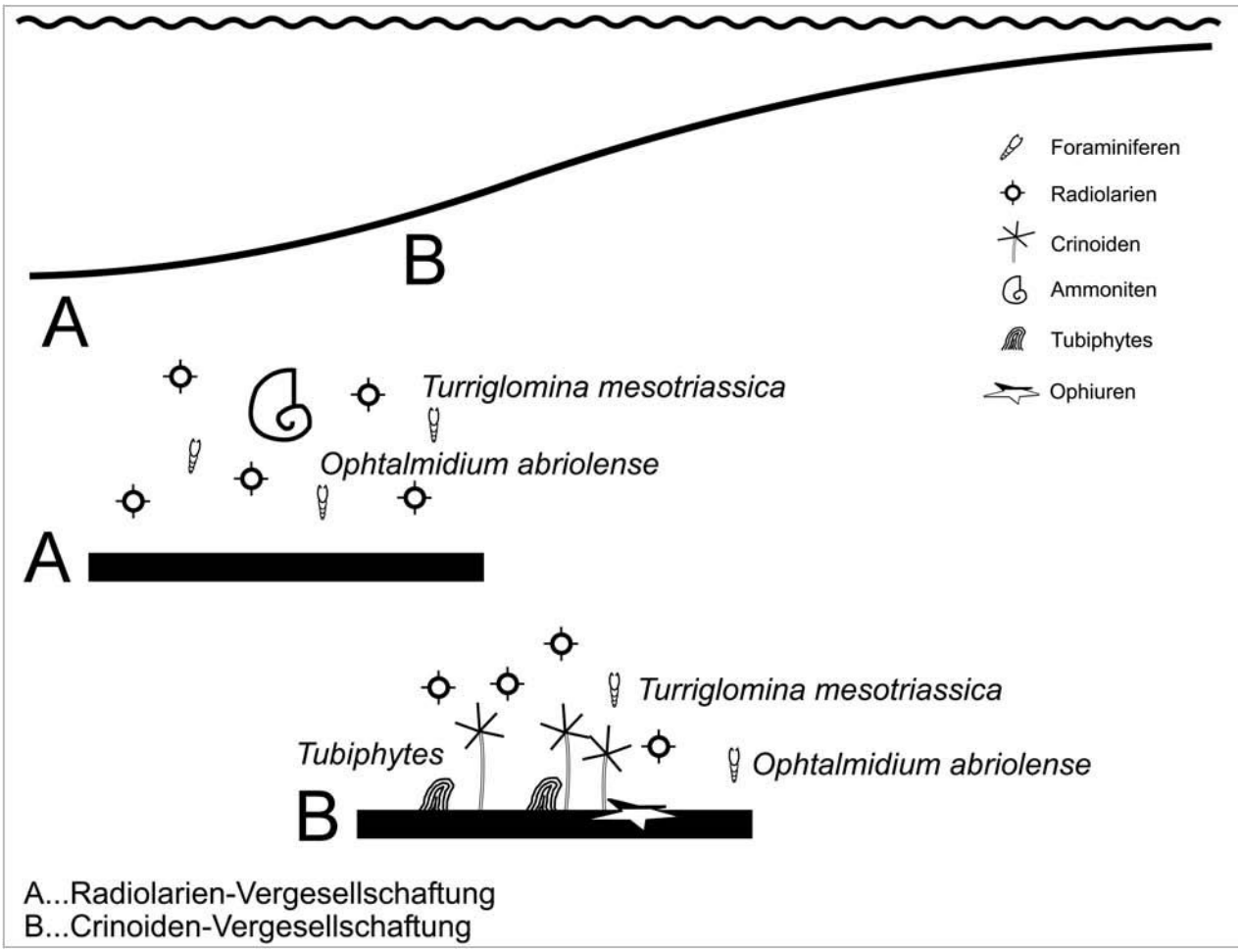

Abb. 10: Schematisches Ablagerungsmodell der Reifling-Formation mit den wichtigsten Fossilvergesellschaftungen. (Die Foraminifere *Turriglomina mesotriassica* ist nach Rettori, 1995, eine planktische Form, Ophtalmidium abriolense eine benthische Form).

Fig. 10: Schematical deposition modell of Reifling-formation with the most important fossile associations.

gen bereits einen Übergangsbereich zwischen dem Becken und dem Riffhang. Dies deutet sich durch gemeinsames Vorkommen von Filamenten, Radiolarien und Riffdetritus, der zum Top hin zunimmt, an.

Die Daten zur Wassertiefe sind in der Literatur sehr verschieden und lassen keine eindeutigen Angaben zu. Bechstädt & Brandner (1970) geben aufgrund von Glomospiren Funden einen ruhigen, schlammigen, etwa 30 m tiefen Sedimentationsraum an, während Bechstädt & Mostler (1974) aufgrund des massenhaften Auftretens von psychrosphärischen Ostracoden, eine Wassertiefe von 500 m und eine Ablagerung der Sedimente in einem riffnahen Becken annehmen. Die lithologisch ähnlich ausgebildeten Buchensteiner Knollenkalke in den Südalpen erreichen eine Wassertiefe von 800 m (Bosellini & Ferri 1980). Auch das Vorkommen von Radiolarien und Filamenten weist lediglich auf offen marine Bedingungen hin. Die Foraminiferen *Ophtalmidium abriolense* und *Turriglomina mesotriassica* geben zwar Hinweise auf tieferes Wasser, nicht aber über die genaue Wassertiefe.

3.3. Wettersteinkalk-Formation

3.3.1. Lithologie

Die Untergrenze der Wettersteinkalk-Formation wäre mit dem letzten Auftreten der Knollenkalke bzw. der Bankkalke der Seegrube-Einheit und dem ersten durchgehendem Einsetzen von riffschuttführenden Kalken zu ziehen. Aufgrund der

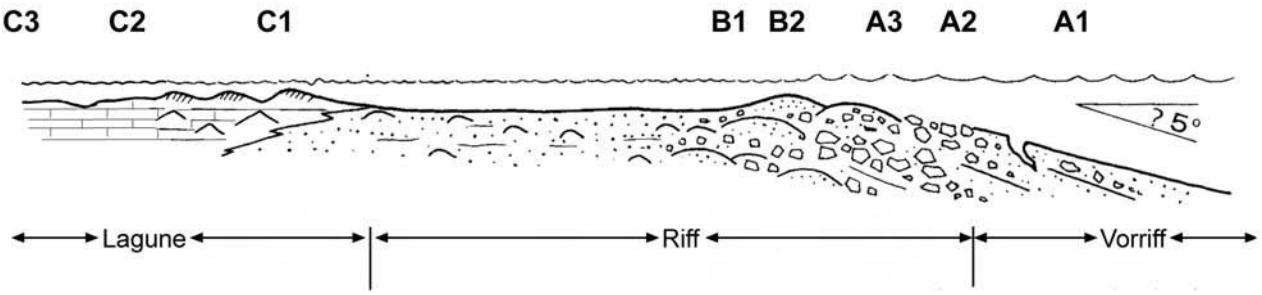

Abb. 11: Schematisches Profil durch den Hafelekar Riffkomplex und die Verteilung der Faziestypen, modifiziert nach Brandner & Resch (1981).

Fig. 11: Schematical section through the „Hafelekar" reef complex and the distribution of the facies types, modified after Brandner & Resch (1981).

Verzahnung von Hintergrundsedimentation (Filamente und Radiolarien) und Calciturbiditen (siehe Kapitel Seegrube-Einheit) ist die Grenze lokal nicht scharf ausgebildet und eine genaue Definition einer solchen ist noch in Diskussion. Die Autorin schließt sich der Meinung von Sarnthein (1966) an und verwendet den Begriff Wettersteinkalk-Formation erst ab einem vollständigen Fehlen von Radiolarien und Filamenten.

Im Arbeitsgebiet wurde eine horizontale Gliederung entsprechend einer Faziesgliederung vorgenommen und die Wettersteinkalk-Formation in Vorriffbereich, Riff und Lagune unterteilt.

Vorriff/Slope

Einige Meter über der Reifling-Formation, meist ohne scharfen stratigraphischen Kontakt, setzen zunächst dunkelgraue bis fast schwarze, massige Kalke ein, die beim Anschlagen mit auffallend planaren Flächen brechen. Schon mit dem freien Auge lassen sich Rifforganismen wie Sphinctozoen oder vereinzelte Korallen erkennen. Es handelt sich bei den über den dunkelgrauen basalen Kalken folgenden Gesteinen, um zumeist gut ausgewaschene Riffschuttbreccien, deren Komponenten (Riffkalke, isolierte Organismen und vereinzelt Lagunenkalke), meist durch dicke Calcitsäume zementiert sind. Vereinzelt sind auch kleinere Hohlräume mit radiaxialen Zementen zu finden.

Die Riffschuttkalke werden nach oben hin heller und weisen teilweise gröbere Riffschuttbreccien auf. Die durchschnittliche Komponentengröße schwankt von ca. 2 cm bis zu mehreren dm. Neben den immer häufiger werdenden Crinoiden, teilweise mit Durchmessern bis zu 1,5 cm, die meist in der Nähe zum eigentlichen Riff zu finden sind, nehmen auch die Hohlraumgefüge an Häufigkeit und Größe zu. Nach Sarnthein (1965) beträgt die Mächtigkeit des Riffschutts im Profil Seegrube 65-75 m.

Das Riff

Der zentrale Riffbereich kann interpretiert werden als ein Gebiet mit randlich ausgesetzten hochenergetischen Zonen, die eine diversifizierte Fauna beinhalten, und geschützten Bereichen im Riff sowie entlang der "reef-flat" (Brandner & Resch, 1981).

Das primäre Riff, bzw. Riffgerüst setzt sich aus gerüstbildenden Organismen zusammen wie Korallen, Kalkschwämme, Rotalgen und *Tubiphytes* und vereinzelt Codiaceen. Im Gegensatz zu früheren Ansichten spielen Korallen sehr wohl eine vorherrschende Rolle (Brandner & Resch, 1981). Unter den inkrustierenden Organismen befinden sich *Tubiphytes*, Kalkschwämme und untergeordnet verschiedene Bryozoen, Problematica wie *Ladinella porata* und Stromatolithischen. Die primäre Funktion von *Tubiphytes* liegt in seiner Kapazität als Gerüstbildner in ruhigen Wasserzonen und ebenso als inkrustierender und bindender Organismus in stark bewegtem Wasser. E.Ott (1972) weist unter anderem auf *Tubiphytes obscurus* als einen der wichtigsten Gerüstbildner und Gerüstbinder hin. Weiters unterstreicht er das Auftreten mehrerer Arten von Sphinctozoen (gegliederte Kalkschwämme). Zwischen den Organismen finden sich

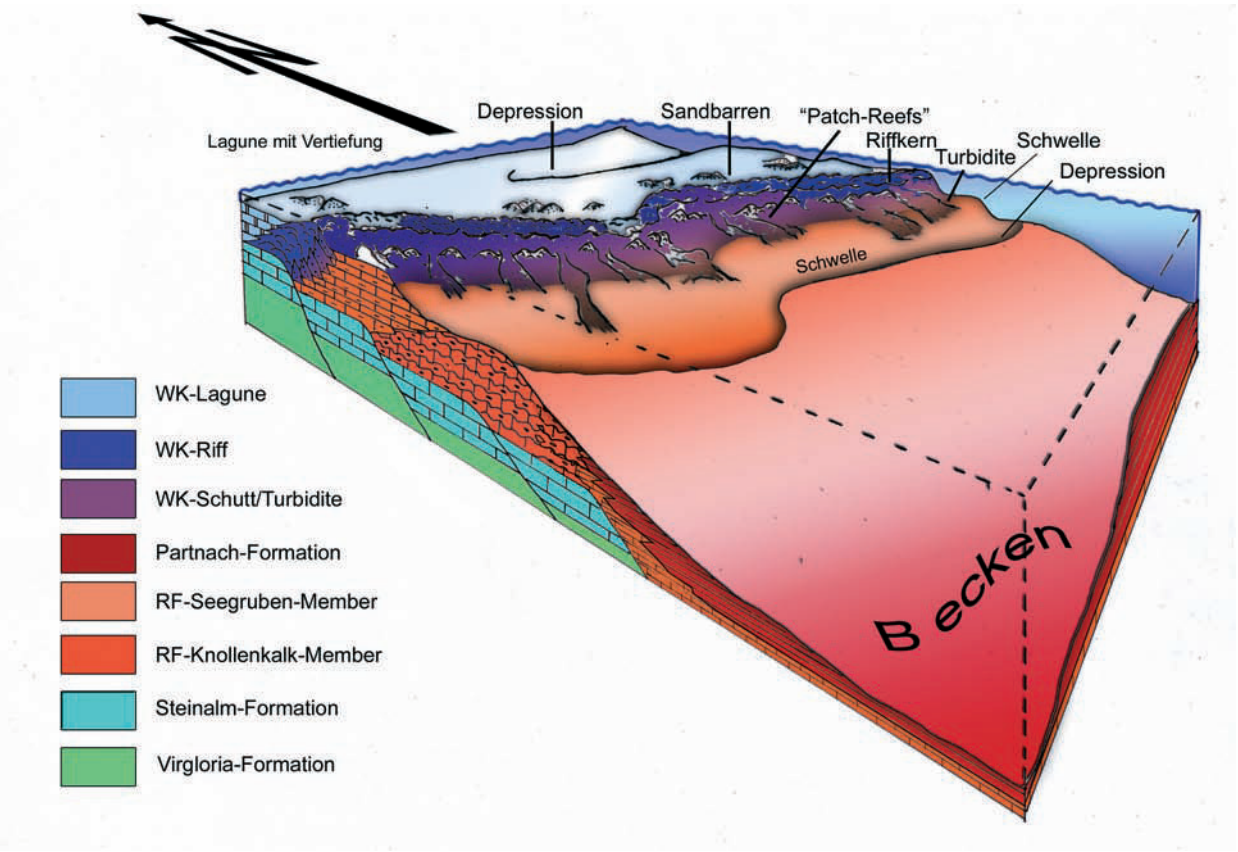

Abb. 12: Paläogeographisches, 3-dimensionales, schematisches Modell zur Lage der Faziesbereiche der Wettersteinkalk-Formation, Reifling-Formation, Partnach-Formation, aus Nittel 2004.

Fig. 12: Paleogeographical, three-dimensional, schematical modell for the locality of the facies rooms of the Wettersteinkalk-, Reifling- and Partnach formation, from Nittel 2004.

Detritus und Resedimente, die wiederum durch schuttbindende Organismen wie mikrobielle Krusten und Porostromata verkrustet und gefestigt werden. Ebenfalls charakteristisch für den Riffkern ist das Auftreten der sogenannten „Großoolithe". Die bis zu m-großen „Großoolithe", die aus einer Wechselfolge von Calcit und Dolomit bestehen, stellen eine Besonderheit im Riff dar, können aber bereits in kleinerer Ausführung in den Riffschuttbreccien des Vorriffs auftreten. Der Wechsel zwischen Calcit und Dolomit lässt auf einen wechselhaften Chemismus der Porenwässer schließen. Eine Ursache für das Eindringen der zum Teil hypersalinen Porenwässer aus der Lagune mit einem relativ hohen Mg/Ca-Verhältnis in die tieferen abgestorbenen Riff- bzw Riffschuttbereiche, ist ein im Cordevol (Jul1/l) verstärktes Vorwachsen der Riffe gegen das Becken hin, verursacht durch einen relative Meeresspiegel - absenkung bzw. Subsidenzstop. (Brandner, 1978).

Die Lagune

Die bei Brandner & Resch (1981) ebenso wie bei Sarnthein (1965) erwähnten „skeletal sand shoals mit Tepeestrukturen" (entspricht der „Unteren Schollenserie" von Sarnthein) bilden die Hauptbarriere zwischen dem Riff und der Lagune. Auch im Arbeitsgebiet waren diese vereinzelt aufgeschlossen und charakterisiert durch "sheet cracks" mit radiaxialem Zement, Tepee Strukturen, invers gradierte Pisolithe mit vertikalen Trockenrissen und kreuzgeschichtete Grainstones, die auf kleine Sanddünen weisen, die zeitweilig ohne Wasserbedeckung waren. Dripstonezemente (=Hängezement, Tafel I, Fig. 7, 8; Tafel V, Fig.7) geben hier den eindeutigen Hinweis.

Dort, wo die „skeletal sand shoals" fehlen, bildet ein ca. 2–4 m mächtiger, braun verwitternder Horizont, der aber immer noch Riffkomponenten

wie Korallen und Sphinctozoen enthält, die Grenze zwischen Lagune und Riff. Direkt darüber folgen die ersten, im dm- Bereich gebankten, teilweise bituminösen Dasycladaceen- Grainstones mit auffallend großen Dasycladaceen, meist *Teutloporella herculea*, die E. Ott (1967) in Riffnähe stellt. Vereinzelt treten auch innerhalb der Dasycladaceenkalke sheet cracks mit Tepee Strukturen auf. Zum Hangenden hin werden auch Stromatolithlagen häufiger, die, ebenso wie die Dasycladaceenkalke, eine braungraue Farbe aufweisen und gut gebankt sind. Die darüber folgenden Bänke werden mächtiger und teilweise fossilärmer. Die gesamte Lagune ist vor allem durch deutliche im dm-m Bereich auftretende Schichtung charakterisiert.

Abb.12

3.3.2. Lithotypen und Fossilführung

A: Riffschutt, Turbidite

Turbidite haben ihren Ursprung an den Plattformrändern und in den höheren Bereichen des Hanges, zusätzliches Material kommt vom unteren Hang. Selten sind aufgearbeitete Becken- und Beckenrandsedimente, wie Radiolarien- und Filament-Mud bis Wackestones zu finden.

Hauptkomponenten sind Bruchstücke von inkrustierenden Organismen und frühdiagenetisch zementierten Lithoklasten.

A1: Distale Turbidite, Hohlräume, Radiolarienmikrite

Charakteristisch für diesen Faziestyp ist das Auftreten mikritischer Bereiche innerhalb biogenreicher Grain- und Rudstones. In den Mud- bis Packstones der mikritischen Bereiche (möglicherweise ehemalige, durch Bioturbation gestörte Internsedimente) treten Radiolarien, Filamente, Ostracoden und Lageniden auf, was auf eine Ablagerung der Turbidite in Beckennähe schließen lässt. Auch *Turriglomina mesotriassica* und *Ophtalmidium tricki* weisen auf tieferes Wasser hin. Eine mikritische Matrix ist nur in distalen Turbiditen innerhalb der Reifling-Formation zu finden (Rüffer & Zamparelli, 1997).

Häufige Komponenten sind porostromate Calcimikroben vom Typ *Cayeuxia*, onkoidische Umkrustungen, Mikroproblematika wie *Tubiphytes obscurus* und *Ladinella porata*. Seltener treten Bruchstücke von Korallen, Serpuliden, Brachiopoden, Gastropoden, Crinoiden, Echiniden und Foraminiferen, wie *Palaeolituonella meridionalis, Astrorhizacea, Turriglomina mesotriassica, Ophtalmidium tricki, Frondicularia* sp., *Endoteba elegans, Duostominidae,* cf. *Planiinvoluta carinata, Tolypammina* sp., *Endotebanella* sp. und *Endotriadella s*p. auf.

A2: Turbidite, Grainstones/Rudstones

Charakteristisch für diese Sedimente sind zerbrochene Biogene von Sphinctozoen, Mikroproblematica und inkrustierenden Organismen. Neben häufigen Biogenen wie *Tubiphytes obscurus,* Sphinctozoen, darunter *Solenolmia manon*, *Solenolmia manon minor*, *Colospongia catenulata*, Inozoa (*?Stolenella* sp.) und seltener Korallen, treten immer mehr onkoidische Krusten von *Tubiphytes* sp., *Girvanella* sp., *Ladinella porata*, *Baccanella floriformis* und inkrustierende Cyanobakterien auf, die als Sedimentbinder und Gerüstbildner fungieren. Seltener sind Crinoiden, Echinidenreste, Seeigelstacheln, Gastropoden, Serpuliden, Brachiopoden, Ostracoden und Foraminiferen wie *Siphonofera* sp., *Agglutisolena conica*, *Palaeolituonella* sp. und *Astrorhizacea,* zu finden.

In den Intrapartikelporen und gelegentlich auftretenden Hohlräumen folgen spätdiagenetische Blockzemente auf vereinzelten, fibrösen, radiaxialen Calcitsäumen, die ein weiterer Hinweis für einen proximalen Ablagerungsraum der Turbidite sind.

A3: Riffschutt/Riffschuttbreccien

Charakteristisch für diesen Faziestyp ist das Auftreten von schlecht sortierten angularen bis subangularen und subgerundeten Klasten aus lithifizierten Riffkarbonaten. Die scharf abgegrenzten Riff-klasten zeigen diverse Microfaziestypen: ungradierte und gradierte Pelsparite mit Aggregatkörnern, Rudstones mit Sphinctozoa, und Biosparite mit vereinzelt auftretenden Echinidenstacheln sowie einzelnen Biogenen, die mit mächtigen Zementsäumen umgeben und verbunden sind. An Biogenen kommen vor: Korallen, Sphinctozoa wie *Folicatena cautica, Vesicocaulus carinthiacus, Colospongia catenulata* und *Solenolmia manon manon*, *Tubiphytes* sp., Bivalvenschalen, Gastropoden, Serpuliden, Brachiopoden, Girvanella, Ostraco-

den und Foraminiferen wie cf. *Ammobaculites* sp., *Duostominidae*, *Palaeolituonella meridionalis*, *Frondicularia* sp., *Aulotortus friedli*, Astrorhizacea und *Frondicularia* sp.

B: Der Riffkern

Brandner & Resch (1981) konnten am Hafelekarriff und Goethewegrifff fünf Riff-Gemeinschaften unterscheiden. Eine Codiaceen-Algen-Gemeinschaft, eine *Tubiphytes*-Gemeinschaft, eine Calcispongien-Gemeinschaft, weiters die Thecosmilien-Calcispongien-Gemeinschaft und die einer Thanatozenose ähnliche Gemeinschaft von Korallen-Echinodermen- und *Tubiphytes.*

Da im Arbeitsgebiet nicht alle Bereiche des Riffs zugänglich waren, konnten nur wenige Faziestypen unterschieden, und keine genaue Zuordnung zu den oben genannten Riff-Biozenosen durchgeführt werden.

B1: Bindstones/Bafflestones, überwiegend Tubiphytes-Inkrustierungen

Die Hauptriffbildner im Wettersteinkalk sind vom Ladin bis ins frühe Karn Organismen wie *Tubiphytes* und Sphinctozoen, die als Gerüstbildner und Sedimentfänger in höheren Bereichen des Hanges und Plattformrandes fungieren. Durch Aufarbeitung werden die Bind- Bafflestones unmittelbar als Rudstones abgelagert oder zu tieferen Bereichen des Hanges transportiert (A2). Häufig sind sie mit inkrustierenden Organismen vergesellschaftet, ebenso wie mit porostromaten Algen, seltener mit Korallen und Bryozoen. Foraminiferen sind generell selten im Riffkern vertreten (*Palaeolituonella sp.*). Frühdiagenetische fibröse Zemente („Zementriff nach Flügel") sind vorherrschend und sind ein Teil des Riffgerüstes.

B2: Bafflestones, Boundstones, Korallenstöcke

Auch in den von Rüffer & Zamparelli (1997) untersuchten Profilen im Lalider Tal und am Gatterköpfl waren die Korallen in den im Allgemeinen selten auftretenden korallenführenden Faziestypen schlecht erhalten. Zu den wenigen Ausnahmen zählen *Retiophyllia, Cassianastrea reussi* und *Volzeia badiotica, die* meist gemeinsam mit Sphinctozoen vorkommen.

Die Korallen sind meist von unterschiedlichen Organismen wie *Tubiphytes obscurus*, *Ladinella porata*, Sphinctozoen (*Solenolmia manon minor*), porostromaten Calcimikroben, Solenoporaceen und sessilen Foraminiferen inkrustiert. Seltener findet man Foraminiferen und andere kleinere Organismen innerhalb der Sedimentfänger und Gerüstbildner.

C: Backreef/Lagune

Eine detaillierte Beschreibung der gesamten Lagune erfolgte durch Sarnthein (1965). Er beschreibt Faziestypen, wie „Kornaggregat-Klumpen-Fazies", „Kotpillenschlamm-Fazies" und „Biogenschlamm-Fazies" mit Anhäufungen von Dasycladaceen, die auch im Arbeitsgebiet vertreten sind. Die von ihm erwähnten „Messerstich-Zyklen" waren nicht aufgeschlossen, sie treten erst nördlich bzw. östlich des Arbeitsgebietes auf.

C1: Plattformrand mit Sandanhäufungen

Die Sedimente des „Plattformrandes mit Sandanhäufungen" werden nach Wilson (1975) oberhalb der Wellenbasis und innerhalb der durchlichteten Zone abgelagert. Sie sind stark von Gezeiten beeinflusst und charakterisiert durch das Auftreten von Sandshoals und Gezeitenbarren.

C1.1: Rud- Grainstones, Backreef

Die Rud und Grainstones der Backreef-Fazies sind einerseits durch eine starke Fragmentierung der Komponenten, gute Auswaschung und mehrphasige, teilweise bitumenhältige Zementsäume, ähnlich wie bei Pisoiden, und andererseits durch das massenhafte Auftreten von *Teutloporella herculea* charakterisiert. Weitere häufig auftretende Komponenten sind porostromate Calcimikroben vom Typ *Cayeuxia* und *Ortonella*, seltener findet man *Diplopora annulata*, *Teutloporella nodosa*, *Clypeina besici*, *Aciculella bacillum*, Bryozoen, Gastropoden, Ostracoden, Echinidenreste Schalenreste und folgende Foraminiferen: *Lamelliconus* sp, *Glomospirella, Aulotortus tenuis, Aulotortus sinuosus, Glomospira* sp., *Trochammina sp, Aulotortus friedli.*

Eine Ausnahme bilden stark zerklüftete, partiell ausgewaschene Pack-bis Wackestones, die charakterisiert sind durch häufig auftretende Dasycladaceen-Sporangien, die in den zementierten

Bereichen der Klüfte zu finden sind. Neben den Sporangien wie *Aciculella* sp., *Aciculella cf. sokaci*, *Aciculella sokaci*, sind unter den Dasycladaceen *Teutloporella nodosa, Teutloporella herculea* und *Teutloporella peniculiformis* vertreten. Seltener treten Ostracoden und Foraminiferen wie *Mesoendothyra isjumiana* und *Glomospira* sp. auf.

C1.2: Grape- Lumpstones- Onkoide, Gezeitenbarren

Auffallend in diesem Faziestyp sind die meist schön gradierten Onkoide und Rindenkörner, die eine Coarsening-Upward-Abfolge zeigen. Meniskuszemente, Hängezemente, vadoser Silt und teilweise offene Porenräume deuten auf ein zeitweiliges Freiliegen an der Oberfläche und eine Ablagerung in der marin-vadosen-Zone hin. Biogene Komponenten treten neben den Onkoiden, Rindenkörnern und Aggregatkörnern eher geringfügig auf. Dazu zählen Fragmente von *Teutloporella* sp., porostromate Calcimikroben, Ostracoden und Foraminiferen wie *Gaudryina* sp., *Glomospirella*, *Duostominidae* und *Trochammina sp*.

C1.3: Pisoidgrainstones

Dieser Faziestyp ist durch das häufige Auftreten von Pisoiden geprägt. Deren Kern wird meist von Lithoklasten oder Fragmenten von porostromaten Algen gebildet. Manchmal besitzen sie aber gar keinen Kern und bestehen nur aus engschichtigen Calcitlamellen. Das Auftreten von zerbrochenen Pisoiden spricht für randmarine Bereiche. Neben den Pisoiden sind Grapestones und Lithoklasten stark vertreten, dazu kommen einige Fragmente von Algen und Gastropoden. Foraminiferen sind nur vereinzelt zu finden. Aufgrund des guten Auswaschungsgrades kann man auf ein mäßig hochenergetisches Gebiet mit ständiger Auswaschung am Rand der Gezeitenbarren schließen. Die Pisoide sind generell Anzeiger eines Auftauchhorizontes einer lagunären Verflachungs - sequenz. Dies wird auch durch Trockenrisse und Tepeestrukturen bestätigt (Tafel I, Fig. 7, 8).

C2: innere Plattform

Die Sedimente der normalmarinen inneren Plattform wurden innerhalb der durchlichteten Zone und über der Wellenbasis abgelagert (Wilson 1975).

C2.1: Biopelsparite

Grapestones und Lumpstones treten zurück, im Vordergrund stehen Peloide und Biogene, sowie fragmentierte Komponenten. Die Biogene werden hauptsächlich von Dasycladaceen wie *Clypeina besici, Poikiloporella duplicata, Physoporella jomdaensis* und *Teutloporella herculea* gebildet, die gemeinsam ein cordevolisches (Jul1/l) Alter angeben. Seltener sind *Aciculella* sp., Ostracoden, Gastropoden und Schalenreste zu finden. Foraminiferen sind relativ häufig, darunter befinden sich *Glomospira* sp., *Gaudryina* sp., *Glomospirella* sp., *Trochammina* sp., *Aulotortus friedli* und *Agathammina austroalpina.*

C2.2: reine Grape- Lumpstones, Bindstones

Die Grape- und Lumpstones bilden vermutlich den häufigsten Faziestyp in der Lagune. Dieser steht für eine Ablagerung im Intertidal und flachem Subtidal, in Gebieten mit geringer Zementation, starker aber wechselnder Wasserbewegung (Illing, 1954). Diese Lithotypen sind durch das überwiegende Auftreten von Aggregatkörnern und LF-Gefügen (Loferite) charakterisiert. Seltener sind Peloide, Dasycladaceenfragmente, unter anderem von *Teutloporella nodosa*, Spirorbis, porostromate Calcimikroben vom Typ *Cayeuxia* sp, Gastropoden und Ostracoden zu finden.

Foraminiferen wie *Trochammina* sp. sind häufig vertreten, vereinzelt kommen *Glomospira* sp., *Endotebanella* sp., *Gaudryina* sp., *Endotriadella* wirzi, *Duostominacea*, *Pseudobolivina tornata*, *Glomospirella*, *Frondicularia woodwardi*, *Ammodiscus* sp. und *Aulotortus friedli* vor.

C3: Innere Plattform mit eingeschränkter Wasserzirkulation

Abgelagert werden diese Sedimente ebenfalls innerhalb der durchlichteten Zone und über der Wellenbasis, aber nur mit geringer Verbindung zum offenen Ozean und damit verbundenen größeren Temperatur- und Salinitätsschwankungen.

3.1: Stromatolithen/Bindstones

Charakteristisch sind zusammenhängende Algenmatten einerseits von Stromatolithen mit den

	Dimensionen	Durchschnittswert
Länge	0,22 – 0,38 mm	0,31 mm
Max. Breite der obersten Kammer, inklusive Kiel	0.9 – 0,12 mm	0,11 mm
Anzahl der Kammern	5 – 7	6
Höhe der obersten Kammer	0,06 – 0,07 mm	0,063 mm

Tabelle 1

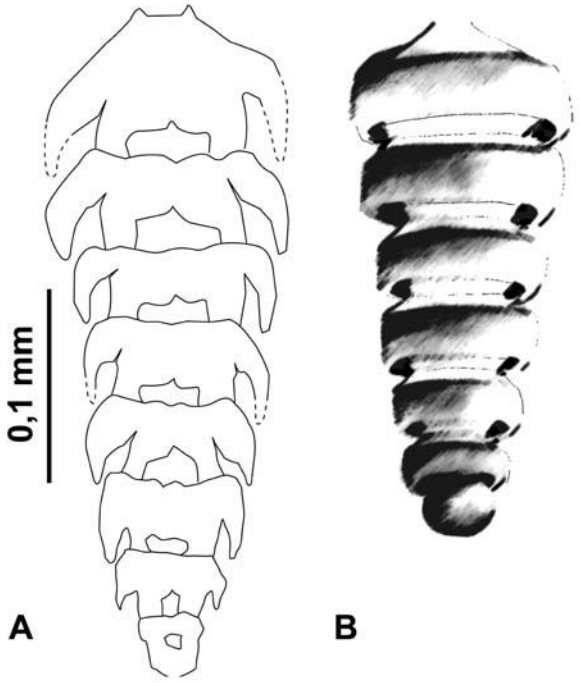

Abb. 13: *Austrocolomia carinata* nov. spec. A. Skizze zum Dünnschliff, B. mögliches dreidimensionales Aussehen, etwas verkürzt durch den Blickwinkel.

Fig. 13: *Austrocolomia carinata* nov. spec. A. Skizze zum Dünnschliff, B. mögliches dreidimensionales Aussehen, etwas verkürzt durch den Blickwinkel. Delineation to the thin section, B. possible three-dimensional appearence, shortened by perspective.

typischen LF- Gefügen, und andererseits von porostromaten Algen. Vereinzelt sind Bryozoen, Dasycladaceenfragmente, Bivalvenschalen, Cyanobakterien und selten Foraminiferen wie *Glomospirella* sp., *Frondicularia* sp., *Trochammina* sp. zu finden.

Seltener sind Grain-Bindstones, die als Hauptkomponenten porostromate Calcimikroben vom Typ

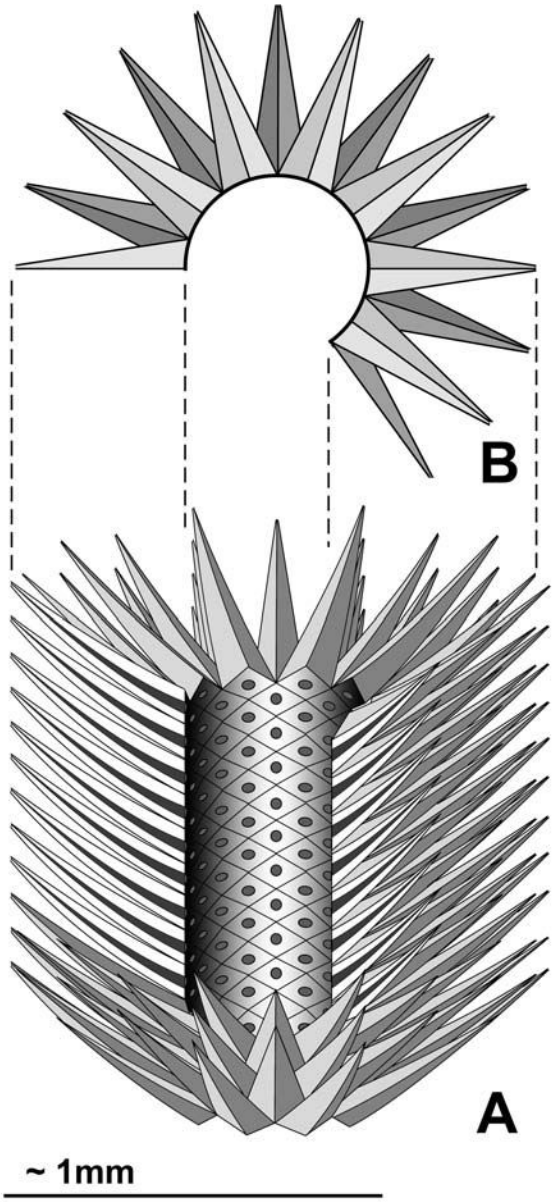

Abb. 14: *Probolocuspis aculeata* nov. spec. A. Rekonstruktion des möglichen dreidimensionalen Aussehens. B. Ansicht von oben, kein Querschnitt

Fig. 14: *Probolocuspis aculeata* nov. spec. A. Reconstruction of the possible three-dimensional appearance. B. View from top, no cross section.

	Dimensionen	Durchschnittswert
Außendurchmesser	1,26 – 5,1 mm	1,66 mm
Innendurchmesser	0,52 – 2,76 mm	0,54 mm
Wandstärke	0,38 – 1,66 mm	0,66 mm
Stachellänge	0,60 – 0,76 mm	0,21 mm
Stachelquerschnitt	0,20 – 0,26 mm	0,69 mm
Stachelkanaldurchmesser	0,036 – 0,10 mm	

Tabelle 2

Cayeuxia, und Tubiphytes führen. Foraminiferen wie *Turriglomina mesotriassica,* cf. *Austrocolomia carinata* nov. spec. sprechen für ein etwas tieferes Wasser und ein Ablagerung in Vertiefungen innerhalb der Lagune. Weitere Foraminiferen sind Endotriadella wirzi, ?Auloconus permodiscoides, *Robuloides*, *Endoteba* sp., *Tolypammininae* und *Frondicularia* sp.

Systematische Beschreibung

Ordnung: FORAMINIFERIDA
Familie : Nodosariidae Ehrenberg 1838
Gattung : *Austrocolomia* Oberhauser 1960

Austrocolomia carinata nov. spec.
(Tafel VIII, Fig.3)

Namensgebung: nach dem rundum laufenden Kiel.
Locus typicus: Lokalität der Probe 228, am Weg vom Brandjochboden zum Brandjochspitz auf 2100 m.
Stratum typicum: Wettersteinkalk-Formation, Lagunenfazies
Material: Drei Individuen in drei Dünnschliffen der Probe 228

Diagnose: Eine sehr kleine Art der Gattung Austrocolomia, von gerader Gehäuseform, mit rundum laufendem Kiel. Proloculum aufgrund der starken Umkristallisation nicht sichtbar.

Beschreibung: (zwei Exemplare) kalkiges Gehäuse, bestehend aus einer geradlinigen Serie von 5-7 Kammern (siehe Tabelle 1). Jede Kammer trägt an ihrer breitesten Stelle (Ansatz im oberen Kammerteil) einen markanten, rundum laufenden Kiel, der fast die ganze Kammer wie ein Kragen umhüllt. Die Zweiwandigkeit ist aufgrund der starken Umkristallisation nur noch erahnbar.

Ordnung: DASYCLADALES
Familie : Acetabelariaceae ? Hauck, 1884
Unterfamilie: Clypeineae ? Elliott, 1968
Gattung : Probolocuspis Brönnimann, Zaninetti, Moshtaghian und Huber, 1974

Probolocuspis aculeata nov. spec.
(Tafel XII, Fig.1-9)

1994 *Teutloporella herculea* - Piros et. al, Tafel 1, Fig. 1-2

Namensgebung: nach dem äußeren, mit „Stacheln" versehenen Aussehen
Locus typicus: Am Weg vom Brandjochboden zum Brandjochspitz auf 2100 m (Probe 228 mit den meisten Exemplaren) und am Klettersteig von der Frau Hitt zum Brandjochspitz auf 2430-2450 m (Probe 327, 328)
Stratum typicum: Wettersteinkalk-Formation, Lagunenfazies, Ladin
Material: wenige Schrägschnitte in Dünnschliffen (228, 327, 328), ein Querschnitt und einige Fragmente von Längsschnitten und eine Vielzahl von einzelnen Stacheln in Quer- und Längsschnitten.

Diagnose: An einer geraden, zylindrischen Stammzelle sitzen dicht gedrängt, euspondyl arrangiert stachelförmige Äste von trichopohrem Typ, was für

Merkmale	*Teutloporella echinata*	*Probolocuspis aculeata* nov. spec.
Anzahl der Äste / Umgang	25- 35 Äste	~ 20 Äste
Abzweigungswinkel der Äste	Zwischen horizontal und 60-70 °, stark divergierend	34-38°, parallel eingeregelt
Verhältnis Außen-/Innendurchmesser	Durchschnitt 4,6 : 1	Durchschnitt 2,5 : 1
Form der Äste	Stark verjüngende trichophore Äste, meist ohne Zentralkanal sichtbar	Breite, trichophore Äste mit deutlichem Zentralkanal
Standort	mitten zwischen Gerüstbildnern des Riffs (Tubiphytes, Sphinctozoen, Pharetronen, Ladinella porata)	Lagune der Wettersteinkalk-Formation

Tabelle 3

die Zuordnung zur Gattung Probolocuspis, nach der Diagnose von Senowbari 2003, entscheidend ist. Die Äste erster Ordnung verkalken frei und isoliert.

Beschreibung: Die in horizontalen Reihen angeordneten „Stachel" oder Äste (10-20 pro Umgang), sind mit der jeweils folgenden Reihe um eine ? Stachellänge gegeneinander versetzt, was zu einem wabenähnlichen Muster führt. Die „Stachel" weisen nahe der Stammzelle stets einen rautenförmigen Querschnitt auf (Höhe:Breite = 1:1,85) mit einem kreisrundem Zentralkanal. Sie sind leicht gekrümmt und wachsen einheitlich eingeregelt in einem Winkel von 34-38° nach oben.

Dimensionen: Durchmesser der Stachelquerschnitte beziehen sich auf die Längsachse der Raute. Die Stachellänge sowie die Wandstärke sind nicht eindeutig messbar, da die Stachel meist schräg angeschnitten sind (siehe Tabelle 2).

Observationen: Die neue Spezies unterscheidet sich von *Probolocuspis espahkensis* zum Einen durch die paralelle Anordnung der Stachel in gleich bleibenden Winkeln und zum Anderen durch die rautenförmigen Querschnitte der Stachel, *Probolocuspis espahkensis* weist kreisförmige Querschnitte auf. Eine Ähnlichkeit mit *Teutloporella echinata* Ott ist nur durch die rautenförmigen Querschnitte der einzelnen „Stachel" gegeben.

Weitere Unterschiede im Vergleich mit *Teutloporella echinata* (siehe Tabelle 3).

Begleitende Fauna sind porostromate Calcimikroben vom Typ Cayeuxia, häufig Tubiphytes, selten *Teutloporella herculea* und einige Foraminiferen.

3.3.3. Ablagerung

Laut Brandner & Resch (1981) und Bechstädt & Mostler (1974) handelt es sich bei den mitteltriadischen Riffen der Nordtiroler Fazies um Riffe mit einer steigenden regressiven Tendenz, das heißt, sie wandern beckenwärts und werden schließlich von der sich dahinter befindenden und ausdehnenden Lagune erstickt.

Abgesehen von lokalen Komplikationen - bedingt durch synsedimentäre Tektonik entlang der Plattformränder - zeigt das Riff infolge variierender Wasserbewegung und Nahrungszufuhr eine Differenzierung in Vorriff und zentralen Riffbereich. Die von Brandner & Resch (1981) beschriebenen linsenförmigen „Fleckenriffe", die den unteren Bereich des Wettersteinkalkes im Hangbereich repräsentieren, sind im Arbeitsgebiet möglicherweise vorhanden, konnten aber wegen Unzugänglichkeit nicht kartiert werden.

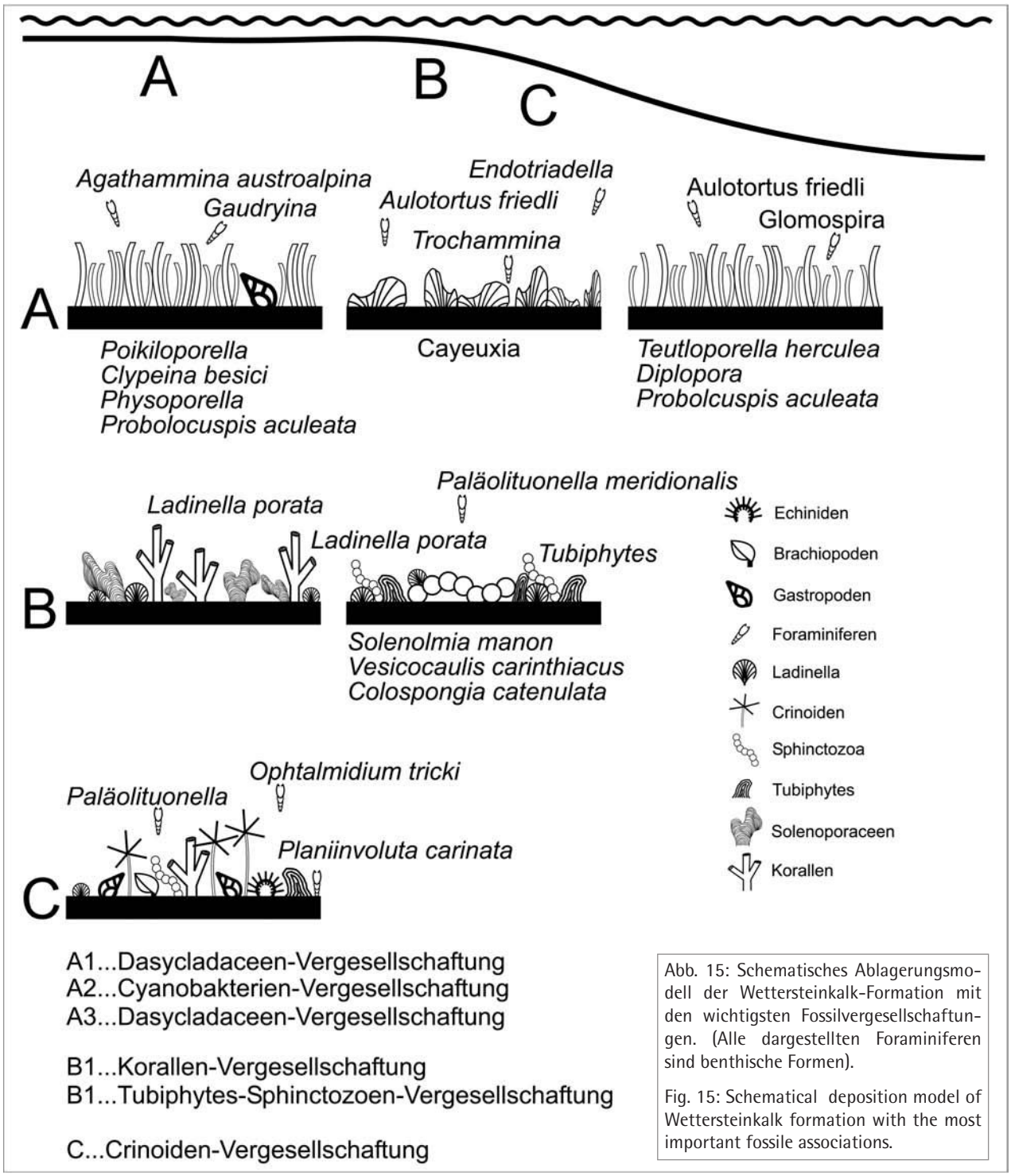

Abb. 15: Schematisches Ablagerungsmodell der Wettersteinkalk-Formation mit den wichtigsten Fossilvergesellschaftungen. (Alle dargestellten Foraminiferen sind benthische Formen).

Fig. 15: Schematical deposition model of Wettersteinkalk formation with the most important fossile associations.

Danksagung

Die vorliegende Studie ist Teil meiner Diplomarbeit an der Universität Innsbruck unter Betreuung von Univ. Prof. Dr. R. Brandner, bei dem ich mich besonders bedanken möchte. Ebenso bei Univ.-Doz. Dr. W. Resch für die Hilfestellung und stets anregenden Diskussionen in der Paläontologie. Weiters bedanken möchte ich mich bei Univ.-Prof. Mag. Dr. Diethard Sanders für die Durchsicht des Manuskripts und bei Felix Heller für die Anfertigung der Dünnschliffe.

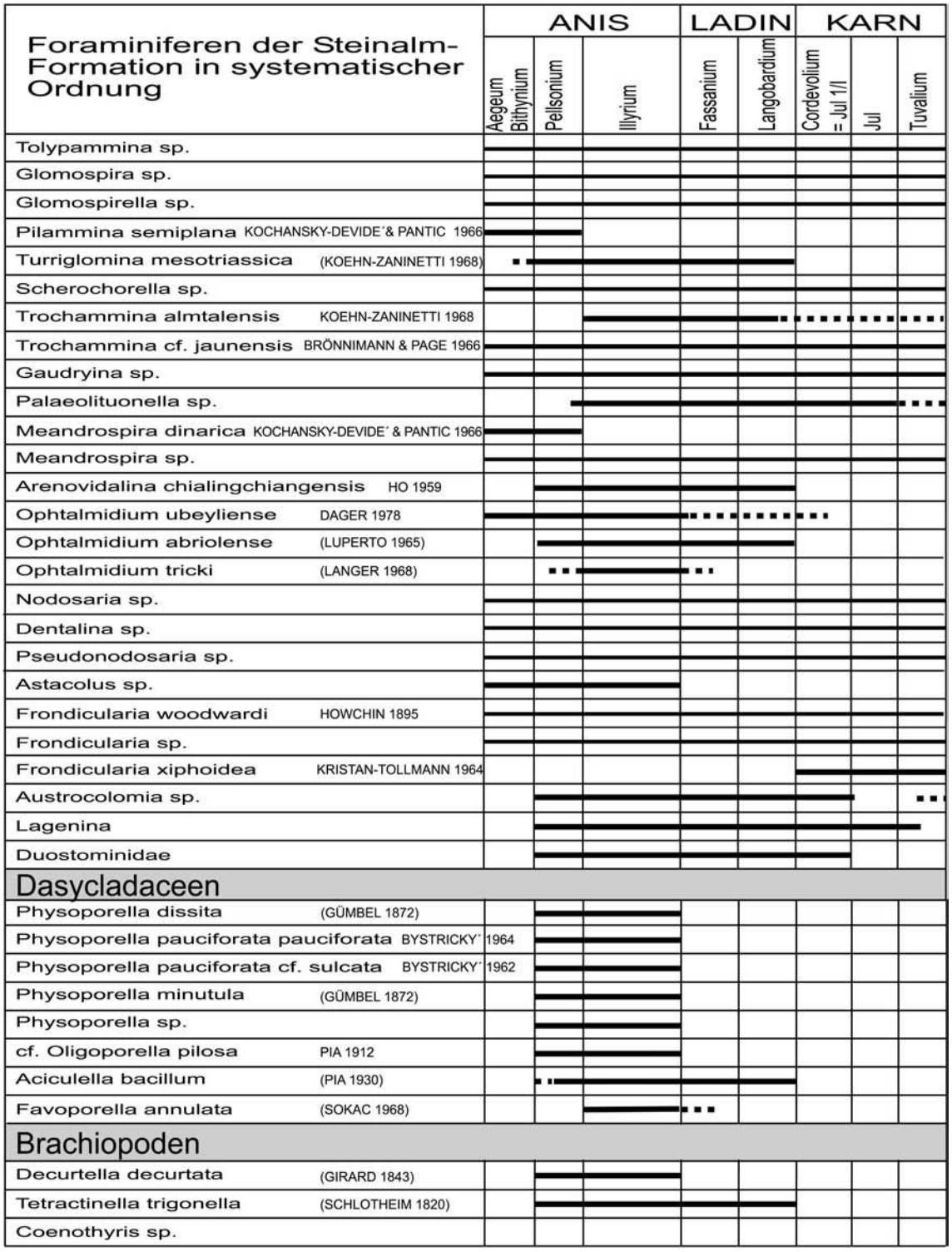

Abb. 16: Tabelle zur zeitlichen Verbreitung der Mikrofossilien der Steinalm-Formation. Chronostratigraphische Stufengliederung der Foraminiferen nach Loeblich & Tappan 1988, Rettori 1995, Salaj et. al. 1983. Chronostratigraphische Stufengliederung der Dasycladaceen nach Ott 1974. Chronostratigraphische Stufengliederung der Brachiopoden nach Siblik 1988.

Fig. 16: Timetable to the microfossils of the Steinalm -formation. Chronostratigraphical distribution of foraminiferas after Loeblich & Tappan 1988, Rettori 1995, Salaj et. al. 1983. Chronostratigraphical distribution of brachiopods after Siblik 1988.

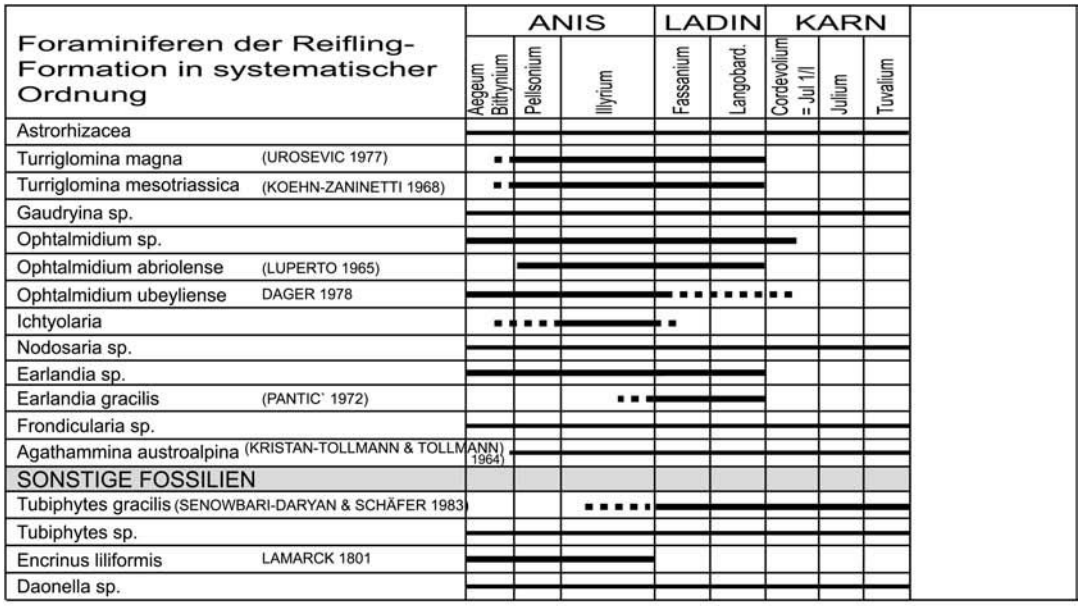

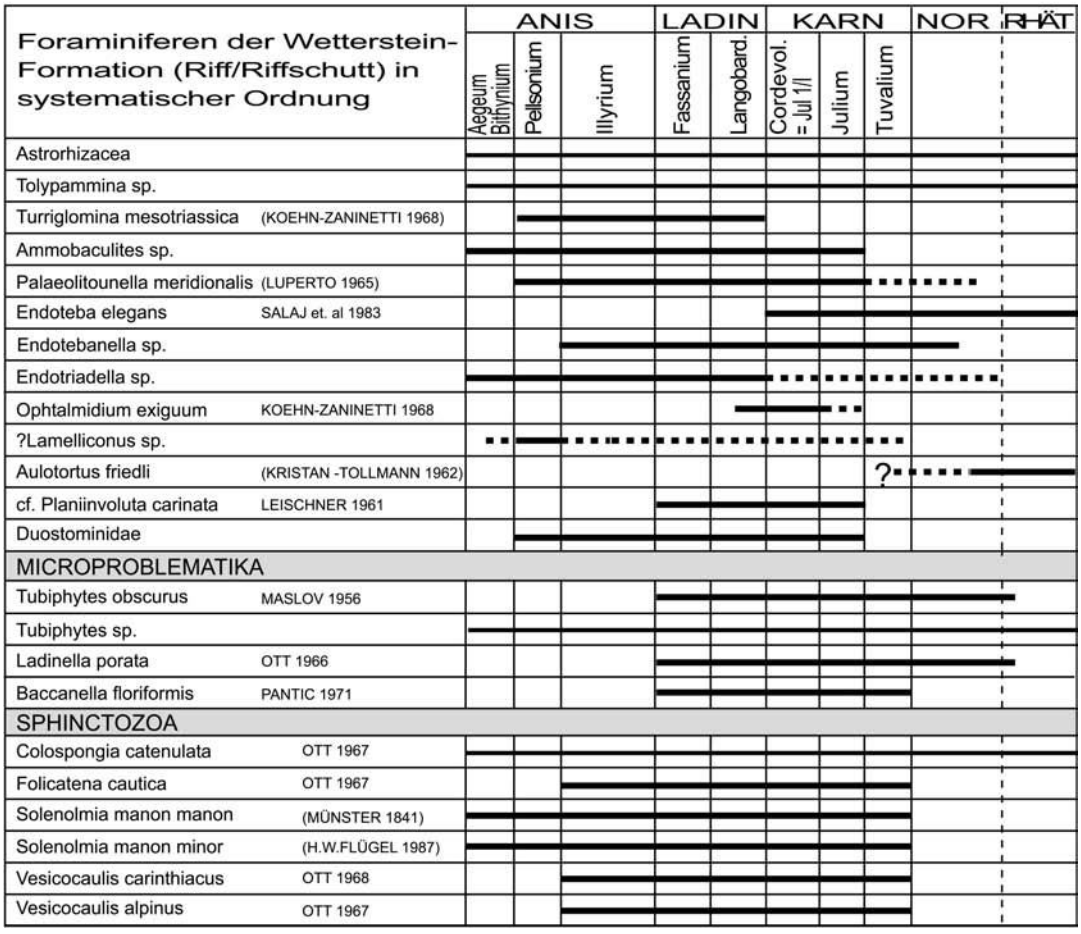

Abb.17: Tabelle zur zeitlichen Verbreitung der Mikrofossilien der Reifling-Formation und Wettersteinkalk-Formation (Riff/Riffschutt). Chronostratigraphische Stufengliederung der Foraminiferen nach Loeblich & Tappan 1988, Rettori 1995, Salaj et. al. 1983. Chronostratigraphische Stufengliederung der Sphinctozoen nach Senowbari –Daryan 1990.

Fig. 17: Timetable to the microfossils of the Reifling- and Wettersteinkalk-Formation (reef, forereef). Chronostratigraphical distribution of foraminiferas after Loeblich & Tappan 1988, Rettori 1995, Salaj et. al. 1983. Chronostratigraphical distribution of sphinctozoans after Senowbari–Daryan 1990.

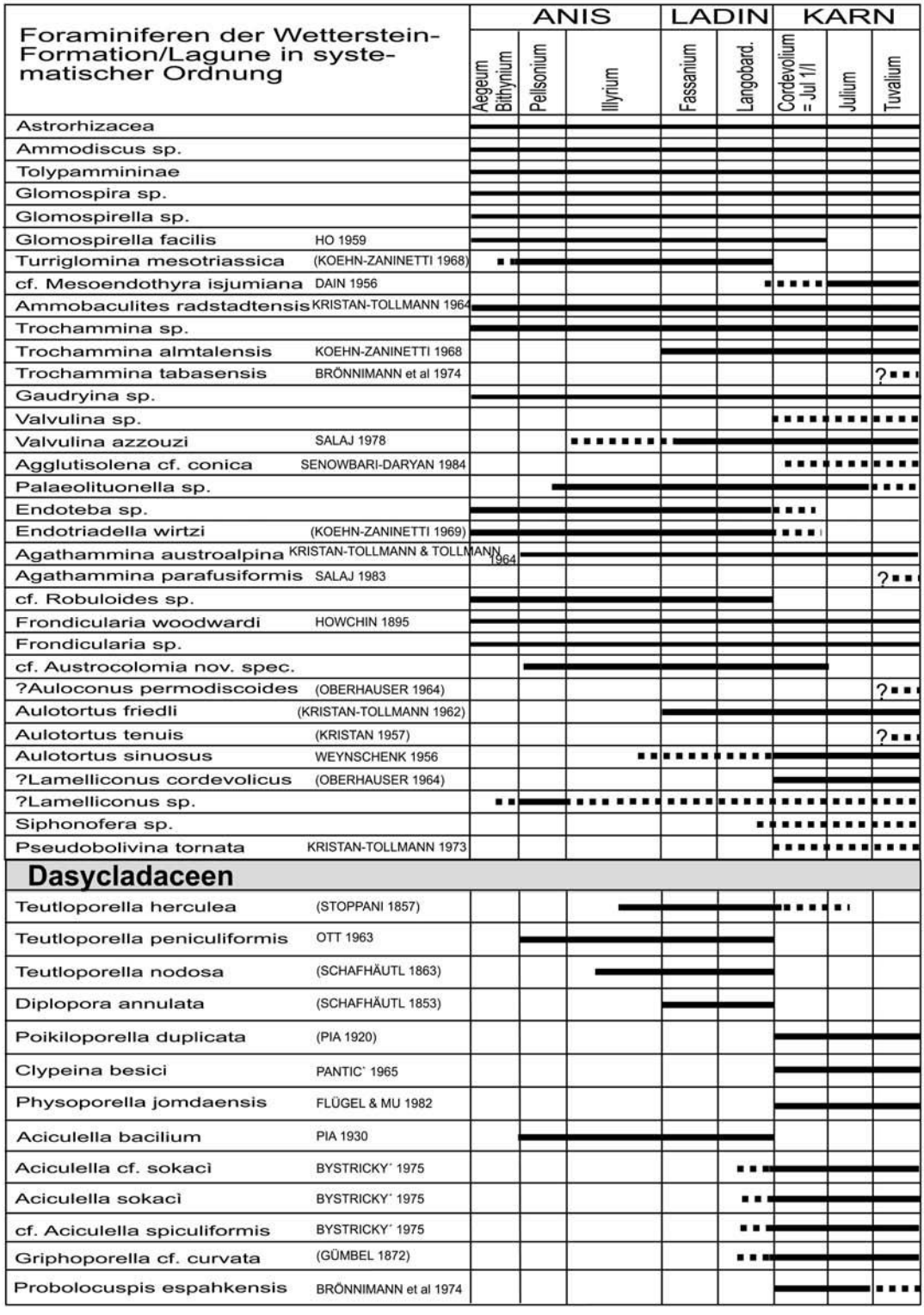

Abb. 18: Tabelle zur zeitlichen Verbreitung der Mikrofossilien der Wettersteinkalk-Formation Lagunenfazies
Chronostratigraphische Stufengliederung der Foraminiferen nach Loeblich & Tappan 1988, Rettori 1995, Salaj et. al. 1983. Chronostratigraphische Stufengliederung der Dasycladaceen nach Ott 1974.

Fig. 18: Timetable to the microfossils of the Wettersteinkalk-Formation (lagoon).
Chronostratigraphical distribution of foraminiferas after Loeblich & Tappan 1988, Rettori 1995
Salaj et. al. 1983. Chronostratigraphical distribution of dasycladaceans after Ott 1974.

Literatur

Amorosi, A. (1993): Use of glauconites for stratigraphic correlation: a review and case hsitories. - Giorn. Geol., 55, 117-137, 14 Figs., 2 Tabs., Bologna

Ampferer, O. & Hammer W. (1899): Geologische Beschreibung des südlichen Theiles des Karwendelgebirges. - Jb. Geol. R.-A., 48, p. 289-374.

Ampferer, O. & Hammer W. (1911): „Geologischer Quer - schnitt durch die Ostalpen vom Allgäu zum Gardasee. -Jb. Geol. R.-A., Bd. 61, p. 531-710.

Ampferer, O. (1903): Geologische Beschreibung des nördlichen Theiles des Karwendelgebirges. - Geol. B.-A. Wien, p. 84.

Bechstädt T. & Brandner R. (1970) - Das Anis zwischen St. Vigil und dem Höhlensteintal (Pragser-und Olanger Dolomiten, Südtirol). Festband des Geol. Inst., 300-Jahr-Feier Univ. Innsbruck, 9-103, Innsbruck.

Bechstädt, T. & Mostler, H. (1974): Mikrofazies und Mikrofauna mitteltriadischer Beckensedimente der Nördlichen Kalkalpen Tirols. - Geol. Paläont. Mitt. Innsbruck, Bd.4, p. 1-74.

Bechstädt, T. & Mostler, H. (1976): Riff-Becken-Entwicklung in der Mitteltrias der westlichen Nördlichen Kalkalpen. - Z.dt. Geol. Ges., 127, p. 271-289.

Bosellini , A. & Ferri, R. (1980): la formatione di Livinallongo (Buchenstein) nella Valle di S. Lucano (Ladinico inferiore, Dolomiti Bellunesi). – Ann. Univ. Ferrara, Sez. IX, VI, 5, 63-89, Ferrara.

Brandner, R. & Poleschinski, W. (1986): Stratigraphie und Tektonik am Kalkalpensüdrand zwischen Zirl und Seefeld in Tirol - Jber. Mitt. oberrhein. Verh., N.F. 68, p. 67-92.

Brandner, R. & Resch, W. (1981): Reef development in the middle triassic of the Northern Limestone Alps near Innsbruck - SEMP, Spec. Publ. 30, p. 203-231.

Brandner, R. (1978): Tektonisch kontrollierter Sedimen - tationsablauf im Ladin und Unterkarn der westlichen Nördlichen Kalkalpen. – Geol. Paläont. Mitt. Innsbruck, Bd 8, Festschrift W. Heissel

Donofrio, D. A., Heißel, G., et al. (1979): Zur tektonischen und stratigraphischen Position des Martinsbühels bei Innsbruck. - Geol. Paläont. Mitt. Innsbruck, Bd. 7, p. 1-43.

Flügel, E. (1972): Fazieslexikon Mikrofazielle Untersu - chungen in der alpinen Trias – Methoden und Probleme. – Mitt. Ges. Geol. Bergbaustud., 21, Inns - bruck, p. 9-64.

Frisch, J. (1968): Sedimentologische, lithofazielle und paläogeographische Untersuchungen in den Reichenhaller Schichten und im Alpinen Muschelkalk der Nördlichen Kalkalpen zwischen Lech und Isar. - Unveröff. Diss. TU. München, 133 p.

Frisch, J. (1975): Sedimentologische, lithofazielle und paläogeographische Untersuchungen in den Reichenhaller Schichten und im Alpinen Muschelkalk der Nördlichen Kalkalpen zwischen Lech und Isar. - Jb. Geol. B. -A., 118, p.75-114.

Gallet, Y. ; Krystyn, L. ; Besse, J. (1998): Upper Anisian to Lower Carnian magnetostratigraphy from the Northern Calcareous Alps (Austria) – J. Geophys. Res. Vol. 103 , No. B1 , p. 605.

Granier, B. R.C. & Grgasovic, T. (2000): Les Algues Dasycladales du Permien et du Trias Nouvelle tentative d'inventaire bibliographique, géographique et stratigraphique.- Geol.Croat., 53/1, Zagreb, p.1-197.

Heissel, G. (1978): Karwendel - geologischer Bau und Versuch einer tektonischen Rückformung. - Geol. Paläont. Mitt. Innsbruck, Bd.8, p. 227-288.

Henrich, R. & Zankl, H., (1986): Diagenesis of Upper Triassic Wetterstein Reefs of the Bavarian Alps. - Reef Diagenesis, p. 245-268.

Hinze, C. & Meischner, D.: Gibt es rezente Rotsedimente in der Adria?- Marine Geol., 6: 53-71; 2 Tab., 6 Abb., Amsterdam 1968.

Hollmann, R., 1964. Subsolutions-Fragmente (Zur Biostratonomie der Ammonoidea im Malm des Monte Baldo/ Norditalien). - N. Jb. Geol Paläont. Abh. 119, p. 22-82.

Illing, L.S. (1954): Bahaman clacareous sands. - Bull. Amer. Ass. Petrol. Geol., 38/1, p.1-95.

Kubanek, F. (1969): Sedimentologie des Alpinen Muschelkalkes (Mitteltrias) am Kalkalpensüdrand zwischen Kufstein (Tirol) und Saalfelden (Salzburg). - Diss. TU Berlin, 202 p.

Kobel, M. (1969): Lithostratigraphische und sedimentologische Untersuchungen in der kalkalpinen Mitteltrias (Anisian and Ladinian) des Rhätikon (Österreich und Fürstentum Lichtenstein). Mitt. Geol. Inst. ETH u. Univ. Zürich, N. F. Zürich, 118, 149 p.

Loeblich, A.R. & Tappan, H. (1988): Foraminiferal genera and their classification. - Van Nostrand Reinhold Company - New York

Logan, B. W., Rezak, R., & Ginsburg, R. N., 1964, Classification and environmental significance of algal stromatolites: Journal of Geology, v. 72, p. 68-83.

Meischner, K.-D., (1964): Allodapische Kalk, Turbidite in riff-nahen Sedimentations-Becken. In: Bouma, A.H., Brouwer, A. (Eds.), Turbidites. Elsevier, Amsterdam, p. 156–191.

Miller, H. (1962): Zur Geologie des westlichen Wetterstein- und Miemingergebirges (Tirol). Unveröffentl. Diss. Univ. München, 118 p.

Mostler, H. (1972): Ein Beitrag zur Genese mitteltriadischer Crinoidenkalke im Gebiet von Reutte, Tirol (Nördliche Kalkalpen) - Geol. Paläont. Mitt. Innsbruck, 2.

Mostler, H. (1986): Zur Mitteltrias westlich von Innsbruck - Jber. Mitt. oberrhein. geol. Ver., 68, p. 15-27.

Mühlöcker, F. (2000): Mitteltriasstratigraphie und Tektonik an der Basis der Inntaldecke der Innsbrucker

Nordkette. - Unveröffentl. Diplomarbeit Univ. Innsbruck, 89 p.
Nittel, P. (2004): Strukturell- stratigraphische Neubearbeitung und mikrofazielle Untersuchungen in der Mitteltrias des Kalkalpensüdrandes in der Umgebung von Innsbruck (Tirol, Österreich). – Unveröffentl. Diplomarbeit Univ. Innsbruck, 165 p.
Ott, E. (1972): Die Kalkalgen-Chronologie der Alpinen Mitteltrias in Angleichung an die Ammoniten-Chronologie.-N.Jb. Geol. Paläont. Abh., Stuttgart, 141, p. 81-115.
Ott, E. (1972): Zur Kalkalgen-Stratigraphie der Alpinen Trias.-Mitt. der Ges.der Geol. Bergbaustudenten in Österr., Innsbruck, Bd.21, p. 455-464.
Ott, E. (1974): Algae (Dasycladaceae).-Catalogus Fossilium Austriae, Wien. Heft XVIIb, p.1-64.
Resch, W. (1977): Zur Faziesabhängigkeit alpiner Trias-Foraminiferen. - Habilitation an der Univ. Innsbruck, 99 p.
Resch, W., (1972). Statistische Untersuchungen der Foraminiferen-Faunen aus dem Profil Köveskal/W-Ungarn (Fassan- tieferes Cordevol).- Mitt. der Ges.der Geol. Bergbaustudenten in Österr., Innsbruck, Bd.21, p. 513-538.
Resch, W., (1979). Zur Faziesabhängigkeit alpiner Trias-Foraminiferen.- Jahrb. Geol. B.-A., Wien, 122, p. 181-240.
Rettori, O et al. (1995): Foraminiferi del Trias inferiore e medio della Tetide: Revisione tassonomica, stratigrafia ed interpretazzione filogenetica.- Publ.du Depart. de Geol.et Palèont., Genève, N° 18, p. 343-362.
Rothpletz, A. (1888): Das Karwendelgebirge. - Z. deutsch. österr. Alpenverein.
Rüffer, T. (1995): Entwicklung einer Karbonatplattform. Fazies, Kontrollfaktoren und Sequenzstratigraphie in der Mitteltrias der westlichen Nördlichen Kalkalpen (Tirol, Bayern). - Gaea heidelbergensis, 1, 282 p.
Rüffer, T. & Zamparelli, V. (1997): Facies and Biota of Anisian to Carnian Carbonate Platforms in the Northern Calcareous Alps (Tyrol and Bavaria). - Facies, 37, p. 26-31.
Salaj, J., Borza, K., & Samuel, O., (1983). Triassic foraminifers of the West Carpathians., 213 p., Bratislava.
Sarnthein, M. (1965): Sedimentologische Profilreihen aus den mitteltriadischen Karbonatgesteinen der Kalkalpen nördlich und südlich von Innsbruck. - Verh. Geol. B. -A., 1-2, p. 119-162.
Sarnthein, M. (1966): Sedimentologische Profilreihen aus den mitteltriadischen Karbonatgesteinen der Kalkalpen nördlich und südlich von Innsbruck. 1. Fortsetzung. - Ber. Naturwiss. Med. Ver. Innsbruck, 54, p. 33-59.
Sarnthein, M. (1967): Versuch einer Rekonstruktion der mitteltriadischen Paläogeographie um Innsbruck, Österreich. - Geol. Rdsch., 56, p. 116-127.
Sarnthein, M. (1968): Bericht 1967 über.geologisch-sedimentologische Aufnahmen am Karwendelsüdrand (Blatt Innsbruck Umgebung). - Verh. Geol. B.-A., 3, p. 51-53.
Senowbari-Daryan, B. (1990): Die systematische Stellung der thalamiden Schwämme und ihre Besdeutung in der Erdgeschichte.- Münchener Geow. Abh, München, 21, p. 1-183.
Senowbari-Daryan, B. & Majidifard, R. (2003): A Triassic "problematic Microfossil" Revealed: probolocusois espahkensis Brönnimann, Zaninetti, Moshtagian and Huber 1974 is Attributed to the Dasycladacean Algae.- Facies, **48**, Erlangen, p. 19-20.
Siblik, M. (2001): Catalogus Fossilium Austriae, Brachiopoda mesozoica – a) Brachiopoda triadica – Supplementum, Wien, Heft Vc2a.
Tollmann, A. (1976): Analyse des klassischen nordalpinen Mesozoikums. - IX, 449 p., Deuticke, Wien.
Wilson, J, L. (1975): Carbonate facies in geologic history. – 471 p., Springer, New York.

Tafeln I-XI: Balkenlänge ohne Text immer 0,1 mm
Tafel I: Geländefotos in Farbe

Fig. 1 Grenze Virgloria-Formation / Steinalm-Formation. Ockerfarbener Wurstelkalk-Horizont der Virgloria-Fm. der die Grenze zur Steinalm-Fm. bildet. VSR-Graben (Seitengraben des Höttinger Grabens)
Fig. 2 Packstone mit Crinoiden- und Brachiopodenbruchstücken, dazwischen Glaukonit als gerundete Komponenten und authigen verteilt. Grenzhorizont zur Steinalm-Fm., Bruchkluppe,(Probe 377)
Fig. 3 Grenze Steinalm-Fm. / Reifling-Fm. im Profil Kranebitter Klamm West. Übergang von massigem zu dm-gebanktem Steinalmkalk, darüber Knollenkalke der Reifling-Fm., bis zum ersten Pietra Verde Horizont.
Fig. 4 Reifling-Fm. / Varietät Schusterbergkalk. Rötliche Karbonatknollen durchzogen von roten mergeligen Schlieren, Reifling-Fm. 2000-er Weg, (Aufschluß 239)
Fig. 5 Dritter und mächtigster Pietra Verde-Horizont mit grünlichen Tuffen im Profil Karwendelbahn, Reifling-Fm.
Fig. 6 Großoolith. Wettersteinkalk-Fm., Rifffazies am Innsbrucker Klettersteig
Fig. 7 Schichtungsparallele Großoolithstrukturen (="sheet cracks") mit Tepeestrukturen, Innsbrucker Klettersteig-Kemacher, Wetterstein-Fm. Lagunenfazies, (Aufschluß 406)
Fig. 8 gradierte Ooidsandbank, Trockenrisse (Pfeil) weisen auf ein Freiliegen an der Oberfläche, Innsbrucker Klettersteig- Kemacher, Wetterstein-Fm. Lagunenfazies, (Aufschluß 406)

Tafel I

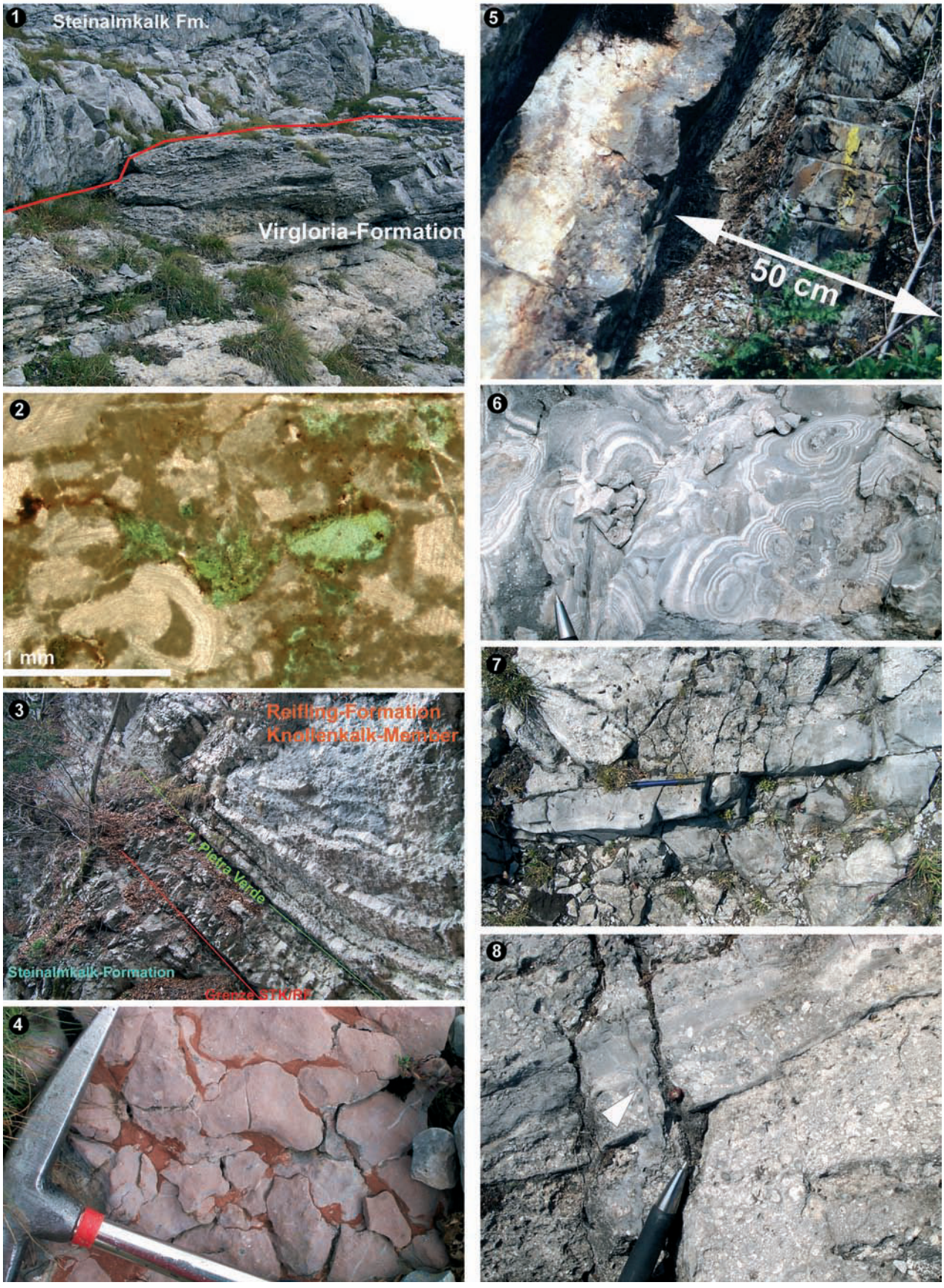
1
Steinalmkalk Fm.
Virgloria-Formation
2
1 mm
3
Reifling-Formation
Knollenkalk-Member
1. Pietra Verde
Steinalmkalk-Formation
Grenze STK/RF
4
5
50 cm
6
7
8

Tafel II: Foraminiferen Steinalm-Fm.

Fig. 1 *Dentalina* sp. Steinalm-Fm., Kranebitter Klamm, (Probe PM8)
Fig. 2 *Frondicularia woodwardi.* Steinalm-Fm., Klammeck, (Probe 110)
Fig. 3 *Frondicularia* sp. Steinalm-Fm., Kranebitter Klamm, (Probe KK1),
Fig. 4 *Frondicularia* cf. *xiphoidea (*sensu Salaj et al 1983; Tafel 83/16). Steinalm-Fm., Kranebitter Klamm, (Probe PM4)
Fig. 5 *Astacolus* sp. Steinalm-Fm., Kranebitter Klamm, (Probe PM4)
Fig. 6 *Austrocolomia* sp. Steinalm-Fm., Bruchkluppe, (Probe 377A)
Fig. 7 *Austrocolomia* sp. Steinalm-Fm. Kranebitter Klamm, (Probe PM 7)
Fig. 8 *Meandrospira dinarica*. Steinalm-Fm., Bruchkluppe, (Probe 186)
Fig. 9 *Duostominidae*. Steinalm-Fm., Bruchkluppe, (Probe 186)
Fig. 10 *Turriglomina mesotriassica*. Steinalm-Fm., Rauschbrunnengegend, (Probe 116)
Fig. 11 *Ophtalmidium abriolense* (ob.)*Ophtalmidium tricki* (unt.). Steinalm-Fm., Bruchkluppe, (Probe 377B)
Fig. 12 *Pilammina semiplana*. Steinalm-Fm., Geigerriß, (Probe 134)
Fig. 13 *Ophtalmidium ubeyliense*. Steinalm-Fm., Rauschbrunnengegend, (Probe 77)
Fig. 14 *Astacolus* sp. Steinalm-Fm., Bruchkluppe, (Probe 377A)
Fig. 15 *Scherochorella* sp. Steinalm-Fm., Rauschbrunnengegend, (Probe 116)
Fig. 16 *Bryozoe*. Steinalm-Fm., Kranebitter Klamm, (Probe PM7)
Fig. 17 *Spirorbis.* Querschnitt. Steinalm -Fm., Karwendelbahn, (Probe KB15)
Fig. 18 *Sprirorbis*. Steinalm-Fm., Kranebitter Klamm, (Probe PM6)

Tafel II

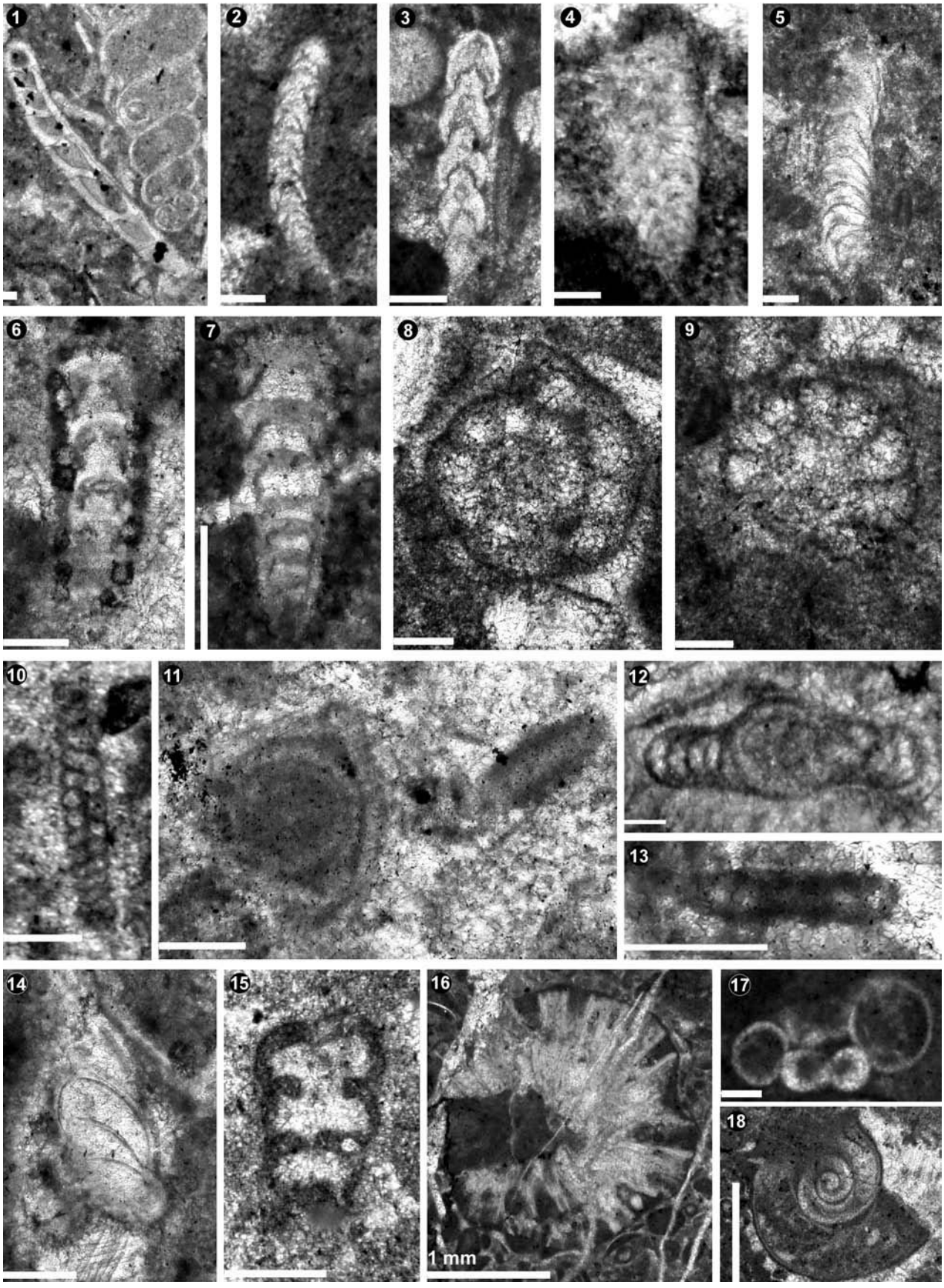

Tafel III: Dasycladaceen Steinalm-Fm.

Fig. 1 *Physoporella dissita.* Längsschnitt. Steinalm-Fm., Klammeck, (Probe 110)
Fig. 2 *Physoporella minutula*. Schrägschnitt. Steinalm-Fm., Klammeck, (Probe 110-2)
Fig. 3 *Physoporella minutula.* Steinalm-Fm., Klammeck, (Probe 110-2)
Fig. 4 *Physoporella dissita*. Fragment Längsschnitt. Steinalm-Fm., Kranebitter Klamm, (Probe PM 1)
Fig. 5 *Physoporella pauciforata*. Querschnitt. Steinalm-Fm., Klammeck, (Probe 110)
Fig. 6 *Oligoporella* sp. Im Längsschnitt mit typischer trichophorer, den Kalkpanzer durchsetzenden Pore. Steinalm-Fm., Klammeck, (Probe 110-2)
Fig. 7 *Favoporella annulata*. Fragmente aus Quer- und Schrägschnitt. Steinalm-Fm., Klammeck, (Probe 110)
Fig. 8 *Aciculella bacillum*. Leicht schräger Querschnitt. Steinalm-Fm., Klammeck, (Probe 110)
Fig. 9 *Aciculella bacillum*. Längssschnitt, Steinalm-Fm., Kranebitter Klamm, (Probe 110-2)
Fig. 10 *Oligoporella* sp. (links unten), *Physoporella dissita* (rechts oben). Steinalm-Fm., Klammeck, (Probe 110-2)
Fig. 11 *Encrinus liliformis* mit Anbohrungen. Steinalm-Fm., Karwendelbahn, (Probe KB 15)
Fig. 12 *Decurtella decurtata.* Steinalm-Fm., Achselkopf, (Probe 76)

Tafel III

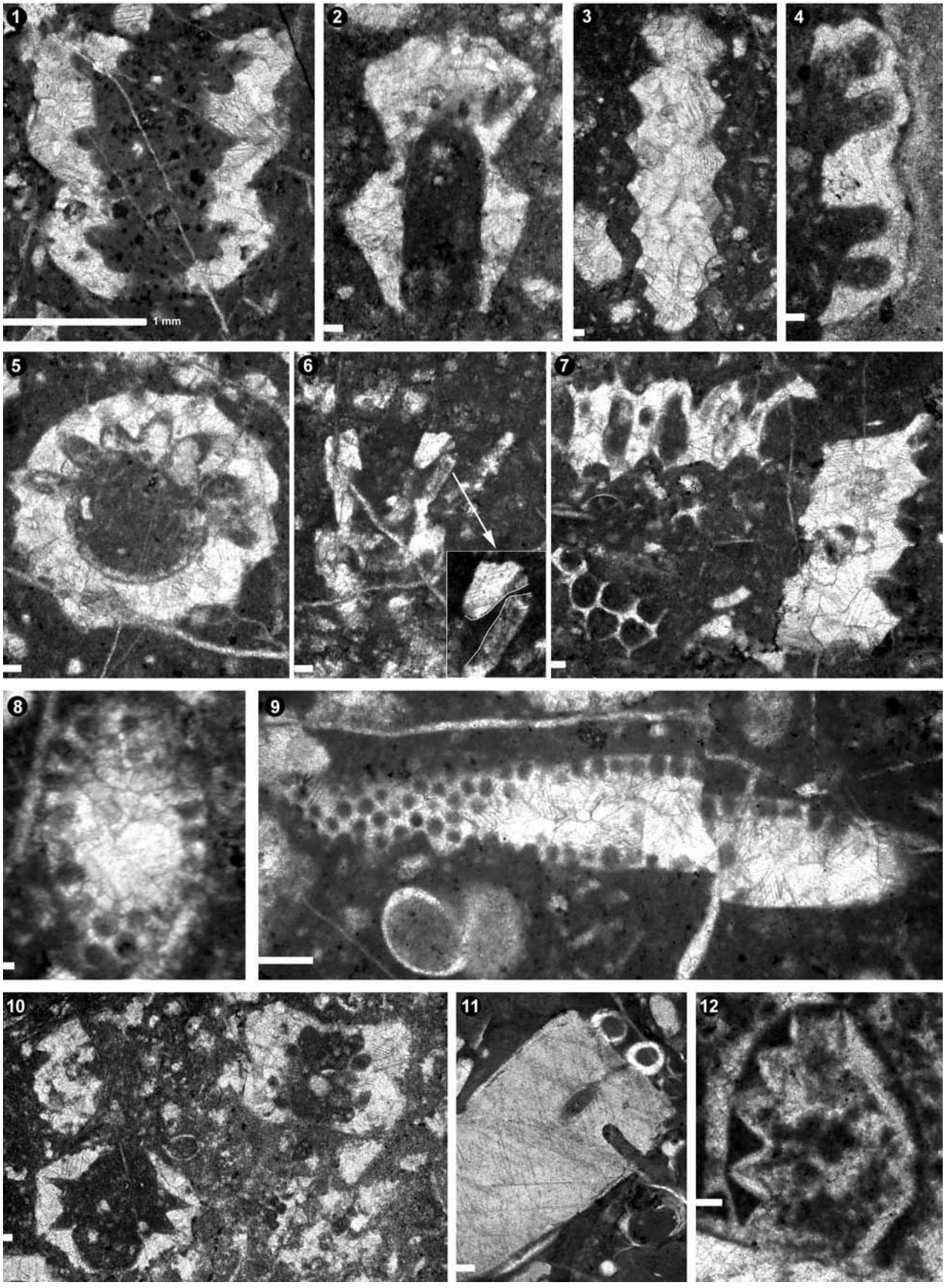

Tafel IV: Foraminiferen und Faziestypen Reifling-Fm.

Fig. 1 FAT A, partiell ausgewaschener, bioturbater Filament-Packstone. Reifling-Fm., Bruchkluppe, (Probe 237)
Fig. 2 FAT B, Geopetal verfüllte Radiolarien zeigen eine aufrechte Lagerung in einem partiell ausgewaschenen Packstone. Reifling-Fm., Kranebitter Klamm, (Probe PM11)
Fig. 3 FAT C, Bioturbater Pack- bis Wackestone mit stromatactoiden Hohlräumen. Reifling-Fm., Klammeck, (Probe 112)
Fig. 4 Durch Stylolithen begrenzte Packstone-Knolle umgeben von eingeregelten Filamenten und Intraklasten. Reifling-Fm., Achselkopf, (Probe 268)
Fig. 5 *Turriglomina mesotriassica*. Reifling-Fm., Geigerriß, (Probe 131)
Fig. 6 *Turriglomina magna*. Reifling-Fm., Kranebitter Klamm, (Probe PM20)
Fig. 7 *Ophtalmidium abriolense*. Reifling-Fm., Bruchkluppe, (Probe 239A)
Fig. 8 *Arenovidalina chialingchiangense*. Reifling-Fm. Schusterbergkalk, Achselkopf, (Probe 268)
Fig. 9 *Ichtyolaria* sp. Reifling-Fm., Bruchkluppe, (Probe 237)
Fig. 10 Frondicularia woodwardi. Reifling-Fm., Seegrube-Einheit, Kranebitter Klamm, (Probe KKC)
Fig. 11 Scheinbar zellig, doppelwandiger Aufbau von fraglichen Kalkalgenresten. Reifling-Fm., Seegrube-Einheit, Kranebitter Klamm, (Probe KKA)
Fig. 12 Earlandia sp. Reifling-Fm., Seegrube- Einheit, Bruchkluppe, (Probe BK14)
Fig. 13 Holothurienrädchen. Reifling-Fm., Seegrube- Einheit, Kranebitter Klamm, (Probe KKA)
Fig. 14 *Tubiphytes* sp. Reifling-Fm., Seegrube- Einheit, Kranebitter Klamm, (Probe KKC)
Fig. 15 *Tubiphytes gracilis*. Reifling-Fm., Seegrube- Einheit, Geigerriß, (Probe 131)

Tafel IV

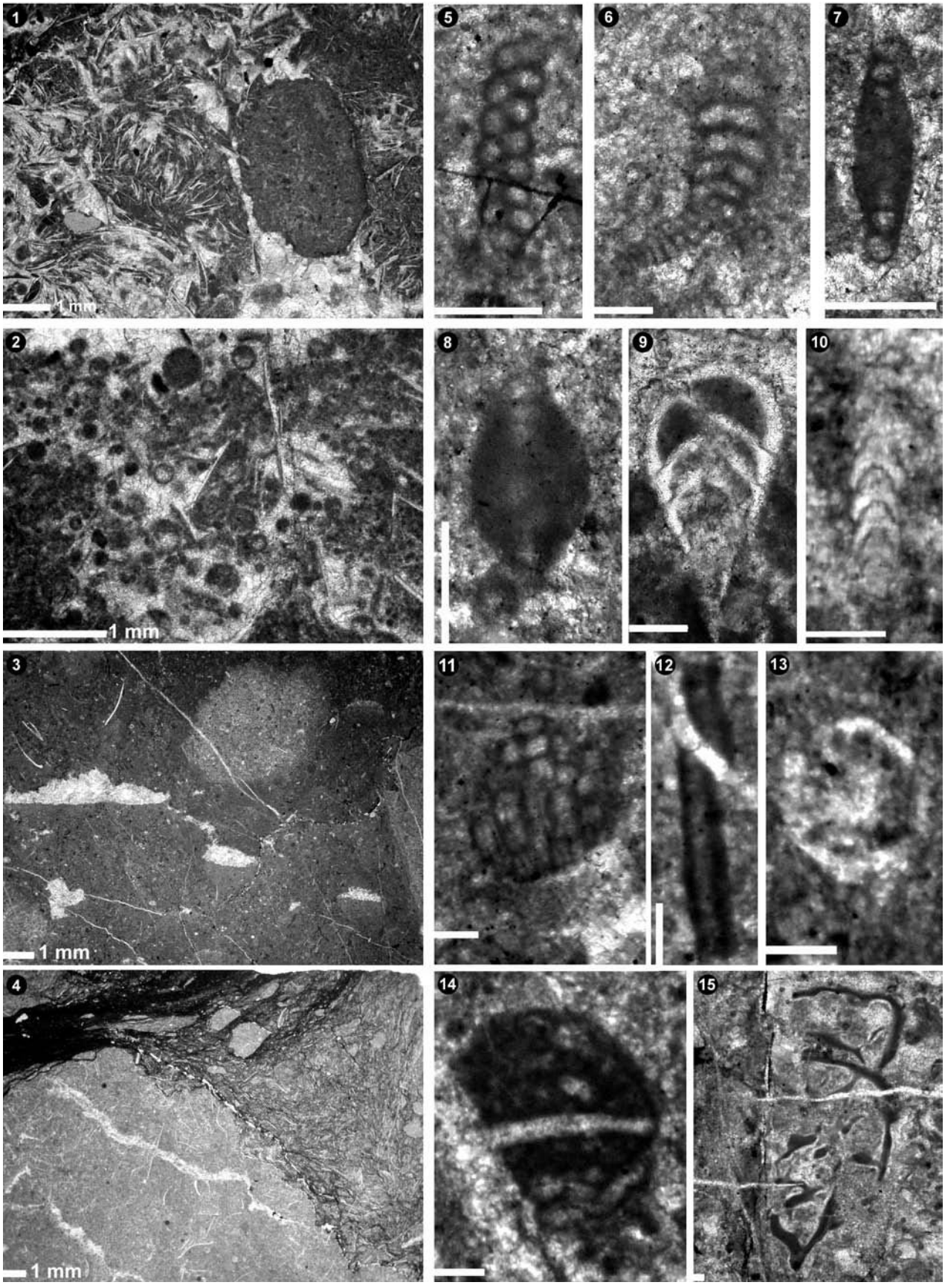

Tafel V: Foraminiferen und Microproblematika WKR/S

Fig. 1 *Paleolituonella meridionalis*. Wetterstein-Fm., Rauschbrunnengegend, (Probe 144C)
Fig. 2 Sifonofera sp. Wetterstein-Fm. Riffschutt, Brandjochkreuz, (Probe 227)
Fig. 3 *Agglutisolena conica*. Wetterstein-Fm. Riffschutt, Brandjochkreuz, (Probe 227)
Fig. 4 *Agglutisolena conica*. Wetterstein-Fm., 2000er-Weg, (Probe 298)
Fig. 5 *Turriglomina mesotriassica*. Wetterstein-Fm., Achselkopf, (Probe 266)
Fig. 6 *Endotebanella sp*. Wetterstein-Fm., Achselkopf, (Probe 266)
Fig. 7 *Ammobaculites* sp. Wetterstein-Fm., Sattelspitze, (Probe 343)
Fig. 8 *Endoteba elegans*. Wetterstein-Fm., Bruchkluppe, (Probe 330)
Fig. 9 *Planiinvoluta carinata*. Wetterstein-Fm., Bruchkluppe, (Probe 330)
Fig. 10 *Ophtalmidium* cf. *exiguum*. Wettersteinkalk-Fm., Bruchkluppe, (Probe 330-2)
Fig. 11 *Aulotortus friedli* (sensu Piller). Wettersteinkalk-Fm., Hölltalgraben, (Probe 358B)
Fig. 12 *Ladinella porata*. Wettersteinkalk-Fm., Bruchkluppe, (Probe 330)
Fig. 13 *Baccanella floriformis*. (Wettersteinkalk-Fm., Achselboden, (Probe 215A)
Fig. 14 Solenoporacee. Wettersteinkalk-Fm., 2000er-Weg, (Probe 301)
Fig. 15 Koralle. Wettersteinkalk-Fm., Rauschbrunnengegend, (Probe 114)
Fig. 16 *Tubiphytes* sp. Wettersteinkalk-Fm., Höttinger Alm-Weg, (Probe 164)
Fig. 17 *Tubiphytes* sp. Wettersteinkalk-Fm., Sparberschrofen, (Probe 281)

Tafel V

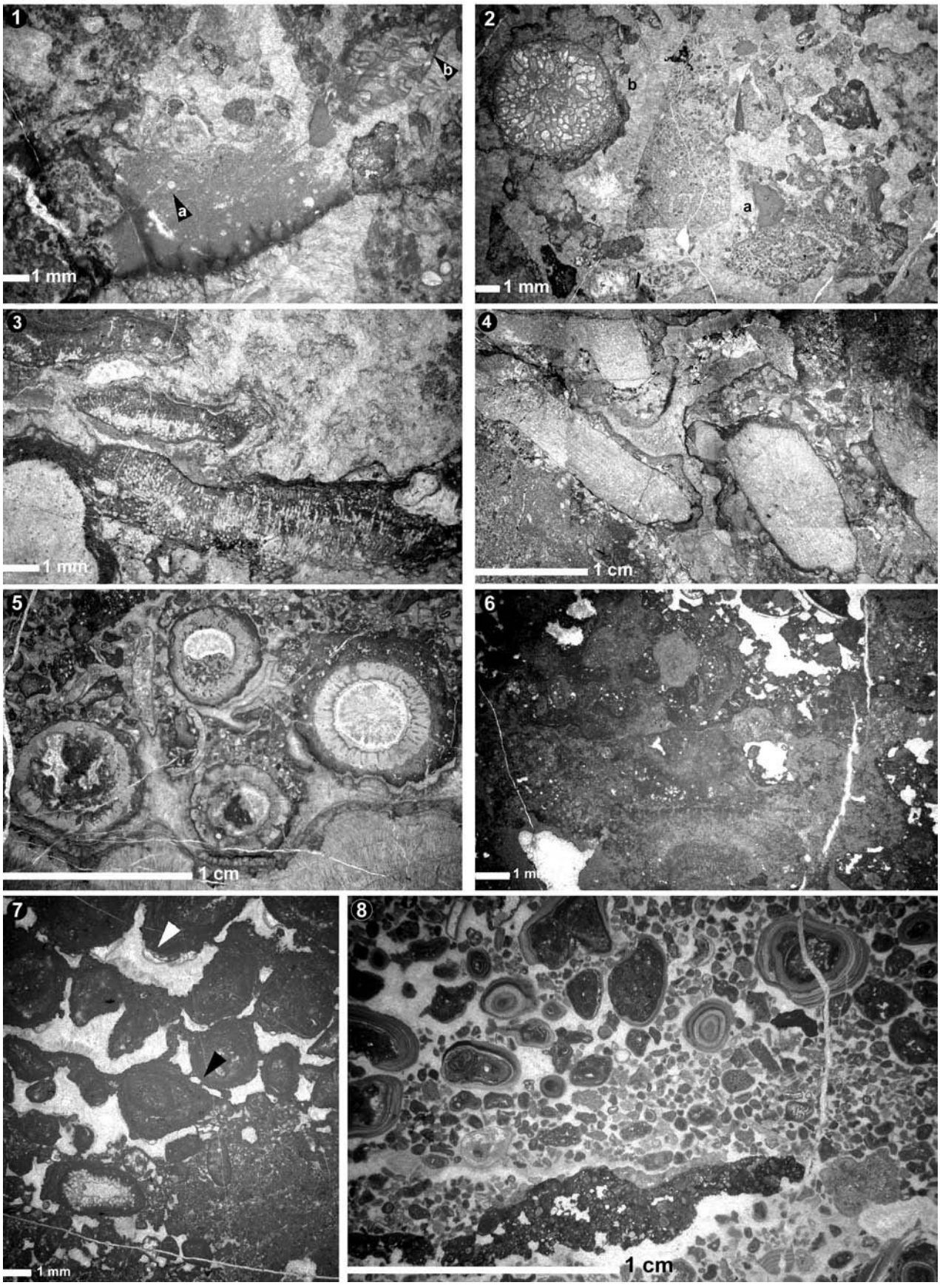

Tafel VI: Schwämme WKR/S

Fig. 1 *Colospongia catenulata*. Wettersteinkalk-Fm., Schneekar, (Probe 350)
Fig. 2 *Colospongia* sp. Wettersteinkalk-Fm., Brandjochspitz, (Probe 329-3)
Fig. 3 *Vesicocaulis carinthiacus*. Wettersteinkalk-Fm., Achselboden, (Probe 150B)
Fig. 4 *Vesicocaulis alpinus*. Wettersteinkalk-Fm., Tramentboden, (Probe 243)
Fig. 5 *Solenolmia manon minor*. Wettersteinkalk-Fm., Achselboden, (Probe 150B)
Fig. 6 *Solenolmia manon manon*. (Pfeil: *Baccanella floriformis*) Wettersteinkalk-Fm., Achselboden, (Probe 164-2)
Fig. 7 *Stolenella* sp. Wettersteinkalk-Fm., Söldensteig, (Probe 87)
Fig. 8 *Vesicocaulis carinthiacus*. Wettersteinkalk-Fm., Rauschbrunnensteig, (Probe 114)
Fig. 9 *Colospongia catenulata*. (Pfeil: *Baccanella floriformis*) Wettersteinkalk-Fm., Achselboden, (Probe 163)
Fig. 10 Sphinctozoa. Wettersteinkalk-Fm., 2000er-Weg, (Probe 298); Balkenlänge 1 mm

Tafel VI

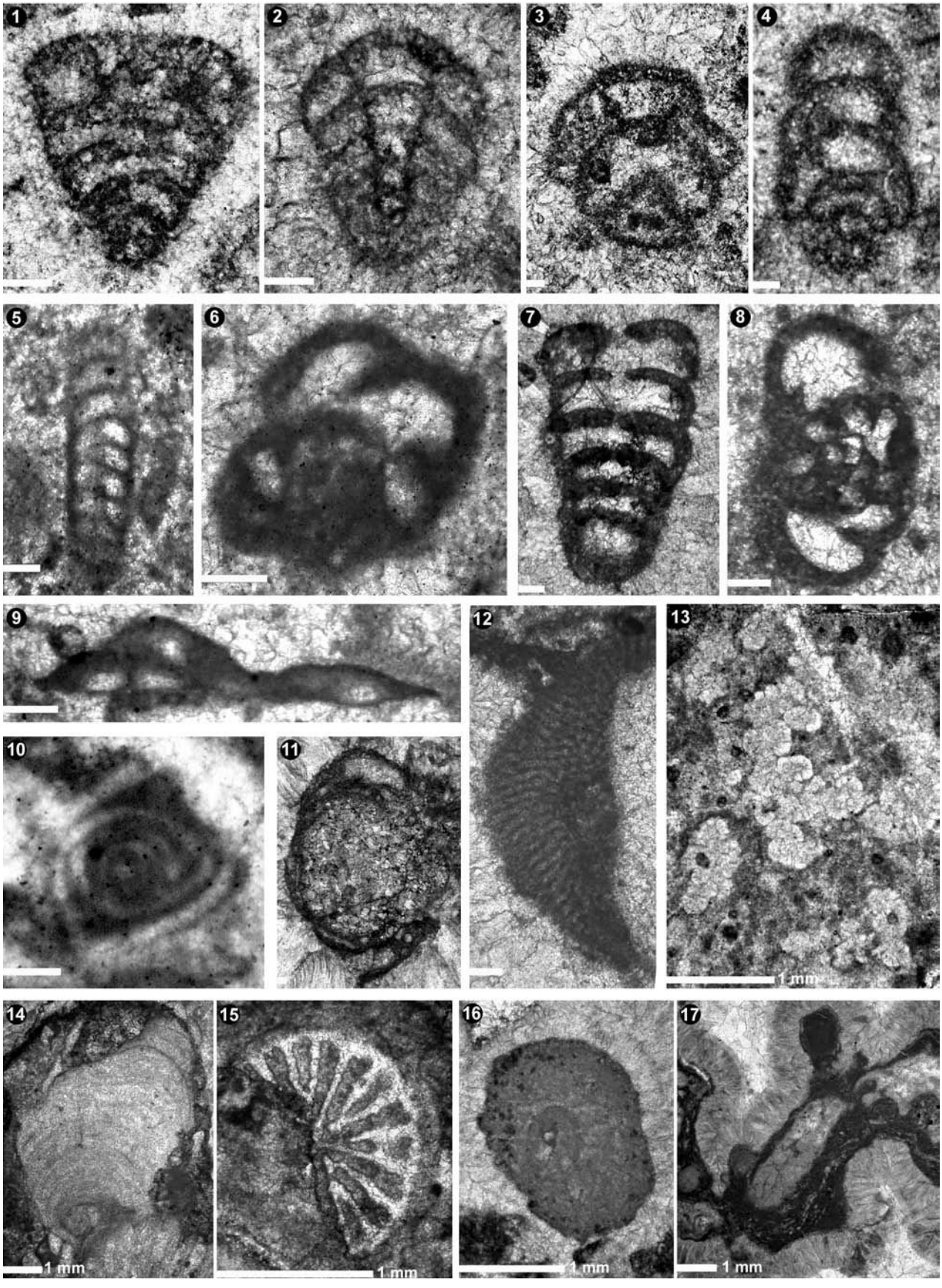

Tafel VII: Faziestypen WKR/S und WKL

Fig. 1 FAT A1, Mikritische Hohlraumfüllungen mit Radiolarien, a) Sphinctozoa. Wettersteinkalk-Fm., Achselkopfweg, (Probe 265)

Fig. 2 FAT A3, schlecht sortierter Lithoklast-Rudstone aus isolierten Organismen a) Tubiphytes, b) *Solenolmia manon* und lithifizierten Riff bzw. Vorriffkarbonaten. Zementiert durch subamarinen und radiaxialen Calcit. Wettersteinkalk-Fm., Achselboden, (Probe 164-2)

Fig. 3 FAT B Schuttbindende porostromate Algen und onkoidische Krusten, Bind- Bafflestone. Wettersteinkalk-Fm., Achselboden, (Probe 216)

Fig. 4 FAT B2, Bafflestone mit teilweise von Solenoporaceen (a), *Tubiphytes* (b) und Sphinctozoen(c) inkrustierten Korallen, Zwischenräume mit ausgewaschenem Riffmaterial aufgefüllt. Wettersteinkalk-Fm., Brandjochboden, Probe 301)

Fig. 5 FAT C1/1, Rud-Grainstone, mit Querschnitten von *Teutloporella herculea*, Riffnähe. Wettersteinkalk-Fm., Brandjochboden, (Probe 231-2)

Fig. 6 FAT C3, Fenestral Bindstone aus porostromaten Calcimikroben vom Typ *Cayeuxia.* Wettersteinkalk-Fm., Achselkopf, (Probe 286/1-2)

Fig. 7 FAT C1/2, Rindenkörner und Onkoide mit einem CU-trend gradiert, Meniskuszement (Pfeil schwarz) und Hängezement (=Dripstone Zement) (Pfeil weiß) sprechen für Freiliegen an der Oberfläche und einer Ablagerung in der vadosen Zone. Wettersteinkalk-Fm., Gipfel Brandjochkreuz, (Probe 232)

Fig. 8 FAT C1/3 Gradierter Pisoidgrain- Rudstone, gut ausgewaschen, Coarsening Upward (CU). Wettersteinkalk-Fm., Innsbrucker Klettersteig-Kemacher, (Probe 406)

Tafel VII

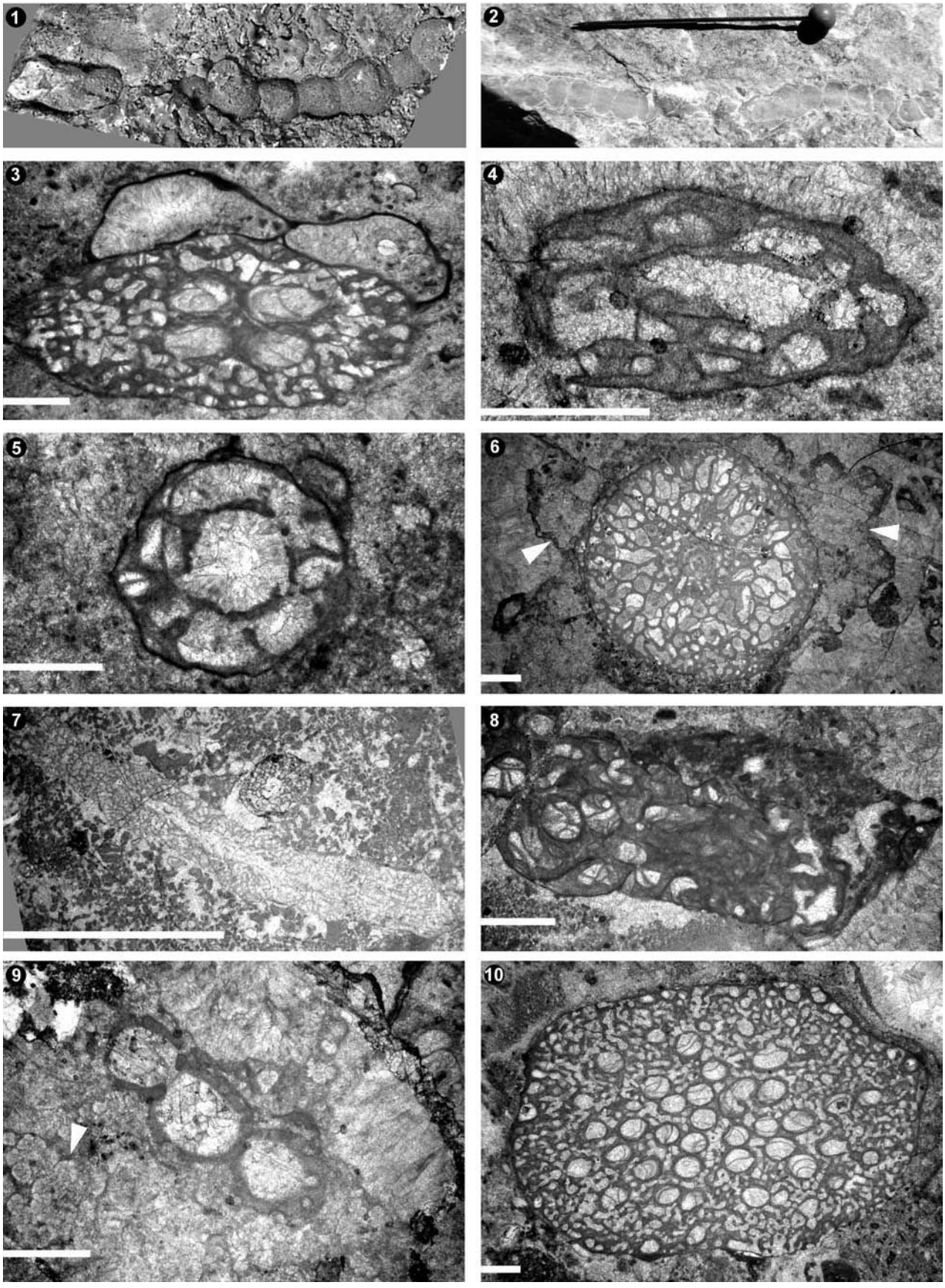

Tafel VIII: Foraminiferen WKL

Fig. 1 *Aulotortus tenuis*. Wettersteinkalk-Fm. Lagunenfazies, Hölltalgraben, (Probe 49/1)
Fig. 2 *Turriglomina mesotriassica*. Wettersteinkalk-Fm. Lagunenfazies, Brandjochkreuz, (Probe 228)
Fig. 3 *Austrocolomia carinata* nov. spec. Wettersteinkalk-Fm. Lagunenfazies, Brandjochkreuz, (Probe 228)
Fig. 4 *Pseudobolivina tornata*. Wettersteinkalk-Fm. Lagunenfazies, Brandjochkreuz- Gipfel, (Probe 233)
Fig. 5 *Aulotortus friedli*. Wettersteinkalk-Fm. Lagunenfazies, Brandjochkreuz, (Probe 234)
Fig. 6 *Lamelliconus* sp. Wettersteinkalk-Fm. Lagunenfazies, Hölltalgraben, (Probe 49/1)
Fig. 7 *Robuloides* sp. Wettersteinkalk-Fm. Lagunenfazies, Brandjochkreuz, (Probe 228)
Fig. 8 *Glomospirella* sp. Wettersteinkalk-Fm. Lagunenfazies, Achselkopf, (Probe 286/1)
Fig. 9 *Endotriadella wirzi*. Wettersteinkalk-Fm. Lagunenfazies, Hölltalgraben, (Probe 49/3)
Fig. 10 ?*Auloconus permodiscoides*. Wettersteinkalk-Fm. Lagunenfazies, Brandjochkreuz, (Probe 228-2)
Fig. 11 Valvulina azzouzi. Wettersteinkalk-Fm. Lagunenfazies, Trammentboden, (Probe 242)
Fig. 12 *Gaudryina* sp. Wettersteinkalk-Fm. Lagunenfazies, Achselkopf, (Probe 74)
Fig. 13 *Ammobaculites radstadtensis*. Wettersteinkalk-Fm. Lagunenfazies, Rauschbrunnengegend, (Probe 361)
Fig. 14 *Glomospirella facilis*. Wettersteinkalk-Fm. Lagunenfazies, Achselkopf, (Probe 286/1-2)
Fig. 15 *Mesoendothyra isjumiana*. Wettersteinkalk-Fm. Lagunenfazies, Brandjochboden, (Probe 371)
Fig. 16 *Trochammina* sp. Wettersteinkalk-Fm. Lagunenfazies, Achselkopf, (Probe 286)
Fig. 17 *Trochammina tabasensis*. Wettersteinkalk-Fm. Lagunenfazies, Aspachhütte, (Probe 83-2)
Fig. 18 Valvulina sp. Im Querschnitt. Wettersteinkalk-Fm., Lagunenfazies, Brandjochboden, (Probe 223)
Fig. 19 *Agathammina austroalpina*. Längsschnitt, Wettersteinkalk-Fm. Lagunenfazies, Aspachhütte, (Probe 83-2)
Fig. 20 *Agathammina austroalpina*. Querschnitt, Wettersteinkalk-Fm. Lagunenfazies, Aspachhütte, (Probe 83)
Fig. 21 *Valvulina azzouzi*. Schräger Schnitt. Wettersteinkalk-Fm. Lagunenfazies, Aspachhütte, (Probe 83-2)
Fig. 22 cf. *Agathammina parafusiformis*. Wettersteinkalk-Fm. Lagunenfazies, Achselkopf, (Probe 74)

Tafel VIII

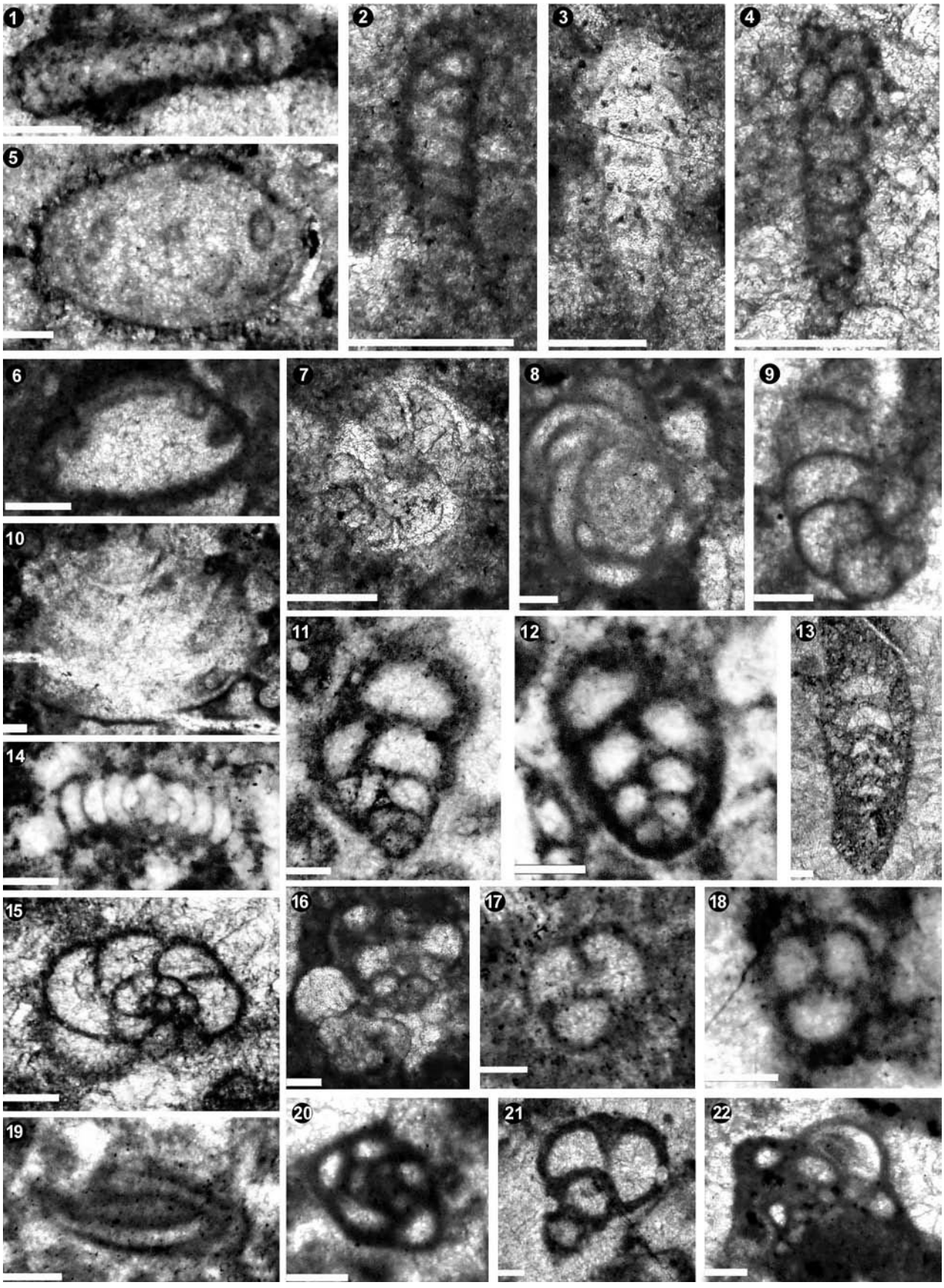

Tafel IX: Dasycladaceen WKL

Fig. 1 *Teutloporella herculea* im Handstück, in Riffnähe. Wettersteinkalk-Fm. Lagunenfazies, Brandjochspitz, (Probe 324-3)
Fig. 2 *Teutloporella nodosa*. Schrägschnitt, Wettersteinkalk-Fm. Lagunenfazies, Achselkopf, (Probe 286/1)
Fig. 3 *Cayeuxia* sp. Wettersteinkalk-Fm. Lagunenfazies, Hölltalgraben, (Probe 49/1)
Fig. 4 cf.*Griphoporella* sp. Wettersteinkalk-Fm., Lagunenfazies, Brandjochboden, (Probe 231-2)
Fig. 5 Porostromate Alge vom Typ *Cayeuxia*. Detailbild: nach oben weisende, spitzwinklige Verzweigung der länglichen Röhren. Wettersteinkalk-Fm. Lagunenfazies, (Probe 327B)
Fig. 6 *Diplopora annulata*. Wettersteinkalk-Fm. Lagunenfazies, Hölltalgraben, (Probe 49/1)
Fig. 7 *Teutloporella herculea*. Querschnitt, Wettersteinkalk-Fm. Lagunenfazies, Brandjochboden, (Probe 231),
Fig. 8 *Teutloporella peniculiformis*. Wettersteinkalk-Fm. Lagunenfazies, Achselboden, (Probe 371)
Fig. 9 *Aciculella sokaci*. Wettersteinkalk-Fm. Lagunenfazies, Achselboden, (Probe 371)
Fig. 10 Gametophore. Wettersteinkalk-Fm. Lagunenfazies, Brandjochboden, (Probe 231)
Fig. 11 Gametophore. Wettersteinkalk-Fm. Lagunenfazies, Brandjochkreuz, (Probe 234B)
Fig. 12 Gametophore. Wettersteinkalk-Fm. Lagunenfazies, Brandjochboden, (Probe 231A-2)
Fig. 13 Gametophore. Wettersteinkalk-Fm. Lagunenfazies, Brandjochboden, (Probe 231-2)
Fig. 14 *Aciculella bacillum*. Wettersteinkalk-Fm. Lagunenfazies, Brandjochboden, (Probe 231-2)
Fig. 15 *Aciculella baccillum*. Wettersteinkalk-Fm. Lagunenfazies, Brandjochboden, (Probe 231)
Fig. 16 *Aciculella sokaci*. Wettersteinkalk-Fm. Lagunenfazies, Achselboden, (Probe 371)
Fig. 17 *Aciculella* cf.*sokaci* . Wettersteinkalk-Fm. Lagunenfazies, Achselboden, (Probe 371)

Tafel IX

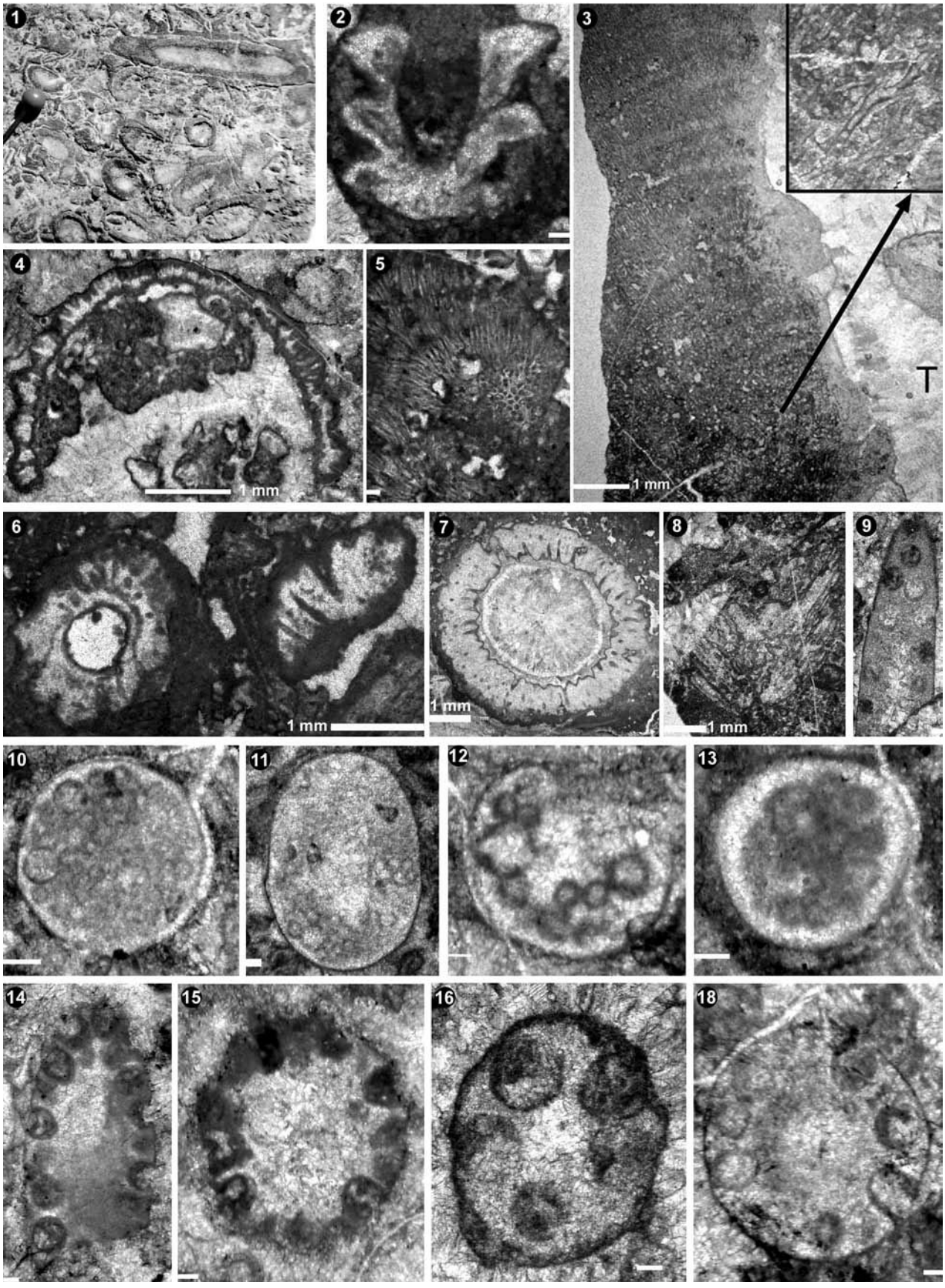

Tafel X Dasycladaceen WKL, Cordevol

Fig. 1 *Clypeina besici*. Schrägschnitt, Wettersteinkalk-Fm. Lagunenfazies, (Probe 231-3)
Fig. 2 *Clypeina besici*. Längsschnitt, Wettersteinkalk-Fm. Lagunenfazies, Durrachsteig, (Probe 83-2)
Fig. 3 *Clypeina besici*. Schrägschnitt, Wettersteinkalk-Fm. Lagunenfazies, (Probe 231-3)
Fig. 4 *Clypeina besici*. Wettersteinkalk-Fm. Lagunenfazies, Achselkopf, (Probe 74)
Fig. 5 *Clypeina besici*. Wettersteinkalk-Fm. Lagunenfazies, Durrachsteig, (Probe 83-2)
Fig. 6 *Clypeina besici*. Wettersteinkalk-Fm. Lagunenfazies, Durrachsteig, (Probe 83)
Fig. 7 *Clypeina besici*. Wettersteinkalk-Fm. Lagunenfazies, Durrachsteig, (Probe 83)
Fig. 8 *Clypeina besici*. Wettersteinkalk-Fm. Lagunenfazies, Durrachsteig, (Probe 83-2)
Fig. 9 *Poikiloporella duplicata*. Längsschnitt, Wettersteinkalk-Fm. Lagunenfazies, Durrachsteig, (Probe 83-2)
Fig. 10 *Physoporella jomdaensis*. Wettersteinkalk-Fm. Lagunenfazies, Durrachsteig, (Probe 83)
Fig. 11 *Poikiloporella duplicata*. Schrägschnitt, Wettersteinkalk-Fm. Lagunenfazies, Durrachsteig, (Probe 83-3)
Fig. 12 *Physoporella jomdaensis*. Wettersteinkalk-Fm. Lagunenfazies, Durrachsteig, (Probe 83)
Fig. 13 *Physoporella jomdaensis*. Wettersteinkalk-Fm. Lagunenfazies, Durrachsteig, (Probe 83-3)

Tafel X

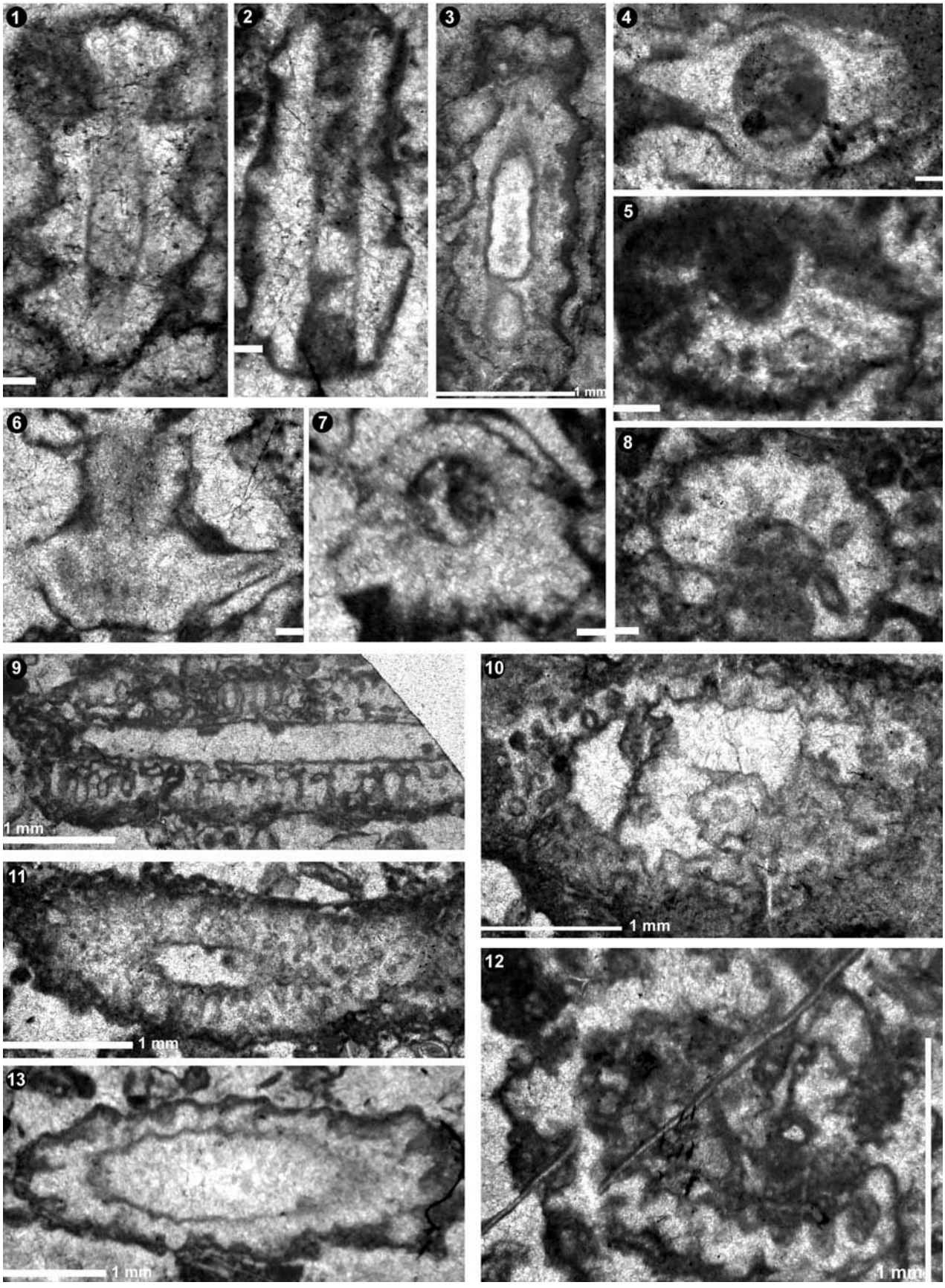

Tafel XI

Fig. 1-8 *Probolocuspis espahkensis*. Wettersteinkalk-Fm., Lagunenfazies,
Fig. 1 steiler Schrägschnitt, die Pfeile markieren die einzelnen Stachel, die in unterschiedlichen Winkeln zur Achse orientiert sind. Wettersteinkalk-Fm. Lagunenfazies, Brandjochboden, (Probe 221)
Fig. 2 flacher Schrägschnitt. Wettersteinkalk-Fm. Lagunenfazies, Brandjochkreuz, (Probe 231-3)
Fig. 3 flacher Schrägschnitt. Wettersteinkalk-Fm. Lagunenfazies, Brandjochkreuz, (Probe 231-3)
Fig. 4 zwei Stachel. Wettersteinkalk-Fm. Lagunenfazies, (Probe 79/2),
Fig. 5 Stachel. Wettersteinkalk-Fm. Lagunenfazies, Brandjochkreuz, (Probe 231-3)
Fig. 6 zwei Stachel. Wettersteinkalk-Fm. Lagunenfazies, Brandjochkreuz, (Probe 234B)
Fig. 7 Stachel. Wettersteinkalk-Fm. Lagunenfazies, Brandjochkreuz, (Probe 231)
Fig. 8 zwei Stachel, Wettersteinkalk-Fm. Lagunenfazies, Hölltalgraben, (Probe 49/1)
Fig. 9 Verdacht auf *Teutloporella* sp. Weit in den Innraum reichenden Poren (Pfeil). Wettersteinkalk-Fm. Riffschutt, Achselkopf, (Probe 282)
Fig. 10 Codiacee. Eventuell proximaler Teil, Längszellfäden sichtbar (Pfeil). Wettersteinkalk-Fm. Riffschutt, Kranebitter Klamm, (Probe 317)
Fig. 11 Verzweigende Kalkalge, Verdacht auf Codiacee. Wettersteinkalk-Fm. Lagunenfazies, Hölltalgraben, (Probe 49/3)
Fig. 12 Codiacee. Ähnlichkeit mit *Collerocodium*. Deutlich erkennbar die cortikale Zone und Reste von Längszellfäden in der Medulla. Wettersteinkalk-Fm. Riffschutt, Bruchkluppe, (Probe 330)
Fig. 13 *Ladinella porata*. Aufsitzend auf fädigen Algen (?*Girvanella*). Wettersteinkalk-Fm. Riffschutt, Bruchkluppe, (Probe 330)
Fig. 14 *Ladinella porata*. Querschnitt mit Zentralkanal. Wettersteinkalk-Fm. Riffschutt, Bruchkluppe, (Probe 330)

Tafel XI

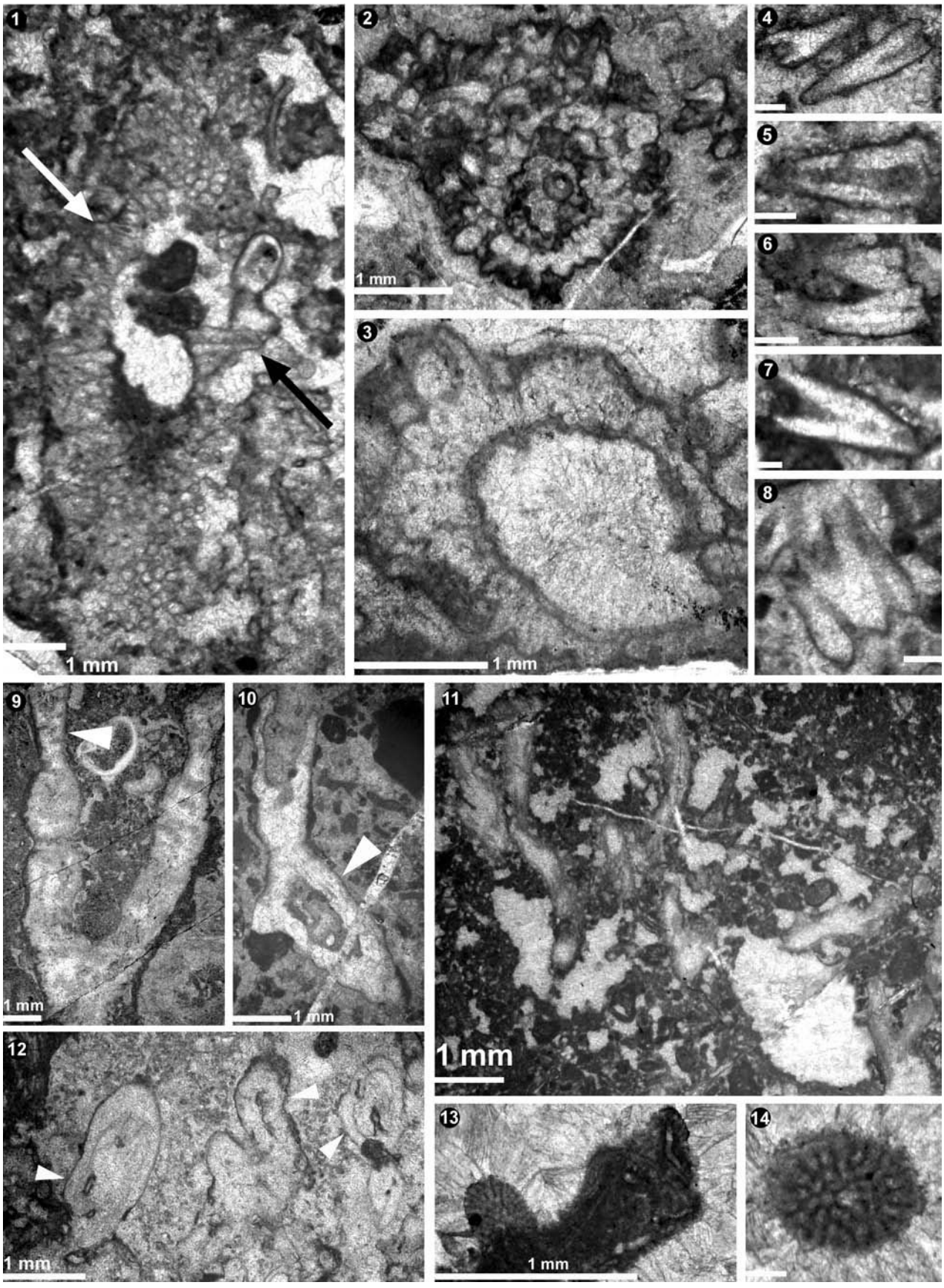

Tafel XII

Fig. 1-9 *Probolocuspis aculeata* nov.spec

Fig. 1 Schrägschnitt mit rautenförmigen Stachelquerschnitten (Pfeil). Wettersteinkalk-Fm. Lagunenfazies, Brandjochkreuz, (Probe 228-3)

Fig. 2 Fragment flacher Schrägschnitt. Wettersteinkalk-Fm. Lagunenfazies, Brandjochspitz, (Probe 328-D)

Fig. 3 steiler Schrägschnitt, mit rautenförmigen Stachelquerschnitten und nach innen an Größe zunehmenden Zentralkanal. Wettersteinkalk-Fm. Lagunenfazies, Brandjochkreuz, (Probe 327)

Fig. 4 Fragment Längsschnitt im Außenbereich der Stammzelle. Wettersteinkalk-Fm. Lagunenfazies, Brandjochkreuz, (Probe 228-3)

Fig. 5 Querschnitte von *Teutloporella herculea* (links) und *Teutloporella* XX nov. spec (Pfeil). Wettersteinkalk-Fm. Lagunenfazies, Brandjochkreuz, (Probe 328D)

Fig. 6 leicht schräger Querschnitt (Ausschnitt aus Fig. 5). Wettersteinkalk-Fm. Lagunenfazies, Brandjochkreuz, (Probe 328D)

Fig. 7 Schrägschnitt mit rautenförmigen Stachelquerschnitten (links) und Fragment Längsschnitt (rechts). Wettersteinkalk-Fm. Lagunenfazies, Brandjochkreuz, (Probe 228)

Fig. 8 Rautenförmiger Querschnitt eines „Stachels" mit Zentralkanal. Wettersteinkalk-Fm. Lagunenfazies, Brandjochkreuz, (Probe 228-3)

Fig. 9 Fragment Schrägschnitt mit rautenförmigen Stachelquerschnitten und deutlichem Zentralkanal (Pfeil). Wettersteinkalk-Fm. Lagunenfazies, Brandjochkreuz, (Probe 228)

Fig. 10 Fragment Schrägschnitt. Wettersteinkalk-Fm. Lagunenfazies, Brandjochkreuz, (Probe 228)

Tafel XII

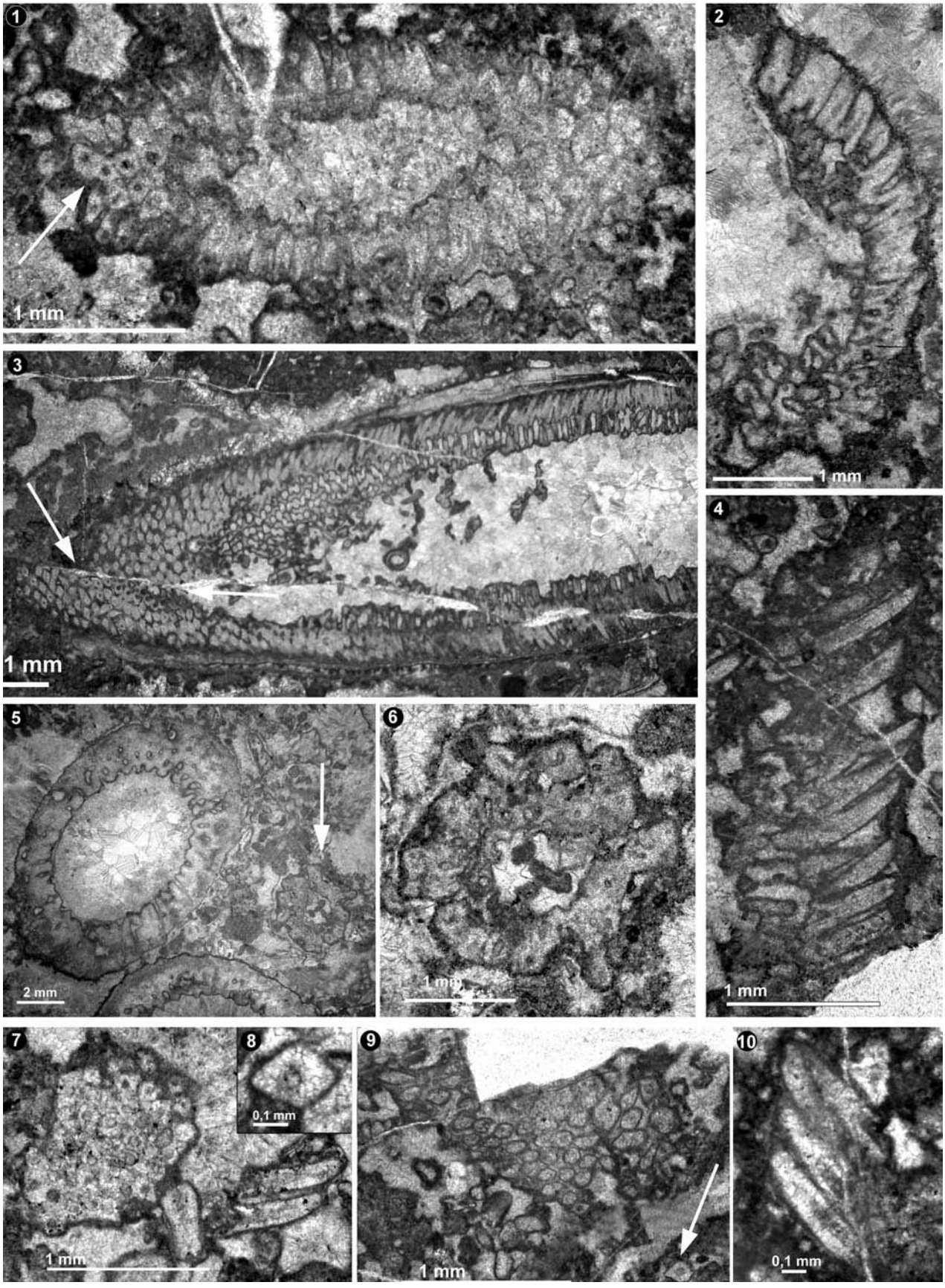

Geo.Alp, Vol. 3, S. 147–166, 2006

SPATIAL FEATURES OF HOLOCENE STURZSTROM-DEPOSITS INFERRED FROM SUBSURFACE INVESTIGATIONS (FERNPASS ROCKSLIDE, TYROL, AUSTRIA)

Christoph Prager[1, 2], Karl Krainer[1], Veronika Seidl[1] & Werner Chwatal[3]

With 11 figures and 2 tables

[1] University of Innsbruck, Institute of Geology and Paleontology, Innrain 52, A-6020 Innsbruck, Austria

[2] alpS Centre for Natural Hazard Management, Grabenweg 3, A- 6020 Innsbruck, Austria

[3] Technical University of Vienna, Institute of Geodesy and Geophysics, Gußhausstrasse 27-29, A-1040 Vienna, Austria

Abstract

A low frequency Ground Penetrating Radar (GPR) system was successfully applied for near subsurface explorations at different accumulation areas of the fossil Fernpass rockslide (Tyrol, Austria), which is one of the largest mass movements in the Alps. Based on detailed field studies and calibrated by drillings down to a depth of 14 m, the reflectors of the processed GPR-data could be well attributed to different depositional units. As a result, the distal rockslide deposits feature intensively varying accumulation geometries and are up to approximately 30 m thick. In addition, the topographically corrected GPR data show that the Toma, i.e. cone-shaped hills composed of rockslide debris, show deeper roots than the topographically less elevated rockslide successions between them. Compiled field-, drilling- and GPR-data indicate that the accumulation pattern and spread of the investigated rockslide deposits was obviously predisposed by the late-glacial valley morphology and that the Sturzstrom surged upon groundwater-saturated, fine-grained lacustrine sediments. Thus we assume that dynamic undrained loading, reducing the effective stresses between the rockslide and its incompetent substrate, enabled the extremely long run-out distance of the sliding mass measuring up to at least 15.5 km. Continuous gravitational spreading, which probably occurred subsequent to the rapid Sturzstrom flow, resulted in a further decomposition of the rockslide deposits and the generation of the present morphology, characterised by the well-known Toma hills and associated funnel- to basin-formed depressions which include several kettle-like lakes. After decomposition, the spreading rockslide deposits have locally been covered by on-lapping fluvial deposits. According to GPR data, these post-rockslide sediments can reach thicknesses of up to at least 20 m.

1. Introduction

"Sturzströme" are rapid moving rock avalanches, commonly greater than 10^6 m^3 in volume and may cover excessive travel distances even on only gently sloped valley floors due to their flow-like behaviour (Heim, 1932; Hsü, 1975). The dynamic disintegration of catastrophic failing rock masses generates unconsolidated attrition breccias of different grain-sizes and with varying contents of fine interstitial material in the pore space. The fracturing and crushing of the sliding mass lower significantly the internal friction coefficient and the shearing resistance, especially when the disintegrating mass and/or its substrate are water-saturated (e.g. Rouse, 1984; Abele, 1997; Erismann & Abele, 2001; Legros, 2002; Hungr and Evans, 2004). Thus, the enhanced mobility of many rockslides may be attributed to lubrication effects that are controlled by grain size reductions and sufficient water supply.

Also one of the largest mass movements in the Alps, the catastrophic Fernpass rockslide in the Northern Calcareous Alps (Tyrol, Austria), shows long run-out distances up to at least 15.5 km in length. Since its complex accumulation path is also characterised by unusually high deflection angles of the sliding debris, some fundamental questions about the processes involved are asked. Detailed field studies show evidence that preferentially in medial to distal accumulation areas the Sturzstrom kinematics could have been favoured by water-saturation of its low permeable fine-grained substrate. Additional questions arise since the distal Fernpass slide deposits are split into numerous isolated outcrops of chain-like arranged, debris-ridges and –hills of unknown thickness and unclear subsurface geometry. Till now the genesis of this hummocky accumulation pattern remained unsolved.

Thus this study aims to present some spatial attributes such as thickness and distribution of distal rockslide deposits, theirs substrate and the groundwater table by testing the applicability of the Ground Penetrating Radar (GPR) system for near-subsurface explorations. In general, this method enables exploration depths in the order of some tens of metres (Davis and Annan, 1989) and was in the Eastern Alps already applied to rock-glaciers and water-unsaturated talus-deposits (Brückl et al., in press; Krainer et al., 2002; Sass and Wollny, 2001). Ideally in the Fernpass region these quick and non-destructive geophysical in-line investigations can also be calibrated by shallow-seated drillings and thus provide spatial information on the varying subsurface geology. Based on the results of the calibrated GPR measurements, we intend to make a contribution to a kinematical model for the accumulation and spread of long run-out Sturzstrom deposits.

2. Location and Geology

The Fernpass is situated in the western part of the Northern Calcareous Alps, approx. 45 km west-northwest of Innsbruck (Tyrol, Austria) and enables an important North-South-passage between the Tyrolean Inn valley in the South and Bavaria (Germany) in the North. Its apex (1332 m a.s.l.) and the valley floors to both sides are covered by at least 16.5 km^2 wide spread rockslide deposits, attributing to one of the largest mass movements in the Alps.

2.1. Scarp area

The source area of the Fernpass rockslide is located within the southernmost Lechtal nappe, a polyphase and heteroaxial folded and faulted major thrust unit of the western Northern Calcareous Alps (Eisbacher & Brandner, 1995). Here the calcareous rockslide debris originated from an exceptional deeply incised, wedge-shaped niche with a present maximum elevation of 2231 m a.s.l., indicating a failure volume of about 1 km^3. The scarp is made up by several hundred metre thick alternations of thin-bedded platy dolomites, limestones and marls belonging to the bituminous Seefeld Fm (Norian, Upper Triassic). These incompetent and low permeable rocks represent an intraplatform-basin succession within the upper Hauptdolomit Group (Norian), one of the main rock units in the Northern Calcareous Alps (Brandner & Poleschinski, 1986, Donofrio et al., 2003). At Fernpass lithological parameters and bedding conditions, but above all, complex intersection of brittle fault systems and fracture zones control the formation of preferred sliding planes and the block size distribution. Crucial slope vulnerabilities result from polyphase faulting along three dominant fault systems, i) E-W-trending normal and reverse faults, ii) NE-trending sinistral and iii) NW-trending dextral faults. Cataclasis induced from brittle faulting along the prominent NE-trending Loisach fault system (Eisbacher & Brandner, 1995) and along a NW-trending fault at Nassereith enabled fluvio-glacial erosion and valley-deepening (Fig. 1). This caused stress redistribution of the valley-slopes and uncovered favourable orientated sliding planes permitting subsequent slope instabilities.

2.2. Accumulation area

Seismic investigations near the Fernpass apex indicate a substantially steepened and undercut slope toe, where the top of the bedrock units is situated in about 700–800 m a.s.l. (Prager et al., in pre - paration). The overlying 500–600 m thick soft rock units are assumed to originate mainly from the Fernpass rockslide and decrease significantly in thickness laterally. Morphologically the medial to distal accumulation areas are characterised by large-scale transversal debris ridges and trenches, exemplary formed Toma-hills and associated funnel- to

basin-formed depressions, some of them filled with kettle-like lakes. According to the morphological definition by Abele (1974:119), the well-known Toma are "isolated, cone- to pyramidal- or roof-shaped elevations, predominately made up by rockslide debris and characterised by more or less planar hill slopes with constant inclination". Formerly these typical hummocky characteristics of several large rockslides in the Alps, among them also the Fernpass slide, were believed to represent late-glacial dead-ice scenery (Abele, 1964, 1969). In contrast, Abele (1991a, 1997) favoured that the intensively structured rockslide scenery may result from pull-apart mechanisms, generating Horst- and Graben-like transversal debris ridges and depressions, during the rapid rockslides motion on water-saturated substrates. But the internal rockslide kinematics that generated the typical cone-shaped Toma, featuring sub-circular basal planes and occurring often as isolated individuals, is not established till now. However, at Fernpass neither these unsmoothed structures nor the rough scarp shows any signs of glacial overprints and indicates a post-glacial genesis of the hummocky rockslide scenery. This assumption was backed up by the cross-check of three independent and remarkably well coinciding dating methods. Rockslide-dammed torrent deposits, situated close to the scarp-front, yielded a C-14 minimum age of at least 3380-3080 cal. BP, whereby an age of between 3300 and 4600 cal. yrs BP (Mid-Holocene) is assumed for the base of this backwater sequence. This coincides well with two cosmogenic radionuclide Cl-36 exposure ages of large-scale sliding planes at the scarp, which are 3600 ± 900 and 4800 ± 1100 yrs old. In addition, small-scale successions of the rockslide deposits are lithified by previously not mentioned carbonate cements. These have been dated by the Th-230/U-234 disequilibrium method and yielded a minimum age of about 4150 ± 100 yrs for the accumulation of the southward-deflected rockslide deposits. All age data indicate a failure event in the middle Holocene at about 4100–4200 yrs BP (Prager et al., in review).

The internal structure of the Holocene Fernpass rockslide is characterised by chaotic deposits featuring varying block-size separation and fragmentation. Upper parts of the proximal depositional facies contain large angular blocks up to a few metres in diameter and occasionally even slabs of 100´s metres in side length. Due to dynamic disintegration and abrasion of the surging debris, medial to distal areas are built up by subangular to even edge-rounded components of different size (centimetre to several metres) mixed with abundant fine interstitial material. Sieve analyses of 9 gravelly samples yielded approx. 5–30 weight-percent clay- to silt-sized matrix. The basal sliding plane of the Fernpass rockslide, supposed to show fine attrition-breccias, is not exposed. Drilling data show that basal deposits of the adjacent Tschirgant-rockslide are made up by silt- to clay-sized, calcareous deposits with a low hydraulic permeability of about 4.0 - 5.0 x 10^{-9} m/s (Hartleitner, 1993).

2.3. Travel path of the Fernpass rockslide

Due to the oblique impact on its opposite slope, the failing rock masses were proximally piled up to a few hundred metre thick succession and subsequently split into two channelled but diametrically opposed Sturzstrom branches (Fig. 1). The northern Sturzstrom, containing the majority of the debris volume, shows a comparable low deflection angle and surged at least 10.8 km towards northeast on to the aggradation plain of the Lermooser Moos at approx. 970 m a.s.l. This accumulation path is kinematically coherent and thus no further aim of this study.

In contrast, the trajectory flow of the southern Sturzstrom is characterised by unusually high deflection angles. First, the eastward sliding debris was deflected from the proximal accumulation area about 140° to southwest and subsequent, due to channelling in the narrow valley, about perpendicular to southeast. Then, after a travel distance of approx. 11 km from the topmost scar, this Sturzstrom entered at Nassereith an unconfined alluvial plain. But instead of continuing its further run-out path straight on, the debris curiously turned about 90° to southwest and flew another 4 km down the Gurgl valley to its lowermost accumulation point at 790 m a.s.l., covering a total run-out distance of at least 15.5 km. Based on this, both rockslide branches show extremely low angles for their overall slopes, i.e. the ratios of drop height versus run-out length along the channel line (referred to as "Fahrböschung", Heim 1932). This may be used as a geometrical criterion to describe landslides mobility and at Fernpass measures about 6.7° for the northern respectively 5.3° for the highly and curiously deflected southern branch.

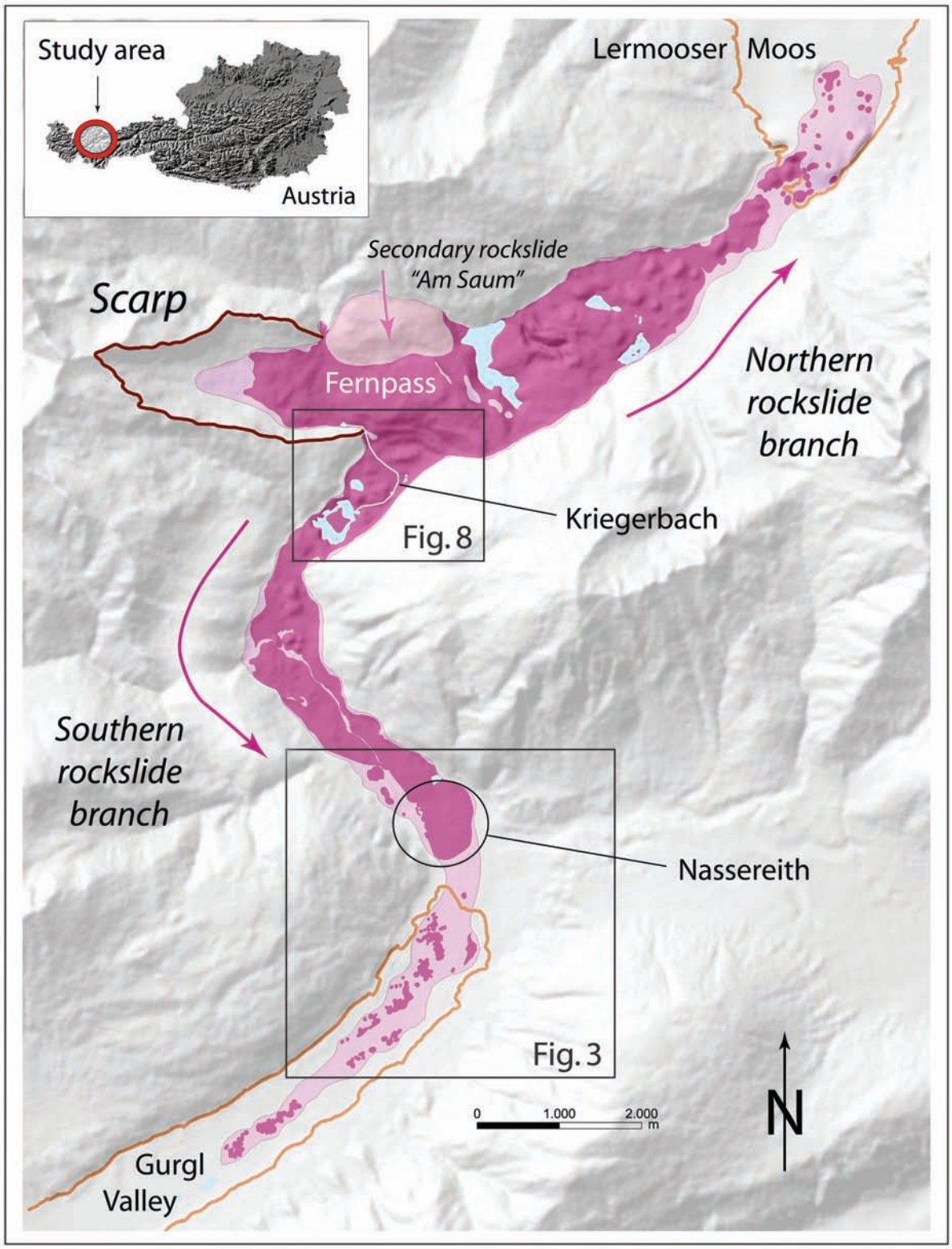

Fig. 1: Digital elevation model of the Fernpass area showing the scarp and the accumulation area of the rockslide deposits (Dark pink: field outcrops of rockslide deposits; light pink: assumed accumulation area; orange line: top of lacustrine deposits, underlying the rockslide debris). Locations of GPR-measurements and drillings are indicated by squares that refer to detail maps (Fig. 3, Fig. 8).

Field investigations (Ampferer 1904, 1924; Ampferer & Ohnesorge, 1924) and drillings (Köhler & Lumasegger, 1992; Poscher, 1993) indicate that the debris of the northern rockslide branch partially rests upon subglacial till, whereas the distal southern Sturzstrom surged upon fine lacustrine sediments. Latter, comprising a thickness of at least 20 m, are interpreted as the bottom set of a late-glacial delta complex covering the Gurgl valley (Bichler, 1995).

Remarkably, based on the absence of field outcrops, the distal accumulation path of the southern rockslide branch seems to be somehow interrupted, as occurring between the southern outskirt of Nassereith and the approx. 10 - 20 m high elevated Toma in the northern Gurgl valley (Fig. 1, Fig. 3). Here this lack is probably due to a post-depositional masking of the rockslide deposits by alluvial debris flows, but may also result from intensive anthropogenic manipulations of the traffic node Nassereith. On the other hand, drilling data show that here only a few metres below surface presumably late-glacial lacustrine deposits are present, containing metamorphic drop-stones in depths below 7–10 m and reaching from the Gurgl valley upstream at least to the Nassereith area (Poscher, 1993). Except for this, here no further subsurface information about the post-glacial valley filling, particularly with regard to the geometry of the Fernpass rockslide deposits, is available. So both, the spatial distribution and the thickness of the apparently disrupted accumulation path of the rockslide deposits as well as the depth of the groundwater-table are relevant research problems for the Sturzstrom kinematics. Based on detailed field studies, the relevant geological discontinuities are assumed in a depth of a few metres (groundwater-table) to maximal a few tens of metres (base of the rockslide deposits). Thus, distinct sections of the Fernpass rockslide are ideal test sites for the applicability of the GPR system as well as for supplementary drilling campaigns to calibrate the geophysical measurements.

3. Methods

Field survey was carried out by a Subsurface Interface Radar (Geophysical Survey Systems Inc., System 2000, Model 3200) equipped with a multiple low frequency antenna. With regard to the best resolution at the intended exploration depth of a few tens of meters, the profiles were measured using a 35 MHz antenna with constant antenna spacing (common-offset profiling) and orientation of the antennae perpendicular to the profile direction. Data were collected by discrete stacking mode. Distance between transmitter and receiver was 4 m, step size, i.e. distance between the data collection points, was 1 m. Detailed descriptions of this method refer to Jol & Bristow (2003) and Milsom (2003). Considering expected water-saturation of the subsurface lithologies, i.e. coarse rockslide deposits upon fine-grained lacustrine deposits, an intermediate dielectric constant of 15 for wet sand (GSSI, 2001) was chosen for the geophysical explorations.

In distal rockslide accumulation areas the measurement campaigns were carried out near the village Nassereith in May 2004 and June 2005 after stable and dry weather- and soil conditions. Special attention was here paid to take field surveys far apart from power supply lines to avoid any electromagnetic interference with the measurement radar signal. A second test site is situated at more proximal deposits southwest of the Fernpass and presumably affected by seasonal varying groundwater-saturation. Thus, to minimize the interfering influence of a high water table, here the field measurements were carried out in winter (February 2005), when also the GPR-antennas could be effectively coupled with the approx. 1 m thick snow pack covering the rough substrate.

Field data were processed by using the software ReflexW version 3.5 and its implemented module 2-D data-analysis (Sandmeier geophysical software, Karlsruhe, Germany). Thereby, to differentiate between geological reflectors and system immanent artefacts, background noises were removed from the raw data by applying following filters: Remove Header Gain, Energy Decay (both amplitudes processing), Background Removal (removal of all horizontal signals deriving from the GPR antennas) and low frequent Bandpass Filter (25–50MHz). Based on this, some vertical elongated and deeper reaching fault signals in the raw data could be attributed to ineffective coupling of the GPR antennas with the substrate and thus were filtered. In contrast, some reflection features such as line- and convex-shaped "air-velocity hyperpoles", come from anthropogenic or natural hindrances (e.g. fences, trees) and are still present in the processed data, but may not be inter-

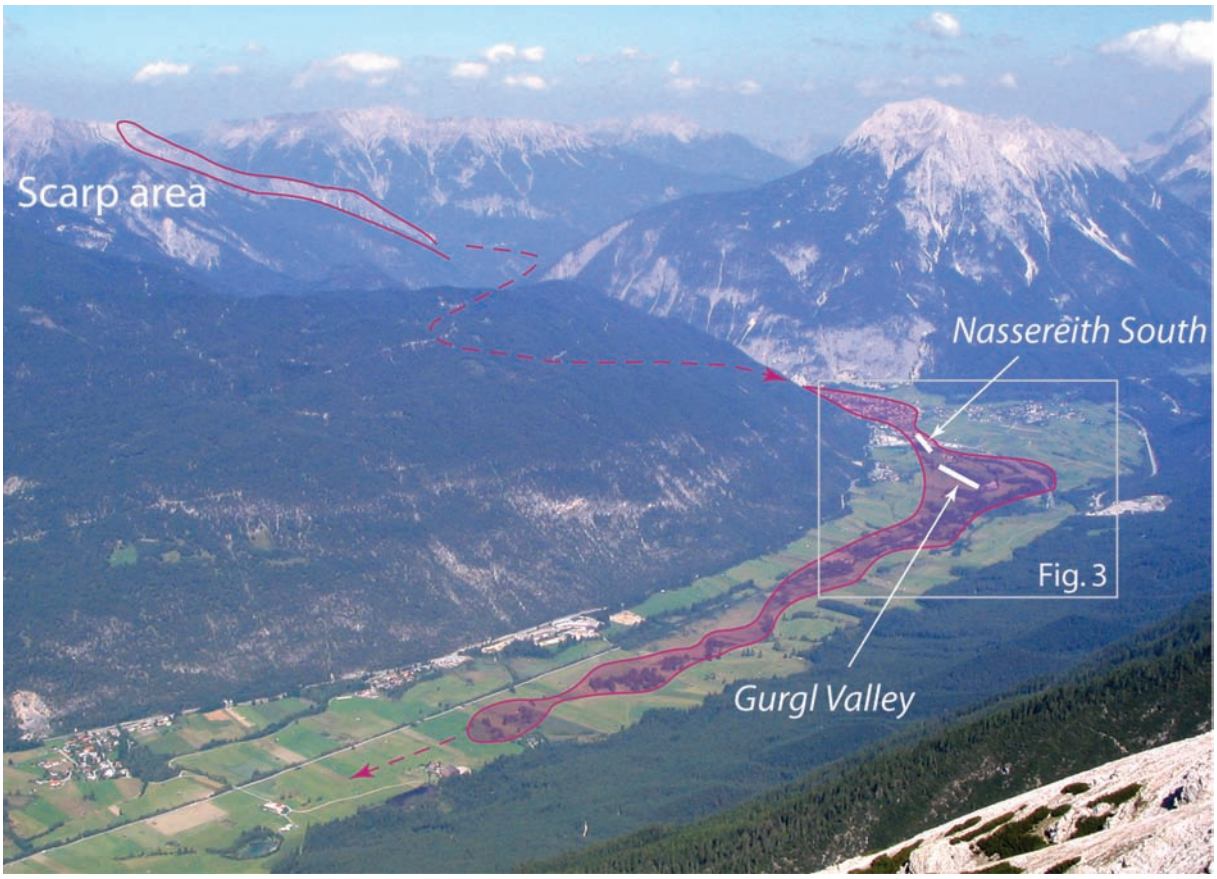

Fig. 2: Oblique view towards northeast to the upper Gurgl valley and the Nassereith area showing the scarp area and the distribution of the Fernpass rockslide deposits. Stippled lines indicate the deflected accumulation path of the southern Sturzstrom branch.

preted as geological discontinuities. Finally, the records were converted to relative depths, with a reliable mean velocity of 0.1 m/ns for the underground, and topographically corrected.

To calibrate the GPR measurements and their interpretations, crucial data concerning lithological parameters and spatial distribution of sediments and groundwater were gained by a shallow-seated drilling campaign. In May 2005 five bore holes up to depths of 14 metres were constructed by using a truck-borne spiral-drill with a diameter of about 15 cm. Fine deposits from clay- to finesand-size were easy to drill and could be well examined, because they stuck on the spirals of the drill, even when water-saturated. In contrast, coarser deposits mostly got lost when pulling out of the drilling hole. In this cases the hardness and duration of the drilling-progress was a criterion for a coarse grain-size classification and recognition of larger boulders. At stable borehole conditions the groundwater table was measured by a light-perpendicular.

4. Field measurements and interpretation

GPR investigations were carried out at three different morphological sites (Fig. 1; Appendix, Table 1): 1. Distal accumulation areas featuring well exposed Toma, 2. Alluvial plain between evident distal rockslide deposits and 3. Alluvial fan between medial rockslide accumulation areas.

4. 1. Toma of distal rockslide deposits

The morphology south of Nassereith is characterised by the confluence of the gently sloped Gurgl valley and a tributary, southwest trending alluvial fan. In the central part of the main valley several well developed, forested Toma rise up to 15 m above the valley floor. There a GRP profile was measured at an elevation of about 810 m a.s.l., trending SSE-NNW almost perpendicular to the run of the valley and running across both lateral slopes of Toma and

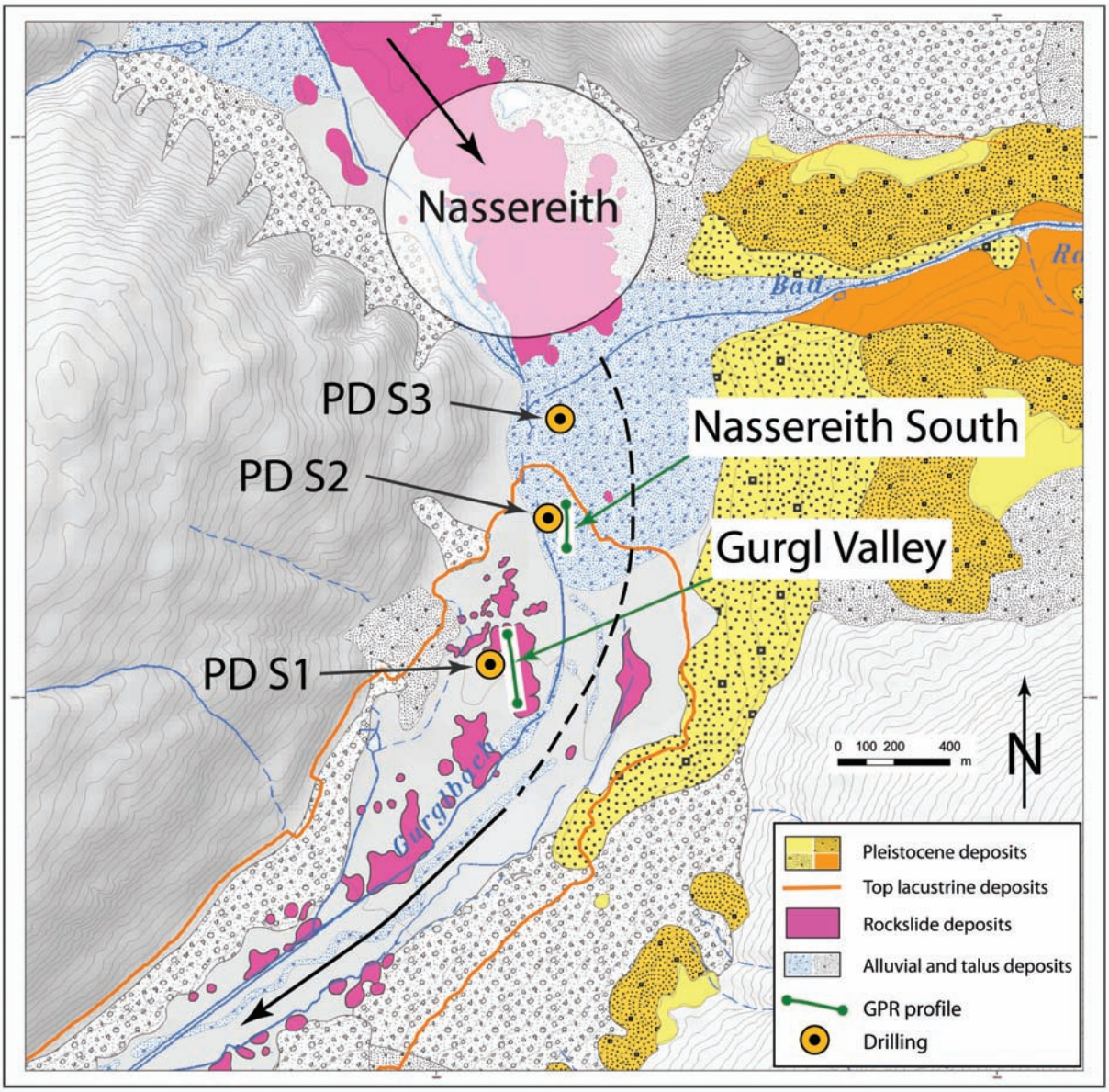

Fig. 3: Geological sketch map of the area Nassereith – upper Gurgl valley showing GPR profiles and drillings. Note the high deflection angle of the rockslide towards SW and lacking field outcrops of rockslide deposits thereat.

flattened to gently inclined alluvial plain between the Toma (Fig. 3, Fig. 4).

This 230 m long radargram is characterised by several densely spaced, subhorizontal discontinuities (Fig. 5). A distinct reflector was recognised at a depth of about 20 m, as best visible within the first 50 profile metres. There it forms a clear concave structure, which is situated straight below a several metres high elevated Toma. Based on the undulating geometry and the geological field situation, we interpret this striking reflector as the base of the Fernpass rockslide deposits that rest on low permeable lacustrine sediments. In central sections of the profile this reflector is superposed by an "air velocity hyperbole", but can be traced further North in about the same depth, i.e. at approx. 790 m a.s.l.. Some accentuated basal reflections, best visible in the raw data between profile-metres 120 - 200 in about 10 m depth, indicate increased lithological contrasts and thus may be attributed to larger and/or less fractured rockslide boulders. However,

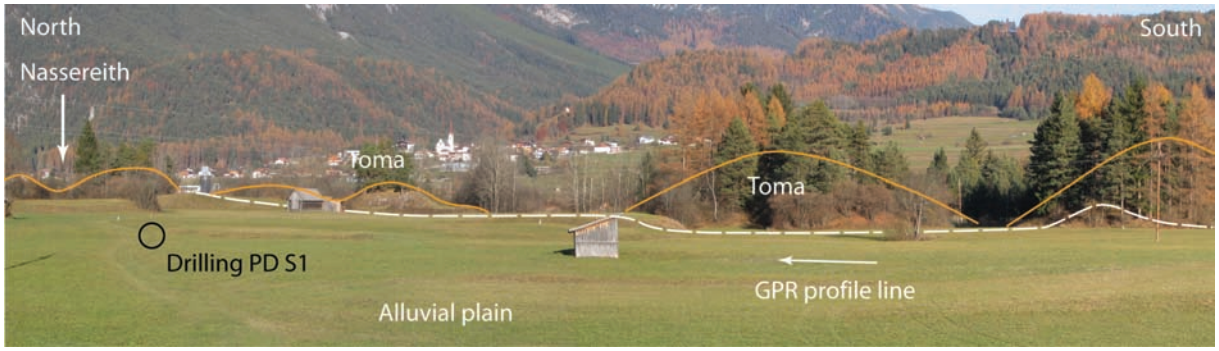

Fig. 4: Typical rockslide morphology of the distal Fernpass rockslide south of Nassereith, featuring the cone-shaped Toma. The location of the GPR profile Gurgl valley is indicated by the stippled white line.

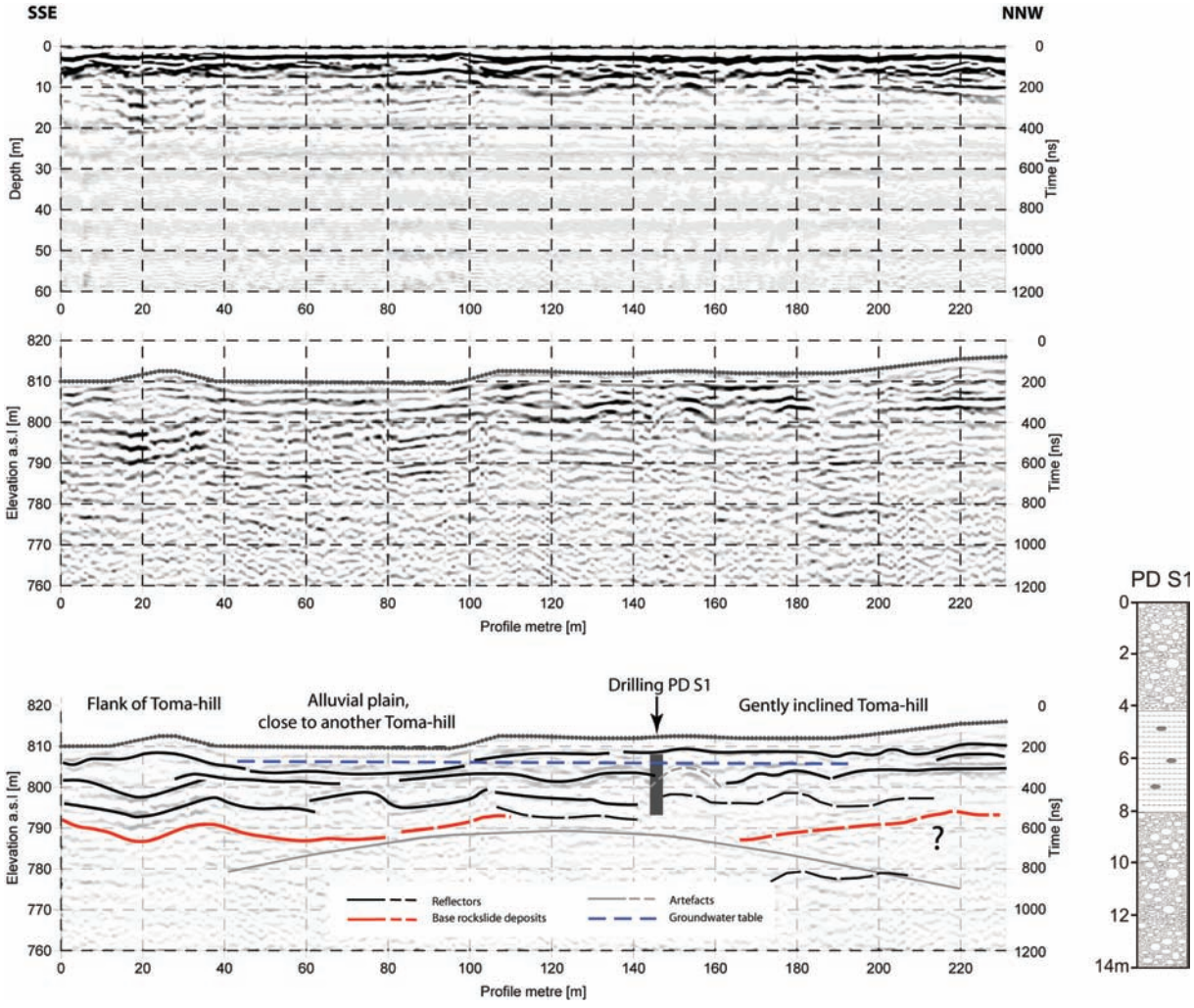

Fig. 5: GPR profile Gurgl valley, from top to bottom: radargram, processed and topographically corrected data, geological interpretation with therein projected drilling PD S1 (c. at profile metre 145) and its lithological succession to the right (for the legend see Appendix, Table 2).

the radargram provides clear evidence that Toma have obviously more pronounced roots than the successions between these debris cones. This indicates substantial subsidence of the rockslide mass into its fine-grained substrate, i.e. glacio-lacustrine silts and clays, due to loading and therefore disables the detection of a primary subplanar basal sliding plane. According to these data (5–15 m high Toma with 15–20 m deep roots), the distal deposits of the Fernpass rockslide show here a total maximum thickness of about 20–30 m.

Another striking reflector was detected at an altitude of about 805 m a.s.l., situated within the uppermost rockslide deposits. The interpretation of this curvilinear reflector is based on subsurface data provided by the adjacent drilling PD S 1 situated about 100 m west of this GPR profile. Surprisingly this borehole, which is bounded to the North, East and South by a chain of Toma at a distance of a few tens of meters, yielded an entirely fluvial-lacustrine succession of alternating fine- to medium-sized clastic deposits, but lacking evidence of larger boulders down to a depth of 14 m. Since the GPR data clearly point to the presence of a basal plane of the rockslide deposits at depths of about 20 m, we assume that the drilled fluvial-lacustrine sediments are, at least partially, younger than the deeper rooting rockslide deposits. These fluvio-lacustrine sediments lap on and fill up the depressions between the individual Toma. In the drilling PD S1 the groundwater table was detected 3.5 m below the surface, i.e. at an altitude of approx. 806.5 m a.s.l. (Fig. 5; Appendix, Table 2). This groundwater table may cause the shallow subsurface GPR reflector detected at about the same depth.

4. 2. Distal rockslide deposits buried by alluvial debris flows

Some distal accumulation areas of the rockslide deposits are poorly exposed due to decreasing thickness, post-depositional burial by fluvial deposits and anthropogenic influences near the surface of the valley-floor. All this may be the case at the southern outskirt of Nassereith, where the field situation provides only little information about shallow subsurface structures. However, no field outcrops of the Fernpass rockslide deposits occur between Nassereith and the nearest Toma approx. 600 m further downstream (Fig. 1, Fig. 3). Moreover, right there the trajectory flow of this Sturzstrom shows a high deflection angle of about 90° and turned towards the upper Gurgl valley. Thus the subsurface geology of the area next to Nassereith is of special interest concerning this curious accumulation path and its causal kinematics.

In the commercial zone of Nassereith a GPR profile was recorded from N to S at an altitude about 815 m a.s.l. (Fig. 3). This profile shows numerous distinct and densely spaced reflectors, and can geophysically be subdivided into three units (Fig. 6). The upper succession of the valley fill is characterised by reflectors that dip about 5–15° relative towards the south. At a depth of about 6 m, i.e. at an altitude of approx. 807 m a.s.l., these planes lap down onto a slightly undulating main discontinuity and its associated reflectors. Below this, several second order reflectors can be traced to another main reflector at a depth of approx. 15 m. Further down, the radar signals are less clear and also superposed by a hyperbolic air reflection.

A calibration drilling, situated approx. 15 m west of this GPR profile, yielded a fluvial succession overlying fine-grained lacustrine deposits, but did not supply material between 7.5–12.5 m (PD S2, Appendix, Table 2). As this depth was almost not to drill, we assume the presence of coarse material, probably larger (rockslide-) boulders, in this section. Thus, the GPR-reflectors, detected at depths of approx. 6 m and less distinct about 15 m, however, may be correlated with the top and with the obviously undulating base of the Fernpass rockslide deposits. The uppermost, clearly inclined reflectors indicate distinct stratification, due to changes in grain size of the prograding fluvial debris flow deposits. The groundwater table was well-defined at a depth of 3.2 m, i.e. at an altitude of about 812 m a.s.l. within the inclined bedded fluvial deposits. These subsurface conditions were backed up by another drilling about 300 m north of the profile (PD S 3). In this borehole water-saturated coarse-grained deposits, which were extremely hard to drill, were recognized at a depth of about 7.5–9.0 m. But it remained unclear whether these sediments all belong to a tributary, Holocene alluvial fan, which progrades here towards south-west into the Gurgl valley (Fig. 3). However, both drillings did not exceed depths of 14 m, but penetrated fine-grained, probably peri-lacustrine deposits below the blocky successions (Appendix, Table 2).

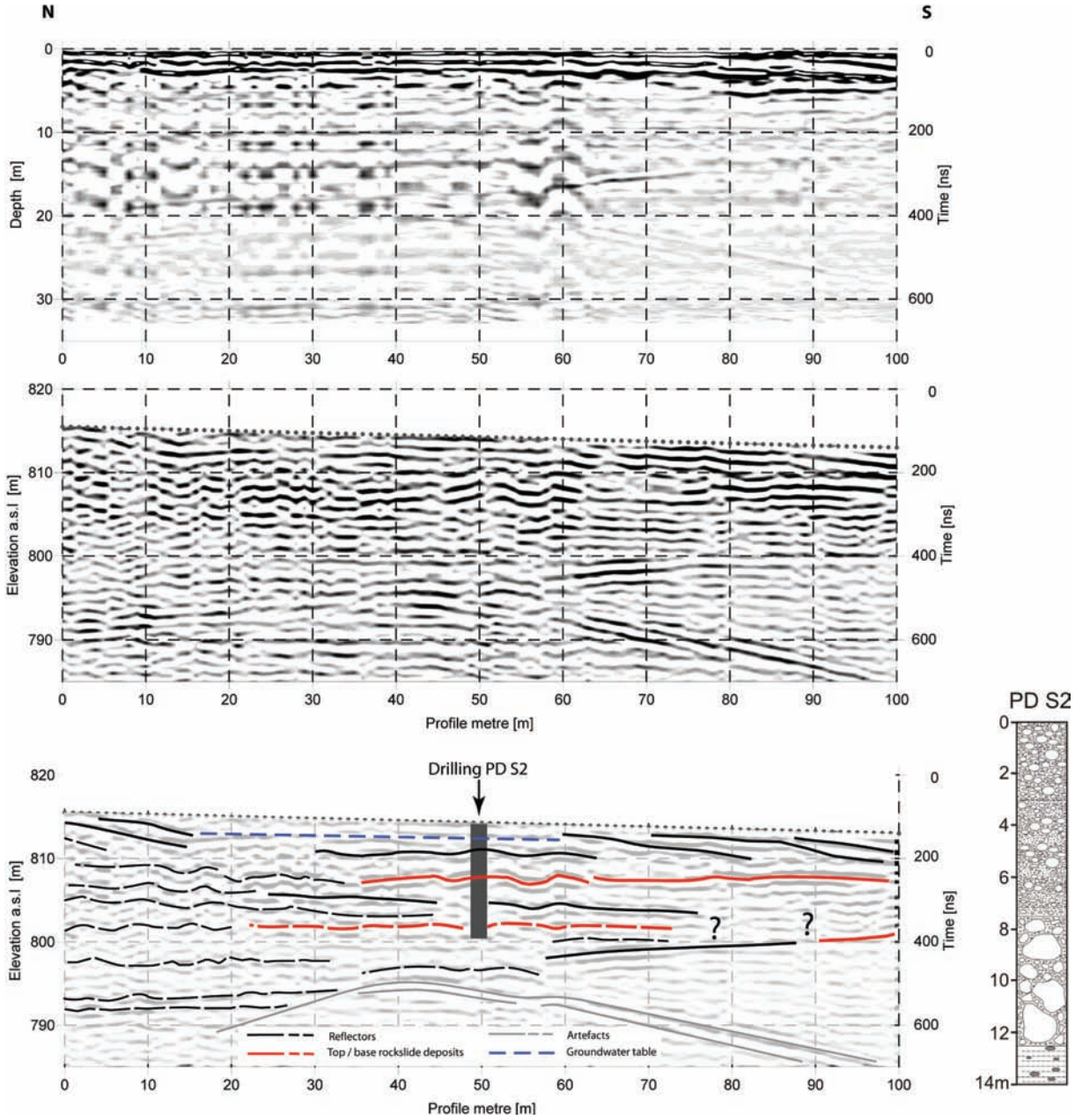

Fig. 6: GPR profile Nassereith South, from top to bottom: radargram, processed and topographically corrected data and interpretation with therein projected drilling S2 (at profile-metre 50.00).

Further information concerning the subsurface lithology is derived from an excavation pit in the commercial area of Nassereith (April 2004). There the uppermost 2.5 m of the valley fill were exposed, composed of dry, polymict fluvial gravels, characterised by mean diameters of less than 20 cm, with thin intercalations of silty layers at its base. Remarkably, the well-rounded clasts of metamorphic and carbonate composition contained a few metre-sized angular boulders of dark grey dolomite. These exotic boulders can clearly be interpreted as rockslide deposits floating in the valley fill.

Compiled field- and subsurface data indicate that near Nassereith the fine-grained lacustrine sediments are overlain by a thin fluvial succession, which covers the coarse rockslide deposits and locally even intermingles. According to both GPR- and drilling-data, in the area next to Nassereith the rockslide deposits are extremely thin with varying

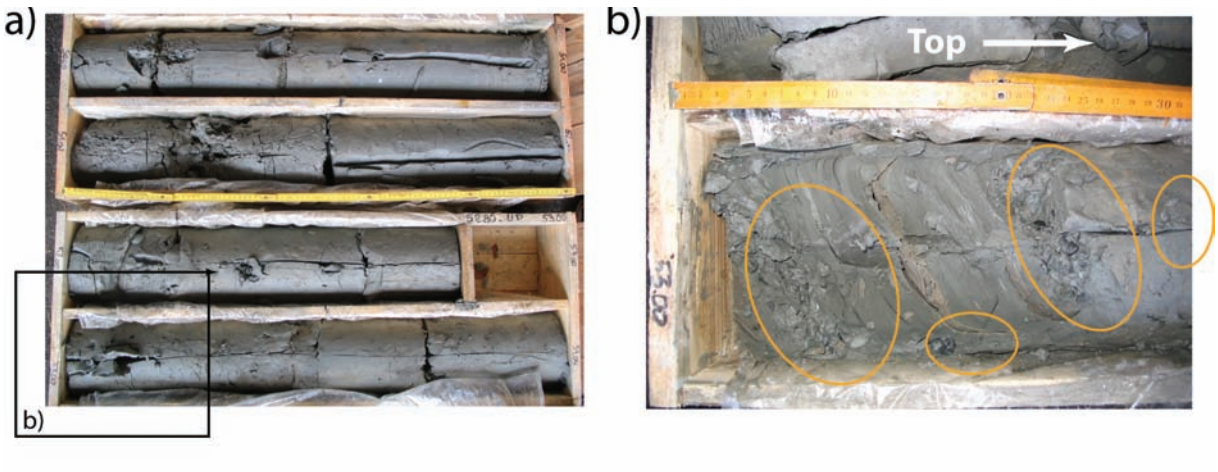

Fig. 7: Substrate of the distal Fernpass rockslide near Nassereith: lacustrine fine deposits ("varved clays") containing several subspherical pebbles ("dropstones", indicated by circles)
(Drilling core Tschirgant KB 9, 858 m a.s.l.; a) section metres 50–54 and b) metre 53.10 in detail).

thicknesses ranging from presumably 1.5 m (PD S3), to 5 m (PD S2) and 9 m (GPR profile Nassereith South). This contrasts clearly with the increased thickness up to 20–30 m further downstream (Fig. 5).

Considering these complex relationships, the underlying substrate of the Fernpass rockslide deposits is of special interest. Borehole data in the course of terrain explorations for the by-pass of Nassereith show that fine-grained lacustrine sediments contain metamorphic dropstones at depths below 7–10 m, i.e. approx. 800 to 810 m a.s.l., pointing to an ice-marginal facies (Poscher, 1993). Also the adjacent drillings PD S1 and PD S2 yielded fine-grained deposits that are similar to lacustrine "varved clays" (Appendix, Table 2). Embedded in the fine-grained matrix are numerous spherical, predominantly carbonate, locally densely packed pebbles with polished grain-surfaces. We interpret these sediments as peri-lacustrine deposits, which were also mined on the southern flank of the uppermost Gurgl valley. There several drillings exposed polymict Pleistocene gravels with tens of meters thick intercalations of lacustrine clays and silts (unpubl. reports by Ilbau, 1996; Asfinag Austria, 2005). These fine-grained deposits commonly show high contents of re-deposited pebbles such as well rounded and sub-spherical polished clasts (Fig. 7), predominantly of carbonate and less common of metamorphic composition. According to Bichler (1995), these mud-supported gravity flows may be part of a delta-complex, where debris from the terrace-slopes interfinger with the proximal bottom set of a presumably late-glacial lake.

However, both the field outcrops and these corresponding subsurface data exhibit a top of lacustrine sediments, i.e. the varved clays of the bottom set, at an altitude of 800 to 810 m a.s.l. Where these fine deposits interfinger with the coarser grained delta forests, the top of the peri-lacustrine facies extends to an altitude of at least 822 m a.s.l. (e.g. KB 9; Asfinag, 2005).

4. 3. Medial rockslide accumulation areas

Medial depositional areas of the Fernpass rockslide show several tens of meters high debris ridges, Toma and corresponding depressions, orientated transversal to the direction of the rockslide propagation, between. At the base of the proximal accumulation area of the thick Fernpass ridge, the rockslide deposits feature a significant, since deeply incised trench-structure at an altitude of about 950 m a.s.l. Therein an approx. 300 m wide, NW-SE-trending alluvial fan of the creek Krieger-Bach is arranged approx. perpendicular to the direction of the former rockslide. On this accumulation plain, which is gently inclined (5°) towards SE, the GPR profiles were measured both parallel to the discharge from NW to SE (profile Kriegerbach 1) and

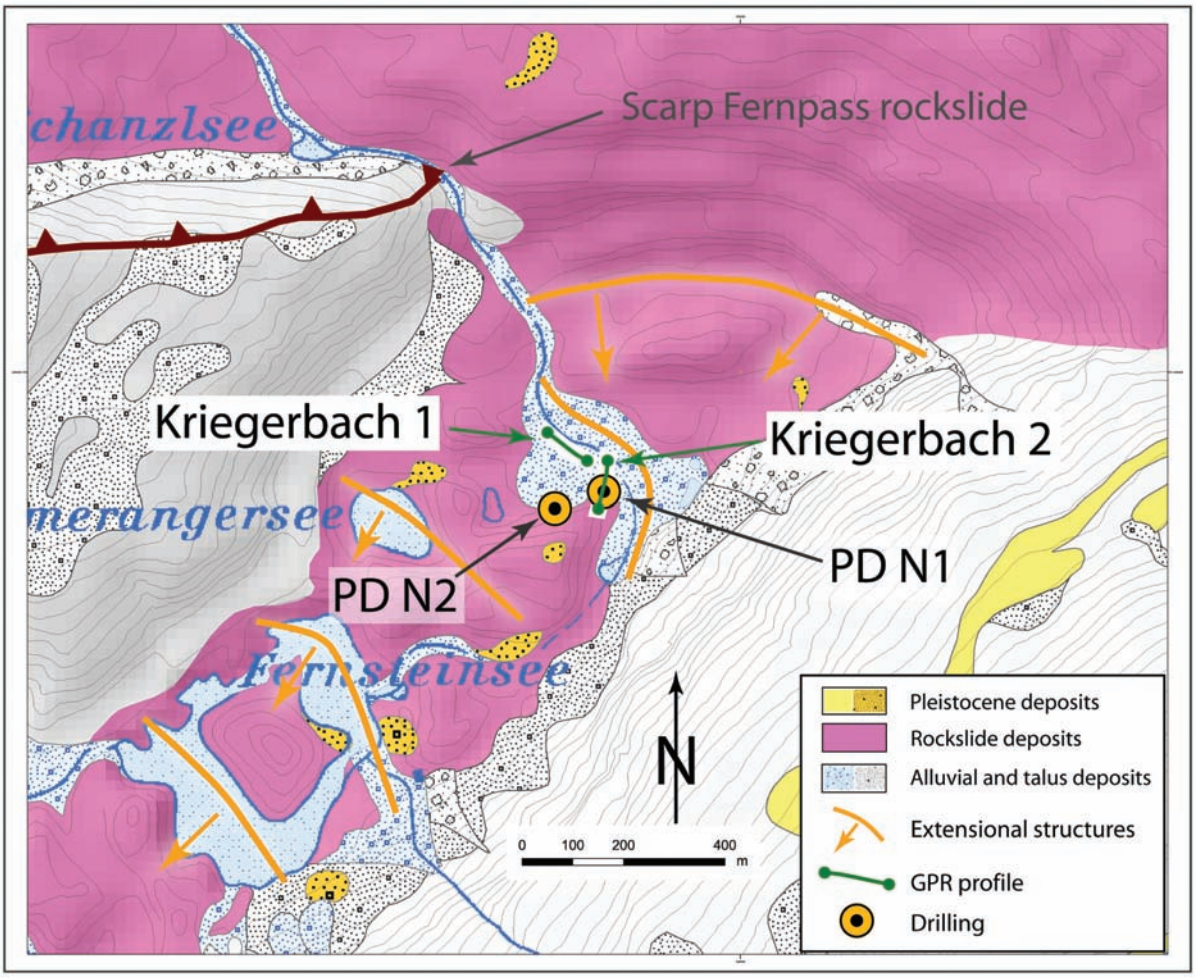

Fig. 8: Geological sketch map of the medial accumulation area of the southern branch of the Fernpass rockslide, showing GPR profiles and drillings on the alluvial accumulation plain of the river Kriegerbach. Note extensional structures within the rockslide deposits, approx. perpendicular to the direction of the Sturzstrom motion; some of these depressions are filled with lakes or fluvial discharge systems such as the river Kriegerbach.

obliquely across the debris fan from N to S, ending near the base of an approx. 30 m high Toma (profile Kriegerbach 2; Fig. 8, Fig. 9).

GPR profile Kriegerbach 1 (Fig. 10) was measured downstream along the orographic right bank of the present torrent channel. The subsurface geometry is characterised by numerous reflectors, which are arranged mainly subhorizontally. In coincidence to field- and drilling-data (PD N1, PD N2; Appedix Table 2), this indicates repeated grain size changes of the stratified debris flow deposits. This radargram shows at least two main unconformities at intermediate depths: an upper one dipping from about 5 m downstream to about 15 m below the surface; and a distinct lower one situated at a depth of about 15-20 m. These main reflectors display a wedge-shaped set of numerous planes that clearly dip subparallel at an angle of approx. 10 - 15° downstream relative towards SE. The thickness of this wedge decreases downstream, where several less inclined on-lapping reflectors discordantly overlie it. Based on the field geometry of the rockslide deposits, we interpret the subhorizontal GPR basal discontinuity at a depth of about 20 m as the top of the Fernpass rockslide deposits. These deposits are buried by down-lapping plane-sets of the prograding fluvial debris flows, which are clearly stratified due to grain-sizes changes. Their lithological composition equals those of the carbonate rockslide deposits. Probably due to channel shift, this sedimentary accumulation wedge is truncated and overlain by less inclined fluvial deposits. Thus, upper sections of this radargram are characterised by the internal

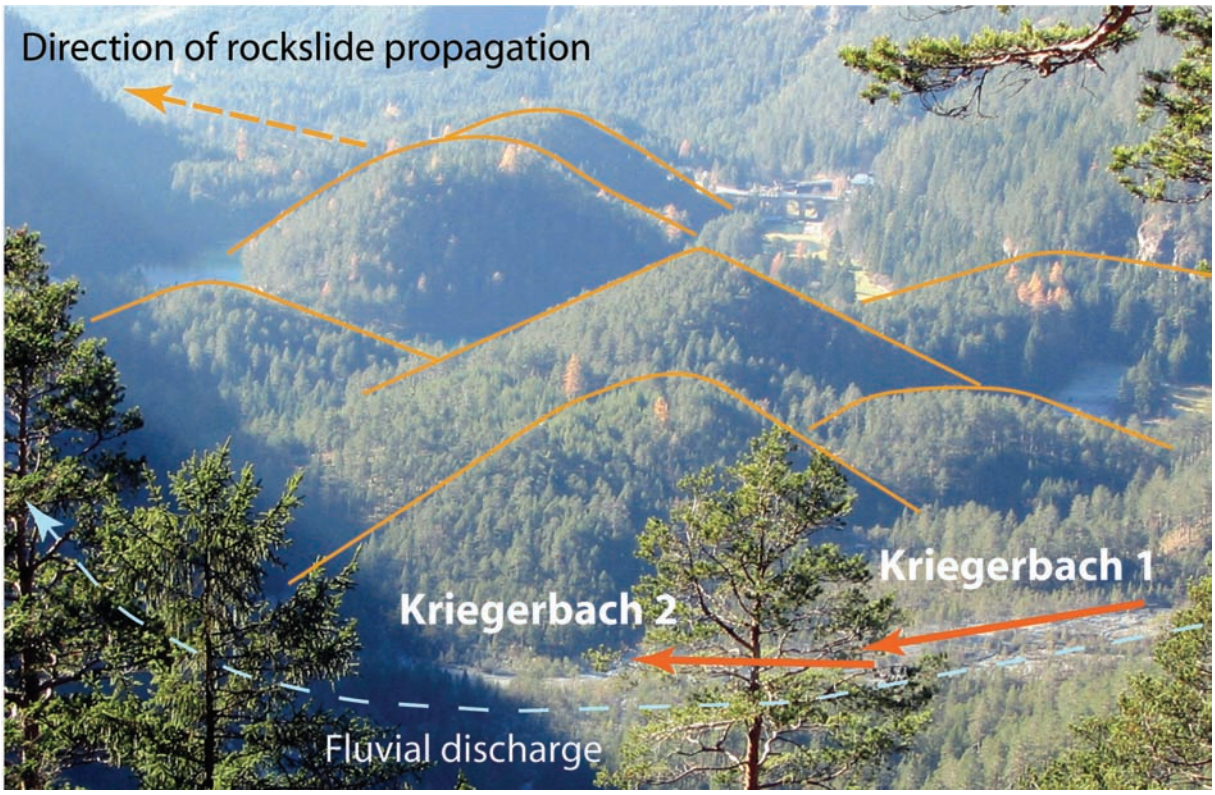

Fig. 9: Morphology of the alluvial plain of the river Kriegerbach (foreground, with thereat measured GPR profiles), surrounded by well exhibited Toma up to 50 m elevation (background).

interplay of fluvial erosion and sedimentation. Reflectors below 25 m are difficult to interpret.

A distinct basal reflector was also detected in the adjacent GPR profile Kriegerbach 2 (Fig. 11). There a main unconformity plunges within the last 30 profile-metres from a depth of 6 m in the S down to a depth of approx. 16–20 m in the N, resulting in a dip angle of about 20°. Based on this geometry, the corresponding field outcrops further south and data from the adjacent drilling PD N1, indicating very coarse material at this position and depth, the basal reflector is interpreted as the top of the Fernpass rockslide deposits. According to the GPR data, the rockslide deposits are discordantly overlain by on-lapping fluvial sediments. Numerous parallel reflectors indicate corresponding sedimentary stratification due to grain size changes, i.e. a sub-horizontal alternation of coarse- and fine-grained torrential debris layers. Sections around profile-meter 10 and at depths between 15–20 m indicate a buried channel situated straight beneath the present torrent (not shown on the radargram; situated just a few metres north of the starting point of this profile).

Remarkably both high-resolving GPR profiles at the locality Kriegerbach, show significant attenuated radar signals below depths of approx. 10 m and further downwards a progressive fading away, as is best indicated by the unprocessed field data. Radar signals vanished along the entire profile length and cut even across the basal main reflector of the buried Toma. Thus we attribute this attenuation not to an increasing amount of fine-grained clastic sediments but more likely to an increased humidity of the debris. The adjacent drillings PD N1 (near the end point of radargram Kriegerbach 2) and PD S2 (approx. 100 m west of PD N1; Fig. 8) reached a depth of 7.5 respectively 14 m, but did not provide stable borehole conditions to measure the water-level. However, clearly wet gravel was drilled at depths of approx. 5 and 7 m respectively below the ground, indicating a close-by groundwater-table within this highly permeable debris (Appendix, Table 2).

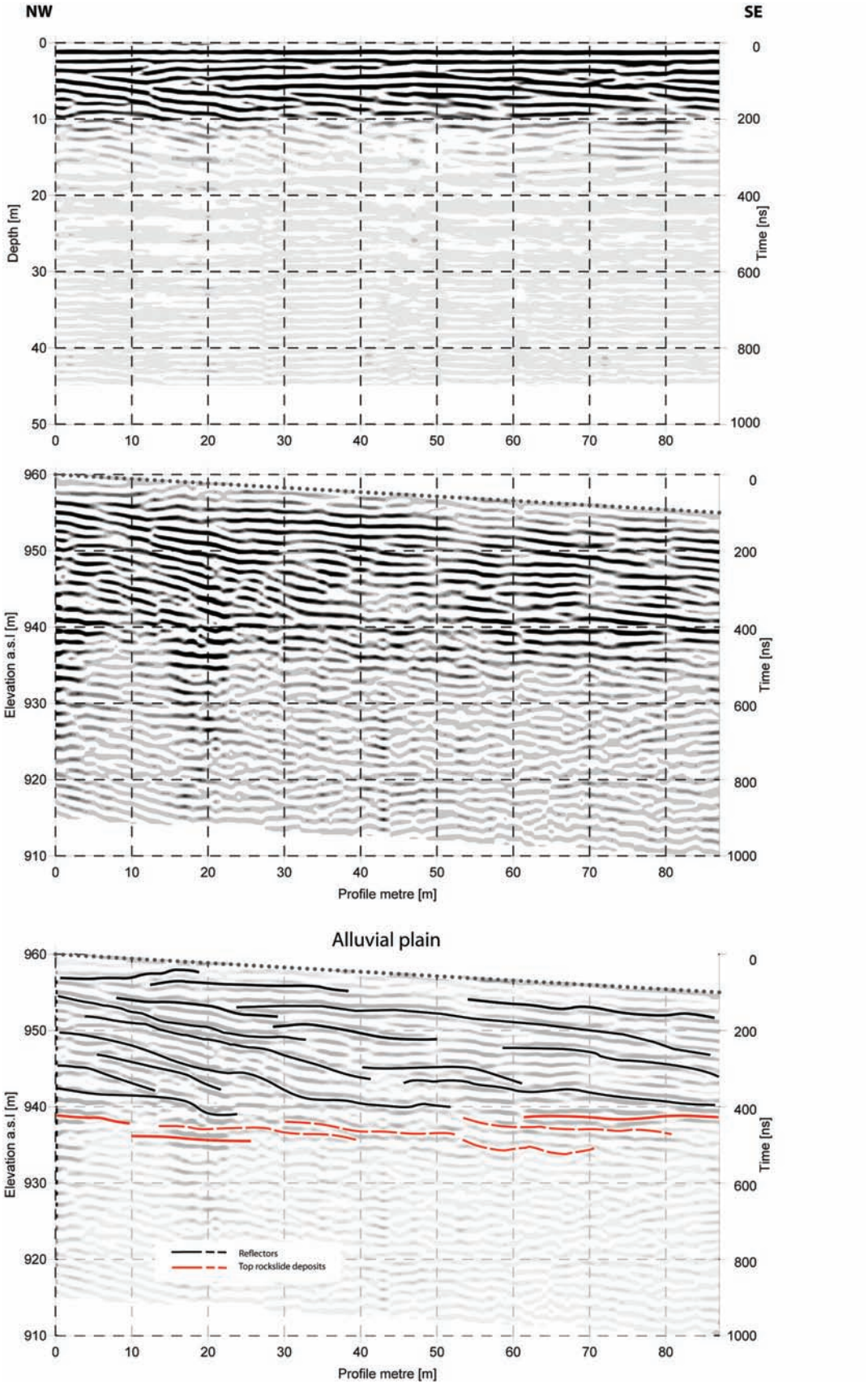

Fig. 10: GPR profile Kriegerbach 1, from top to bottom: radargram, processed and topographically corrected data and interpretation.

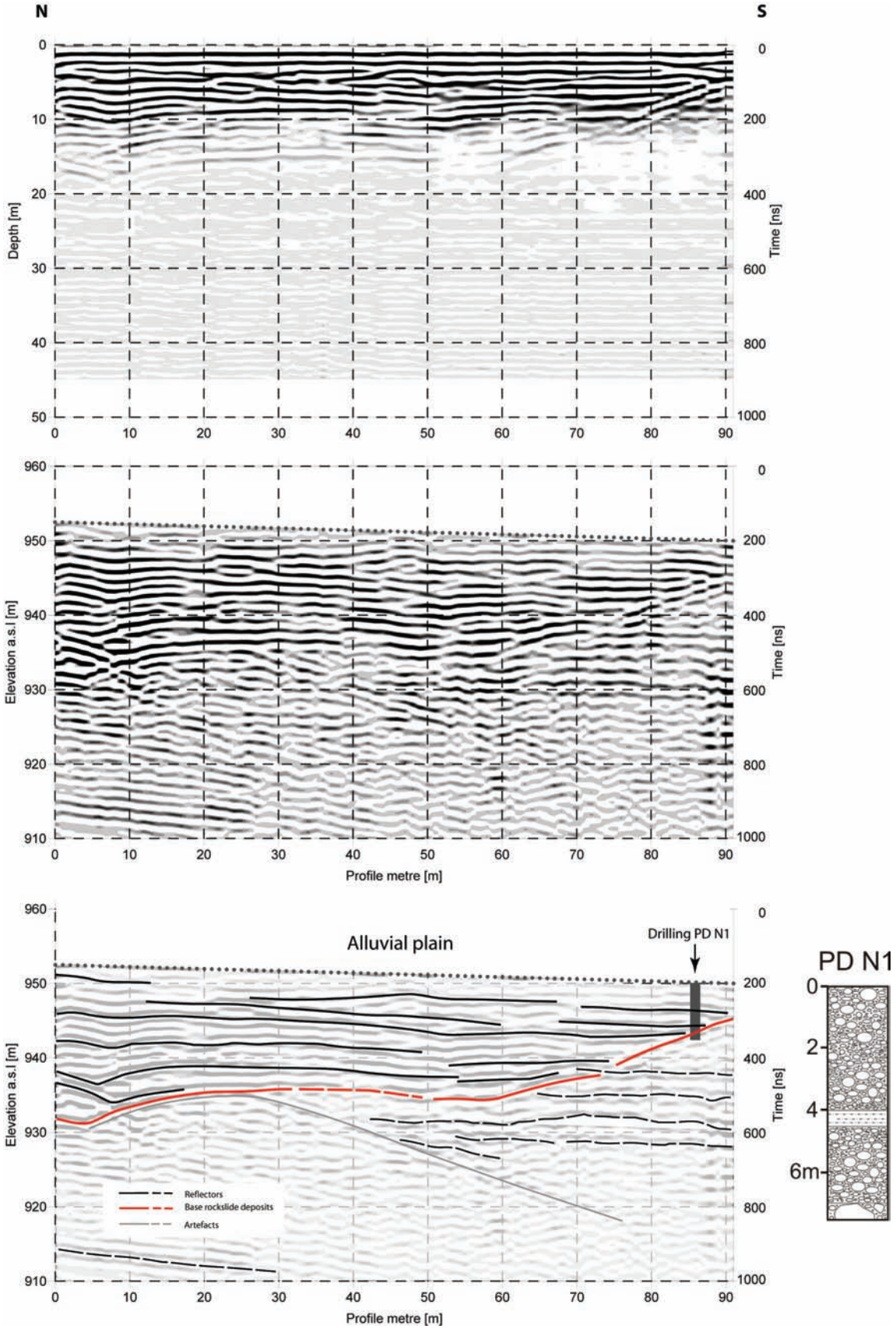

Fig. 11: GPR profile Kriegerbach 2, from top to bottom: radargram, processed and topographically corrected data and interpretation with therein projected drilling N1 (approx. at m 4.00).

5. Results

Different accumulation sites of the fossil Fernpass rockslide (Northern Calcareous Alps) were successfully explored by a low frequency GPR system down to a depth of at least 20–30 m. Some fault signals, e.g. coming from ineffective coupling of the antennas with the substrate or from superficial reflections, were effectively filtered from the raw data. All processed radargrams show several distinct reflectors with varying intensities and geometries.

Based on detailed field studies and calibrated by drillings, these geophysical discontinuities were attributed to different depositional units and also to varying groundwater-saturation of the substrate. As a result, the distal Fernpass rockslide deposits rest upon fine-grained peri-lacustrine sediments and show strong variations in thickness. Measurements taken at the flanks of Toma-hills, at a distance of approx. 11 km from the uppermost scarp area, clearly point to a maximum thickness of the distal slide debris of about 20–30 m. There the undulating basal reflectors indicate a differential subsidence of the rockslide debris into its fine-grained substrate due to loading. Thus, a distinct subplanar sliding plane is not detectable.

Another test site, a few hundred metres up-stream, does not show any field outcrops of rockslide deposits along a length of approx. 600 m along the streamline. The assumption, that the accumulation path of the Sturzstrom could have been somehow interrupted was backed up by the GPR explorations and drilling-data. Both show an extremely reduced thickness of the rockslide material, ranging between approximately 2 and 9 m. Locally these coarse but extremely thinned out deposits even intermingle with the uppermost fluviatil valley filling. Drilling campaigns in the distal rockslide accumulation area, down to depths of 14 m, established a shallow groundwater-table only at between 3–6 m below surface. According to this, the present groundwater flow in the quaternary valley fill is inclined approx. 0.5° downstream. However, the GPR signals were not effectively shielded by this shallow water-table but penetrated down into deeper successions of the water-saturated rockslide deposits and its fine substrate.

Further GPR measurements, carried out at medial accumulation areas, could not penetrate the several decametre thick rockslide deposits, but show clearly an on-lapping of prograding debris flows onto the hummocky rockslide relief. Also the internal stratification of the 5 - 20 m thick fluviatile debris is best recognisable in the radargrams and demonstrates the high resolution of the applied GPR system.

6. Discussion and Conclusions

Due to an oblique impact at its opposite slope, the Fernpass rockslide was split into two diametrically opposed Sturzströme. Regardless of the resulting loss of kinetic energy, both cover long travel distances up to 15.5 km. Compiled data of rockslides in the Alps indicate, that increased mobility correlates well with the rockslides volume, whereas lengths of 10 km were only exceeded by events containing a volume of about 1 km^3 and above (Heim, 1932; Scheidegger, 1973; Abele, 1974). But at Fernpass the moderately deflected northern rockslide branch, which clearly contains the majority of the debris, shows a shorter travel path than the less thick southern rockslide branch. In addition, latter is also characterised by remarkable high deflection angles of its curiously curved accumulation path. This field data point out, that here the run-out of the slide debris cannot be attributed mono-causal to size-effects.

Since many landslides cover larger travel distances than might be expected from their morphological settings and their material properties, several kinematical models have been established to explain enhanced landslide mobility, all of them somehow dealing with reducing the dynamic coefficient of friction. Among these are frictional melting and acoustic fluidization due to internal vibrations, the dynamic disintegration of the rock masses and attempts of adopting granular flow models. But most models concentrate on lubrification mechanisms and the presence of fluidising media such as air, water and/or vapour (e.g. Rousse, 1984; Erismann & Abele, 2001; Legros, 2002; Hungr & Evans, 2004). Based on field studies, interactions of descending rockslides with water-saturated valley-fillings are common features of several large rockslides and have already been observed at Flims/Switzerland (Pavoni, 1968; Poschinger et al., in press), in Austria at Wildalpen (Fritsch, 1993), Almtal (Abele, 1991b; Van Husen, 1995) and Tschirgant (Abele 1991a, 1997; Patzelt & Poscher, 1993). However, the spread of rockslides on water-

saturated substrates is believed to be the most favourable parameter enabling excess run-out distances. According to the geotechnical basic principle of undrained dynamic loading (Hutchinson & Bhandari, 1971), rapid mass movements may abruptly load water-saturated deposits and cause a sudden increase of both the pore-pressure and the total vertical stress therein. This, in turn, increases the shear stress within the zone of principal displacement and thus substantially facilitates the further landslide propagation, even along low-angle slopes and valley-floors. Fine and low permeable attrition breccias at the base of large catastrophic rockslides, as drilled at the Tschirgant rockslide deposits (Hartleitner, 1993) adjacent to the Fernpass region, may prevent the vertical escape of confined pore-water from the water-saturated sliding zone up into the permeable rockslide debris and thus hold up an excess pore-pressure.

At Fernpass, the long run-out of the southern rockslide branch was certainly favoured by the dynamic disintegration of the failing rock masses and a substantial channelling in the narrow valley. But above all, the mobility of the distal Fernpass rockslide was favoured by two aspects: 1) the water-saturation of the uppermost valley fill and 2) the Sturzstrom discharged, at least from the Nassereith area on, onto low permeable, lacustrine deposits. Both field studies and drilling data show that fine lacustrine sediments, underlying the distal rockslide deposits, are present upstream at least to Nassereith and extend at the valley flanks up to elevations of 810–820 m a.s.l. In contrast to this, here the central valley floor exhibits distal rockslide deposits that show a bottom surface at elevations of about 790 m a.s.l. Subsurface data inferred from GPR measurements show that adjacent rockslide deposits root at a depth of about 15–20 m. Thus, the top of the lacustrine deposits does not form a horizontal plane, but a smooth concave-curved depression towards the middle of the valley. This geometrical implication suggests that the spatial distribution of the distal rockslide deposits was substantially controlled by the late-glacial valley morphology. Movements on an incompetent fine substrate with a trenched and confining topography may explain the curious rockslide deflection at Nassereith: instead of continuing its straight accumulation path towards SE, the sliding debris turned here approx. perpendicular towards SW. Obviously the distal rockslide was not able to override a predisposed channel-like topography, but forced to accumulate as chain-like arranged Toma in the middle of the valley floor.

In addition, straight within this zone of deflection, the accumulation path of the slide debris was somehow interrupted. Between well-exposed Toma further up- and downstream, here evident field outcrops of rockslide deposits are absent for several hundred metres along the channel line. Both GPR- and drilling data backed up, that south of Nassereith the rockslide deposits are extremely reduced in thickness and accumulated within an only 2–9 m thick layer. Remarkably the very front of the rockslide, which travelled from this zone of disintegration more than 4 km further downstream, maintained as a more coherent debris mass with a thickness up to approx. 20–30 m. These geometrical relations suggest the distal Fernpass rockslide was obviously affected by differential accelerations, which caused a pulling-apart and splitting into several individual slide-units. Once preferential water supply from the substratum must have somehow favoured the dynamic undrained loading and thus the mobility of the frontal rockslide and left the main debris mass behind. Drilling campaigns showed a shallow groundwater-table, close below the present surface at between -3 to -6 m, and thus an effective water-saturation of both, the subsurface rockslide deposits and its fine lacustrine substrate. Whether the southern branch of the Fernpass rockslide discharged into a relict reservoir of a late-glacial lake or, more likely, just surged onto water-saturated lacustrine deposits, cannot be reconstructed yet.

Based on field observations, already Abele (1991a, 1997) suggested that catastrophic rockslide masses may disintegrate by being stretched and pulled-apart, especially when moving along water-saturated valley fills. Such distensive movements may generate debris ridges and associated depressions in between, both being striking morphological features of several large landslides. However, we do not assume that these pull-apart mechanisms attribute exclusively to rapid moving, high-energy Sturzströme. This cannot satisfyingly explain both the observed intensively varying thickness of the rockslide deposits along the channel line and also the in-line configuration of the cone-shaped Toma. Also one of the most significant extensional structures, containing the alluvial plain of the creek Kriegerbach where two GPR profiles were measured,

is genetically certainly not only due to the rapid Sturzstrom flow.

Rather all these features indicate that the semi-coherent rockslide-debris, and presumably also the uppermost parts of the incompetent substrate included, were affected by creeping processes and gravitational spreading. These distensive movements along water-saturated, basal sliding planes probably occurred at lower kinetic energy levels, however subsequent to the rapid Sturzstrom surge (Prager & Zangerl, 2005). This resulted in a further decomposition of the rockslide deposits and the generation of the present morphology, which is characterised by the well-known Toma and associated funnel- to basin-formed depressions including several kettle-like lakes. Cohesion, which is needed to form the cone-shaped Toma from the collapsing debris mass, was provided by the jig-saw-fitting of several shattered clasts and by the considerable amount of fine interstitial matrix. Since then, the spreading rockslide deposits have locally been covered by on-lapping fluvial clastics. According to GPR data, these post-rockslide sediments can reach thicknesses up to at least 20 m.

Acknowledgement

We gratefully acknowledge Wolfram Mostler (Univ. Innsbruck, Austria) for his help during the GPR field measurements and for providing insights in to unpublished drilling data (Ilbau, 1996) of the gravel-pit near Nassereith. Also Intergeo Consultants (Salzburg, Austria) kindly provided insights into drilling cores (Asfinag Austria, 2005) from Quaternary deposits at the southern flank of the Gurgl valley. Christian Zangerl (alpS, Innsbruck, Austria) is gratefully acknowledged for fruitful discussions and his input to the development of some ideas, concerning the rockslide kinematics, presented herein. Financially this study was supported by the ILF Consulting Engineers Ltd. and the TIWAG Tyrolean Hydroelectric Power Company Ltd. (both Innsbruck, Austria).

References

Abele, G. (1964): Die Fernpaßtalung und ihre morphologischen Probleme. - Tübinger Geograph. Stud., 12: 1-123.

Abele, G. (1969): Vom Eis geformte Bergsturzlandschaften. - Zs. f. Geomorph. N. F., Suppl. 8: 119-147.

Abele, G. (1970): Der Bergsturz im Almtal im Toten Gebirge. - Mitt. Österr. Geograph. Ges., 122: 120-124.

Abele, G. (1974): Bergstürze in den Alpen. Ihre Verbreitung, Morphologie und Folgeerscheinungen. - Wiss. Alpenvereinsh., 25: 1-230, München.

Abele, G. (1991a): Der Fernpaßbergsturz. Eine differentielle Felsgleitung. - Österr. Geograph. Ges., Zweigver. Innsbruck Jhrber. 1989/1990: 22-32.

Abele, G. (1991b): Durch Bergstürze mobilisierte Muren und durch Muren transportierte Bergsturzmassen. - Österr. Geograph. Ges., Zweigver. Innsbruck, Jhrber. 1989/1990: 32-39.

Abele, G. (1997): Rockslide movement supported by the mobilization of groundwater-saturated valley floor sediments. - Zs. f. Geomorph. N. F., 41/1: 1-20.

Ampferer, O. (1904): Die Bergstürze am Eingang des Ötztales und am Fernpaß. - Verh. Geol. R.-A., 1904: 73-87.

Ampferer, O. (1924): Erläuterungen zur Geologischen Spezial-Karte der Republik Österreich Blatt Lechtal (5045). - 55 pp., Geol. B.-A,. Wien.

Ampferer, O. & Ohnesorge, T. (1924): Erläuterungen zur Geologischen Spezial-Karte der Republik Österreich Blatt Zirl-Nassereith (5046). - 68 pp., Geol. B.-A., Wien.

Bichler, B. (1995): Quartärgeologie im Gurgltal unter besonderer Berücksichtigung der Pitztalmündung (Bezirk Imst/Tirol). - Ph.D. thesis, 77 pp., Univ. Innsbruck.

Brandner, R. & Poleschinski, W. (1986): Stratigraphie und Tektonik am Kalkalpensüdrand zwischen Zirl und Seefeld in Tirol (Exkursion D am 3. April 1986). - Jber. Mitt. oberrhein. Geol. Ver. N.F., 68: 67-92, Stuttgart.

Brückl, E., Hausmann, H., Krainer, K. & Mostler, W. (in press): Internal structure, composition and dynamics of Reichenkar rock glacier (western Stubai Alps, Austria). – Permafrost and Periglacial Processes.

Davis, J.L. & Annan, A.P. (1989): Ground penetrating radar for high-resolution mapping of soil and rock stratigraphy. - Geophysical Prospecting, 37: 531–551.

Donofrio, D. A., Brandner, R. & Poleschinski, W. (2003): Conodonten der Seefeld-Formation: Ein Beitrag zur Bio- und Lithostratigraphie der Hauptdolomit-Plattform (Obertrias, Westliche Nördliche Kalkalpen, Tirol). - Geol. Paläont. Mitt. Innsbruck, 26: 91-107.

Eisbacher, G.H. & Brandner R. (1995): Role of high-angle faults during heteroaxial contraction, Inntal Thrust Sheet, Northern Calcareous Alps, Western Austria. - Geol. Paläont. Mitt. Innsbruck 20, 389-406.

Erismann, T. H. & Abele, G. (2001): Dynamics of rockslides and rockfalls. - 316 pp., Springer.

GSSI (2001): Operation Manual, SIR-System 2000, Model 3200. - Geophysical Survey Systems Inc., North Salem, 2001.

Fritsch, A. (1993). Das Quartär der westlichen Hochschwab-Nordabdachung unter Berück-sichtigung des Bergsturzes von Wildalpen.- Ph.D. thesis, 122 pp., Univ. Vienna.

Hartleitner, K. (1993): Die Planung der 'Neuen Bahn' im Abschnitt Ötztal-Landeck: Geologische Ergebnisse. - In: Hauser, C. & Nowotny, A. (Eds.): Arbeitstagung 1993 Geol. B.-A., Geologie des Oberinntaler Raumes, Schwerpunkt Blatt 144 Landeck: 139-140.

Heim, A. (1932): Bergsturz und Menschenleben. - 218 pp., Wasmuth, Zürich.

Hsü, K. (1975): Catastrophic Debris Streams (Sturzstroms) generated by Rockfalls. - GSA Bull., 86: 129-140.

Hungr, O. & Evans, S. G. (2004): Entrainment of debris in rock avalanches: An analysis of a long run-out mechanism. - GSA Bull., 116: 1240-1252.

Hutchinson, J. N. & Bhandari, R. K. (1971): Undrained loading; a fundamental mechanism of mudflows and other mass movements. - Geotechnique, 21: 353-358.

Jol, H.M. & Bristow, C.S. (2003): GPR in sediments: advice on data collection, basic processing and interpretation, a good practice guide. - In: Bristow, C.S. & Jol, H.M. (Eds), Ground Penetrating Radar in Sediments. Geological Society, London, Spec. Publ., 211: 9-27.

Köhler, M. & Lumasegger, M. (1992): Hydrogeologische Untersuchung des Fernpassgebietes. - 239 pp., Unpubl. Report, ILF Consulting Engineers Ltd, on behalf of Amt der Tiroler Landesregierung, Abt. IIIg - Kulturbauamt, Innsbruck.

Krainer, K.; Mostler, W. & Span, N. (2002): A glacier-derived, ice-cored rock glacier in the western Stubai Alps (Austria): evidence from ice exposures and Ground Penetrating Radar investigation. – Zs. f. Gletscherkunde u. Glazialgeologie, 38/1: 21-34, Innsbruck.

Legros, F. (2001): The Mobility of long-runout landslides. - Eng. Geol., 63: 301-331.

Milsom, J. (2003): Field Geophysics (3rd Ed.). – 232 pp., John Wiley, Chichester (The Geological Field Guide Series).

Patzelt, G. & Poscher, G. (1993): Der Tschirgant-Bergsturz. – In: Hauser, C. & Nowotny, A. (Eds.): Arbeitstagung 1993 Geol. B.-A., Geologie des Oberinntaler Raumes, Schwerpunkt Blatt 144 Landeck, Exkursion D: Bemerkenswerte Geologische und Quartärgeologische Punkte im Oberinntal und aus dem äußerem Ötztal: 206-213.

Pavoni, N. (1968): Über die Entstehung der Kiesmassen im Bergsturzgebiet von Bonaduz-Reichenau (Graubünden). - Ecl. Geol. Helv., 61: 494-500.

Poscher, G. (1993): Neuergebnisse der Quartärforschung in Tirol. – In: Hauser, C. & Nowotny, A. (Eds.): Arbeitstagung 1993 Geol. B.-A., Geologie des Oberinntaler Raumes, Schwerpunkt Blatt 144 Landeck: 7-27.

Poschinger, A. v.; Wassmer, P. & Maisch M. (in press): The Flims Rockslide: History of Interpretation and new Insights. in: Evans, S.G., Scarascia-Mugnozza, G., Strom, A., Hermanns, R.L. (eds.), Massive rock Slope Failures, 341-369, Kluwer Academic Publ., Dordrecht.

Prager, C. & Zangerl, C. (2005): Kinematics of a long run-out rockslide: a case study from the Fernpass-region (Northern Calcareous Alps, Tyrol, Austria). - Geophys. Res. Abstr. 7: 02737, EGU 2005, Vienna.

Prager, C.; Ivy-Ochs, S.; Ostermann, M.; Synal, H.-A. & Patzelt, G. (in review): Geology and age of the catastrophic Fernpass rockslide (Tyrol, Austria). - Geomorphology, Spec. Iss., Large slope instabilities: from dating, triggering and evolution modelling to hazard assessment.

Rouse, W.C. (1984): Flowslides. - In: Brunsden, D. & Prior, D.B. (Eds.): Slope instability, 491-522, Wiley.

Sass, O. & Wollny, K. (2001): Investigations regarding alpine talus slopes using ground-penetrating radar (GPR) in the Bavarian Alps, Germany. - Earth Surf. Process. Landforms, 26: 1071–1086.

Scheidegger, A. (1973): On the prediction of the reach and velocity of catastrophic landslides. – Rock Mechanics and Rock Engeneering, 5/4: 231-236.

Van Husen, D. (1995): Bericht 1994 über geologische Aufnahmen im Quartär auf Blatt 67 Grünau/Almtal. – Jb. Geol. B.-A., 138/3: 490-491, Wien.

Appendix: Basic data of GPR profiles and drillings cited in this study.

Profile	Date of measurement	Start	End	Length	Main reflectors	Interpretation	Relevant Drilling
Gurgl valley	11.05.2004	188290 239980	188255 240210	230	4 - 6 20	Groundwater -3,5 m Base rockslide / Top lacustrine deposits	PD S1
Nassereith South	29.07.2005	188420 240700	188415 240605	100	6 15	Base fluvial deposits / Top rockslide Base rockslide / Top lacustrine deposits	PD S2 (PD S3)
Kriegerbach 1	04.02.2005	187675 245870	187725 245800	91	5 - 15 15 - 20	Debris flows (prograding) Top Rockslide	PD N1, PD N2
Kriegerbach 2	04.02.2005	187740 245850	187725 245760	96	6 - 20	Base debris flows / Top Rockslide	PD N1, PD N2

Remarks: Geographic Information (National Austrian Grid Bundesmeldenetz, Meridian M 28) measured by GPS and controlled by ortho-corrected images. Length of profiles quoted in metres, depth of reflectors in metres below ground surface. Interpretation of the reflectors implies their depth (quoted in below ground surface) as observed in probe drillings (Tab. 2).

Tab. 1 – Basic data of measured GPR profiles.

Drilling	Locality	Long. (E)	Lat. (N)	Elevation	Depth	Lithology	Interpretation	Groundwater
PD S1	Nassereith, field track	188195	240130	ca. 810	0 - 4.2	Polymict gravel (carbonatic and crystalline) with varying content of sand and silt	Fluviatil deposits (debris flows)	
					4.2 - 8.0	Clayish silt with little content of sand and several polished (drop-?)stones	Stillwater deposits ("varved clay")	- 3.50 (806.5)
					8.0 - 14.0	Polymict gravel (coarse from 10.0 - 12.5) with clayish - sandy matrix	Fluviatil deposits (debris flows)	
PD S2	Nassereith, industrial area	188405	240640	ca. 815	0 - 3	Polymict gravel	Fluviatil deposits, anthropogenic affected	
					3 - 7.5	Polymict gravel (carbonatic and crystalline) with varying content of sand and silt	Fluviatil deposits (debris flows)	
					7.5 - 12.5	Boulders (very hard to drill) in sandy - silty matrix	Rockslide (mingled with fluviatil deposits ?)	- 3.20 (811.8)
					12.5 - 14.0	Clayish silt with numerous polished (drop-?)stones	Lacustrine deposits ("varved clay")	
PD S3	Nassereith, communal road	188440	240995	ca. 820	0 - 13.2	Polymict gravel with varying content of sand and silt, therein loose layers of silty clays and occasional (7.5 - 9.0 m) occurrence of boulders	Fluviatil deposits (debris flows) with overbank deposits and boulders (rockslide ?)	- 6.00 (814.0)
					13.2 - 14.0	Clayish silt with sandy gravel (polymict, but crystalline-dominated)	Distal debris flows / proximal lacustrine deposits	
PD N1	Kriegerbach, forest track	187745	245760	ca. 950	0 - 4.0	Carbonatic gravel (fine) and sand with varying content of silt	Torrential deposits (debris flows)	
					4 - 4.5	Sand with clayish-silty matrix		clearly wet gravel underneath - 7.00 (*)
					4.5 - 7	Carbonatic gravel (coarse) and sand with varying content of silt (hard to drill)		
					7.0 - 7.5	Boulders (not to drill)	Rockslide ?	
PD N2	Kriegerbach, forest track	187635	245725	ca. 950	0 - 8.0	Alternation of fine and coarse carbonatic gravel and sand, both with varying content of silts (easy to drill)	Torrential deposits (debris flows)	
					8.0 - 12.5	Carbonatic gravel (coarse) and sand (hard to drill)	Debris flows ?	clearly wet gravel/sand underneath - 5.00 (*)
					12.5 - 14.0	Boulders (not to drill)	Rockslide ?	

Longitude and Latitude (based on National Austrian Grid Bundesmeldenetz, Meridian M 28) measured by GPS and controlled by ortho-corrected images, Elevation from Austrian Map. Depth of lithological changes quoted in metres below ground surface. Ditto groundwater level, this additionally also quoted in metres above sea level.

(*) SB-N N1-2: Drilling hole unstable, no water table measurable.

Geo.Alp, Vol. 3, S. 167–189, 2006

MICROBIALLY INDUCED CALCIUM CARBONATE IN TUFAS OF THE WESTERN EASTERN ALPS: A FIRST OVERVIEW

Diethard Sanders[1], Michael Unterwurzacher[2] & Beate Rüf[1]

With 1 figure, 4 plates and 2 tables

[1] Institute of Geology and Palaeontology

[2] Institute of Mineralogy and Petrography, Faculty of Geo- and Atmospheric Sciences, University of Innsbruck, A-6020 Innsbruck, Austria (EU)

E-mail: Diethard.G.Sanders@uibk.ac.at, Michael.Unterwurzacher@uibk.ac.at

Abstract

Most of fourteen tufa locations mainly in the western part of the Eastern Alps contain a significant to prevalent portion of microbially-induced calcium carbonate.

The investigated tufas are situated on substrata of limestone, dolostone, marlstone, conglomerate, gneiss, phyllite and slate. Most larger tufa occurrences comprise significant areas wherein tufa formation is low or had halted. Two major groups of "microbial tufas" are distinguished, (1) crystalline microbial calcium carbonate, and (2) micropeloidal to micritic calcium carbonate. Crystalline microbial calcium carbonate is present in two major fabrics. (1A) Calcified "microbushes" of outward-radiating clusters of slightly tangled tubuli each encased by a single crystal of calcite of subrounded to subcircular cross-section. Larger volumes of tufa may be composed of stacked laminae built by laterally arrayed microbushes. (1B) Knobs to crusts that, internally, consist of fan-like arrays of tubuli encased within large single crystals of calcite. Both the microbushes and the microfans are interpreted as calcified cyanobacterial aggregates of *Rivularia* type. The crystalline microbial calcites may readily recrystallize and provide a substrate for further, "inorganic" calcite growth, resulting in cementstone texture that shows little evidence of its microbially-induced origin.

(2) Micropeloidal to micritic calcium carbonate includes micropeloidal grainstone, "filamentous-micropeloidal" grainstone, (fenestral) lime mudstone with stromatolithic or cauliflower lamination, and thrombolithic lime mudstone. The micropeloids and the filamentous-micropeloidal arrays may have been produced by coccoid and filamentous cyanobacteria, at or near the tufa surface. A major portion of calcium carbonate of this category, however, is present within the pore space of tufas, where it formed in association with light-indepedent microbes and/or with dead microbes, small phytoclasts and organic compounds. Deduced rates of present tufa formation are within the range of known rates, but show distinct variations both within and among locations.

Zusammenfassung

Die meisten von vierzehn Kalktuff-Vorkommen vorwiegend in den westlichen Ostalpen bestehen aus einem bedeutenden bis überwiegenden Anteil aus Kalziumkarbonat, dessen Fällung von Mikroben induziert wurde.

Die untersuchten Tuffe liegen auf verschiedenen Gesteinsuntergründen wie Kalkstein, Dolomitstein, Mergel, Konglomerat, Gneis, Phyllit und Schiefer. In den meisten Vorkommen findet noch aktive Tuff-Bildung statt, jedoch enthalten die meisten der grösseren Vorkommen auch Bereiche, in denen kaum oder keine Tuff-

Neubildung stattfindet. Wir unterscheiden zwei Hauptgruppen "mikrobieller Tuffe", (1) kristallines mikrobielles Kalziumkarbonat (zumeist Kalzit), und (2) mikropeloidales bis mikritisches Kalziumkarbonat.

Das kristalline mikrobielle Kalziumkarbonat zeigt zwei Gefüge. (1A) Verkalkte "Mikrobüsche" aus Büscheln von leicht unregelmässigen und "verfilzten" Röhrchen, deren jedes von einem stark gelängten, im Querschnitt rundlichen Einzelkristall meist aus Kalzit eingehüllt wird. Die Mikrobüsche können alleine vorkommen oder zu Laminae aufgereiht stehen, zusammen mit anderen Arten von Tuff, oder bilden selbst Tuffe, die aus vielen Laminae aufgereihter Büschchen bestehen. Jeder Mikrobusch besteht aus einem einzigen oder wenigen Kristallen von Kalzit; innerhalb jedes Mikrobusches sind daher ganze ganze Bündel von Röhrchen oder die Röhrchen des gesamten Mikrobusches von Kalzit umgeben, der trotz des diskreten Wachstums der Röhrchen eine einzige optische Orientierung zeigt. Die Mikrobüsche starten an ihrer Basis von "keulenförmigen" Kalzitkristallen, die an ihrer Oberseite die Öffnungen der Röhrchen zeigen. (1B) Knoten bis Krusten, die im Schnittbild aus regelmässigen "Fächern" von gleichmässig aufgefächerten, diskreten Röhrchen bestehen. Jedes Röhrchen wird von Kalzit umgeben. Büschel von Röhrchen oder ganze Fächer von Röhrchen sind von Kalzit mit einer einzigen optischen Orientierung umgeben, sodass jedes Röhrchen-Büschel bzw. jeder Fächer in einen grossen Einkristall aus Kalzit eingebettet ist. Die Krümmung der Aussenseite der Kalzitkristalle ist parallel der Krümmung der Röhrchen. Die Organismen, die die beschriebenen Typen 1A und 1B von kristallinem Kalzit bilden, werden der Gattung *Rivularia* (Nostocales, Cyanobacteria) zugeordnet. Die Kalzite der Typen 1A und 1B sind von sub-Millimeter dünnen, zueinander in etwa parallelen Laminae von Mikrit bis Mikrosparit durchsetzt. Das "Wachstum" jeder Lage von Rivularien geht von einer dieser Mikrit/Mikrosparit-Lamina aus. Auf diese Weise werden Laminae von wenigen Millimetern bis etwa 1 cm Dicke von verkalkten Rivularien gebildet. Feldexperimente legen nahe, dass die Mikrit/Mikrosparit-Laminae Unterbrechungslagen darstellen, die sich meist in Verbindung mit einem winterlichen Aussetzen bzw. Verringern der Rate der Kalkfällung bzw. des Rivularien-Wachstums bilden. Bei Lingenau (Vorarlberg) besteht der weitaus grösste Anteil des gesamten aktiven Tuffvorkommens aus Rivularien-Tuff, der die beschriebene Lamination zeigt, die wahrscheinlich auf jahreszeitliche Schwankungen der Kalkfällungsrate in Verbindung mit dem Wachstum der Cyanobakterien zurückzuführen ist. Feldexperimente und die erwähnte ?jährliche Lamination der Tuffe machen sehr wahrscheinlich, dass die Fällung des Kalkes in ursächlicher Verknüpfung mit dem Wachstum der Cyanobakterien steht, diese also entscheidend die Kalkfällung beeinflussen.

(2) Mikropeloidales bis mikritisches Kalziumkarbonat umfasst im wesentlichen mikropeloidale grainstones, "filamentös-mikropeloidale" grainstones, (fenestrale) lime mudstones mit stromatolithischer oder "blumenkohl-artiger" Lamination, und thrombolithische lime mudstones. Die Arten des Kalziumkarbonats der zweiten Gruppe bildeten sich wahrscheinlich im Zusammenhang mit coccoiden (Mikropeloide) und filamentösen Cyanobakterien ("filamentös-mikropeloidale" Aggregate) an oder nahe der Oberfläche der Tuffe, zu einem grossen Teil aber auch durch licht-unabhängige Mikroben, die im Porenraum der Tuffe leben, sowie durch Kalkfällung in Verbindung mit unbelebter organischer Substanz (z. B. tote Mikroben, Phytoklasten, organische Verbindungen) im Porenraum. Ein seltener Typ von Tuff, der sich möglicherweise unter signifikanter Beteiligung von Mikroben bildete, ist durch einen fossilen Vadolith vertreten. Die ermittelten Raten heutiger Tuff-Bildung liegen im Bereich bekannter Raten, zeigen jedoch zwischen verschiedenen Tuff-Lokalitäten als auch auch innerhalb einer "Lokalität" starke Unterschiede. Unter intensivem Wasserzutritt, wie etwa an den Prallstellen frei fallender Wasserfäden oder an Vorsprüngen von wasserüberronnenen Tuff-Vorhängen rekristallisiert der kristalline mikobielle Kalzit meist rasch und dient als Unterlage für weitere, "anorganische" Kalzitfällung, was zu einem mehr oder weniger homogenen, sehr harten cementstone-Gefüge führt, das kaum noch Spuren seines mikrobiell induzierten Ursprungs zeigt.

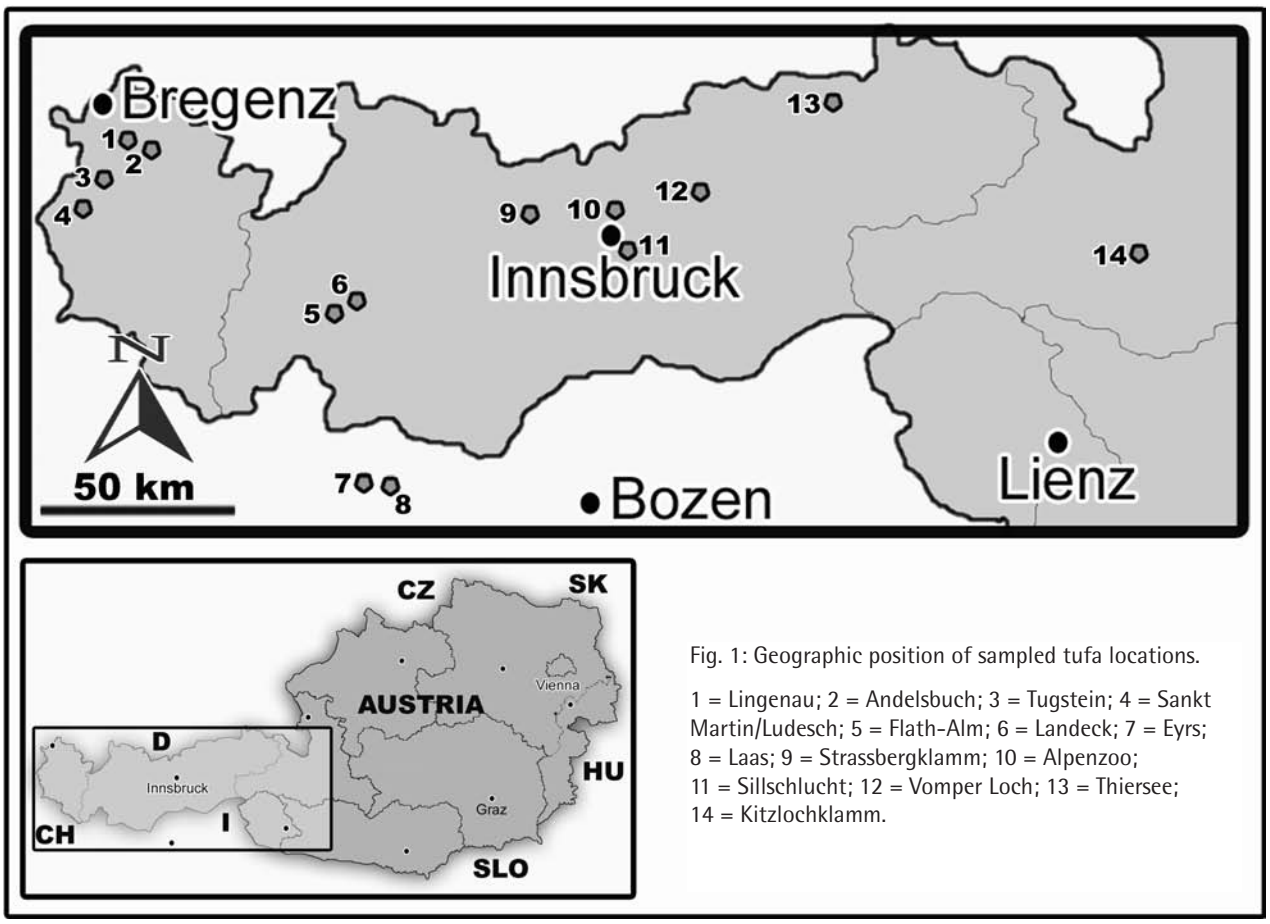

Fig. 1: Geographic position of sampled tufa locations.

1 = Lingenau; 2 = Andelsbuch; 3 = Tugstein; 4 = Sankt Martin/Ludesch; 5 = Flath-Alm; 6 = Landeck; 7 = Eyrs; 8 = Laas; 9 = Strassbergklamm; 10 = Alpenzoo; 11 = Sillschlucht; 12 = Vomper Loch; 13 = Thiersee; 14 = Kitzlochklamm.

1. Introduction

In the days before concrete, tufa limestone was a highly appreciated building stone. By contrast to travertine limestone (lapis tiburtinum) that forms around hot springs associated with volcanism, calcareous tufa forms by precipitation of calcium carbonate from "cool" spring and river waters (Ford & Pedley, 1996). Tufa limestone was widely used in masonry as a light-weight yet stressable, easily workable stone resistant to frost cracking. Numerous are the castles, churches and other buildings that contain or even largely consist of blocks of tufa. By contrast to all other building materials except for wood, tufa "re-grows" after quarrying by precipitation of calcium carbonate. In addition, in many cases, a single or several locations of tufa were situated (relatively) near the building site, hence costs for transport were low. Aside of these profane considerations, tufas are interesting for other reasons, too. First of course stands the question "Why precipitation of calcium carbonate just here and not at every other spring?", touching upon hydrology, water chemistry, climate, type of geological substrate, and ecology and biochemistry of the organisms involved. Spring tufas form by precipitation of calcium carbonate from waters supersaturated up to about 10 times. Supersaturation is mostly attained, or is highest, some distance downstream the emergence of the spring or, in large tufa-precipitating systems such as Plitvice, also within-stream to downstream of rapids and water falls. There is general aggreement that degassing of CO_2 out of the water is the single most important process in producing the necessary degrees of supersaturation for precipitation (Viles & Goudie, 1990; Chen et al., 2004).

To a carbonate sedimentologist, however, a simple yet tackling question is "How do these tufas look like in thin section and how do the observed fabrics form?" All geologists can predict how a thin section of oolite should look like and how the constituent ooids originate. For spring tufas, despite investigations into their water chemistry and aspects of fabrics (Emeis et al., 1987; Sancho et al., 1997; Janssen

et al., 1999; Freytet & Verrecchia, 1999), we are as yet still off a concept relating the field appearance of different types of tufas to their microfabrics and, finally, from establishing a predictive concept of formation of spring tufa fabrics (cf. Merz-Preiß & Riding, 1999). This holds in particular for calcium carbonate precipitation induced by microbes. Cyanobacteria, for instance, secrete extracellular polymeric substances that might profoundly modify the shape of crystallized calcium carbonate (cf. Cölfen, 2003). In the present paper, major types of microbially-induced tufa observed at locations visited by us are characterized and discussed. Microbially-induced tufa is widespread and, at a number of locations, comprises the major part of total carbonate volume. For spring tufas of the Eastern Alps, the significant to prevalent contribution of microbially-induced calcium carbonate to date has not been appreciated, and bears implications for the general mode of tufa formation. This contribution is in acknowledgement to the first author's (D. S.) first academic teacher, Rainer Brandner, who accompanied his first steps into the wide world of carbonate rocks.

2. Methods and settings

A total of fourteen locations of spring tufas situated in Vorarlberg, Northern Tyrol, Southern Tyrol, and Salzburg was documented and sampled (Fig. 1). For a short characterization of the sampled tufa locations, the reader is referred to table 1. In order to include as many different types of tufa-depositing systems (fossil to active) as possible, no specific selection of tufa locations was made. Each location is classified with respect to its prevailing tufa deposystem (e. g. springline tufa) and the types of tufa as identified on the surface (e. g. waterfall tufa, moss tufa) (Tab. 1). The different types of tufas as classified in the field were sampled. Cut slabs and thin sections of resin-indurated samples provided documentation of microfabrics. A total of 134 thin sections has been investigated. SEM investigation of selected samples provided additional information on surfaces and internal fabrics. The investigated spring tufas are situated on different rock substrata (Tab. 1). In addition, at most locations, the substrate is overlain by glacial till, or reworked glacial till, or glacial till is present in the environs of the tufa formation. Where tufa occurrences are situated on substrata of gneiss or phyllite, these rocks typically are riddled by more-or-less wide cataclastic to phyllonitic zones.

3. Types of microbially induced calcium carbonate

Based on descriptive features, herein we distinguish two major classes of calcium carbonate precipitated under microbial mediation, (1) crystalline microbial calcium carbonate, i.e. microbially-induced tufa composed of $CaCO_3$ crystals that are recognizable by standard light microscopy, and (2) micritic microbial calcium carbonate, in which the crystals are so small that they can hardly be resolved with a petrographic microscope.

3.1. Crystalline microbial calcium carbonate

3.1.1. Laminated "microbush" tufa

In this category, the most conspicuous facies and microfacies is represented by laminated, porous tufas. These laminated tufas may build steep to overhanging, yellowish tufa curtains up to a few tens of meters in height associated with water falls (Pl. 1/1-3). Individual tufa laminae typically are between about 4 to 8 mm in thickness (Pl. 1/4, 5). The laminae are vertically separated by very thin intercalations typically less than a millimetre thick of microsparite and/or of micrite; the microsparite consists of more-or-less equigranular calcite rhombohaidra. Each tufa lamina consists of laterally arrayed, more-or-less dense "microbush-like" arrangements of calcite crystals that are obvious as "microbushes" also under crossed polars (Pl. 1/5). Individual branches of the calcite microbushes are bifurcating (Pl. 1/6). Upon bifurcation, the optical orientation of the calcite crystals commonly remains constant. In laterally adjacent microbushes, however, the calcite is typically of different optical orientation, giving rise to microbushes of distinct extinction under crossed polars (Pl. 1/5-7). Within the center of the calcite crystals that comprise individual microbush branches, elongate tubes parallel to the vertical extent of the crystals are present (Pl. 1/6). In cross-section, the calcite crystals that comprise the individual branches of the microbushes show a subcircular to circular pore in their center, corresponding to the mentioned tubes (Pl. 1/7). In

young, "fresh" samples of laminated tufa, the space between the calcified branches is open pore space (Pl. 1/6, 7). In SEM, the surface of the described tufa laminae of microbushes consists of a dense array of round, tower-like calcite crystals each with a sub-circular hollow in its center, resulting in very small calcite tubelets (Pl. 1/8). Whereas the upper and outer surface of the calcite tubelets shows crystal growth surfaces according to the rhombohaidral symmetry of calcite, the inner surface of the tubelets is round and/or slightly rugged (Pl. 2/1, 2). The outer boundary of these calcite may show numerous sub-micron sized steps according to the rhombohaidral calcite symmetry or, in the best-preserved samples, the boundary of the laminae is nearly perfectly smooth and round (Pl. 2/2). At Laas, a similar spectrum of microstructures of inferred microbial origin is observed, but is preserved within more-or-less calcitized aragonite. At March 18th, 2005 at Lingenau (Vorarlberg), an active pavement of laminated tufa as described was sampled, by excavating a cavity with a chisel. The same spot was re-sampled on September 8th, 2005, i. e. nearly six months later. Because the first sampling had truncated the laminae of the tufa, any newly precipitated calcium carbonate should be easily recognizable by geometrical relations in thin section. Indeed, the truncated laminae of previous years became overlain by a lamina up to about 6 millimeters of calcified microbushes identical to those in the older, underlying laminae (Pl. 2/3, 4). This proves that this style of tufa formation is still active at Lingenau. The tufa lamina formed between 18.3.-8.9.2005 shows lateral variations in the intensity of calcification. Within densely calcified portions, the tubuli of the microbushes are enveloped by dense calcite of low porosity. In scarcely calcified portions, it is just the tubuli - or some stretches thereof - that are enveloped by elongate to "worm-like" curved, optically single crystals of calcite.

At several locations, laminated tufas of the described type comprise the major portion of total tufa volume. At Lingenau, the light-yellow cascades and curtains of waterfall tufas consist practically entirely of this type of tufa. This laminated tufa seems to form on well-sunlit, steep to vertical substrata overrun by thin sheets of water. By contrast, under impacting water from water falls or water "shoots", and under shooting water more than roughly 1-2 cm in depth, this type of tufa is intercalated with and is replaced by a brown, massive calcite with a botryoidal surface (Pl. 1/2). At Lingenau, however, also the major part of phytoclastic tufa of the moderately steeply inclined creek downstream the upper waterfalls consist of laminated microbush tufa (Pl. 2/5). There, this type of tufa also commonly forms "mini-rimstones", with rims up to a few millimeters high and pools are a few centimeters to about 10 cm in width (Pl. 2/6, 7). In thin section, the mini-rimstones also consist of microbush tufa as described above (Pl. 2/8). Also at other locations, however, the described type of tufa may locally represent a significant portion of the total volume.

Interpretation: For the described laminated "microbush calcite", the elongate organic structures that comprise the nucleus for calcite precipitation are identical in size and growth pattern to calcified filamentous cyanobacteria, probably *Rivularia* (cf. Obenlüneschloß, 1991; Riding, 1991; Kano et al., 2003). Within the described tufa, the regular interruptions of growth along thin laminae of micrite to microsparite may represent a seasonal or quasi-seasonal pattern. This is indicated by the absence of a lamina of micrite to microsparite along the contact to the laminae artifically truncated by us in spring 2005, followed by growth of a summer-2005 lamina of rivularian calcite. The thickness of this lamina of about 4 to 8 mm compares well with that of the older laminae (see Pl. 2/3). Thus, during a single spring to summer cycle, cyanobacterially-induced calcification adds a few millimeters at least to the tufa surface. Whereas calcified cyanobacterial microbushes and laminae built thereof were observed also within moss tufas and in phytoclastic tufas, massive laminated tufas of this type form mainly in association with water falls. The described "mini-rimstones" of rivularian tufa in such abundance to date were observed only at Lingenau. Seasonally laminated cyanobacterial tufas similar to those described by us have been described, for instance, from Belgium (Janssen et al., 1999) and Japan (Kano et al. 2003). Growth thicknesses of up to 1 cm/a of these laminated tufas are considered as likely (Janssen et al., 1999, p. 83), and this is supported by our data (see also below). In most laminated cyanobacterial tufas, however, the cyanobacterial filaments are encrusted by calcitic micrite and/or microsparite (cf. Arp et al., 1999; Janssen et al., 1999; Kano et al., 2003), not by optically single calcite crystals (but see Obenlüneschloß, 1991). Cyanobacteria secrete protective, mucus-like, extra-

No. in figure 1 Name of location Size Rock substrate in immediate environs	Field classification of tufa deposystem (acc. to Ford & Pedley, 1996) Prevalent tufa on active surface, field classification	Abundance of microbially-induced tufas	Prevalent types of microbially-induced tufa	Active/Inactive relation
1 Lingenau Large Conglomerates, sandstones, marlstones	Proximal springline tufa Waterfall tufa	Abundant	Microbush calcite, microfan calcite	Moderately active to low-active
2 Andelsbuch Moderate Marlstones	Fluvial barrage tufa (of perennial creek) Moss tufa	Common to abundant	Micropeloidal grainstones, crystalline microbial calcites, thrombolites	Moderately active to fully active
3 Tugstein Small Limestone	Proximal springline tufa Moss tufa	Common to few	Micropeloidal grainstones, thrombolites (in pore space)	Fully active
4 St. Martin (Ludesch) Large Sandstone, marlstone	Paludal tufa Moss tufa	Abundant	Micropeloidal grainstones, thrombolites (in pore space)	Moderately to ?fully active
5 Flath-Alm Moderate to ?large Gneiss and slate, glacial till	Fossil. Proximal springline tufa. Phytoclastic tufa	Uncommon	Micropeloidal grainstones, crystalline microbial calcites	Fossil
6 Landeck Moderate Quartz phyllite	Springline tufa, paludal tufa Phyto/lithoclastic tufa, moss tufa (few)	Uncommon	Micropeloidal grainstones, lime mudstones in part of ?microbial orgin	Moderately active to ?low-active
7 Eyrs Moderate Gneiss with shear zones, glacial till	Fossil. Springline tufa, paludal tufa Lithoclastic tufa	not identified in our samples; perhaps uncommon to rare	(not specified)	Fossil

Tab. 1: Locations sampled for tufas (see Fig. 1 for location). Field classification of tufa deposystems is based on Ford & Pedley (1996). The size of tufa locations (including both actively forming tufa and older, inactive to fossil tufa at each location) is here subdivided into four categories. Very small: up to a few meters; Small: a few meters to about 20 m (longest measure); Moderate: 20 m to about 100 meters; Large: distinctly more than about 100 meters in longest measure. For each location, because of limitations of outcrop, the relation of active tufa-depositing area relative to inactive tufa occurrence (Active/Inactive relation) provides a semi-quantitative impression only, and is subdivided into four categories. Fully active: Inactive areas absent or of insignificantly small size relative to active areas; Moderately active: Active and inactive areas roughly of the same size; Low-active: Active area much smaller than inactive area; Fossil: no active tufa formation.

No. in figure 1 Name of location Size Rock substrate in immediate environs	Field classification of tufa deposystem (acc. to Ford & Pedley, 1996) Prevalent tufa on active surface, field classification	Abundance of microbially-induced tufas	Prevalent types of microbially-induced tufa	Active/Inactive relation
8 Laas (several occurrences) Moderate (for most occurrences) Gneiss with shear zones, glacial till (locally)	Springline tufas Lithoclastic tufa, waterfall tufa, phytoclastic tufa	Abundant: waterfall tufas Common: litho/phytoclastic tufas (in part fossil)	Active waterfall tufa: Microbush aragonite, microfilamentous aragonite Litho/phytoclastic tufas (in part fossil): micropeloidal grst-pkst, lime mudst (thrombolites), microbush aragonite, microfilamentous aragonite	Total of all occurrences: low-active
9 Strassbergklamm Large Dolostones	Springline tufa Waterfall tufas, moss tufas	Common to abundant	Micropeloidal grainstones	Low-active to fossil
10 Alpenzoo Moderate Lodgement till, cellular dolostone	Springline tufa Moss tufa	Abundant	Crystalline microbial calcites, micropeloidal grainstone, thrombolites	Moderately active to ?low-active
11 Sillschlucht (several occurrences) Small and very small (two occurrences are fossil) Quartz phyllite	Springline tufa Waterfall tufa, moss tufa	Common to abundant (as pore fills and as crusts)	Stromatolithically to cauliflower laminated lime mudst, fenestral lime mudst, micropeloidal grainstones, Crystalline microbial calcites,	Total of all occurrences: low-active
12 Vomper Loch Very small Limestones	Springline tufa Moss tufa	Abundant	Micropeloidal grainstones, laminated lime mudstones	Fully active
13 Thiersee Fossil part: Large Active part: Very small Limestones	Fossil part: waterfall tufa, fluvial barrage tufa? Phytoclastic tufas, waterfall tufas Active part: Moss tufa (small)	Common to abundant	Waterfall tufas: Microbush calcite, micropeloidal grainstone Vadolithic tufas: micropeloidal to clotted-micropeloidal grainstone, lime mudstone	Low-active to fossil
14 Kitzlochklamm Small Slates	Springline tufa associated with short cave Moss tufa, with lateral transition into speleothems	Overall few, confined to spring tufa, in cave only flowstones	micropeloidal grst-pkst, cauliflower/stromatolithically laminated lime mudst, lime mudst (thrombolites)	Fully active

Tab. 1 (continued)

cellular polymeric substances (EPS) rich in polysaccharides and in organic acids, such as aspartic amino acid (Obenlüneschloß, 1991; Decho et al., 2005). Biopolymers within gels or gel-like substrates, such as provided by EPS embedding cyanobacteria, are efficient modifiers of the shape of crystallizing calcium carbonate (cf. Cölfen, 2003). Aspartic amino acid, for instance, binds to specific step edges of calcite crystal surfaces; this, in turn, results in curved to finely stepped crystal edges and surfaces. The resulting "chiral" modifications of crystal shape (see Cölfen, 2003, p. 24) are broadly reminiscent to the curved to very finely serrated outer surface of the observed *Rivularia* calcite.

3.1.2. Microfan tufa

A similar, less widespread type of tufa of this category is primarily associated with subhorizontal to steeply inclined to overhanging, wet (spray water and/or seep water) but not intensely water-run portions of water fall tufas (e. g. at the location Lingenau), but also at locations dominated by moss tufas and phytoclastic tufas, where it is present as well-indurated, dense carbonate crusts on gravels, tufa intraclasts and phytoclasts (e. g. at the locations Ludesch, Andelsbuch, Alpenzoo). In the field, this tufa is present in small, protruding, cream to yellow to pink or light brown-coloured, calcified patches or crusts a few millimeters to a few square meters in size. Small patches of crust are of knobby to hemispherical shape; wider crusts up to 10 cm and more in extent may show a mammillated to pustular-"meandroid" surface (Pl. 3/1). The crusts may be present in isolated knobs to small patches, or may comprise areas up to a few square meters in size (e. g. at the location Andelsbuch). The crusts are present on bare rock surfaces, but are equally common on lithoclasts, tufa intraclasts (Pl. 3/1-3) as well as on phytoclasts. In thin sections oriented vertical relative to the surface of the crusts, they consist of a highly regular array of outward-fanning calcite crystals (Pl. 3/4, 5). Within the calcite crystals, a highly regular array of branched, curved, outward-fanning tubelets is present, forming "microfans" of tubuli. The curvature and extent of the tubelets is concordant with extent and curvature of the calcite crystals (Pl. 3/6). Each individual microfan as defined by the patterns of the tubelets consists of several curved calcite crystals, i. e. outwards, each crystal becomes larger as the tubelets fan out. Near their outer termination, individual calcite crystals as identified by extinction under crossed polars are up to about 10 mm in width. The outer surface termination of individual crystals of calcite is the same surface than that of the entire crust, i. e. of convex and concave shape in thin section. In addition, also within the calcite fans, individual bush-like arrays of calcite crystals may terminate sharply along a curved surface.

Interpretation: The calcitic knobs to crusts are interpreted as calcified cyanobacterial aggregates, but of a different type than the above-described calcite. In this type of tufa, the fans built by the tubuli are of quite smooth and continuous curvature, and of highly regular arrangement. Additionally, individual calcite crystals extend across the concentric lamination, resulting in large single crystals. Three extant species, or morphospecies, of *Rivularia* are known to produce such regular, radially-fanning sparry calcite (Obenlüneschloß, 1991; see also Janssen et al., 1999, p. 81). *Rivularia* is very similar to the fossil genus *Cayeuxia* (see also Kershaw & Guo, 2003, their Fig. 4), and is considered by some authors as a synonym (Flügel, 2004, p. 409, 410). *Cayeuxia*, or *Rivularia*, for that matter, consists of a radially-fanning array of tubuli very similar to the fans of calcified tubuli observed by us. We thus assign the described, regularly-fanning tubuli/calcite crystal aggregates to *Rivularia*. The close correspondence of calcite crystals with the shape, curvature and fanning of the cyanobacterial filaments indicates that calcite crystallization is influenced or steered by the cyanobacteria. The precise reasons for the changes, or apparent changes, in the optical orientation of calcite crystals during growth and outward-fanning are not known. The optical orientation of the calcite crystals may be set since the start of growth of a cyanobacterial aggregate (calcification with different orientations on different sides of the cell?), or it may result from changes in orientation during later growth of the crystal/cyanobacterial-ensemble. The formation of both of the described types of crystalline microbial calcite in association with photosynthetic organisms is also indicated by the microstratigraphy observed in thin sections; calcified fabrics of these kinds always are form first during the formation of tufa fabric successions, and no calcified rivularians or other cyanoids were observed within macropores of tufa.

3.2. Micropeloidal to micritic calcium carbonate

3.2.1. Micropeloidal grainstones

Aside of both "inorganically" precipitated cements (not treated herein) and the above-described tufas, micropeloidal grainstone to, subordinately, packstone and non-geopetal crusts of stromatolithically laminated/fenestral lime mudstones are the most significant types of microfacies types in the investigated spring tufas. In the field, micropeloidal grainstones to packstones appear as light brown to ocre-coloured crusts to masses a few millimeters to more than 10 cm in thick. Such crusts have been found also in low-lit locations such as short, artifically excavated caves or below overhangs, below thin sheets of flowing water and on permanently wet spots around drip impacts or at water seeps. In general, in locations of low to moderate illumination, such as in caves, half-caves and below overhangs, crusts more than 10-20 square meters in size of microbial calcium carbonate may comprise the largest part or all of the tufa calcium carbonate, like at Andelsbuch. Crusts and patches of micropeloidal grainstone/packstone are common to widespread in all types of spring tufas, but typically this lithology is most abundant in moss tufas and in phytoclastic tufas. In moss tufas, micropeloidal grainstone may have formed first in the diagenetic succession. Conversely, in phytoclastic tufas, the first stages of diagenesis typically are represented by crystalline microbial calcites and/or by fringes of cement, whereas the remaining abundant pore space is partly to entirely filled by micropeloidal grainstone to packstone. Overall, the micropeloidal grainstones to packstone show little variation with respect to fabric. They consist of a more-or-less porous grainstone composed of micropeloids cemented by fringes of very finely crystalline rhombohaidral calcite spar. (Pl. 3/7) In thin section, some micropeloidal grainstones show a more-or-less systematic, "pearl-necklace" like arrangement of micropeloids (Pl. 3/8), or an array of tangled, very narrow "tubes" encrusted along all or most of their extent by micrite (Pl. 4/1). In the grainstones, fenestral pores and/or dissolution veins less than a millimeter to more than a centimeter in width may be common. Some of the micropeloidal grainstones to packstones also contain layers of fenestrae that probably result from larval conducts of insects, such as of chiromonids and/or trichopterids. In addition, phyto- and zooclasts (e. g. gastropod shells) may float within the grainstone. The micropeloidal grainstone to packstone may comprise entire thin sections, i. e. patches built exclusively of this lithology are at least about 6 cm in width, or it is present as one of several spring tufa fabrics (e. g. cement crusts, moss stems) within the same sample. To simulate moss tufa formation, at Tugstein (Vorarlberg), a hair brush was fixed on March 18th, 2005 onto a wall of tufa thinly overrun by water. About six months later, on September 8th, 2005, the bristles of the brush were completely clogged and overgrown by indurated calcium carbonate (Pl. 4/2). In thin section, the calcium carbonate that clogs the bristles is a fenestral micropeloidal grainstone as described, and relatively rich in very small-sized phytoclasts. At the surface of the indurated clogging of micropeloidal grainstone, beyond the extent of the bristles, "mini-stromatolites" and micritic crusts of calcium carbonate had formed (Pl. 4/3). By contrast to moss tufas (not described herein), however, the bristles of the brush are not immediately overlain by a layer of micrite to microsparite, or cement. At waterfall tufas, on steeply-dipping to overhanging surfaces of tufa and/or of substrate rock, crusts up to a few centimeters thick of stromatolithically to cauliflower-like laminated or fenestral lime mudstone to micropeloidal grainstone locally are common. At the toe of tufa-encrusted rockwalls, chips of tufa spalled off by frost action may accumulate. These chips, in turn, may be coated by laminated crusts of lime mudstone to micropeloidal grainstone as described, giving rise to a specific type of intraclast coated grain.

Interpretation: Micropeloids formed by calcification of clumps (probably mostly consortia) of non-filamentous microbes are among the most widespread types of microbially-induced calcium carbonate, and have been described from numerous habitats ranging from deep-marine to terrestrial (e. g. Reid, 1987; Reitner, 1993; Camoin et al., 1999; Rivadeneyra et al., 2000, 2004). In calcium-rich environments such as sea water and tufa-precipitating waters, active expellence of calcium out of the cell is a physiological must. Because the cell surface of microbes is negatively charged, particularly dead microbes are attractors of calcium ions; in addition, most microbial aggregates or consortia are embedded in extracellular polymeric substance rich in bicarbonate (from respiration). Microbial calcification thus proceeds in habitats both lit and dark,

albeit at different rates. Furthermore, precipitation of calcium carbonate may proceed in association with dead microbes, small phytoclasts and organic substances within the pore space of tufa. This at least in part explains the widespread presence of micropeloidal grainstone to packstone both in surface and subsurface habitats, and both on the surface of actively forming tufas and in the pore space of tufas.

3.2.2. Thrombolites

Lime mudstone, typically with a highly variable proportion of small phytoclasts, small tufa intraclasts and/or a few extraformational grains derived from the local rock substrate, is widespread in larger pores of all types of tufa. The possible contribution of microbially-mediated micrite precipitation to these mudstones, however, is difficult to assess. A portion or all of the lime mudstone may have been passively spilled into the pore space via the typically swift pore water flow within spring tufa lithosomes. In some cases, however, faint cauliflower-like laminae within relatively pure mudstone, and a close association of micropeloidal grainstone interfingering, in a non-geopetal fashion, with lime mudstone suggest that at least some of the lime mudstone may represent thrombolithic microbialites. Whether passively infilled or precipitated, the lime mudstones within micro- to macropores make up a significant proportion of the total rock of many tufas.

Interpretation: Because the described thrombolites are present within the pore space of tufas, this type of microbially-induced calcium carbonate results from non-photoautotrophic organisms. At the present state of investigations, precipitation of isolated crystals and/or "dark calcification" of thoroughly micrite-calcified biofilms may be assumed, but is difficult to prove. A portion or all of the lime mud may have been produced by microbially induced precipitation, whereas another portion probably represents a fine-grained sediment passively swept in. That passive sweep-in was active in at least many cases is suggested, but equally not proven, by common presence of small phyto-, intra- and extraclasts in the lime mudstone. Conversely, non-geopetal, homogeneous to faintly clotted masses of micrite, and cauliflower-like, non-geopetally laminated masses of lime mudstone are ascribed to dark calcification of biofilms. A few groups of cyanobacteria also are capable to thrive in the dark by facultative chemoautotrophy on sugars (Schwoerbel, 1999), but as yet it is not known whether the interstitial waters of spring tufas contain enough (poly)saccharides to sustain sizeable dark-cyanobacterial populations. Aside of the potential presence of interstitial cyanobacteria, the pore space of tufa may be colonized by light-independent, aerobic to facultatively anaerobic, heterotrophic and chemoorganotrophic bacteria. These bacteria thrive within a wide range of pH, T and oxygen, and are quite resilient against changes in these parameters (cf. Schwoerbel, 1999). Aerobic or anaerobic oxidation of organic compounds such as carbohydrates and organic acids results in release of carbon dixoide and/or of bicarbonate which, in association with expellence of calcium out of the cell, leads to precipitation.

3.3. Vadoid grainstones to rudstones

At the location Thiersee, aside of fossil phytoclastic waterfall tufas and Recent moss tufa, a type of tufa is present that to date (November 2005) was observed by us in abundance only there. This tufa consists exclusively, or nearly so, of subspherical to ellipsoidal vadoids and cyanoids a few millimeters to more than a centimeter in diameter (Pl. 4/4). The nuclei of the vadoids commonly are or were phytoclasts. The vadoid cortices typically show an inner, subspherical part and an outer layer that may abut with fitted boundaries (reminiscent of compromise boundaries within freely precipitated cement) to the adjacent vadoids (Pl. 4/5). In addition, along point contacts or along the described fitted boundaries, the vadoids are cemented by micrite and/or by finely crystalline fringes of equant calcite spar. The vadoid cortices consist of numerous, very thin laminae of micrite and/or of micropeloidal grainstone, and/or of laminae of micropeloidal grainstone or clotted lime mudstone, and/or of micro-dendrolithic to "cloudy" aggregates of micrite within a finely crystalline equant calcite cement (Pl. 4/6). Many of the piso- to macro-vadoids are aggregates built by smaller-sized vadoids of similar to identical type (Pl. 4/6). Along the surface of megapores (e. g. after tree trunks) to cavern-sized framework pores in phytoclastic tufas, the cement crusts that merge the grains together laterally coalesce, resulting in dis-

tinctly botryoidal surfaces (Pl. 4/7). The botryoids consist of numerous very thin laminae of cement, and/or of laminated micrite, and/or of micropeloidal grainstone, or of micritic micro-dendrolites embedded within finely crystalline equant calcite spar (Pl. 4/8).

Interpretation: The described coated grains are interpreted as vadoids that formed in an episodically to near-permanently turbulent vadose surface environment (cf. Flügel, 2004). Within the vadoid cortices, the inner subspherical portion records a first, mobile phase when the vadoids were still subject to episodic overturning. By contrast, the outer layers of cortices, i. e. the layers that abut the adjacent vadoids along "compromise-like" boundaries, record a subsequent immobile phase during which the grains became bound to each other. This second phase may have resulted from very shallow burial within the vadolithic sediment, in a depth no longer affected by episodic sediment reworking, or resulted from a prolonged phase of sediment immobility. Within the vadoid cortices, the diversified laminae of clotted wackestone to micropeloidal grainstone may represent microbialites. Conversely, the micrite micro-dendrolite/calcite cement fabrics and for the "cloudy" micrite patches within laminae that consist of very finely crystalline calcite spar cement, may not be of primary origin, but more probably resulted from recrystallization of the micrite. The spring tufa occurrence near Thiersee once probably was a few hundreds of meters in size at least, perhaps even more. Today, except very minor precipitation of moss tufa and of thin calcareous crusts on rock surfaces of waterfalls of local creeks, nearly no precipitation of calcium carbonate takes place. Erosional relicts of tufa still adherent to a cliff of limestones consist of tufas as described, and contain moulds of tree branches and trunks, and locally show indistinct subhorizontal bedding. Most of the tufa occurrence consists of an interval at least about 5-10 meters thick down to base of outcrop, but today is subject to erosion and is largely covered by forest. The spring tufa from this location had been quarried to build the Josefsburg, the western outlier of the fortress of Kufstein; this underscores the volume of this occurrence. The spring tufas at Thiersee perhaps accumulated from a fluvial barrage tufa system, within a lentic fluvial reach with vadolithic tufas and at least one waterfall with both phytoclastic tufas and vadolithic tufas. Today, lacustrine oncoids still form in lake Thiersee.

4. Rates of tufa formation

Experimental precipitation substrata placed at three tufa occurrences (Strassbergklamm, Lingenau, Tugstein, see Fig. 1 and Tabs. 1, 2) in spring 2005 and removed in fall 2005 indicate highly different rates of tufa formation depending on location, exposition and field type of tufa formed (e. g. moss tufa, waterfall tufa). Artificial precipitation substrata include (a) hard substrates such as flower pots of burnt clay, stones, or formatted rods of wood, and (b) soft substrata, such as a hairbrush and small paint rollers with very thin, soft hair.

In Strassbergklamm, flower pots placed within water-run tufa curtains and in water shoots immediately below the curtains showed only a thin film of calcium carbonate formed closely above the level of standing water within the pots, and closely above the impact halo of the water on the outer surface. Similarly, paint rollers were impregnated by an ocre-coloured, firm (but not hard) substance that consists only in part of micrite. Thus, in Strassbergklamm, tufa formation at present is very slow to halted.

At Lingenau, by contrast, all artifical substrata became covered by crusts of rivularian tufa up to about 8 mm in thickness during the time between 18.3.05 (placement of substrates) to 8.9.05 (removal of some substrata). The growth of the filamentous cyanobacteria probably halts somewhen in late fall and starts during spring, thus the rate of tufa formation of about 8 mm/6 months will be close to the maximum present rate of local tufa formation. This is underscored by the thickness of the laminae in the rivularian tufas, which do not exceed a thickness of about 6-8 mm.

At Tugstein, a hair brush was fixed on 18.3.2005 onto a wall of tufa thinly overrun by water. On 8.9.2005 (date of removal), the bristles (25 mm in length) of the brush were completely embedded by and overgrown by cemented, hard micropeloidal grainstone and other types of microbialites (see above). This indicates that micropeloidal grainstone may accrete, by combined baffling and precipitation, at rates of at least about 2-2.5 cm per year, provided that a suitable substrate is present.

In Vomper Loch, a low rock cliff blast in 1966 upon road cutting is covered by a spring tufa about 4 m in length and 3.8 m in height. Types of tufas include moss tufa and, subordinately, phytoclastic and cyanobacterial tufa. In May 2001, the

Location	Type of tufa	Rates of growth	Reference
Strassbergklamm	waterfall tufa	close to zero	this paper
Lingenau	cyanobacterial waterfall tufa	up to 8-10 mm/a	this paper
Tugstein	waterfall tufa (at site of artificial substrate)	micropeloidal tufa: 25 mm/a (experimentally deduced rate)	this paper
Vomper Loch	moss tufa	8.5 mm/a (maximum 35 years average of a single station) 5 mm/a (average of several stations)	this paper
England (several locations)	cyanobacterial (Nostocales) tufa built by *Rivularia haematites*	5 mm/a: summer growth rate 0.7 mm/a: winter growth rate	Pentecost (1987)
Global review of tufa locations with rate data	all types of "cool spring" tufa	1-50 mm/a, up to 52 mm/a (last figure: Drysdale & Gillieson, 1997)	Viles & Goudie (1990)
Stuttgart (Germany)	spring tufas (Pleistocene interglacial)	average rate: up to 5 mm/a	Frank et al. (2000)
Louie Creek (Australia)	fluviatile tufas	average rate: 4.15 mm/a	Drysdale & Gillieson (1997)
Two tufa creeks in Germany	fluviatile tufas	2 mm/a on artificial substrates	Merz-Preiß & Riding (1999)
Mijares gorge (Spain)	fluviatile tufas	average long-term rate: 1-5 mm/a	Pena et al. (2000)

Tab. 2: Comparison of rates of tufa precipitation

thickness of the tufa was determined at 17 sites. For the maximum thickness of 30 cm of moss tufa, with an age of 35 years of the artificial cliff, this transfers to a mean accretion rate of about 8.5 mm/a. The average thickness of sites with a cover of apparently pure moss tufa is about 18.5 centimeters, corresponding to an average rate of moss tufa formation of 5 mm/a. After excavation of the rock wall, a colonization phase of unknown duration must be assumed before moss cover and efficient precipitation started to develop. Not withstanding this uncertainty in the rate estimate, the deduced rates of moss tufa formation in Vomper Loch compare well with the rates as determined by the experimental substrata, and with short-term (years) to to long-term (hundreds to thousands of years) rates of tufa formation of other areas (see Tab. 2).

5. Discussion

Cyanobacteria are among the most significant biological inducers of calcium carbonate precipitation, but are considered as facultative calcifiers in that both external, inorganic factors and biological factors must be set to allow for precipitation (Riding, 1992; Merz-Preiß & Riding, 1999). In tufa-depositing systems, the prevalence of cyanobacteria over other photosynthetic microbes can be explained by the fact that the latter are both obligate anaerobes and most commonly depend on hydrogen sulfide which, in oxygenated freshwater, is practically absent. Moreover, cyanobacteria are best-adapted to thrive in oligotrophic waters (Schwoerbel, 1999). As mentioned, the actively forming cyanobacterial tufas are of ocre to yellow tints. By contrast, except for a single red species, uncalcified cyanobacterial accumulations show dark green to blackish-blue or brown tints (Schwoerbel, 1999). This fits with our observation that permanently or episodically wet tufa curtains that are inactive or of very low activity with respect to $CaCO_3$ precipitation are typically coated by a greenish to dark brown to blackish biomat that is only slightly calcified or uncalcified, such as in Strassbergklamm and in the inactive portions of Lingenau and Laas (see Tab. 1).

At all investigated locations, microbially-induced tufa makes up a significant to even prevalent portion of tufa volume. Equally, the tufa curtains of Lingenau, Strassbergklamm and Laas would not exist (in that style) without microbially induced precipitation. Because the crystalline microbial calcites readily "age" to more-or-less equicrystalline cementstones, the contribution of microbially-induced calcium carbonate to total tufa volume might be underestimated. The microbially-induced tufas also act as a template for further precipitation of calcite by recrystallization of microbial tufa accompanied by additional, inorganic $CaCO_3$ precipitation. The resultant final fabric may show little record of microbial induction of precipitation. At the waterfall of Lingenau, if an accretion rate of 5-10 mm/a is back-extrapolated, this implies that a tufa layer 5-10 m thick formed within only 1000 years. If the spring that nourishes present-day tufa formation at Lingenau was active at that location since about 5000 ka b. p., this would imply that a tufa 25-50 m in thickness had accreted; scattered small outcrops of subsurface rocks, however, suggest that the tufa cover is up to a few meters in thickness only. At Lingenau, the total area covered by inactive tufa is significantly larger than the presently active one, and inactive waterfall tufas are as widespread as the active one. In Strassbergklamm, as mentioned, an array of tufa curtains is present over hundreds of meters along the left flank of the gorge, yet the present rate of calcification is very low to zero. At Laas, several occurrences of inactive and of fossil tufas are present, but active tufa formation still takes place. Thus, locations with active tufa formation, locations of inactive tufa but overrun by water, and fossil "dry" tufas today all may co-exist within the same geographic area, and at the same location.

Although the data base is limited, for the tufa occurrences investigated so far, an overall correlation between total size and active/inactive ratio (in the following shortly: activity) is suggested (Tab. 1). Whereas for very small and small occurrences, their typical full activity may in part also be an artefact of distinction, the clear-cut prevalence of low and zero total activity in the moderately large and large occurrences is not. The negative relation between size and total activity perhaps reflects the perceived „late Holocene tufa decline" (Goudie et al., 1993; Ford & Pedley, 1996), and might result from three factors. (1) Moderately large and large tufa systems are produced by cumulation of small active systems in time and space, thus necessarily will be characterized by a lower total activity. In this view, small active systems comprise the „building blocks" of larger systems. Such a concept would necessitate changes, in space, of spring emergence or of levels of spring emergence. (2) The moderate to large systems result from environmental conditions no longer verified today. In this context, it is notable that most, but not all, of the tufas visited by us are associated with glacial till either in their directly underlying substrate or in the supposed recharge area of tufa-depositing waters. The glacial till probably favoured the formation of groundwater supersaturated for calcium carbonate. Our hypothesis that calcium carbonate from glacial till may nourish most of the investigated tufa occurrences is supported by cementation patterns in the Quaternary of northwestern Germany, where glacial till is the major source of calcium carbonate (Elbracht, 2002). Fine-grained glacigenic calcium carbonate is vulnerable to dissolution because particle surfaces are not coated by iron hydroxides, organic substances,

or biofilms (Elbracht, 2002; see also Fairchild et al., 1994). In addition, in glacial tills, very fine-grained carbonate particles produced by shear-induced cataclasis below glaciers may contain residual strain in their lattice. Both, the "edge effect" of very small crystallites and residual lattice strain, render such particles highly soluble (cf. Bathurst, 1975). Thus, progressive exhaustion of soluble carbonate particles from glacial tills may lead to an overall decline of tufa deposition over time. (3) The moderate- to large-sized tufa occurrences relate to former climatic conditions that, perhaps, were more wet and warmer (cf. Goudie et al., 1993). In Northwestern Europe, however, tufa-depositing systems became rapidly established early after post-glacial ice retreat, before the establishment of extensive forests (Taylor et al., 1994). For the fossil tufas at Flath-Alm and some locations near Laas (e. g. Gsalerweg), a limitation of activity to the pre-forestation interval can be excluded because these contain coarse phytoclastic tufas including calcium-carbonate metasomatized tree fragments (Ostermann et al., 2006).

There is probably no straightforward relation between climate and deposition of calcareous tufa. A comparison of the annual gauges of shedding, temperature and conductivity of 54 springs monitored by the federal hydrographic services of Austria shows that many "groundwater springs" are characterized by comparatively high *and* comparatively stable values of electrical conductivity (conductivity = rough proxy for anorganic ions in solution) (see: Quellbeobachtung im Hydrographischen Dienst in Österreich, 2005, for data and terminology of spring classification). By contrast, karst springs and talus springs show marked fluctuations in both shedding and conductivity up to more than one order of magnitude, within hours to days. For most but not all karst and talus springs, conductivity inversely correlates with shedding. For talus springs as well as for karst springs fed by shallow subsurface waters, snow melt can lead to a marked lowering of conductivity over weeks to months (cf. Quellbeobachtung im Hydrographischen Dienst in Österreich, 2005). For these latter spring types, thus, the overall lower (relative to many "groundwater springs") and fluctuating conductivity seems less favourable to mineral precipitation. For such spring types, a mere increase of shedding may do little to propel tufa precipitation. In addition, the marked and rapid changes in conductivity probably are hostile to microbes involved in induction of calcium carbonate precipitation. Conversely, for many groundwater springs, increased shedding under a more humid climate may still result in waters supersaturated enough to allow for precipitation.

The above-mentioned potential causes of the late Holocene tufa decline are not mutually exclusive, because there is more than a single way to produce as well as to quench tufa-depositing spring. One of the major obstacles to better understand the origin and environmental significance of tufa is the lack of absolute ages and the lack of precise hydrogeological information of individual tufa-depositing springs. Absolute age-dating by the Th-U method of a number of tufa occurrences will be indispensable to better understand the relation between Holocene climate and tufa formation. In the marine realm, with marked fluctuations, microbial carbonates became more rare until at present, they are nearly absent and limited to special habitats, most probably mainly as a result of a decrease in oceanic saturation state (Arp et al., 2001; Riding & Liang, 2005). Most tufa occurrences differ from common carbonate factories in that they do not have a significant source of metazoan- and/or plant-controlled calcium carbonate. Tufa-depositing systems are more similar to carbonate systems driven only by microbially induced precipitation and by physico-chemical conditions. Startling perhaps, however, is the fact that cyanobacteria and other microbes also are among the most aggressive biodegraders of buildings (Warscheid & Braams, 2000; Gaylarde & Gaylarde, 2005). Investigations into biodegradation, from a geological perspective, may help in a better understanding of the relation between microbes and carbonates.

Acknowledgements

Rudolf Pavuza (Vienna), Martin Zuschin (Vienna) and Karl Krainer (Innsbruck) are thanked for reviews. Eugen Rott (Innsbruck) is acknowledged for discussions and advice on cyanobacterial growth forms. Financial support from project "Kalktuff in Vorarlberg" supported by *inatura Erlebnisschau Dornbirn* is gratefully acknowledged. Felix Heller prepared excellent thin sections of even the most awkward microbial mats, and Monika Tessadri-Wackerle is thanked for arranging the photographs into plates.

References

Arp, G., Thiel, V., Reimer, A., Michaelis, W. & Reitner, J. (1999): Biofilm expopolymers control microbialite formation at thermal springs discharging into the alkaline Pyramid Lake, Nevada, USA. - Sediment. Geol., **126**: 159-176.

Arp, G., Reimer, A. & Reitner, J. (2001): Photosynthesis-induced biofilm calcification and calcium concentration in Phanerozoic oceans. - Science, **292** (5522): 1701-1704.

Bathurst, R. C. (1975): Carbonate sediments and their diagenesis. - Developments in Sedimentology, **12**: 1-658, (Elsevier) Amsterdam.

Camoin, G.F., Gautret, P. & et al. (1999): Nature and environmental significance of microbialites in Quaternary reefs: the Tahiti paradox. - Sediment. Geol., **60**: 15-49.

Chen, J., Zhang, D.D., Wang, S., Xiao, T. & Huang, R. (2004): Factors controlling tufa deposition in natural waters at waterfall sites. - Sediment. Geol., **166**: 353-366.

Cölfen, H. (2003): Precipitation of carbonates: recent progress in controlled production of complex shapes. - Current Opinion in Colloid and Interface Science, **8**: 23-31.

Decho, A.W., Visscher, P.T. & Reid, R.P. (2005): Production and cycling of natural microbial exopolymers (EPS) within a marine stromatolite. - Palaeogeogr., Palaeoeclimatol., Palaeoecol., **219**: 71-86.

Drysdale, R. & Gillieson, D. (1997): Micro-erosion meter measurements of travertine deposition rates: A case study from Louie Creek, northwest Queensland, Australia. - Earth Surf. Process. Landforms, 22: 1037-1051.

Elbracht, J. (2002): Karbonatische Zementation pleistozäner Lockersedimente NW-Deutschlands. – 1-214, Unpubl. Ph. D. thesis, University of Hannover.

Emeis, K.-C., Richnow, H.-H. & Kempe, S. (1987): Travertine formation in Plitvice National Park, Yugoslavia: chemical versus biological control. - Sedimentology, **34**: 595-609.

Fairchild, I.J., Bradby, L. & Spiro, B. (1994): Reactive carbonate in glacial systems: a preliminary synthesis of its creation, dissolution and reincarnation. - In: Deynoux, M., Miller, J. M. G., Domack, E. W., Eyles, N., Fairchild, I. J. & Young, G. M. (eds.): Earth's Glacial Record. - World and Regional Geol., **5**: 175-192 (Cambridge).

Flügel, E. (2004): Microfacies of carbonate rocks. - 1-976, (Springer) Berlin.

Ford, T.D. & Pedley, H. M. (1996): A review of tufa and travertine deposits of the world. - Earth-Sci. Rev., **41**: 117-175.

Frank, N., Braum, M., Hambach, U., Mangini, A. & Wagner, G. (2000): Warm period growth of travertine during the last interglaciation in Southern Germany. - Quatern. Res., **54**: 38-48, Washington.

Freytet, P. & Verrechia, E.P. (1999): Calcitic radial palisadic fabric in freshwater stromatolites: diagenetic and recrystallized feature or physicochemical sinter crust? - Sediment. Geol., **126**: 97-102.

Gaylarde, C.C. & Gaylarde, P. M. (2005): A comparative study of the major microbial biomass of biofilms on exteriors of buildings in Europe and Latin America. - International Biodeterioration and Biodegradation, **55**: 131-139.

Goudie, A.S., Viles, H.A. & Pentecost, A. (1993): The late-Holocene tufa decline in Europe. - The Holocene, **3**: 181-186.

Janssen, A., Swennen, R., Podoor, N. & Keppens, E. (1999): Biological and diagenetic influence in Recent and fossil tufa deposits from Belgium. - Sediment. Geol., **126**: 75-95.

Kano, A., Matsuoka, J., Kojo, T. & Fujii (2003): Origin of annual laminations in tufa deposits, southwest Japan. - Palaeogeogr., Palaeoclimatol., Palaeoecol., **191**: 243-262.

Lowenstam, H. A. & Weiner, S. (1989): On biomineralization. - 1-416, (Oxford University Press) New York.

Merz-Preiss, M. & Riding, R. (1999): Cyanobacterial tufa calcification in two freshwater streams: ambient environment, chemical thresholds and biological processes. - Sediment. Geol., **126**: 103-124.

Obenlüneschloß, J. (1991): Biologie und Ökologie von drei rezenten Süßwasser-Rivularien (Cyanobakterien) - Übertragbarkeit artspezifischer Verkalkungsstrukturen auf fossile Formen. - Göttinger Arb. Geol. Paläont., **50**: 1-86.

Ostermann, M., Sanders, D. & Kramers, J. (2006): Calcium-carbonate metasomatized wood and moss in Th-U age-dated spring tufas (Tyrol, Eastern Alps): significance for post-glacial re-forestation (abstr.). - European Union Geol. Sci., Vienna, in press.

Pena, J. L., Sancho, C. & Lozano, M. V. (2000): Climatic and tectonic significance of Late Pleistocene and Holocene tufa deposits in the Mijares river canyon, Eastern Iberian Range, Northeast Spain. - Earth Surf. Process. Landforms, **25**: 1403-1417.

Pentecost, A. (1987): Growth and calcification of the freshwater cyanobacterium *Rivularia haematites*. - Proc. Roy. Soc. London, ser. B., **232**: 125-136.

Quellbeobachtung im Hydrographischen Dienst in Österreich, 2005. - Mitteilungen des Hydrographischen Zentralbüros, **70**: 68 text-pp., and anonymized data appendix (no author's names given) without page

numbers. Bundesministerium für Land- und Fortwirtschaft, Umwelt und Wasserwirtschaft, Vienna.
Reid, R. P. (1987): Nonskeletal peloidal precipitates in Upper Triassic reefs, Yukon Territory (Canada). - J. Sediment. Pet., **57**: 893-900
Reitner, J. (1993): Modern cryptic microbialite/metazoan facies from Lizard Island (Great Barrier Reef, Australia). Formation and Concepts. - Facies, **29**: 3-40.
Riding, R. (1991): Calcified cyanobacteria. - In: Riding, R. (ed.), Calcareous Algae and Stromatolites, 55-87, (Springer) New York.
Riding, R. (1992): Temporal variation in calcification in marine cyanobacteria. - J. Geol. Soc. London, **149**: 979-989.
Riding, R. & Liang, L. (2005): Geobiology of carbonates: metazoan and seawater saturation state influences on secular trends during the Phanerozoic. - Palaeogeogr., Palaeoclimatol., Palaeoecol., **219**: 101-115.
Rivadeneyra, M. A., Delgado, G., Soriano, M., Ramos-Cormenzana, A., Delgado, R., 2000, Precipitation of carbonates by *Nesterenkonia halobia* in liquid media. - Chemosphere, **41**: 617-624.
Rivadeneyra, M. A., Párraga, J., Delgado, R., Ramos-Cormenzana, A. & Delgado, G. (2004): Biomineralization of carbonates by *Halobacillus trueperi* in solid and liquid media with different salinities. - FEMS Microbiology Ecology, **48**: 39-46.
Rüf, B. (2006): Typen und Bildung von Kalktuff in ausgesuchten aktiven Vorkommen Vorarlbergs (Österreich), und deren Bedeutung für historische Bauwerke. - Unpubl. M. Sc. thesis, University of Innsbruck, in prep.
Sancho, C., Pena, J. L. & Melendez, A. (1997): Controls on Holocene and present-day travertine formation in the Guadalaviar River (Iberian Chain, NE Spain). - Z. Geomorph., N. F., **41**: 289-307.
Schwoerbel, J. (1999): Einführung in die Limnologie. - 1-465, (Gustav Fischer) Stuttgart.
Taylor, D. M., Griffiths, H. I., Pedley, H. M. & Prince, I. (1994): Radiocarbon-dated Holocene pollen and ostracod sequences from barrage-dammed fluvial systems in the White Peak, Derbyshire, U.K. - The Holocene, **4**: 356-364.
Viles, H. A. & Goudie, A. S. (1990): Tufas, travertines and allied carbonate deposits. - Progress Phys. Geogr., **14**: 19-41.
Warscheid, Th. & Braams, J. (2000): Biodeterioration of stone: a review. - International Biodeterioration & Biodegradation, **46**: 343-368.

Plate 1

1: Tufa curtains along and below the emergence of a spring line (Strassberg gorge, Tyrol). The rock substrate is Hauptdolomit. Width of view about 6 meters.
2: Ocre-coloured aragonitic waterfall tufa in active formation (Laas, Southern Tyrol). The darker grey (brown in the field) patches represent coarsely-crystalline botryoidal aragonite; this type of aragonite forms mainly at locations of water impact and along steep to vertical runs with shooting water flow. Width of view about 1 metre.
3: Overhanging tufa curtain (Lingenau, Vorarlberg). This curtain consists of tufa as shown in the next thin section photograph. Height of view about 1 m.
4: Thin section of tufa curtain shown in Pl. 1/3. The tufa consists of laminae each a few millimeters thick of „bushy" calcite that are vertically separated by thin, intercalated laminae of micrite and/or microsparite. Width of view 17 mm.
5: As preceeding photo, but with crossed polars. Individual tufa laminae consist of arrays of elongate-"bushy" calcite crystals that branch towards the upper surface of the tufa carbonate. The "bushy" calcite arrays internally consist of patches of calcite with uniform optical orientation. The laminae of bushy calcite are vertically separated by laminae of micrite to microsparite. Note that each array of calcite "bushes" starts from the intercalated, very thin micrite-microsparite laminae, and branches upward. Width of view 17 mm.
6: Laminated tufa from a tufa curtain overrun by a sheet of water with shooting flow (Lingenau, Vorarlberg). Detail of a tufa lamina that consists of an array of "bushy" calcite aggregates. Section is slightly oblique to the lamination. Note that the optically uniform calcite crystals are slightly curved, and that they are centered by an elongate "channel". Petrographic thin section, crossed polars. Width of view 3.2 mm.
7: Laminated tufa from a tufa curtain overrun by a sheet of water with shooting flow (Lingenau, Vorarlberg). Detail of a tufa lamina that consists of an array of "bushy" calcite aggregates. Section is subparallel to the lamination. Note that each of the thin calcite tubes is centered by a subcircular hollow space. Petrographic thin section, crossed polars. Width of view 4.2 mm.
8: SEM image of calcite crust on a phytoclast (Ludesch, Vorarlberg). The calcite consists of numerous narrow tubes that locally appear to branch or to „bud" onto each other. Elongate forms are diatomeans.

Plate 1

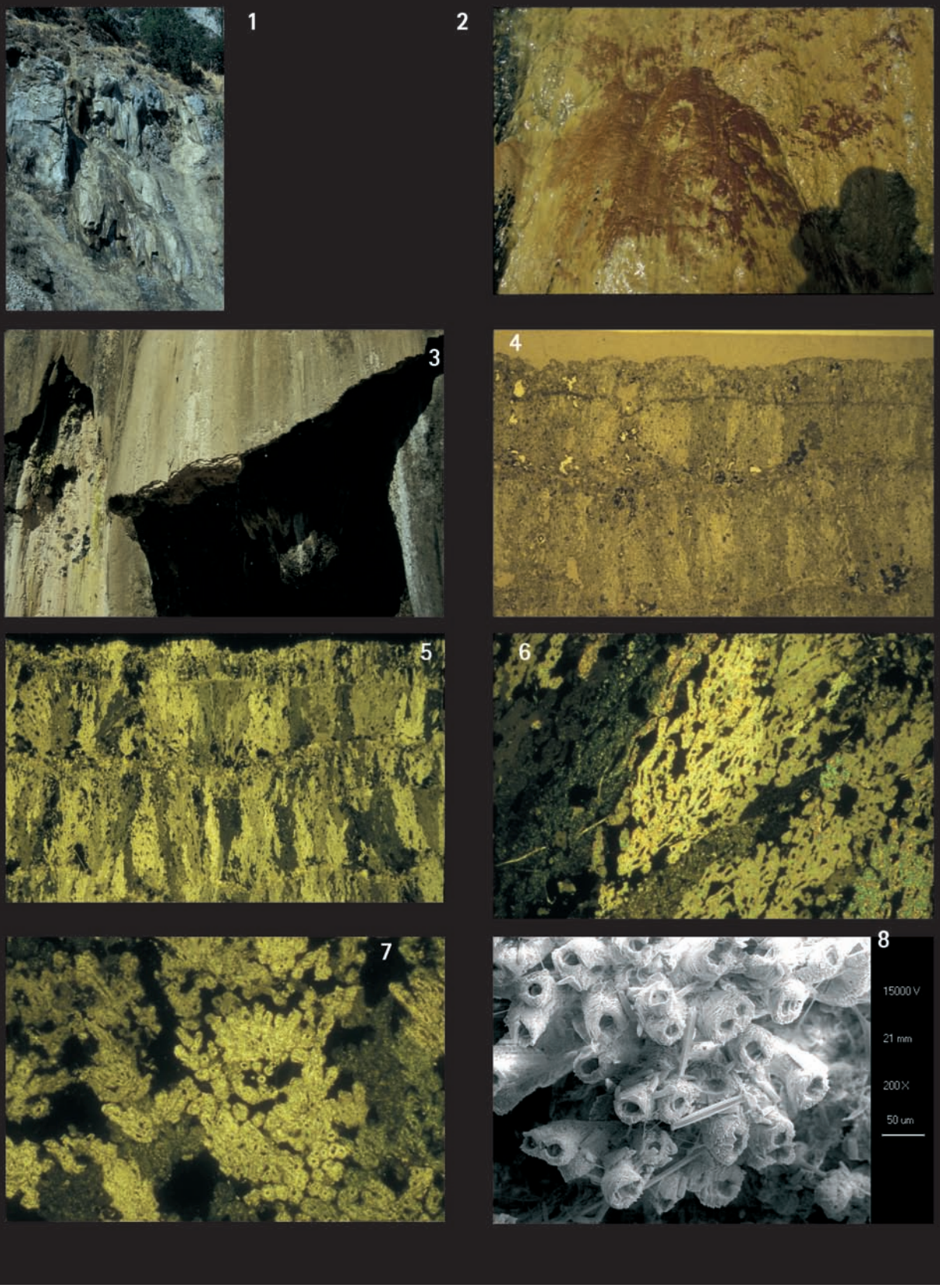

Plate 2

1: SEM image of calcite crust on a leave (Lingenau, Vorarlberg). The calcite consists of numerous tiny tubes that, on their outer surface, show the characteristic surface steps according to the rhombohaidral shape of crystalline calcite. The inner surface of the tubes is relatively rough and does not show crystal surfaces.
2: SEM image. Detail of calcite tubes as shown in Pl. 2/1. The inner surface of the tube does not show crystal surfaces, but is relatively irregular and rough. The outer surface shows numerous, tiny steps according to the symmetry of calcite. The steps, however, disappear towards the debouch of the tube, where the calcite surface appears completely smooth and nearly perfectly circular. The entire structure seems to be built by subcircular, stacked lamellar units of subcircular calcite rings less than 1 micron in thickness.
3: Laminated tufa of tufa curtain (Lingenau, Vorarlberg). The tufa was excavated with a chisel on 18.3.2005, and resampled on 8.9.2005 (nearly six months later). The truncated older laminae of "bushy" calcite became unconformably overlain by a lamina of "bushy" calcite that precipitated during nearly six months. Petrographic thin section, crossed polars. Width of view 17 mm.
4: Detail of previous photograph. Note that the newly-grown (=18.3. - 8.9.2005) lamina of "bushy" calcite is not underlain by a lamina of micrite to microsparite. Petrographic thin section, crossed polars. Width of view 6.5 mm.
5: "Big brother is watching you": Phytoclastic tufa (Lingenau, Vorarlberg). Cross-section through two twigs, overgrown by calcitic tufa as also illustrated in Plate 1. Note, within the calcite crystals, the thin elongate grey traces. Cross polars. Width of view 17 mm.
6: Detail of tufa creek (Lingenau, Vorarlberg) paved by inactive, dry "mini-rimstones", i. e. by a grey calcium carbonate crust with numerous elevated rims oriented subperpendicular to water flow. One-cent coin for scale.
7: Actively forming "mini-rimstone" (Lingenau, Vorarlberg), i. e. by a yellow calcium carbonate crust with numerous rims oriented subperpendicular to water flow. In thin section, these mini-rimstones consist of the same calcite than illustrated in plate 1. Five-cent coin for scale.
8: Cross-section of "mini-rim" from a mini-rimstone as shown in previous photograph. Width of view 3.2 mm.

Plate 2

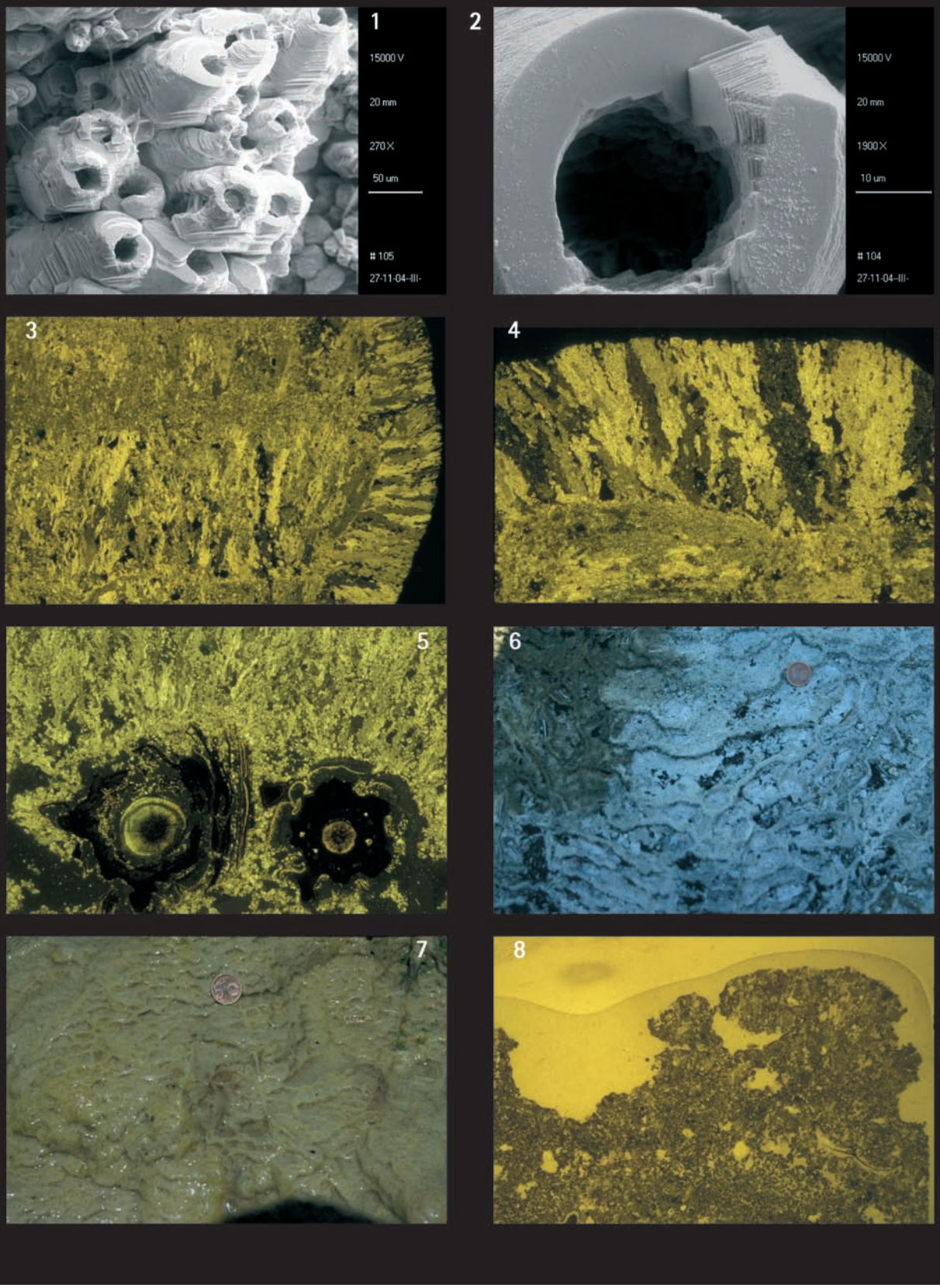
1
15000 V
20 mm
270 X
50 um
105
27-11-04-III-
2
15000 V
20 mm
1900 X
10 um
104
27-11-04-III-
3
4
5
6
7
8

Plate 3

1: Carbonate crust on permanently wet, well-lit, but not intensely water-run location (Lingenau, Vorarlberg). The crust shows a pustular to mammillated to "meandroid" surface. Such crusts, albeit in most cases not very conspicuous, are common in many of the investigated spring tufa occurrences. Width of view about 20 cm.
2: Lithoclasts coated by crust of dense, light-ocre calcium carbonate (Andelsbuch, Vorarlberg). In thin section, the crust shows as well-preserved "*Rivularia*". Clast is about 10 cm in size.
3: Tufa intraclast, coated by mammillary crust of ocre-coloured calcium carbonate (Andelsbuch, Vorarlberg). Such encrusted clasts (tufa intraclasts, lithoclasts, phytoclasts) locally are common. Width of view about 15 cm.
4: Section through carbonate crust on lithoclast (Andelsbuch, Vorarlberg). Note the outward-fanning appearance of the carbonate. Width of view 5.3 mm.
5: Same as Pl. 3/4, but with crossed polars. Note the outward fanning of calcite crystals of discrete optical orientation, and the indistinct lamination subparallel to upper surface of the crust. Width of view 5.3 mm.
6: Thin section through the crust shown in Pl. 3/1. Crossed polars. The crust consists of patches of outward fanning calcite crystals that are arranged into patches each of distinct optic orientation. Width of view 12 mm.
7: Micropeloidal grainstone from an occurrence of moss tufa (Alpenzoo, Tyrol). Width of view 8.5 mm.
8: Thin section of a white, mammillary crust a few centimeters thick (field appearance) (Andelsbuch, Vorarlberg) that consists of micropeloidal grainstone, with the micropeloids arranged in "string fabrics". This crust has been found at the floor of a low-lit location of a short cave excavated by man, in the course of a very small "creeklet" along the floor. Width of view 6.5 mm.

Plate 3

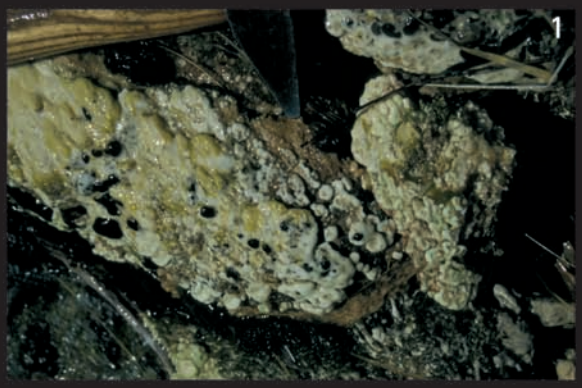

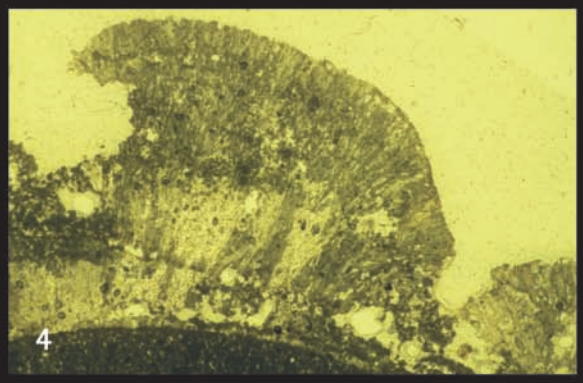

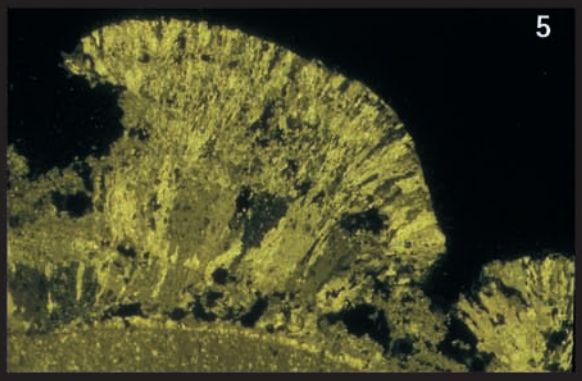

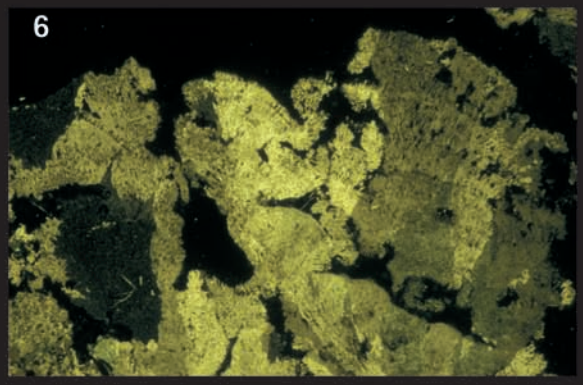

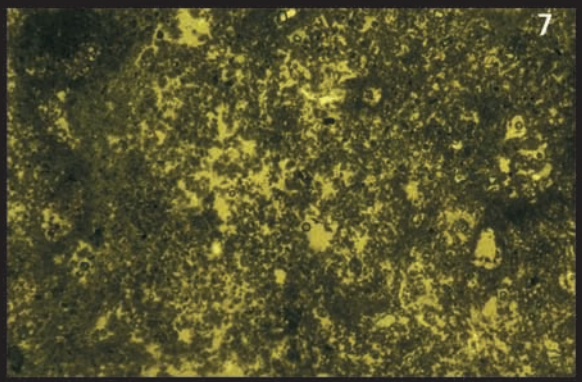

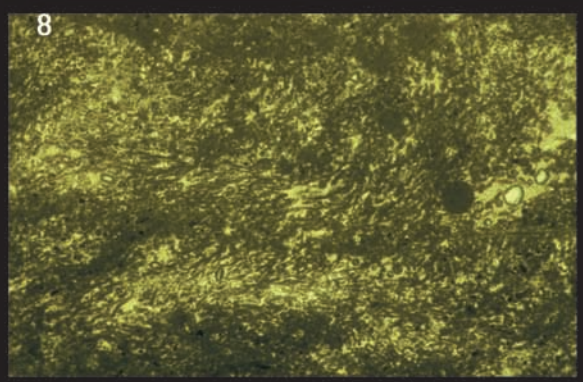

Plate 4

1: Detail of a tufa from a moderately lit location below a natural overhang (Andelsbuch, Vorarlberg). This tufa consists of tangled, very small-sized tubes encrusted along their extent by micrite. Crossed polars. Width of view 6.5 mm.
2: Wooden brush (turned outside from the vertical tufa wall to take the photograph) with bristles clogged by an indurated mass of micritic calcium carbonate (Tugstein, Vorarlberg). The brush was placed on 18.3.2005, and was removed on 8.9.2005, i. e. nearly six months later.
3: Thin section of the calcium carbonate within the bristles of the brush shown in Pl. 4/2. The bristles are clogged by a micropeloidal grainstone relatively rich in small-sized phytoclasts, and with open fenestrae. At the top of the grainstone, a lamina to microdendrolithic overgrowth of micropeloidal to micritic calcium carbonate had formed. Width of view 17 mm.
4: Micro- to piso-oncolite consisting of coated grains built by laminae that consist of micrite and/or of micropeloidal grainstone to micro-dendrolithic grainstone (Thiersee, Tyrol). The oncoids are cemented to each other. Crossed polars. Width of view 17 mm.
5: Fine-grained vadoid rudstone (Thiersee, Tyrol). Note that the vadoids show an inner cortex fringed by more or less dense micrite, and an outer cortex of porous micrite. The outer cortices of the vadoids abut each other along boundaries broadly reminiscent of compromise boundaries of cement crystals. The vadoids are locally cemented to each other by the porous micrite. Width of view 8.5 mm.
6: Macro-oncoid composed of laminae of micrite to micropeloidal grainstone, within oncolite composed mainly of piso-oncoids (Thiersee, Tyrol). Note that the oncoids are cemented to each other. Width of view 17 mm.
7: Botryoidal surface of tufa that consists of calcium carbonate as illustrated in Pls. 4/4, 4/6. Note the cracks both within and between individual botryoids. Two-cent coin for scale.
8: Micro-dendrolithic micrite, separated by patches and layers of finely crystalline cement. Locally, the micro-dendrolithic micrite shows faint subparallel lamination. Crossed polars. Width of view 6.5 mm.

Plate 4

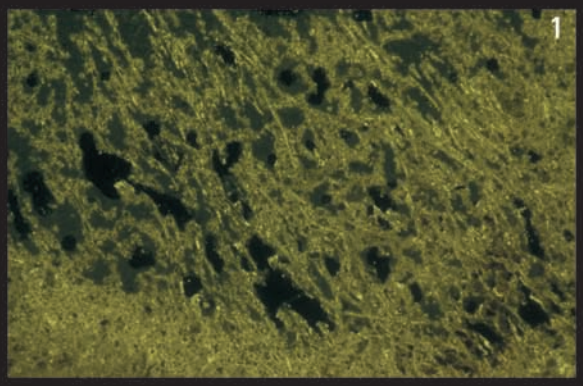

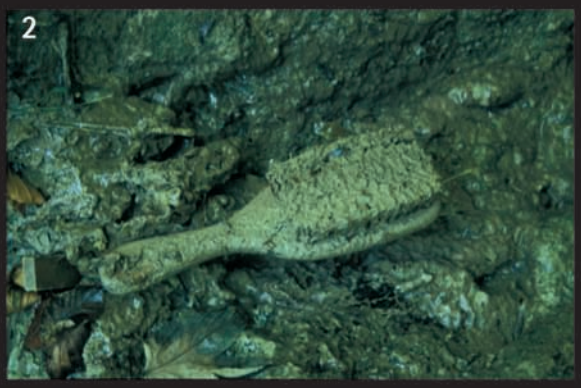

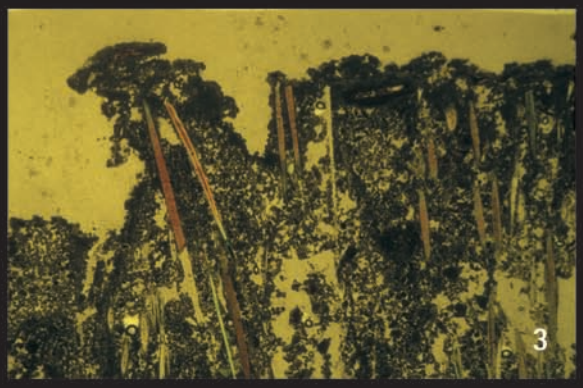

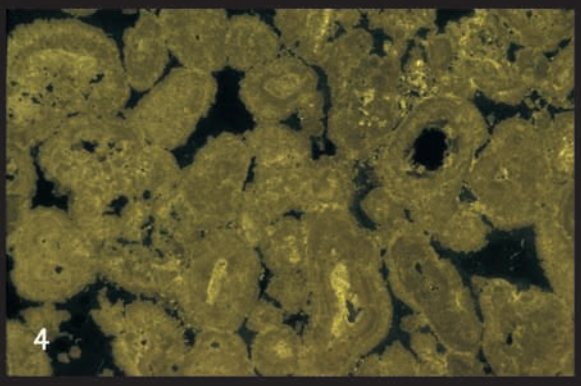

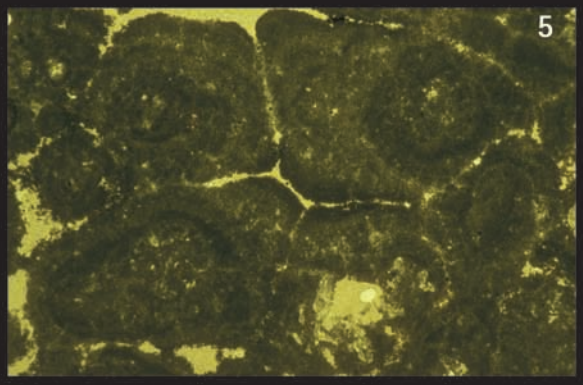

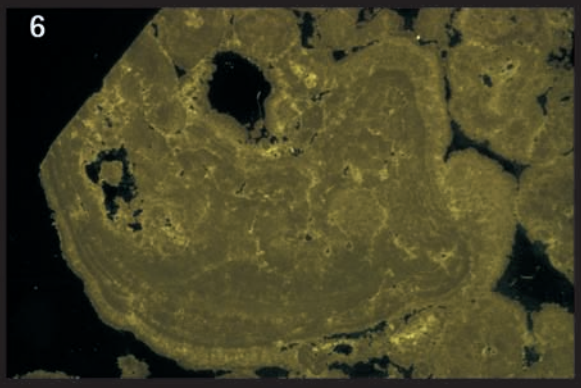

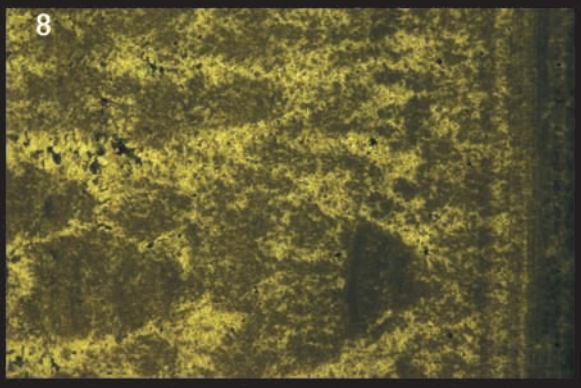

Geo.Alp, Vol. 3, S. 191–206, 2006

NUTRIENT MODELS FOR THE DEVELOPMENT AND LOCATION OF ANCIENT REEFS

Robert J. Stanton Jr.

With 5 figures and 1 table

Department of Invertebrate Paleontology, Natural History Museum of Los Angeles County,
900 Exposition Boulevard, Los Angeles CA 90007, USA

Abstract

The primary function of reef builders, from a geological perspective, is the in situ production of carbonate sediment at a relatively high rate to create a biogenic carbonate body with relief above the sea floor. Reef-building metazoans fall into two broad categories based on the mechanism by which they produce skeletal carbonate — those with primary (autotrophic or photosymbiotic) production through the aid of photosynthetic algae or bacteria, and those with secondary (heterotrophic) production. In modern reefs, carbonate production by photosymbiotic organisms is strongly correlated with low-nutrient, oligotrophic settings and efficient metabolism, whereas carbonate production by heterotrophic reef builders depends on high concentrations of organic nutrients.

Photosymbiotic reef builders are largely responsible for the construction of modern tropical shallow-water reefs, and this appears to have been the case back into the Mesozoic. This conclusion is based on the geologic range of scleractinian corals, the dominant constructors of modern shallow–water reefs. However, the existence of photosymbiotic reef builders in the geologic record cannot otherwise be definitively established. Heterotrophs are responsible for modern deep- and cold-water reefs as well as contributing to the growth of shallow-water reefs. In the absence of firm evidence for photosymbiotic carbonate producers in the geologic record, they are postulated to have been the dominant carbonate-producing metazoans responsible for ancient reefs as well.

In addition to metazoans, photoautotrophs (algae and bacteria growing independently of a metazoan host) were also major carbonate contributors to ancient reefs and mounds. Because carbonate production by both photoautotrophs and heterotrophs depends on nutrient supply rather than the oligotrophic conditions optimal for modern photosymbionts, explanations for the sites and characteristics of ancient reefs must focus on the phenomena and settings that result in sources of abundant nutrients at the geographic scale of reef growth. These nutrient sources consist of localized terrestrial influx, cold seeps, endo-upwelling, and the oceanographic phenomena of upwelling, oxygen minimum zones, and internal waves. Analysis of ancient reefs in terms of nutrient source provides the opportunity, through an alternative paradigm than that provided by modern shallow-water reefs, to understand fundamental controls on growth and distribution of reefs in the geologic record.

Introduction

Modern shallow-water reefs have historically provided the paradigm for the study of ancient reefs. Recognition of ancient reefs was initially through comparison of their external geometry with that of modern reefs; subsequent analysis included comparisons of lithofacies and biofacies. The explication of the ecologic reef by Lowenstam (1950) strongly incorporated in reef study the role of the organisms as members of a distinctive reef community producing in situ carbonate sediment and forming a rigid wave-resistant skeletal framework. Although the incorporation of ecologic fac-

tors was an important step forward in reef analysis, it introduced the problem that modern deep- and cool-water reefs, as well as many ancient reefs (including mud mounds) appeared to lack a skeletal framework and wave-resistance, and thus did not fit the ecologic-reef definition that had been derived from modern reefs. This limiting effect of a strict uniformitarian application of the ecologic reef definition has been circumvented by emphasizing in situ biogenic carbonate production and deemphasizing skeletal frame and wave resistance, as for the example in the definition of reefs "...as laterally confined biogenic structures, developed by the growth or activity of sessile benthic organisms and exhibiting topographic relief and (inferred) rigidity." (Flügel and Kiessling 2002, p. 3). This shifts the focus to the environmental conditions conducive for inordinately high, localized carbonate production, and to the physical processes of its accumulation, destruction and transportation that created a reef's distinctive external form and internal facies pattern (Stanton, 1967).

Numerous factors have been discussed as being important in determining the geologic history of reefs; these include seafloor topography (Wright, 1994), nutrients and productivity (Allmon and Ross, 2001; Bambach, 1993; Hüneke, et al., 2001; Wood, 1993; Wright, 1994), and the biota (Fagerstrom, 1987). These are well summarized by Kiessling (2002). Settings typical of abundant carbonate production and accumulation — 'carbonate factories' — have been described by Schlager (2003). The objective of this paper, in contrast, is to focus on the environmental factors important to heterotrophs and photoautotrophs because of their postulated dominant role in the formation of ancient reefs. Because reefs are sites of high rates of carbonate production, the most important factors are those that controlled nutrient supply.

Major carbonate producers in modern low-latitude shallow-water reefs are photoautotrophs (algae and bacteria) and photosymbiotic metazoans, most important of which are corals containing zooxanthellae, but also including sponges, mollusks and other organisms. For the host organism, photosymbiosis typically results in rapid growth, large size, and a high rate of skeletal calcification. It is most effective in oligotrophic settings because if nutrients are abundant, phytoplankton production reduces water clarity and thus photosynthesis for the zooxanthellae, organisms of the destroyer guild are more effective in removing carbonate skeletal sediment, and filamentous cyanophytes and macrophytes out-compete the photosymbiont macro-invertebrates for space (Hallock, 2001).

Historically, the photosymbiont paradigm has been the model used in the interpretation of ancient reefs. The alternative, heterotroph paradigm, that carbonate production depends on abundant nutrients to nourish heterotrophic and photoautotrophic organisms, has been applied increasingly to ancient reefs because unequivocal evidence of photosymbiotic organisms is lacking for much of the Phanerozoic. Recognition of the appropriate paradigm is important in the study of ancient reefs because the different paradigms lead to divergent explanations for the setting and pattern of reef growth.

The Phanerozoic record of photosymbiosis

The appropriate paradigm for the study of ancient reefs depends on the ability to determine whether photosymbiosis was present in the geologic record and was an important factor in reef growth. This question of photosymbiosis in earth history has received considerable attention (e.g. Wood, 1993, 1999; Kiessling, 2002). Because the photosynthesizing guest lived within the soft tissue of the host organism, photosymbiosis can not be directly observed in fossils. Consequently, criteria based on secondary attributes of modern photosymbionts have been proposed. These include:

1 Rapid growth is typical of modern photosymbionts. This is generally true, but growth rate is generally unknown for fossils. Consequently, large size is commonly used as a surrogate criterion. This, also is generally true, but is also of limited value because size is correlated with age, which, again, is generally unknown for fossils. Furthermore, because not all modern photosymbionts are large, as exemplified by numerous scleractinian corals and by the mollusk *Fragum*, assumption of photosymbiosis from growth rate or size yields a possible rather than definitive answer for fossils.
2 In general, photosymbionts have life habits by which they maximize the solar-energy uptake for the benefit of the symbiotic algae or bacteria. This is reflected in their habitat preference and morphology, but these characteristics provide only probable interpretations for fossils. Modern zoox-

anthellate corals, for example, all live within the photic zone, but not all corals within the photic zone are zooxanthellate. Among bivalves, the zooxanthellate *Tridacna* fits the photosymbiotic model by being large, living in very shallow water, and having a distinctive epifaunal, gaping posture so the zooxanthellae within the mantle will obtain the maximum sunlight. In contrast, however, the zooxanthellate *Fragum*, is small and infaunal (Ohno et al., 1995). Size and life habit are poor criteria for recognizing zooxanthellate fossil corals or clams. Wood (2000) has reached a similar conclusion with regard to Devonian stromatoporoids.

3 Growth forms and corallite structures present in modern corals are correlated with photosymbiosis (Coates and Jackson, 1987). In the faunas they analyzed, the full range of growth forms is present in both zooxanthellate and azooxanthellate corals, but zooxanthellate corals tend to be multiserial whereas azooxanthellate corals are predominantly solitary or pseudo-colonial. Although the range of corallite diameter in each group is comparable, corallites in zooxanthellate corals tend to be much smaller than in azooxanthellate corals. Corallite integration ranges from high to low in both groups, but tends to be much higher in zooxanthellate corals. These group tendencies can be used to infer whether an assemblage might have included photosymbiotic species, but not to infer beyond a probability as to whether a particular fossil species in the assemblage was a photosymbiont. Further, because these tendencies are also correlated with type and rate of sediment input (Sanders and Baron-Szabo, 2005), they can not be interpreted uniquely in terms of photosymbiosis.

4 Skeletal geochemistry, particularly isotope composition, may provide valuable criteria to distinguish zooxanthellate and azooxanthellate corals. The most thorough evaluation of the use of carbon and oxygen isotopes for this purpose has been that of Stanley and Swart (1995). In their study, modern azooxanthellate corals ..."always show a strong positive correlation between the $\delta^{13}C$ and $\delta^{18}O$ isotopes in their skeletons". This is the case, however, for only 4 of the 7 species they document. They also conclude that "In contrast, within individual zooxanthellate corals there is usually no strong correlation between these isotopes". However, they use only a small part of the total isotopic range for zooxanthellate corals in arriving at this conclusion. With these criteria, they concluded that the 13 Late Triassic coral species they studied were zooxanthellate (they questioned whether the correlation between the isotopes in two of the species was weak, but if uniform scales are used for their isotope plots this uncertainty is not visually apparent).

An essential requirement in such a study is that diagenesis had not altered the isotopic composition of the fossils. Although their careful analytical procedures and thorough discussion of the effects that diagenesis might have had support their conclusions and the potential value of isotopes in recognizing photosymbiosis in fossil corals, diagenetic alteration of their samples is nevertheless probable for a number of reasons, even though they could not detect it: 1) Seasonal isotopic variations are absent in the specimens. These should have been present if the corals had lived within the photic zone and were dependent for sunlight on their growth. Thus it appears that diagenesis had obliterated the original seasonally variable, isotopic signal. 2) The species analyzed cover the full morphologic range from solitary to multi-serial. That all would be zooxanthellate is contrary to the guidelines of Coates and Jackson (1987) that relate morphologic characteristics of a coral to the probability of its being zooxanthellate. 3) The species that Stanley and Swart (1995) postulated to be zooxanthellate are from very early in the history of scleractinian corals and are from diverse scleractinian taxa. In contrast, it is estimated that the percentage that were photosymbiotic increased during the evolutionary history of scleractinians, but was only about 25% in the Late Triassic (Kiessling, 2002). The high percentage for the samples of Stanley and Swart (1995) again suggests a ubiquitous diagenetic alteration. The existence of zooxanthellate corals in the Late Triassic is possible, but it is not established by isotopic criteria in this study, nor is it by the criteria of size and life habit that Stanley (1981) had postulated earlier (Wood, 1999).

Lacking definitive skeletal criteria by which to recognize photosymbiont fossils, a strictly uniformitarian argument has been that because high carbonate production in modern reefs is due to photosymbiosis in a wide range of organisms, and high carbonate production was responsible for fossil reefs, photosymbiosis therefore must also have been present in ancient as in modern reefs (Cowen, 1988; Talent, 1988). The present consensus, howev-

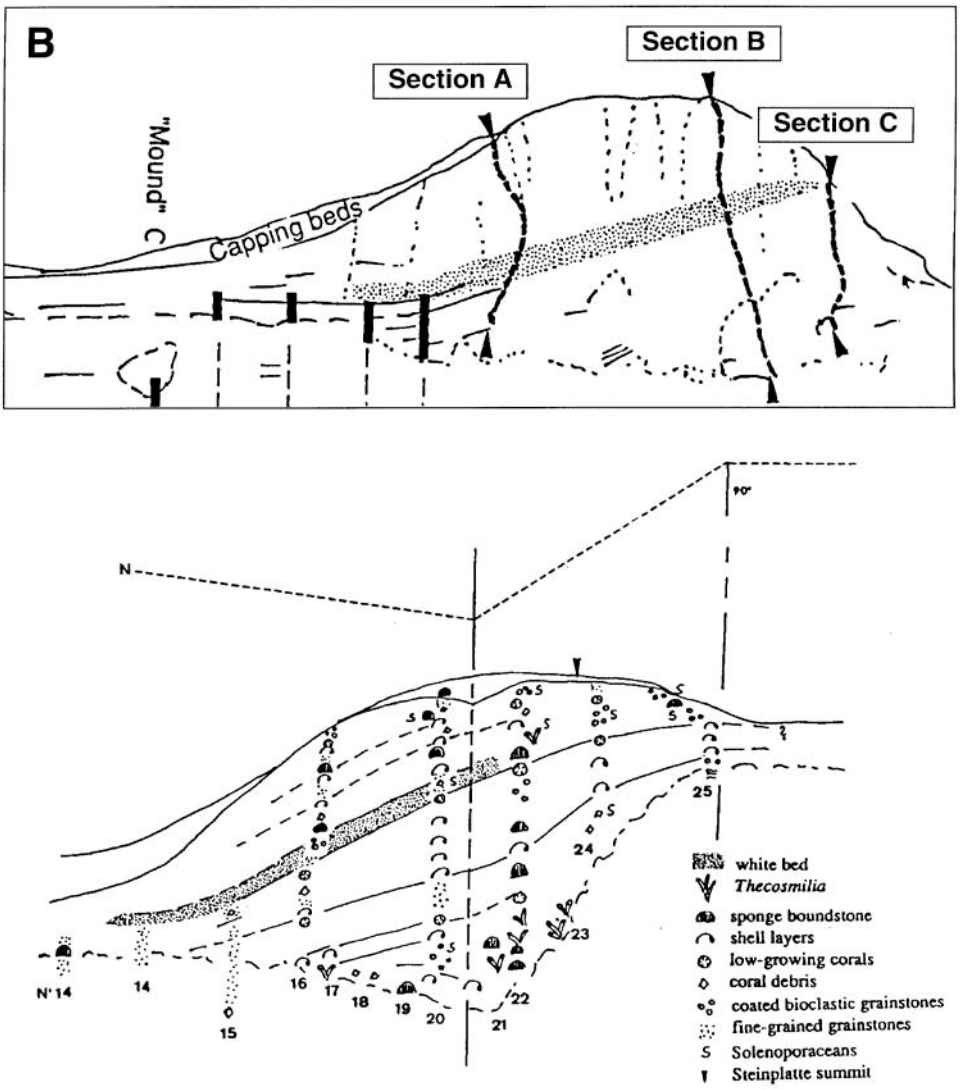

Fig. 1: Biotic content of. A. Profile at the Steinplatte as exposed on outcrop showing the platform-edge transitions: 1) from ramp (right) at about Section B to the distal steepened ramp slope, and 2) from the distal steepened ramp slope to basin floor (left) at about location of Mound C. B. Dominant biota in this platform edge: Note prevalence of shell layers. Dashed line indicates changes in orientation of the outcrop. From Flügel and Koch, 1995.

er, is that although photosymbiosis may reasonably be inferred for scleractinian corals back into the Jurassic (Leinfelder, 2001), it was not an important factor in reef growth until the Cenozoic (Kiessling, 2002). For much of the Phanerozoic, the photosymbiotic paradigm can not be proven, and appears to be unlikely. Consequently, the alternative heterotrophic paradigm focussing on localized nutrient supply should be utilized to explain and predict reefs in the geologic record.

Triassic examples of the heterotrophic paradigm

The validity of the heterotrophic paradigm for ancient reefs has been increasingly recognized (e.g. Dupraz and Strasser, 2002). Two Triassic examples from the Alps are presented here. One is the distally steepened ramp that formed the platform-margin at the Steinplatte (Fig. 1A; Piller, 1981; Stanton and Flügel, 1989, 1995; Flügel and Koch, 1995). Here, the colonial scleractinian coral *Retiophyllia* would

appear to be the dominant reef constructor (Piller, 1981). It forms patches in four settings: a) on the outer ramp surface, b) at the slope break from ramp to distally steepened ramp, at an estimated depth of 70-140 m, c) on the distal ramp slope, and d) at the base of the prograding carbonate ramp in what must have been a water depth approximately 100 m deeper than at the slope break, e.g., 170 to 240 m (Stanton and Flügel, 1995). Although some *Retiophyllia* colonies grew to a height of at least 3 m, it is unlikely that they were zooxanthellate: 1) because their depth range extended to below the base of the photic zone, and 2) because morphologic differences that would be expected across this depth range if they had been zooxanthellate (e.g. Chappell, 1980) are absent. In any case, corals were minor contributors to the Steinplatte carbonate mass both as colonies and as sediment grains. Instead, bivalves, microfossils and sponges the were major sediment contributors (Fig. 1B; Stanton and Flügel, 1989; Flügel and Koch, 1995). Thus, carbonate production depended primarily on heterotrophic organisms, and by inference on abundant nutrients. Coral colonies are minor contributors to other Triassic reefs, as well, as has been described, for example, at Hohe Göll by Zankl (1969) and at Rötelwand by Schäfer (1979). In these examples, coral patches make up perhaps 10% of the mass of reef. It has commonly been assumed that these coral thickets or Riffknospen were point sources of skeletal sediment for the adjacent sea floor, and thus corals were probably much more abundant than is apparent from the abundance of intact colonies in the scattered patches (Zankl, 1969). This was not the case at the Steinplatte, as noted above, and was probably not the case in general because of the relative resistance of the coral skeleton to attrition (Ginsburg, 1956).

Coquinas consisting predominantly of shells of pteriid bivalves form the upper Norian platform-edge in the Julian Alps (Fig. 2; Schlaf et al., 1999). The platform edge was the primary site of mollusk production, with bivalve-rich packstone lower on the slope derived in large part by down-slope transport. Although the coral *Retiophyllia* is a major component of framestone patches scattered on the upper surface of the platform margin, pteriid bivalves are also abundant in these patches. Recognizing that the platform edge is primarily the result of carbonate production by heterotrophs, Schlaf et al. (1999) invokes the heterotrophic paradigm and attributes the dominance of the bivalves and the resultant carbonate production to high nutrient supply. This platform margin, as well as other similar Triassic platform margins, including that at the Steinplatte, border intraplatform basins. Black shale in all these basins is indicative of basin-floor anoxia and high rates of organic-carbon accumulation, suggesting high nutrient concentrations as a general feature associated with the growth of all these reefs.

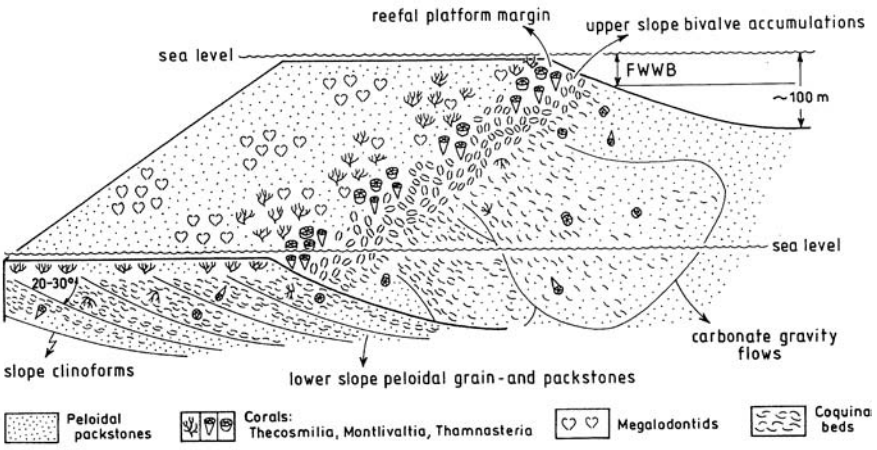

Fig. 2: Upper Norian platform edge, Julian Alps. From Schlaf et al., 1999.

Nutrient sources

Four types of localized nutrient sources are most useful as a framework for analyzing ancient reefs in terms of the heterotrophic paradigm (Table 1).

Table 1. Nutrient sources for heterotrophic reef growth

Terrestrial input
Cold seeps
Endo-upwelling
Oceanographic phenomena
Upwelling
Oxygen minimum zones
Internal waves

1. Terrestrial input. Organic matter in the oceans is ultimately derived from land. Indicative of this is: 1) some 80% of organic carbon buried in marine sediments is of terrestrial origin (Hay, 1995); and 2) carbon influx from oceanic islands in the southwest Pacific, which contribute perhaps as much as one-third of the particulate organic carbon entering the world oceans, is directly correlated with river runoff (Lyons et al. 2002).

It is difficult to link, however, the input of terrestrial particulate and dissolved organic nutrients to carbonate production because of their riverine origin. One reason is that the oceans off river mouths are characterized by low carbonate accumulation because the associated low salinity and high turbidity are generally inimical to carbonate-producing organisms. Another reason is that because of the high fluvial sediment influx, what skeletal carbonate is produced makes up a minor part of the total sediment budget. On the other hand, scleractinian corals and coral buildups are common within terrigenous to marl sediments in the geologic record and the environmental range of scleractinian corals terms of sediment parameters has expanded during the Mesozoic and Cenozoic (Sanders and Baron-Szabo, 2005). Corals adapted to higher levels of turbidity, sediment influx, and nutrient supply than are characteristic of the stereotypical shallow, clear-water and oligotrophic settings of modern reefs. Terrestrial nutrient supply and associated sediment influs are more important factors for scleractinian corals than the photosymbiotic/oligotrophic paradigm would suggest. The example of Jurassic corals flourishing in areas of terrigenous sedimentation also indicates that potential deleterious clastic sedimentation is counterbalanced by increased nutrient availability (Leinfelder, 2001).

Control of reef growth by terrestrial nutrient supply has been used to explain biotic changes in Devonian reefs in the Western Canada Sedimentary Basin (Eliuk, 1988). Tabulate corals and stromatoporoids were the dominant reef-building skeletal macro-organisms whereas megalodont bivalves, of lesser abundance, were important components of younger, reef-capping and fore-reef-slope strata. Eliuk (1988) proposed that as a terrestrial flora developed during the Devonian on the shelf, soil formation increased and both sediment and organic matter were washed from the shelf into the basin. He explained the decrease in abundance of corals and stromatoporoids by both the increasing turbidity and by nutrient poisoning (this assumes that they were photosymbiotic, and does not take into account the adaptability of both tabulate corals and stromatoporoids to sediment influx as described by Sanders and Baron-Szabo (2005) for scleractinian corals). The contemporaneous increase in heterotrophic megalodonts is explained by the increasing nutrients. It is noteworthy that the Devonian reefs, like the previously described Triassic reefs, bordered on an intra-platform basin containing abundant black shale indicative of high nutrient input.

2. Cold seeps. Venting of hydrocarbons occurs at numerous localities on the modern sea floor and may result in carbonate masses that fall within the size range of reefs. On convergent plate margins, compaction of unconsolidated sediment and migration of interstitial water and hydrocarbons along faults or mud diapirs (Orange et al., 1999) is due to tectonic deformation and compactional loading. On passive plate margins, venting occurs along faults above salt domes. Hydrocarbons may also seep along permeable strata from underlying petroleum reservoirs, as in the North Sea (Hovland et al., 1998).

Both methane and hydrogen sulfide are used for carbonate production at modern seeps and to support a wide diversity of chemoautotrophic organisms (Sibuet and Olu-Le Roy, 2002). In the Gulf of Mexico, for example, symbiotic bacteria in chemoautotrophic lucinid and mytilid bivalves use exclusively either methane or hydrogen sulfide. In addition to skeletal carbonate, bacterially precipitated interstitial carbonate cement is a significant component of the carbonate accumulation at cold seeps. These carbonate bodies have discrete distribution patterns that are determined by the conduits along which the hydrocarbons flow. In the northern Gulf of Mexico, they occur in linear belts along fault traces overlying salt domes. Although seepage has been active since at least the Late Pleistocene (Aharon et al., 1997), the duration of an individual seep is generally less than a few hundred years because movement on the faults appears to turn the hydrocarbon flow on and off (Callender and Powell, 2000).

Carbonate mounds formed by the azooxanthellate coral *Lophelia* occur in the North Sea and north-east Atlantic and have lateral dimensions of up to 1 by 5 km and relief above the sea floor of as much as 100m (Freiwald, 2002). Upward growth of the mounds is as much as 2 cm/yr. (Freiwald et al.,

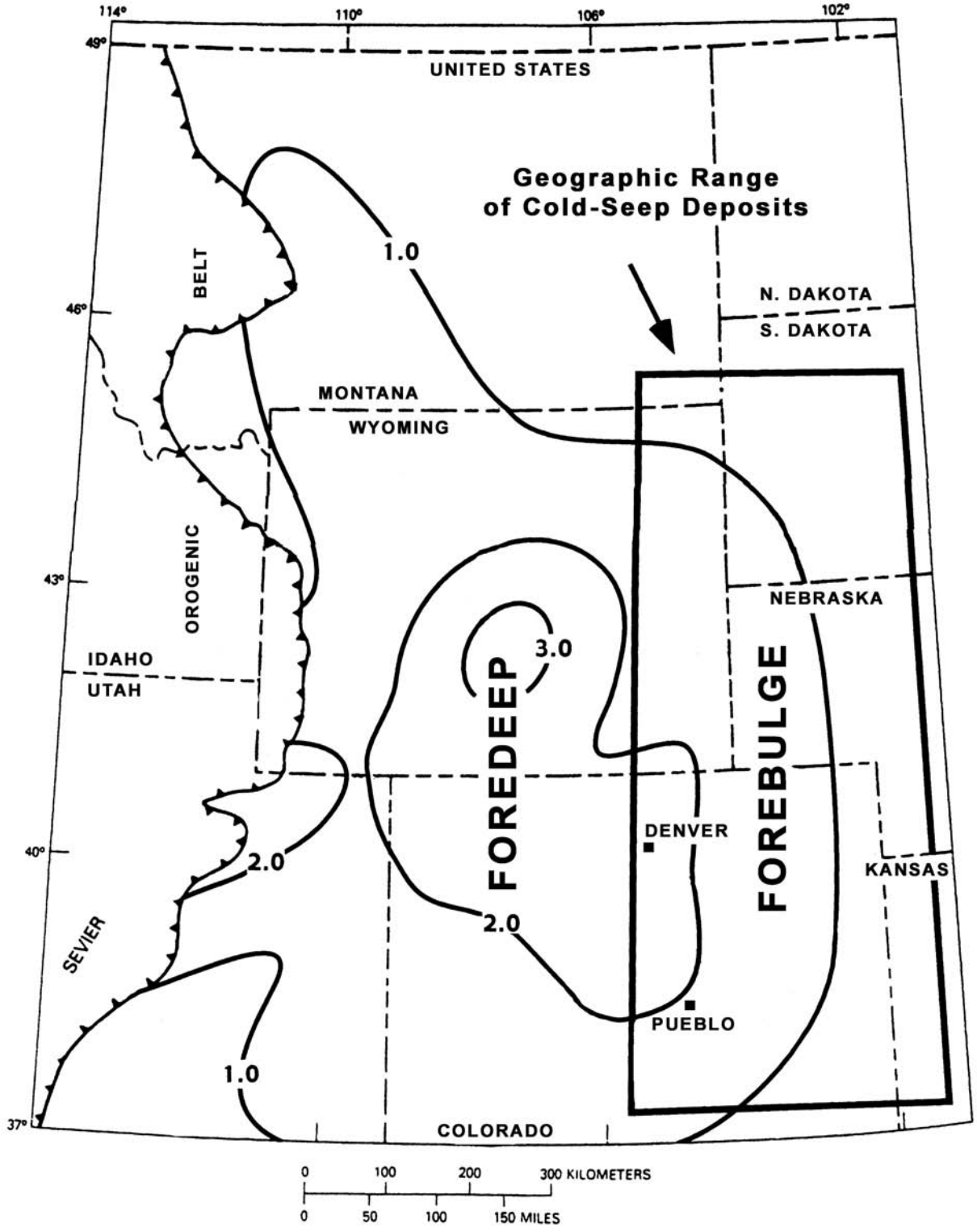

Fig. 3: Sedimentary-tectonic setting of the Tepee Buttes cold-seep deposits in the western interior of the United States. Contours are isopachs in kilometers. From Metz, 2000.

1997). Some of these mounds occur at sites of seepage of light hydrocarbons from the sea floor, leading to the hypothesis that the growth of *Lophelia* and location of the mounds are determined by the hydrocarbon seeps as nutrient sources (Hovland, 1990; Hovland and Risk, 2003). A strong presumptive argument may be made for this connection of seep and mound, but control of nutrient supply and location by ocean currents is probable for many of the mounds, and may be the general explanation in the absence of direct evidence of how *Lophelia* is nourished by the hydrocarbon seepage (Freiwald et al., 2002).

The Tepee Buttes in the United States have a cold-seep origin (Kauffman, et al., 1996) and have served as a model for other cold-seep carbonate buildups (e.g., Gaillard et al. 1992). They are irregular columnar carbonate masses consisting of dense aggregations of mollusk shells, primarily lucinid bivalves, in authigenic bacterial carbonate cement. Their biota and lithology are similar to modern seep deposits in the Gulf of Mexico (Callender and Powell 1997).

The Buttes occur within the Western Interior Cretaceous Basin; they range in age from early Campanian to early Maastrichtian but are restricted within this time span to periods during which thick accumulations of sediment were derived from an orogenic belt to the west, as indicated by major regressive pulses of sedimentation. The distribution of the Buttes was controlled by both regional and local factors. Regionally, the mounds are situated on the forebulge of the Cretaceous fore-arc basin because tensional arching on the outer margin of the foredeep during intervals of rapid sedimentation created avenues for upward migration of fluids (Fig. 3; Metz, 2000). Locally, they occur in linear trends determined by faults and flexures. Thus, their age and location were determined by sediment loading and by tectonic deformation; the distribution patterns of both modern seep deposits and the Tepee Buttes provide a predictive model for the discovery of other seep mounds.

3. Endo-upwelling. The paradox of prolific coral growth and carbonate production on coral reefs in low-nutrient, oligotrophic settings in the tropical oceans has been explained by efficient nutrient recycling and by the photosymbiotic enhancement of skeletal carbonate production. Endo-upwelling may provide an additional nutrient source for reef growth: As a result of geothermal gradients in volcanic islands of the Pacific Ocean, heat flow and upward convection of fluids from deep water adjacent to and within the islands may bring nutrients to the shallow-water reefs to increase productivity there (Rougerie and Wauthy, 1993). Thus, endo-upwelling may help to explain reef growth in this oligotrophic setting by adding nutrients and essential minerals to replace the inevitable loss from the nutrient-poor shallow-water environment. The concept has not been widely accepted by other students of modern reefs, however, for two reasons (Tribble et al., 1994): 1) nutrient recycling is considered adequate to maintain the coral-reef system without a large external source of nutrients, and 2) endo-upwelling at a rate great enough to create a significant nutrient source has yet to be documented.

Endo-upwelling may have been a more important factor in the growth of ancient than in modern reefs because it provided a nutrient source in the absence of photosymbiosis. Devonian reefs in Morocco provide one possible example of endo-upwelling. These reefs grew on topographic highs formed by a ridge of volcanic rocks of earlier Devonian age. The influence of the ridge on currents and storms was emphasized in an early study of these reefs (Brachert et al.,1992). The ridge topography also may have focussed ocean currents to raise the levels of nutrients and oxygen at the reef sites, and may have increased water flux through the accumulating carbonate sediment, which would have promoted early cementation (Hüssner, 1994). More recently, Belka (1998) and Mounji et al. (1998) proposed that the underlying volcanic rock was a source of hydrothermal fluids that could have both provided nutrients for organisms on the mound and promoted early cementation, inorganic precipitation of carbonate micrite, and formation of hardgrounds for epifaunal organisms (Fig. 4). The explanation for these reefs has evolved from the physical effects of sea-floor topography to local sources of nutrients, including the effects of an underlying geothermal gradient and heat flow. The nutrient source may have been a hydrocarbon cold seep, as documented for the Hollard Mound (Peckmann et al., 1999). In any case, endo-upwelling driven by the underlying heat source appears to have been a probable and fundamental cause.

Devonian reefs in the Harz Mountains of northern central Germany formed as atolls on volcanic highs within a clastic-filled basin (Fig. 5; Fuchs,

1990; Gischler et al., 1991; Gischler, 1995). On the basis of isotopic data, Peckmann et al., (2001) concluded that methane provided the nutrients for a chemoautotrophic biota. The methane could have been thermogenic as a result of the volcanic heat source, or could have been derived from the organic-rich basin sediments. In either case, the underlying volcanic rock played a more active role in reef location and growth than merely providing an elevated site for reef growth — fluid migration due to a thermal gradient above the volcanic basement is a clear indication of endo-upwelling of methane from the adjacent marine sediments and probably from nutrient-rich basinal seawater as well.

4. Oceanographic phenomena. Upwelling, oxygen minimum zones, and internal waves may concentrate or localize nutrients and thus strongly affect site-specific carbonate production and reef growth.

Upwelling — The food chain in the oceans is driven by organic material created within the photic zone. Through gravitational settling, however, the organic material is depleted in shallow water; upwelling is important in recycling it and inorganic nutrients back into the photic zone where they are essential for continuing primary production.

Upwelling is strongly controlled by geography: At the regional scale, it is concentrated along the eastern sides of the world's oceans (Flügel and Kiessling, 2002); at a finer scale, it is created through the interaction of ocean currents with seafloor or coastal topography. In coastal upwelling, in which surface water moves ocean-ward and is replaced by deeper and nutrient-rich water, the depth from which the upwelling water is derived, at the base of the mixed layer, is 100 to 200 m in most areas, but may be considerably shallower. For example, off Peru north of 15° S, it is only 25 to 75 m (Hutchings et al., 1995), and off the coast of Oregon and northern California, the surface layer extends to a depth of only 20 m (Smith, 1995). High organic productivity in the present ocean is strongly concentrated in areas of coastal upwelling (Jahnke and Shimmield, 1995; Hay, 1995); distribution of heterotrophic carbonate production and reefs may also have been similarly controlled during much of the Phanerozoic.

Oxygen minimum zone –Dissolved oxygen is low in the oxygen minimum zone (OMZ) as a result of decomposition of organic material that has settled from the overlying water. The development and persistence of an OMZ requires a stratified water mass because vertical mixing by turbulence or upwelling would both disperse the organic matter and introduce oxygenated water. The depth at which an OMZ might occur in the geologic past is difficult to predict, given that the strength and bounding surfaces of present-day OMZs fluctuate seasonally and with oceanographic conditions (Pickard and Emery, 1992; Cannariato and Kennet, 1999), and over longer time spans as well, as for example during glacial and inter-glacial intervals of the Pleistocene (Dean and Gardner, 1998).

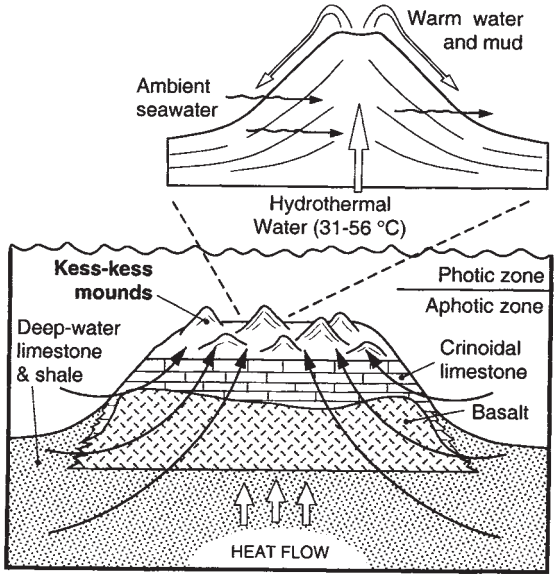

Fig. 4: Postulated geothermally-driven fluid flow, Kess-kess mounds, Morocco. From Mounji et al., 1998.

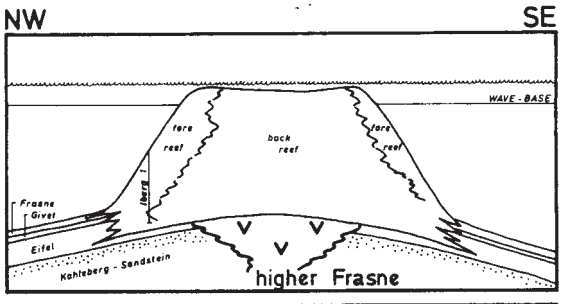

Fig. 5: Cross section of Upper Devonian reef, Harz, Mountains, Germany. Heat flow from the underlying earlier Devonian volcanic rock is postulated to have driven fluid flow from underlying basinal organic-rich sediments. From Gischler et al., 1991.

In the modern ocean, the top of the OMZ is commonly the thermocline, at the base of the photic zone, which corresponds to the boundary between warmer water above and cooler water below, and thus to the resultant pycnocline, dividing less dense water of the mixed layer above from denser and more stable water below (Pickard and Emery, 1992). The thermocline at low and middle latitudes in modern oceans is generally between 100 and 200 m (Defant, 1961).

The OMZ is a nutrient maximum in the ocean (Hay, 1995) because organic matter, both residual and that formed by in situ bacterial production, accumulates there (Kepkay et al., 1979). Bacteria are particularly abundant in the OMZ (Mullins et al., 1985; Thompson et al., 1985) and reduce biologically useful nitrate to nitrite, which then diffuses to the boundaries of the OMZ where it is re-oxidized to useable nitrate. The combination of more abundant dissolved oxygen, useable nitrate, and an optimal habitat for sulfate-reducing bacteria results in heightened biologic productivity at the upper OMZ boundary in contrast to either inside or outside the OMZ (Vercoutere et al., 1986). One result is that mats of non-photosynthetic bacteria that grow on the substrate are more common at the edges of modern OMZs than within them (Williams and Reimers, 1983). The fact that microbialite carbonate production is enhanced in OMZs due to the increased abundance of bacteria, but skeletal production is lower than in more oxygenated shallower water, provides an obvious explanation for deep-water mud mounds in the geologic record. In the northeastern Atlantic, *Lophelia* distribution is strongly concentrated at the top of the OMZ just below the thermocline (Freiwald et al., 1997; Freiwald, 2002).

Internal waves — Internal waves at density interfaces such as at the base and top of an OMZ are common and well-studied features in the ocean (Roberts, 1975; Apel, 1987). They have a significant effect on sediment reworking and movement and on vertical mixing within the water column (Ivey and Nokes, 1989; Cacchione and Pratson, 2004); they also significantly enhance organic production (Pingree and Mardell, 1981; Sandstrom and Elliot, 1984; Holligan and Groom, 1986; Rice et al., 1990), and provide nutrients to modern reefs (Andrews, 1983). These effects are accentuated if the slope of the sea floor is such that the internal waves will break where the pycnocline impinges against it. Through resulting wave agitation of the sea floor, organic matter from the substrate is re-suspended into nepheloid layers in the water column, to be distributed within the area of agitation and into adjacent shallower and deeper areas (Cacchione and Drake, 1986; McCave, 2002). This benthic-pelagic coupling (Graf, 1992) of organic material that is of pelagic origin but is inaccessible to suspension-feeding benthic organism once it has settled on the sea floor unless there is some mechanism of re-suspension was probably extremely important for the growth of deep-water reefs.

The interaction of internal waves with the local sea-floor topography and the re-suspension of organic material where the waves impinge on the sea floor has been correlated with the distribution of *Lophelia* banks around the Faroe Islands (Frederiksen et al., 1992). Internal waves have also been invoked to explain biotic and lithologic features on the ancient sea floor. Thompson and Newton (1987), for example, proposed that the Devonian sea in New York was stratified and that a distinctive brachiopod fauna inhabited the sea floor at the upper boundary of an OMZ. Internal waves on the pycnocline were inferred from current-oriented brachiopods and from winnowed sediment containing small-scale cross-laminations and ripples. Baird and Brett (1991), in another study of Devonian black shales, also concluded that the depositional setting was a dysoxic to anoxic OMZ and they inferred that erosional features and disconformities were the consequence of sub-tidal turbulence and erosion caused by internal waves where the pycnocline impinged on the sea floor.

Upwelling, an OMZ, and internal waves have been integrated to explain the distribution and developmental history of Tournaisian Waulsortian mounds in the Sacramento Mountains of New Mexico (Stanton et al., 2000). The mounds grew on a southward-dipping homoclinal ramp at water depths ranging from approximately 110 to 250 m (Jeffery and Stanton, 1996a). They are situated on and around positive topographic features on the ramp that have been attributed to tectonism and to local erosion and deposition (Ahr, 1989; Jeffery and Stanton, 1996b; Jeffery, 1997).

Mound growth was within an OMZ as indicated by color, total organic content (TOC), and Fe and Mn content of inter-mound ramp strata. Organic carbon accumulation on this part of the ramp corresponds to modern examples of shelf or slope anoxia

resulting from organic carbon input exceeding the available oxygen for its decomposition (Tyson and Pearson, 1991). Upwelling as a control on the growth of Waulsortian mounds has been discussed by Wright (1994), Bridges et al. (1995), Pickard (1996), and Lasemi et al. (1998). It is a likely explanation for the combination of abundance of organic material, the resulting OMZ, and the location of the mounds within this nutrient maximum, but upwelling is a broad, facies-scale explanation. It does not explain carbonate production at the local scale of individual mounds.

Specific locations of mounds may be explained, however, if internal waves on the pycnocline at the top of the OMZ are incorporated into the analysis. Inter-mound strata on the ramp are characterized by fine and homogeneous texture and the absence of scour surfaces or fossil lags. Evidence of local current / wave action is present, however, in several mounds (Wanless and Tedesco, 1991). Considering that the mounds formed well below wave base, these sedimentary features indicate that internal waves impinged against the mounds but not against the adjacent gently sloping inter-mound sea floor.

The explanation of mound growth integrating all the available data is that initial ramp topography accentuated and localized the effects of internal waves at the pycnocline, causing local turbulence on the sea floor, vertical mixing, and enhanced upwelling and phytoplankton productivity. Resuspension of organic matter from the substrate was important for the predominantly suspension-feeding macrofauna, and particularly for the abundant siliceous sponges, which require dissolved nutrients or thoroughly degraded colloidal material for subsistence rather than cellular organic matter that would have been derived from a primary, phytoplankton source (Krautter, 1997; Pisera, 1997). These effects were at a more site-specific scale than that of upwelling alone induced by wind stress and Ekman transport of surface water. With mound growth, topographic disparity on the ramp increased so that the effects of internal waves were increasingly accentuated at the scale of individual mounds in a positive feedback loop (Hüssner, 1994). Enhanced local productivity as a result of benthic-pelagic coupling at the mound sites benefited the suspension-feeding macrofauna, and particularly the heterotrophic carbonate-producing bacteria responsible for the bulk of the lime mud, of which the mounds are largely constructed.

Conclusions

Study of reefs in the Alps, and elsewhere, has had two significant components. The first has been reef description and comparison in terms of lithology, paleontology, external shape and internal facies geometry, and the external factors of paleogeography and paleobathymetry, but with relatively little attention paid to what determined the specific site at which a reef grew. This, however, is precisely the question necessary to understand their origin and development and to explore for them in the subsurface as petroleum reservoirs or sites of mineral deposits.

The second component has been the historical use of modern shallow-water reefs as models for ancient reefs even though the significant characteristic of these modern reefs – the photosymbiotic nature of the major carbonate producers – generally can not be demonstrated and probably did not exist in ancient reefs, at least prior to the Jurassic or perhaps Late Triassic. Morphologic criteria for photosymbiosis in fossils yield conclusions that are only probabilistic and commonly apply only to assemblages but not individual taxa. Isotopic criteria are potentially more useful, but their validity has not been established.

Uniformitarian arguments for the existence of photosymbiosis are also of limited value. The assumption that abundant carbonate production throughout the Phanerozoic required photosymbiosis as in modern shallow-water reefs is countered by carbonate production in modern deeper- and cooler-water reefs. Another uniformitarian argument is that ancient reefs occur in the same setting as modern shallow-water reefs, and therefore the carbonate producers were also photosymbionts. This hypothesis is countered first by observing that modern and ancient reefs are distinctly different in the relatively greater abundance of microbial mud and cement in ancient reefs (Webb, 1996); the microbial contribution to the reefs is of photoautotrophic origin in shallow-water reefs, but must have been of heterotrophic origin in deep-water mud mounds. It is also countered by the fact that many ancient reefs do not occur in settings similar to those of modern reefs. Sub-photic mud mounds

are one example of ancient reefs not replicated in the present seas. Jurassic reefs in Bavaria grew in a complex pattern of mounds and inter-mound basins on a shallow shelf. Many ancient platform-margin carbonate reef systems occurred in intra-platform settings rather than facing the open ocean. Examples are the Triassic and Devonian reefs discussed above and the Permian reef of West Texas.

Thus, modern tropical reefs provide a limited model for fossil reefs. The photosymbiotic paradigm is based on reef growth in shallow-water oligotrophic settings. The alternative, heterotrophic paradigm, that abundant nutrients were required for carbonate production and reef growth, is proposed as the more robust model for the study of reefs during much of the Phanerozoic. Its application requires quite different environmental characteristics to explain the location and nature of nutrient sources and resulting reef growth.

The most significant of these are terrestrial nutrient sources, endo-upwelling, cold-seep hydrocarbon venting, and oceanographic factors of upwelling, oxygen minimum zones, and internal waves. Analyzing ancient reefs in terms of nutrient supply as controlled by these environmental features should promote better understanding of their origin and development.

Acknowledgements

This research has benefited greatly from interactions in the field and numerous conversations with Wayne Ahr and David Jeffery. I thank Martin Zuschin for his invitation for me to discuss this topic at the First Austrian Reef Workshop; it provided the impetus for this paper. Jennifer Abell helped with the figures. Wayne Ahr, Al Fagerstrom, André Freiwald, and Martin Zuschin have made suggestions that have improved the manuscript.

References

Aharon, P., Schwarcz, H.P. and Roberts, H.H. (1999): Radiometric dating of submarine hydrocarbon seeps in the Gulf of Mexico. - Geological Society of America Bulletin, 109: 568–579.

Ahr, W.M. (1989): Sedimentary and tectonic controls on the development of an Early Mississippian carbonate ramp, Sacramento Mountains area, New Mexico. – In: Crevello, P.D., Wilson, J.L., Sarg, J.L. and Read, F.J. (eds.): Controls on carbonate platform and basin development, Soc. Econ. Paleont. Min. Spec. Publ. 44: 203-212.

Allmon, W.D. and Ross, R.M. (2001): Nutrients and evolution in the marine realm. - In: Allmon, W.D. and Bottjer, D.J., (eds.): Evolutionary paleoecology: the ecological context of macroevolutionary change, 105-148. Columbia University Press, New York.

Andrews, J.C. (1983): Thermal waves on the Queensland shelf. - Australian Journal of Marine and Freshwater Research, 34: 81-96.

Apel, J.R. (1987): Principles of Ocean Physics. - 631 pp., Academic Press, London.

Baird, G.C. and Brett, C.E. (1991): Submarine erosion on the anoxic sea floor: stratinomic, palaeoenvironmental, and temporal significance of reworked pyrite-bone deposits - In: Tyson, R.V. and Pearson, T.H. (eds.): Modern and ancient continental shelf anoxia. - Geol. Soc. London Spec. Publ. 58: 233-257.

Bambach, R.K. (1993): Seafood through time: changes in biomass, energetics, and productivity in the marine ecosystem. - Paleobiology, 19: -372-397.

Belka, Z. (1998): Early Devonian Kess-Kess carbonate mud mounds of the eastern Anti-Atlas (Morocco), and their relation to submarine hydrothermal venting. - Journal of Sedimentary Research, 68: 368-377.

Brachert, T.C., Buggisch, W., Flügel, E., Hüssner, H.M., Joachimski, M.M., Tourneur, F. and Walliser, O.H. (1992): Controls of mudmound formation: the Early Devonian Kess-Kess carbonates of Hamar Laghdad, Antiatlas, Morocco. - Geologische Rundschau, 81: 15-44.

Bridges, P.H., Gutteridge, P. and Pickard, N.A.H. (1995): The environmental setting of Early Carboniferous mud-mounds. - In: Monty, C.L.V., Bosence, D.W.J., Bridges, P.H. and Pratt, B.R. (eds.): Carbonate mudmounds: Their origin and evolution. - Int. Ass. Sed. Spec. Publ. 23: 171-190.

Cacchione, D.A. and Drake, D.E. (1986.): Nepheloid layers and internal waves over continental shelves and slopes. - Geo-Marine Letters, 6: 147-152.

Cacchione, D. A. and Pratson, L.F. (2004): Internal waves and the continental slope. - American Scientist, 92: 130-137.

Callender, W.R. and Powell, E.N. (1997): Autochthonous death assemblages from chemoautotrophic communities at petroleum seeps: Palaeoproduction, energy flow, and implications for the fossil record. - Historical Biology, 12: 165-198.

Callender, R. and Powell, E.N. (2000): Long-term history of chemoautotrophic clam-dominated faunas of pe-

troleum seeps in the Northwestern Gulf of Mexico. - Facies, 43: 177-204.

Cannariato, K.G. and Kennett, J.P. (1999): Climatically related millennial-scale fluctuations in strength of California margin oxygen-minimum zone during the past 60 k.y. - Geology, 27: 975-978.

Chappell, J. (1980): Coral morphology, diversity and reef growth. - Nature, 286: 249-252.

Coates, A.G. and Jackson, J.B.C. (1987): Clonal growth, algal symbiosis and reef formation by corals. - Paleobiology, 13: 363-378.

Cowen, R. (1988): The role of algal symbiosis in reefs through time. - PALAIOS, 3: 221-227.

Dean, W.E. and Gardner, J.V. (1998): Pleistocene to Holocene contrasts in organic matter production and preservation on the California continental margin. - Geological Society of America Bulletin, 110: 888-899.

Defant, A. (1961): Physical Oceanography, v. 1. - 729 pp., Macmillan, New York.

Dupraz, C. and Strasser, A. (2002): Nutritional modes in coral-microbialite reefs (Jurassic, Oxfordian, Switzerland): Evolution of trophic structure as a response to environmental change. - PALAIOS 17: 449-471.

Eliuk, L.S. (1998): Big bivalves, algae, and the nutrient poisoning of reefs: A tabulation with examples from the Devonian and Jurassic of Canada. - In: Johnston, P.A. and Haggart, J.W. (eds.): Bivalves: an Eon of Evolution, 157-184, University of Calgary Press, Calgary.

Fagerstrom, J.A. (1987): The Evolution of Reef Communities. - 600 pp., John Wiley and Sons, New York.

Flügel, E. and Kiessling, W. (2002): A new look at ancient reefs. - In: Kiessling, W., Flügel E. and Golanka, J. (eds.): Phanerozoic reef patterns - Soc. Econ. Paleont. Min. Spec. Publ. 72: 3-10.

Flügel, E. and Koch, R. (1995): Controls on the diagenesis of Upper Triassic carbonate ramp sediments: Steinplatte, Northern Alps (Austria). - Geol. Paläont. Mitt. Innsbruck, 20: 283-311.

Frederiksen, R., Jensen, A. and Westerberg, H. (1992): The distribution of the scleractinian coral *Lophelia pertusa* around the Faroe islands and the relation to internal tidal mixing. - Sarsia, 77: 157-171.

Freiwald, A. (2002): Reef-forming cold-water corals. - In: Wefer, G., Billett, D., Hebbeln, D., Jørgensen, B.B., Schlüter, M. and Van Weering, T. (eds.): Ocean Margin Systems, 365-385. Springer-Verlag, Berlin.

Freiwald, A., Henrich, R. and Pätzold, J. (1997): Anatomy of a deep-water coral reef mound from Stjernsund, West Finnmark, Northern Norway. - In: James, N.P. and Clarke, J.A.D. (eds.): Cool-water carbonates, Soc. Econ. Paleont. Min., Spec. Publ. 56: 141-161.

Freiwald, A., Hühnerbach, V., Lindberg, B., Wilson, J. and Campbell, J. (2002): The Sula Reef Complex, Norwegian shelf. - Facies, 47: 179-200.

Fuchs, A. (1990): Charakter und Ende der devonischen Riffentwicklung im Elbingeröder Komplex (Harz). - Facies, 23: 97-108.

Gaillard, C., Rio, M., Rolin, Y. and Roux, M. (1992): Fossil chemosynthetic communities related to vents or seeps in sedimentary basins: The pseudobioherms of southeastern France compared to other world examples. - PALAIOS, 7: 451-465.

Ginsburg, R.N. (1956): Environmental relationships of grain size and constituent particles in some South Florida carbonate sediments. - American Association of Petroleum Geologists Bulletin, 40: 2384-2427.

Gischler, E. (1995): Current and wind induced facies patterns in a Devonian atoll: Iberg reef, Harz Mts., Germany. - PALAIOS, 10: 180-189.

Gischler, E., Weller, H. and Weyer, D. (1991): Devonian reefs of the Harz Mountains, Germany. - VI. International Symposium on fossil Cnidaria including Archaeocyatha and Porifera, Münster, Excursion Guidebook A4, 104 pp.

Graf, G. (1992): Benthic-pelagic coupling: a benthic view. – Oceanogr. Mar. Biol. Annual Review, 30: 149-190.

Hallock, P. (2001): Global reefs, carbonate sediments, nutrients, and global change. - In: Stanley, G.D., Jr. (ed.): The history and sedimentology of ancient reef systems, 387-427. Kluwer Academic/Plenum Publishers, New York.

Hay, W.W. (1995): Paleoceanography of marine organic-carbon-rich sediments. - In: Huc, A.-Y. (ed.): Paleogeography, Paleoclimate, and Source Rocks, AAPG Studies in Geology, 40. 21-59.

Holligan, P.M. and Groom, S.B. (1986): Phytoplankton distributions along the shelf break. - Roy. Soc. Edinburgh Proc, 88B: 239-263.

Hovland, M. (1990): Do carbonate reefs form due to fluid seepage? - Terra Nova, 2: 8-18.

Hovland, M., Mortenson, P.B., Brattegard, T., Strass, P. and Rokoengen, K. (1998): Ahermatypic coral banks off mid-Norway: Evidence for a link with seepage of light hydrocarbons. - PALAIOS, 13: 189-200.

Hovland, M. and Risk, M. (2003): Do Norwegian deep-water coral reefs rely on seeping fluids? - Marine Geology, 198: 83-96.

Hüneke, H., Joachimski, M., Buggisch, W. and Lützner, H. (2001): Carbonate facies in response to climate and nutrient level: The Upper Carboniferous and Permian of central Spitsbergen (Svalbard). - Facies, 45: 93-136.

Hüssner, H.M. (1994): Reefs, an elementary principle with complex realizations. - Beringeria 11: 99p.

Hutchings, L., Pitcher, G.C., Probyn, T.A. and Bailey, G.W. (1995): The chemical and biological consequences of coastal upwelling. - In: Summerhayes, C.P., Emeis, K.-C., Angel, M.V., Smith, R.L. and Zeitzschel, B. (eds): Upwelling in the Ocean: Modern Processes and Ancient Records. 65-81. John Wiley & Sons, Chichester.

Ivey, G.N. and Nokes, R.I. (1989): Vertical mixing due to the breaking of critical internal waves on sloping boundaries. - Jour. Fluid Mechanics, 204: 479-500.

Jahnke, R.A. and Shimmield, G.B. (1995): Particle flux and its conversion to the sediment record: Coastal ocean upwelling systems. - In: Summerhayes, C.P., Emeis, K.-C., Angel, M.V., Smith, R.L. and Zeitzschel, B. (eds): Upwelling in the Ocean: Modern Processes and Ancient Records. 83-110. John Wiley & Sons, Chichester.

Jeffery, D.L. (1997): Tectonic control on sea-floor relief and the localization of Lower Mississippian Waulsortian mounds, New Mexico. - Geology, 25: 1011-1014.

Jeffery, D.L. and Stanton, R.J., Jr. (1996a): Biotic gradients and depth phases on a homoclinal ramp: The Alamogordo Member of the Lake Valley Formation, Lower Mississippian, New Mexico. - In: Strogen, P., Somerville, I.D. & Jones, G. Ll. (eds): Recent advances in Lower Carboniferous geology. - Geol. Soc. London Spec. Publ., 107: 111-126.

Jeffery, D.L. and Stanton, R.J., Jr. (1996b): Growth history of the Lower Mississippian Waulsortian mounds: Distribution, stratal patterns and geometries, New Mexico. - Facies, 35: 29-58.

Kauffman, E.G., Arthur, M.A., Howe, B. and Scholle, P.A. (1996): Widespread venting of methane-rich fluids in Late Cretaceous (Campanian) submarine springs (Tepee Buttes), Western Interior seaway, U.S.A. - Geology, 24: 799-802.

Kepkay, P.E., Cooke, R.C. and Novitsky, J.A. (1979): Microbial autotrophy: A primary source of organic carbon in marine sediments. - Science, 204: 68-69.

Kiessling, W. (2002): Secular variations in the Phanerozoic reef ecosystem. – In: Kiessling, W., Flügel, E. and Golanka, J. (eds.): Phanerozoic reef patterns. - Soc. Econ. Paleont. Min. Spec. Publ., 72: 625-690.

Kiessling, W., Flügel, E. and Golanka, J. (2000): Fluctuations in the carbonate production of Phanerozoic reefs. – In: Insalaco, E., Skelton, P.W. and Palmer, T.J. (eds.): Carbonate platform systems: components and interactions. - Geological Society London, Spec. Publ. 178: 191-215.

Kiessling, W., Flügel, E. and Golanka, J. (2002): (eds.): Phanerozoic reef patterns. 775 pp., Soc. Econ. Paleont. Min. Spec. Publ., 72, Tulsa.

Krautter, M. (1997): Aspekte zur Paläoökologie postpaleozoischer Kieselschwämme. - Profil, 11: 119-324.

Lasemi, Z., Norby, R.D. and Treworgy, J.D. (1998): Depositional facies and sequence stratigraphy of a Lower Carboniferous bryozoan-pelmatozoan carbonate ramp in the Illinois Basin, mid-continent USA. – In: Wright, V.P. and Burchette, T.P. (eds): Carbonate Ramps. - Geol. Soc. London Spec. Publ. 149: 369-395.

Leinfelder, R.R. (2001): Jurassic reef ecosystems. - In: Stanley, G.D., Jr. (ed.): The history and sedimentology of ancient reef systems. 251-309, Kluwer Academic/Plenum Publishers, New York.

Lowenstam, H.A. (1950): Niagaran reefs of the Great Lakes area. - Journal of Geology, 58: 430-487.

Lyons, W.B., Nezat, C.A., Carey, A.E. and Hicks, D.M. (2002): Organic carbon fluxes to the ocean from high-standing islands. - Geology, 30: 443-446.

McCave, I.N. (2002): Sedimentary settings on continental margins – an overview. – In Wefer, G., Billett, D., Hebbeln, D., Jørgensen, B.B., Schlüter, M., and Van Weering, T., (eds.) Ocean Margin Systems, 1-14. Springer-Verlag, Berlin.

Metz, C.L. (2000): Ancient hydrocarbon emission sites, North America Western Interior Cretaceous Basin cold seep mounds (Tepee Buttes) - geographic, stratigraphic, and age distribution. - American Association of Petroleum Geologists Annual Meeting, Abstracts with Programs: 120.

Mounji, D., Bourque, P-A., and Savard, M.M. (1998): Hydrothermal origin of Devonian conical mounds (kess-kess) of Hamar Lakhdad Ridge, Anti-Atlas, Morocco. – Geology, 26: 1123-1126.

Mullins, H.T., Thompson, J.B., McDougall, K. and Vercoutere, T.L. (1985): Oxygen-minimum zone edge effects: Evidence from the central California coastal upwelling system. - Geology, 13: 491-494.

Ohno, T., Katoh, T. and Yamasu, T. (1995): The origin of algal-bivalve photo-symbiosis. – Palaeontology, 38: 1-21.

Orange, D.L., Greene, H.G., Reed, D., Martin, J.B., McHugh, C.M., Ryan, W.B.F., Maher, N., Stakes, D. and Barry, J. (1999): Widespread fluid expulsion on a translational continental margin: Mud volcanoes, fault zones, headless canyons, and organic-rich substrate in Monterey Bay, California. - Geological Society of America Bulletin, 111: 992-1009.

Peckmann, J., Gischler, E., Oschmann, W. and Reitner, J. (2001): An Early Carboniferous seep community and hydrocarbon-derived carbonates from the Harz Mountains, Germany. – Geology, 29: 271-274.

Peckmann, J., Walliser, O.H., Riegel, W. and Reitner, J. (1999): Signatures of hydrocarbon venting in a Middle

Devonian carbonate mound (Hollard Mound) at the Hamar Laghdad (Antiatlas, Morocco). – Facies, 40: 281-296.

Pickard, G.L. and Emery, W.J. (1982): Descriptive Physical Oceanography, 4th ed. - 249 pp., Pergamon Press, Oxford.

Pickard, N.A.H. (1996): Evidence for microbial influence on the development of Lower Carboniferous buildups. - In: Strogen, P., Somerville, I.D. & Jones, G. Ll. (eds): Recent advances in Lower Carboniferous geology. Geol. Soc. London Spec. Publ., 107: 65-182.

Piller, W. E. (1981): The Steinplatte reef complex, part of an Upper Triassic carbonate platform near Salzburg (Austria). – In: Toomey D.F. (ed.): European Reef Models. - Soc. Econ. Paleont. Min. Spec. Publ., 30: 261-290.

Pingree, R.D. and Mardell, G.T. (1981): Slope turbulence, internal waves and phytoplankton growth at the Celtic Sea shelf-break. - Roy. Soc. London Phil. Trans., A302: 663-682.

Pisera, A. (1997): Upper Jurassic siliceous sponges from the Swabian Alb: Taxonomy and paleoecology. - Palaeontologica Polonica, 57: 1-216.

Rice, A.L., Thurston, M.H. and New, A.L. (1990): Dense aggregations of a hexactinellid sponge, Pheronema carpenteri, in the Porcupine Seabight (northeast Atlantic Ocean), and possible causes. - Progress in Oceanography, 24: 179-196.

Roberts, J. (1975): Internal Gravity Waves in the Ocean, Marcel Dekker, 274 pp., New York.

Rougerie, F. and Wauthy, B. (1993): The endo-upwelling concept: from geothermal convection to reef construction. - Coral Reefs, 12: 19-30.

Sanders, D. and Baron-Szabo, R. C. (2005): Scleractinian assemblages under sediment input: their characteristics and relation to the nutrient input concept. - Palaeogeography, Palaeoclimatology, Palaeoecology, 216: 139-181.

Sandstrom, H. and Elliott, J.A. (1984): Internal tide and solitons on the Scotian Shelf, a nutrient pump at work. - Jour. Geophys. Res., 89: 6415-6426.

Schäfer, P. (1979): Fazielle entwicklung und Palökologische zonierung zweier obertriadischer riffstrukturen in den nördlichen kalkalpen ("Oberrhät"-riff-kalke, Salzburg). – Facies, 1: 3-245.

Schlaf, J., Zuschin, M. and Piller, W. (1999): Origin and palaeoenvironment of thick coquina accumulations on a lower Norian (Upper Triassic) carbonate slope (Julian Alps, Slovenia). - Zbl. Geol. Paläont. Teil 1. 1997, H. 7-9: 1153-1166.

Schlager, W. (2003): Benthic carbonate factories of the Phanerozoic. - International Journal of Earth Sciences, 92:445-464.

Sibuet, M. and Olu-Le Roy, K. (2002): Cold seep communities on continental margins: Structure and quantitative distribution relative to geological and fluid venting patterns. - In Wefer, G., Billett, D., Hebbeln, D., Jørgensen, B.B., Schlüter, M. and Van Weering, T. (eds.) Ocean Margin Systems, 235-251. Springer-Verlag, Berlin.

Smith, R.L. (1995): The physical processes of coastal upwelling systems. - In: Summerhayes, C.P., Emeis, K.-C., Angel, M.V., Smith, R.L. and Zeitzschel, B. (eds): Upwelling in the Ocean: Modern Processes and Ancient Records. 39-64, John Wiley & Sons, Chichester.

Stanley, G.D. (1981): Early history of scleractinian corals and its geological consequences. – Geology, 9: 507-511.

Stanley, G.D. and Swart, P.W. (1995): Evolution of the coral-zooxanthellae symbiosis during the Triassic: a geochemical approach. - Paleobiology, 21: 179-199.

Stanton, R.J., Jr. (1967): Factors controlling shape and internal facies distribution of organic carbonate buildups. - American Association of Petroleum Geologists Bulletin, 51:2462-2467.

Stanton, R.J., Jr. and Flügel, E. (1989): Problems with reef models. The Late Triassic Steinplatte "reef" (Northern Alps, Salzburg/Tyrol, Austria). - Facies, 20: 1-138.

Stanton, R.J. Jr., and Flügel, E. (1995): An accretionary distally steepened ramp at an intrashelf basin margin: an alternative explanation for the Upper Triassic Steinplatte "reef" (Northern Calcareous Alps, Austria). - Sedimentary Geology, 95: 269-286.

Stanton, R.J., Jr., Jeffery, D.L. and Guillemette, R.N. (2000): Oxygen minimum zone and internal waves as potential controls on location and growth of Waulsortian mounds (Mississippian, Sacramento Mountains, New Mexico). - Facies, 42: 161-176.

Talent, J.A. (1988): Organic reef-building: episodes of extinction and symbiosis? - Senckenbergiana lethaea, 69: 315-368.

Thompson, J.B., Mullins, H.T., Newton, C.R. and Vercoutere, T.L. (1985): Alternative biofacies model for dysaerobic communities. - Lethaia, 18: 167-179.

Thompson, J.B. and Newton, C.R. (1987): Ecological reinterpretation of the dysaerobic *Leiorhynchus* fauna: Upper Devonian Geneseo Black Shale, central New York. - PALAIOS, 2: 274-281.

Tribble, G.W., Atkinson, F.J., Sansone, F.J. and Smith, S.V. (1994): Reef metabolism and endo-upwelling in perspective. - Coral Reefs, 13: 199-201.

Tyson, R.V. (1995): Sedimentary Organic Matter. 615 pp., Chapman and Hall, London.

Tyson, R.V. and Pearson, T.H. (1991): Modern and Ancient continental shelf anoxia. - In: Tyson, R.V. and Pearson, T.H. (eds.): Modern and ancient continental shelf anoxia. - Geol. Soc. London Spec. Publ. 58: 1-26.

Vercoutere, T.L., Mullins, H.T., McDougall, K. and Thompson, J.B. (1986): Sedimentation across the central California oxygen minimum zone: an alternative coastal upwelling sequence. - Jour. Sed. Petrol., 57: 709-722.

Wanless, H.R. and Tedesco, L.P. (1991): A re-evaluation of Mississippian mud mounds based on their internal stratigraphy. - Geol. Soc. Amer. Abstracts with Programs, 23 (5): 226.

Webb, G.E. (1996): Was Phanerozoic reef history controlled by the distribution of non-enzymatically secreted reef carbonates (microbial carbonate and biologically induced cement)? - Sedimentology, 43: 947-971.

Williams, L.A. and Reimers, C. (1983): Role of bacterial mats in oxygen-deficient marine basins and coastal upwelling regimes: Preliminary report. - Geology, 11: 267-269.

Wood, R. (1993): Nutrients, predation and the history of reef-building. - PALAIOS, 8: 526-543.

Wood, R. (1999): Reef evolution. 414pp. Oxford University Press, Oxford.

Wood, R. (2000): Palaeoecology of a Late Devonian back reef: Canning Basin, Western Australia. - Palaeontology, 43: 671-703.

Wright, V.P. (1994): Early Carboniferous carbonate systems: an alternative to the Cainozoic paradigm. - Sedimentary Geology, 93: 1-5.

Zankl, H. (1969): Der Hohe Göll. Aufbau und Lebensbild eines Dachsteinkalk-riffes in der Obertrias der nördlichen Kalkalpen. - Abh. Sencken. Naturforsch. Ges., 519: 1-123.

Geo.Alp, Vol. 3, S. 207–214, 2006

ENCAPSULATION PARAMETERS IN WASTE DEPOSIT TECHNOLOGY: GEOLOGIC BARRIERS AND LINER SYSTEMS

Kurt Czurda

With 9 figures and 2 tables

Kurt Czurda, Department of Applied Geology, Karlsruhe University, Kaiserstr. 12, D-76128 Karlsruhe, kurt.czurda@agk.uka.de

Abstract

According to the state of technology any waste deposition has to be secured by a multibarrier encapsulation system. Surface liners and base liners have to be constructed in different ways because they serve different purposes. Surface liners have to prevent precipitation water to infiltrate into the waste and base liners seal the waste from the underground rock resp. groundwater. Standard combined systems consist of mineral barriers and geomembranes. A drainage system at the base for seapage control and a gas collection installation at the surface in case of municipal waste complete the system.

1. Clay Liners and waste disposal

As populations grow and technologies advance, ever-more wastes are produced in ever-growing quantities . Of the many and varied environmental problems, encapsulation of wastes in order to restore sites and protect the environment is the topic of this chapter. Encapsulation means sealing the waste body by geological and engineered liner systems which in most cases partly consist of clay liners in different modifications. Encapsulation systems are as varied as the environments in which they are built, and the components of an encapsulation system are as multiple and complex as the wastes therein. For all waste types, encapsulation is the only option: permanent isolation from the accessible environment (Caldwell & Reith, 1993). The requirements for an encapsulation system are basically the same, whether the waste is municipial refuse in a landfill, hospital debris in a low level waste dump , or mixed wastes of diverse industrial productions or construction activities. This leads us to the need to classify wastes because encapsulation systems consist of engineered liner components according to the magnitude of the risks originating from the waste.

From the beginning: sophisticated engineered liners serve two purposes. They have to guarantee practical imperviousness to prevent leachates from infiltrating the environment and secondly have to prove retention or at least retardation properties to prevent contaminant migration by convection and diffusion (Drescher, 1997). In many cases - but not absolutely - the surface barrier might be designed as slightly permeable layer, because further decomposition of sanitary wastes by precipitation moisture could be achieved. Because of the different functions of the surface and the base encapsulation barriers, different systems are state of the art. In any case, for most of the required properties, clay liners are optimal.

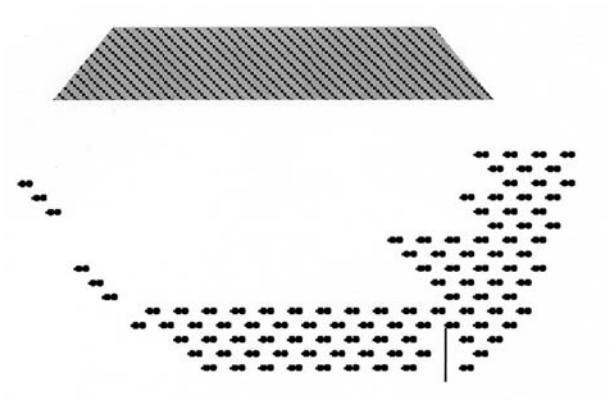

Fig. 1: principle of the multibarrier system for waste encapsulation. Geologic in situ barriers and engineered technical barriers (compacted mineral layers and geomembranes) are the main parts of the system.

have to classify waste categories not by means of the input of waste components but mainly by leaching the waste and determining quantitatively the contaminant content (Czurda, 1992). The European Union, most of the European states, the USA, Canada, Japan etc. follow this system and ended up with similar waste categories. Taking radioactive waste into account as well we roughly have to follow the scheme:

– inert construction and industrial waste
– domestic waste
– toxic industrial waste
– incineration ashes and slags
– radioactive waste

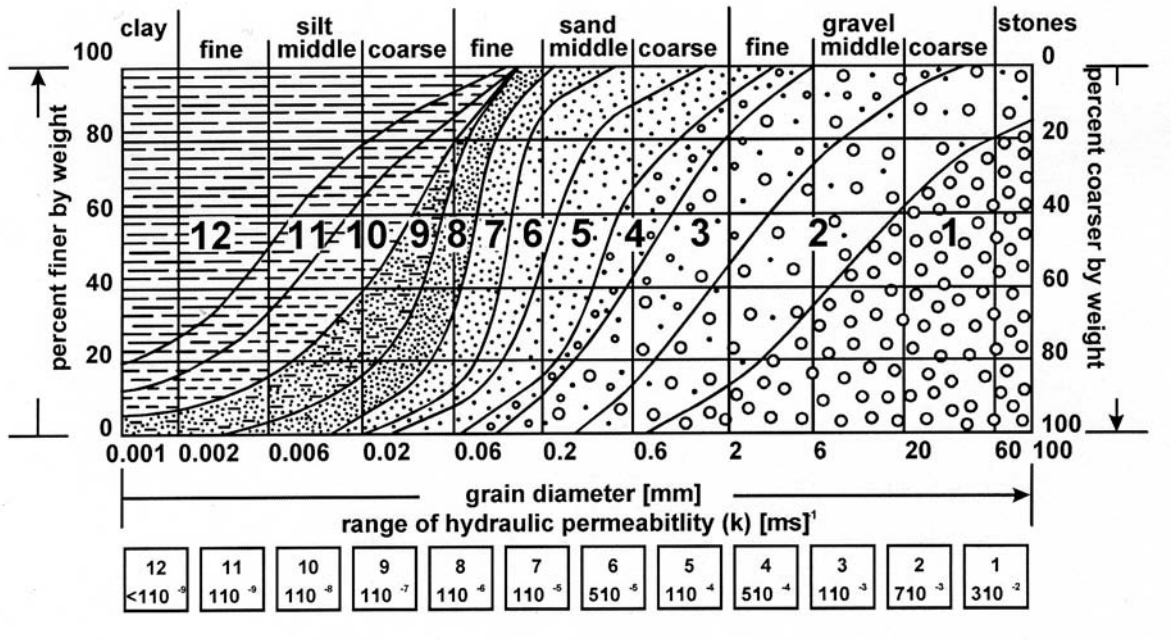

Fig. 2: Practical imperviousness is the main function of liner systems. Hydraulic permeabilities are expressed in k-coefficients in $m.s^{-1}$. The range of $k < 1.10^{-7}$ m/sec is considered as one of the most important barrier features for mineral sealing units in most of the national regulations. Grain size distribution area 10, 11 and 12 refers to this.

1.1 Waste categories

Different waste compositions require different sealing units. E. g. it is not economical to use a multilayer system for inert construction wastes or to design the same systems for sanitary landfills and toxic industrial wastes (Bradshaw et al., 1992). Therefore all regional waste repository regulations

Nuclear waste repositories have to follow special national regulations and are not further treated in this chapter.

As an example for waste assignments some threshold values according to German regulations (TA Abfall, 1991. TA Siedlungsabfall, 1993, Deponieverordnung, 2002) are shown in table 1. They are close to European Union values (EU-Richtlinie, 1999)

	I	II	III
conductivity	6000 µS/cm	50000 µS/cm	100000 µS/cm
uniaxial strength	50 kN/m_	50 kN/m_	50 kN/m_
TO C	20 mg/l	100 mg/l	200 mg/l
phenole	0,2 mg/l	50 mg/l	100 mg/l
mercury	0,005 mg/l	0,020 mg/l	0,100 mg/l
cadmium	0,050 mg/l	0,100 mg/l	0,500 mg/l
lead	0,200 mg/l	1,000 mg/l	2,000 mg/l
sulfate	500 mg/l	1400 mg/l	5000mg/l
soluble part	3 %	6 %	10 %

Table 1: Assignment criterion for waste categories according to the German regulations TA-A and TA-Si. Selected examples. Waste category I means inert waste, II domestic waste and III toxic industrial waste. The leachable parts are listed as examples for very common toxic waste constituents.

1.2 Mineral barriers

As mineral barriers within engineered sealing layers, but as well as constituents of in situ geological barriers - which means the waste deposit location - clay rocks, clay mineral admixtures and zeolite admixtures are the most important and widely used natural materials. Alternative materials like amorphous silica, fly ashes, fly ash zeolites, clay remnants from coal flotation etc. are not treated in the following chapters.

1.2.1 Clay rocks and clay minerals

In using clays and zeolites and other fine grained material for sealing purposes, two main issues are persued: leachate retention by low hydraulic conductivities and toxic constituent retention or retardation by retention mechanisms like adsorption, precipitation, redox processes and others. Soil barriers, containing enough and function adequate clay minerals to provide low permeability, are used extensively to prevent rapid advective migration by various leachates from waste disposal sites (Hiltmann & Stribnry, 1998). The clayey barriers vary from thin geosythetic clay liners (GCL) with 1–3 cm thickness, to compacted clay liners (CCL) up to 300 cm thickness, to natural undisturbed clayey barriers up to 30 m or more in thickness. The hydraulic conductivity of undisturbed clayey deposits depend on the mineralogy, the environment of deposition and the stress history of the deposits. The same is valid for GCL's and CCL's.

The outstanding properties of clay minerals are to be seen in their extremely small grain size (by definition < 2 µm), their negatively charged surface properties of the basal planes, the positively charged broken ends of the platelets and the large surface areas. Most clays in natural settings have a phyllosilicate or sheet structure. Clay minerals have a common structure but they are almost always the result of chemical changes or thermal variations in the range of near surface conditions. Clays attract water, other polar liquids and cations. A dried out clay will expand greatly as it adsorbs water between its layers when attached by aqueous solutions. If toxic ions are constituents of the solution an ion exchange on charged surface sites will result. That is to say, they can accept or release ions depending upon the concentration of the ions in solution relative to that of the clays. This ions, e. g. from the leachate, are not finally fixed but are at disposal for further exchange process depending on the chemical environment. Table 2 gives an overview on cation exchange capacities (CEC) and specific surfaces.

mineral	CEC millimol equv./100g	spec. surface m_/g
allophan	50 - 100	500 - 700
kaolinite	3 - 15	10 - 20
illite	20 - 50	90 - 100
smectite	70 - 130	750 - 800
bentonite	95 - 100	800
vermiculite	150 - 200	750 - 800
Fe- + Al-hydroxide (pH 8,0)	3 - 25	25 - 42
humic material	150 - 250	800

Table 2: CEC (cation exchange capacity) and specific surfaces for different clay mineral spezies and other materials

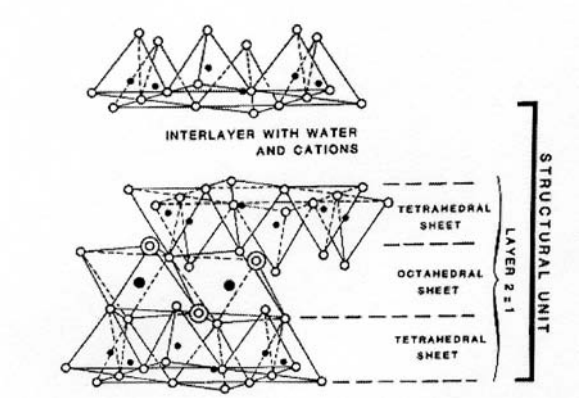

Fig. 3a: 3-layer clay mineral illite with tetraeder/octaeder/tetraeder arrangement and interlayer space between the O-planes of the tetraeders.

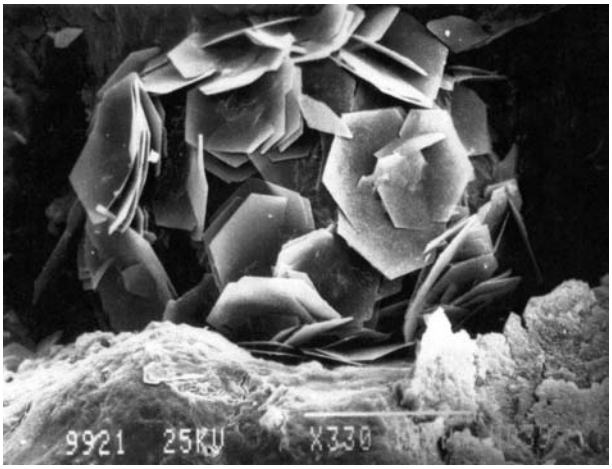

Fig. 3b: Illite aggregate with hexagonal clay flakes, scale: 330x

Of decisive influence on sorption potentials are the primarily fixed cations, e.g. from the marine environment, on the crystallographic basal surfaces. According to the diameter of hydrated cations and their valency they are differently sorbed to the clay surface and are therefore to different quantities exchangeable. For base liner clays as an example Na-bentonites are especially suitable because of their high swelling potential and sorption capacities and therefore fulfil the high degree of imperviousness and the high contaminant retention potential required.

1.2.2 Zeolites

Zeolites are tectosilicates with 3-dimensional alumosilicate structures containing water molecules, alkali and alkaline earth metals in their structural framework. They have proven a high potential as contaminant sorbents due to their high exchange capacity and their selectivity for certain constituents such as NH_4, Pb, Cd, Sr and others, especially when they are activated by sodium chloride. The selectivity of certain zeolite minerals for specific chemical compounds is defined by pore size and

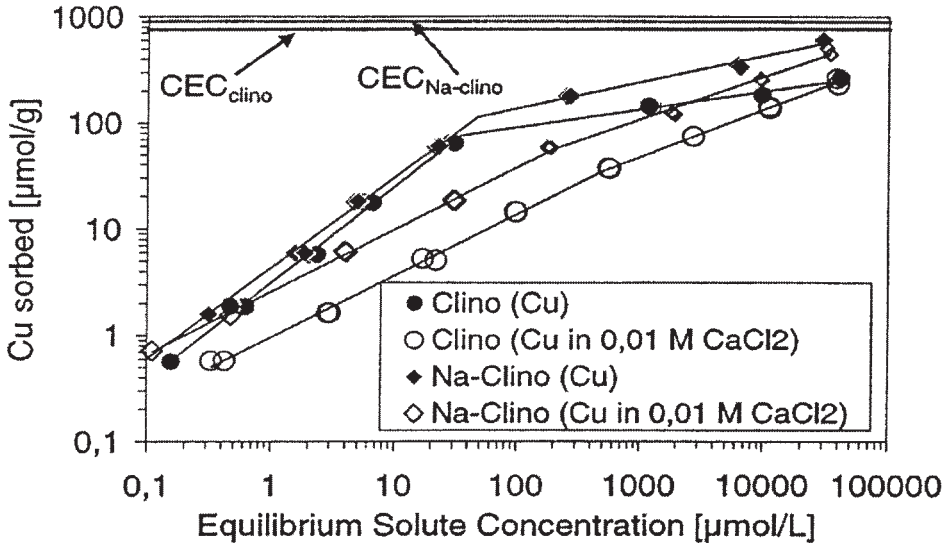

Fig. 4: Freundlich adsorption isotherms of Cu on natural clinoptilolite and Na-clinoptilolite in deionised water and in 0,01 M $CaCl_2$ solution, respectively (1g sample in 40 ml copper solutions, contact time 96 h, at 20° C). The CEC is also represented (clinoptilolite: 720 µmoleq/g and Na-clinoptilolite: 900 $\mu mol_{eq}/g$).

I. Inert waste

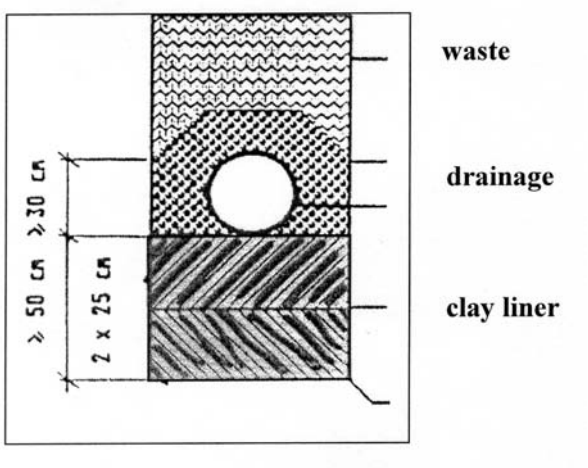

Fig. 5a: base liner system for inert waste. Two compacted clay liners without geomembrane.

II. Domestic waste

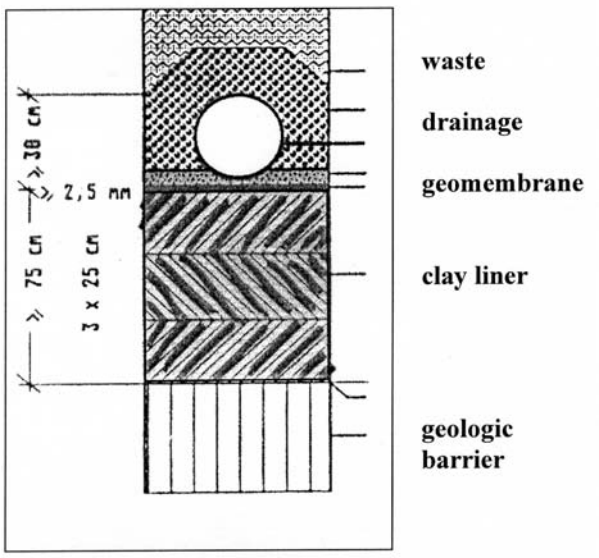

Fig. 5b: base liner system for domestic waste. Three compacted clay liners combined with a geomembrane.

charge properties of the structure. The unbalanced substitution of Si^{4+} by Al^{3+} in the crystal lattice leads - like in clay minerals - to a net negative charge and, subsequently, to the high cation exchange capacity of most natural zeolites.

Natural zeolites occure in sediments, lava vesicules, deuteric altered plutonic rocks and hydrothermal systems associated with alkaline volcanic rocks. In summary, natural zeolites generally originate from a volcanic glass precursor and are therefore very common in nature.

In Fig. 4, in order to show the retention potential, sorption isotherms are presented (Huttenloch et al., 2001). The example shows the sorption of Cu form

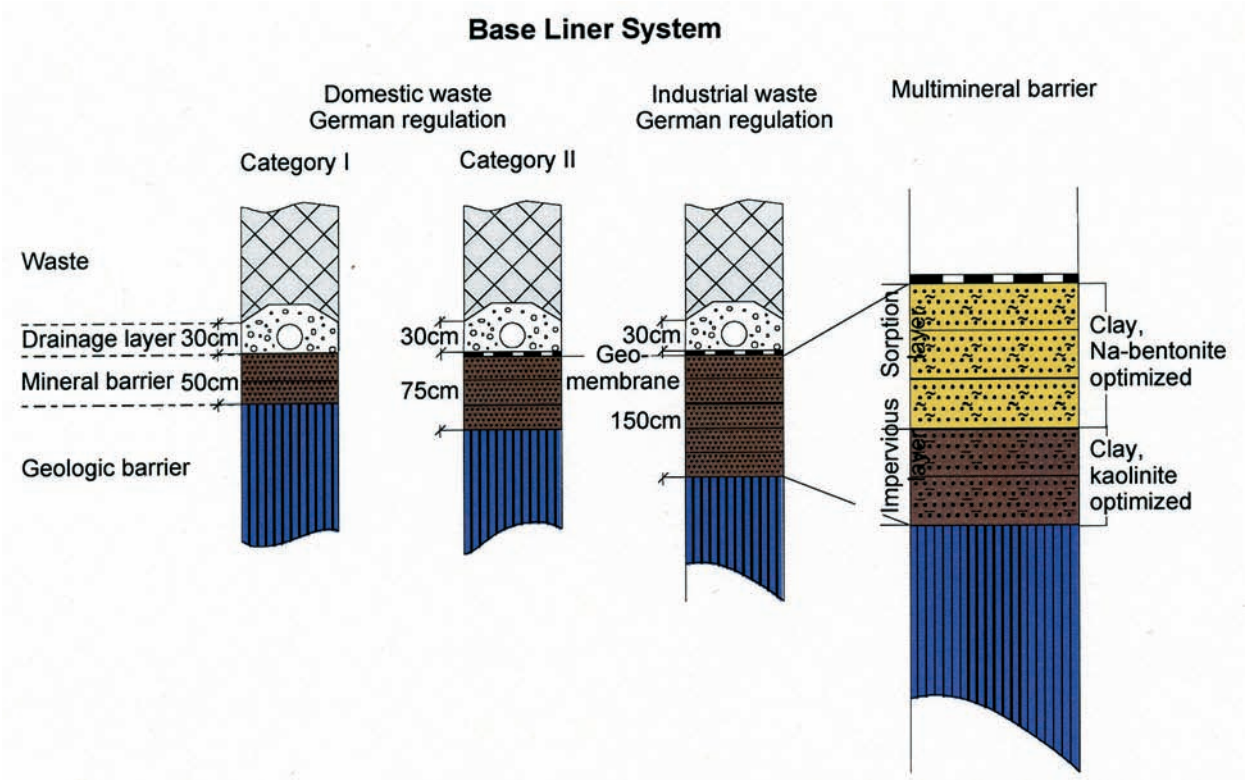

Fig. 6: base liner systems in comparison. The multibarrier system consists of two clay units: an adsorbing bentonite unit and a sealing kaolinite unit.

Fig. 7: REM image of kaolinitic clay, scale 5000x. High non communicating microporosity, electrically neutral two layer mineral without swelling potential. Preferable mineral phase for surface sealing.

Two layer minerals

- low swelling / shrinkage
- low sorption
- low self healing
- high permeability

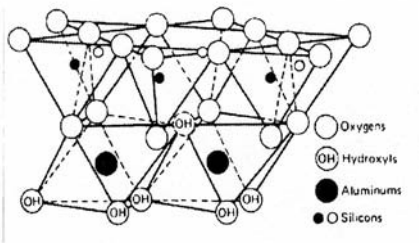

Fig. 8: Crystal structure of two layers clay mineral (e.g. kaolinite).

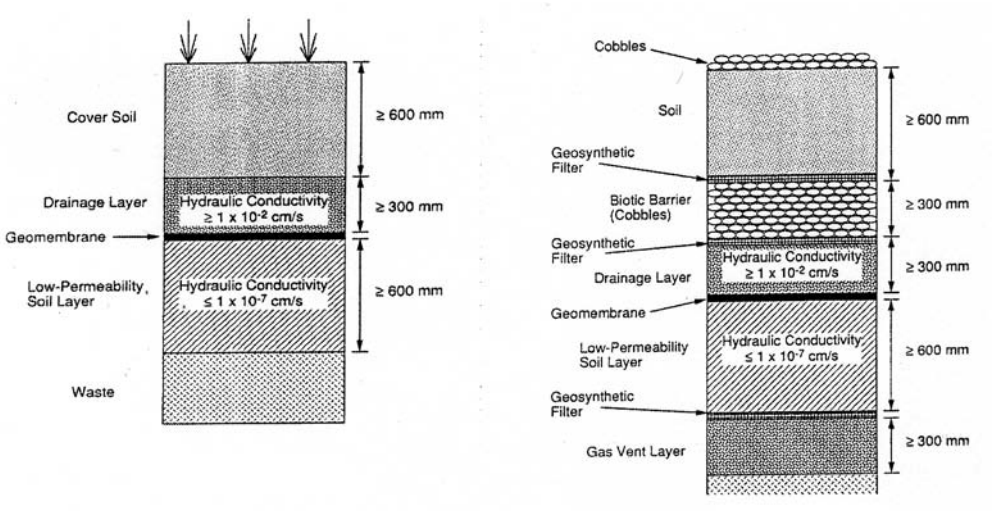

Fig. 9a and b: EPA recommendation for surface liner system in the USA. Clayey mineral barriers are combined with geomembranes. The optional system (right) comprises filter systems in addition: a biotic filter on top of the sealing units and a gas collection layer below.

dionised water and Cu from a 0,01 M Ca Cl_2 matrix solution on clinoptilolite (a very common natural zeolite spezies) and Na-clinoptilolite respectively. The isotherms indicate a non-linear sorption behaviour between sorbed and aqueous concentration of the contaminant, that can be described by the Freundlich equation: $c_s = K_f \cdot cw\ N_f$, where c_s designates the amount of the solute sorbed per unit mass of the sorbent, c_w = the equilibrrium solute concentration, K_f and N_f are empirical parameters specific to the sorption material used.

1.3 Waste deposit multibarrier system

Waste deposits can in principle be constructed as underground storages and at the surface as slope storage, slope dump or depression storage. The common domestic waste, incineration remnants, inert construction wastes etc. are stored at the surface. Underground storage as a special deposition mode is not treated in this chapter.

1.3.1 Base liners

Base liner systems have to prevent leakage from the waste to infiltrate into the subsoil and in addition to guarantee a high potential in toxicant retention by sorption, precipitation and/or redox processes (Rowe et al., 1995). Sorption on mineral surfaces means ion exchange according to chemical environment changes and surface charge properties. In many cases toxicants can be retarded during their migration through the sealing layers.

As an example Figs. 5 a and b show the base liner construction according to German regulations for inert wastes and domestic wastes. Essential are compacted clay layers and in case of domestic wastes a geomembrane in addition to the mineral layers and of course the geological barrier. The basal system contains a leakage collecting layer, connected with a leakage purification plant. There are different leakage detection systems on the market.

1.3.2 Surface liners

The functions of the surface liner systems have exclusively to be seen in preventing the precipitation water from infiltrating into the waste. In case of household wastes the capping system in addition has to have a gas drainage system. Capping layers for all types of waste of course are constructions with a drainage layer (usually gravel 16/32 mm) in case of leaks in the system.

Like in the case of basal systems, compacted clay liners (CCL), and geomembranes are the prevailing sealing elements. But there is an important differ-

ence in the clay mineral composition of the CCLs. Whereas the base CCL-clay should contain 3-layer-minerals as index minerals, e.g. montmorillonite, vermiculite etc., the surface CCL-clay should contain 2-layer-minerals as index minerals, e. g. kaolinite, etc. The 3-layer-clays enable retardation by adsorption and guarantee a high degree of impermeability and the 2-layer-clays of the surface sealing unit combined with sand/silt-matrix are practically impermeable as well but are weak in their adsorption potential. The latter is not required for the surface.

Fig. 7 shows the crystal lattice scheme of kaolinites, a two layer mineral, which combines an aluminium octahedron layers and silica tetrahedron layers. The center, and by their valency electrically balancing ion, is Al^{3+} respectively Si^{4+}. Because of the lack of negative surface charges the ion adsorption potential is extremely low. Because the particle is - like all other clay mineral particles - extremely small (< 2 µm), a sand-silt-kaolinite admixture for the mineral surface sealing can gain very low permeability values (k_f 10^{-8} to 10^{-12} cm/sec).

Conclusion

For hazardous industrial wastes and toxic sanitary landfills we have to locate a site which is primarely a geologic barrier, $k_f < 10^{-6}$ m/sec and at least of 3 m thickness. In case of inert (non toxic) wastes a geologic barrier is not necessary. Essential however is to follow the multibarrier concept and to add on top of the geologic barrier a system of engineered barriers and drainage layers. The engineered barriers comprise as a core unit the combined CCL and geomembrane double layer. A similar multibarrier system has to be constructed for the cover sealing. The difference is expressed in the type of GCL and the drainage layers. The GCL should not contain expanding three layer minerals like montmorillonite or vermiculite. They tend to dry out, forming desiccation cracks. Therefore non swelling two layer minerals like kaolinite or tectosilicates like zeolites should be the index minerals for the sand-silt-clay surface GCL. In case of untreated household waste, a gas drainage layer has to be foreseen to divert the methanol, developing during the waste decay.

References

Bradshaw, A.D., Southwood, R., Warner, F., 1992. The Treatment and Handling of wastes. Chapman & Hall, London, 302 p.

Bundesministerium für Umwelt, Naturschutz und Reaktorsicherheit, 2002. Verordnung über Deponien und Langzeitlager, Berlin.

Caldwell, J.A., Reith, C.C., 1993. Principles and Practice of Waste Encapsulation. Lewis Publishers, Michigan, 414 p.

Czurda, K.A. 1992. Deponie und Altlasten. EF-Verlag für Energie- und Umwelttechnik GmbH, Berlin, 406 p.

Drescher, J., 1997. Deponiebau. Alphabet KG, Berlin, 294 p.

Gassner, E., 1991. Gesamtfassung der Zweiten allgemeinen Verwaltungsvorschrift zum Abfallgesetz 1. Teil. Verlag Franz Rehm, München, 131p.

Hiltmann, W., Stribrny, B., 1998. Tonmineralogie und Bodenphysik. Springer-Verlag, Berlin, Heidelberg, New York, 297 p.

Huttenloch, P., Roehl, K.E., Czurda, K.A., 2001. Sorption of Nonpolar Aromativ Contaminants by Chlorosilane Surface Modified Natural Minerals. Environ. Sci. Technol., 35, pp. 4260 –4264.

Ministerium für Umwelt, Rheinland-Pfalz, 1993. TA Siedlungsabfall – Technische Anleitung zur Verwer - tung, Behandlung und sonstigen Entsorgung von Siedlungsabfällen. Bundesanzeiger, Köln, 117 p.

Rat der Europäischen Union, 1999. Richtlinie über Abfalldeponien. Amtsblatt der Europäischen Union, Brüssel.

Rowe, R. K., Quigley, R. M., Booker, J. R., 1995. Clayey Barrier Systems for waste disposal Facilities. Chapman & Hall, London, 390 p.

Buchbesprechungen

Geo.Alp, Vol. 3, S. 217–219, 2006

Buchbesprechung
von Diethard Sanders

DER ABGRUND DER ZEIT. DIE ENTWICKLUNG DER GEOHISTORIK 1670–1830 VON HELMUT W. FLÜGEL

Im Buch wird auf 250 Seiten in elf Abschnitten die Entstehung der kulturellen und naturwissenschaftlichen Grundlagen des Konzepts der „tiefen" Zeit dargelegt. Diese tiefe Zeit, heute zu einer scheinbaren Selbstverständlichkeit geworden, und die Methoden zu ihrer Unterteilung und Messung sind der vielleicht bedeutendste Beitrag der Geologie zu Wissenschaft und Kultur.

Der Autor Helmut Flügel beginnt mit einem persönlichen Erlebnis, der Betrachtung einer Ikonographie von 1430 von Jan van Eyck, in dem der Maler eine Fossilbank anscheinend gewollt präzise darstellte. Von Fragen bei der Betrachtung dieses Bildes ausgehend, wird die Entwicklung der Geohistorik dargelegt. Dabei muss sich der Autor notwendigerweise auf charakteristische Episoden zu bestimmten Zeiten mit bestimmten Akteuren beschränken. Das Buch zeigt dabei ein umfangreiches und den Leser unterhaltendes Wissen um Details, die nicht unbedingt genau dem Titelthema entsprechen. Es unterscheidet sich von bereits bestehenden Büchern und Büchlein zur Geschichte der Geologie zum einen durch diese Fülle an Detailwissen, zum anderen durch konsequentes Verbleiben dicht an einem reichhaltigen Material historischer Fakten. Insoferne hat es auch eine gewisse Eignung als Nachschlagewerk. Das mag man im Vergleich zu in brilliantem Stil geschriebenen, stark philosophielastigen Büchern wie „Time's arrow, time's cycle" von Stephen Jay Gould als einen Nachteil empfinden. Es hätte jedoch keinen Sinn, mit einem subtilen Meister dieses Genres, wie Gould es war, konkurrieren zu wollen oder ihn epigonenhaft zu kopieren, was leicht zum krampfhaften philosophischen Hinterfüttern von Platitüden führt.

Ein weiteres Verdienst des Autors besteht darin, immer wieder darauf hinzuweisen, dass auch die größten oder wenigstens großartigsten Wissenschafter durchaus den tiefer liegenden kulturellen Beschränktheiten und Mythen ihrer jeweiligen Zeit unterliegen, denn Wissenschaftsgeschichte ist unausweichlich auch zum guten Teil Kulturgeschichte. Dieser Verweis geschieht wiederum weit seltener durch explizites Anschreiben, sondern vielmehr durch Darlegung geschichtlicher Tatsachen, die für sich sprechen. Besonderen Wert hat Flügel darauf gelegt, die Widersprüchlichkeit und Kurvigkeit des Ganges wissenschaftlicher Erkenntnis aufzuzeigen, wobei auch dies zum guten Teil ein Ergebnis der Präsentation des historischen Faktenmaterials ist. Denn wirklich grundlegende Erkenntnisse wie die Entdeckung und Aufschlüsselung der geologischen Zeit geschehen - um mit Kurt Tucholsky zu sprechen - „nicht Mittags um zwölf Uhr zehn", sie sind das Ergebnis eines langwierigen Austausches und oft genug auch Konfliktes des einzelnen Wissenschafters mit sich selbst sowie mit seinem wissenschaftlichen und kulturellen Umfeld. Dies erscheint wichtig in einer Zeit, in der bestimmte Kreise die wirklichkeitsferne Vorstellung hegen oder wenigstens dem Mythos nachhängen, wissenschaftliche Grundlagenerkenntnis sei ähnlich kalkulierbar (auch finanziell) wie die Herstellung von Zahnpasta oder Tennissocken.

Das Buch ist in Deutsch geschrieben und nimmt so jenen, die zwar anstandslos englische Computermenus bedienen, aber klagen, wenn sie einen englischen Text lesen sollten, wenigstens eine Ausrede weg. Das Konzept der tiefen Zeit war und ist gerade durch seinen Widerspruch zur Alltagserfahrung immer wieder verhüllten und offenen Angriffen außerwissenschaftlicher Institutionen ausgesetzt, auch heute noch. Nicht zuletzt deshalb ist es sehr begrüßenswert, wenn ein Geowissenschafter über sein Fach schreibt und sich damit in eine im englischen Sprachraum bereits länger bestehende Tradition stellt. Dies spiegelt sich vielleicht auch darin wider, dass der Haupttitel des Buches die deutsche

Übersetzung eines ähnlichen, allerdings kürzeren wissenschaftsgeschichtlichen Werkes von Claude C. Albritton (1980) „The Abyss of Time" ist. Der einzige potentielle Nachteil des Buches könnte in der Länge des Gesamttextes gesehen werden, der etliche der zunehmend nur noch an Kurzbotschaften gewöhnten Leser vielleicht zur Resignation bringen mag. Glücklicherweise ist der Text jedoch größtenteils so strukturiert, dass auch einzelne Kapitel eigenständig gelesen werden können. Insgesamt bietet das Buch eine sehr gelungene und facettenreiche Darstellung der langsamen, von Zweifeln und Konflikten durchsetzten Annäherung des christlichen Abendlandes an eine Erscheinung, die in anderen Hochkulturen bereits lange davor eine selbstverständliche Größe war - der Abgrund der Zeit.

Helmut W. Flügel (2004): Der Abgrund der Zeit. Die Entwicklung der Geohistorik 1670-1830. Verlag für Geschichte der Naturwissenschaften und Technik. Berlin, Diepholz, 2004, 250 pp.
(service@gnt-verlag.de, http://www.gnt-verlag.de)

Buchbesprechung
von Diethard Sanders

EINFÜHRUNG IN DIE GEOLOGIE SÜDTIROLS. VON VOLKMAR STINGL & VOLKMAR MAIR

Auf nur 80 Seiten eine Einführung in die sehr vielfältige Geologie Südtirols zu schreiben ist eine Herausforderung, der sich die Autoren Volkmar Stingl (Innsbruck) und Volkmar Mayr (Bozen) gestellt haben. Dabei kommt den Autoren zugute, dass sie die besprochenen Abfolgen durch zahlreiche Feldaufenthalte selbst gut kennen und zum Teil auch an Neu-Deutungen aktiv mitgewirkt haben. Dies zeigt sich auch an den vielen sehr guten Fotos. Solche Bildersammlungen bekommt nur zusammen, wer auch selbst viel draussen ist.

Das Buch stellt die erste umfassende, dabei kurze Publikation über die Geologie Südtirols dar, und wurde zum Anlass des 32. International Geologen-Kongresses (Sommer 2004) in Florenz geschrieben, um verschiedene Exkursionen im Rahmen des Kongresses inhaltlich zu unterlagern. Dementsprechend ist die Sprache: knapp, klar und ohne Schnörkel. Meistens schreibt man von solchen Büchern, dass sie sich an Studierende wenden doch, Hand aufs Herz, auch der sogenannte Fachmann ist ab und zu recht froh, etwas, das er zu seinem grossen Wundern nicht mehr augenblicklich memoriert ganz im Stillen rasch nachschauen zu können. Die vom Verlag vorgegebene Kürze der Gesamtdarstellung erlaubte nicht die Darstellung von Säulenprofilen. Das Buch ist auch in Englisch erhältlich (An introduction to the geology of South Tyrol), wobei die englische Übersetzungskunst allerdings etwas zu wünschen übrig lässt. Dennoch ist das Buch vorwiegend Studenten - auch englischsprachigen - sehr zu empfehlen, die sich einen raschen Überlick über die verschiedenen Baueinheiten Südtirols, ihre Abfolge und ihre Metamorphose verschaffen wollen, ist aber sicher auch kein Schandfleck im Bücherregal des Experten.

Stingl, V., Mair, V. (2005), Einführung in die Geologie Südtirols. Autonome Provinz Bozen-Südtirol, Bozen. Kraler Druck, Bressanone/Varna, 80 Seiten.

Diethard Sanders, Institut für Geologie und Paläontologie, Leopold-Franzens-Universität Innsbruck, Innrain 52, a-6020 Innsbruck; e-mail: Diethard.G.Sanders@uibk.ac.at

Buchbesprechung
von Wolfgang Mette

MITTELMIOZÄNE OSTRACODEN AUS DEM WIENER BECKEN (BADENIUM/SARMATIUM, ÖSTERREICH) VON MARTIN GROSS & WERNER E. PILLER (HG.)

Der erste Sonderband der Schriftenreihe der Erdwissenschaftlichen Kommissionen bietet eine umfassende und detaillierte taxonomische Analyse flachmariner Ostrakoden aus dem Mittelmiozän der Zentralen Paratethys, die von Martin Gross im Rahmen seiner Dissertation durchgeführt wurde. Es werden 64 Arten beschrieben und anhand von 589 REM-Fotos (!) dokumentiert. Das sehr gut erhaltene und reichhaltige Material wurde aus 10 Kernbohrungen nahe Bad Deutsch-Altenburg am Südostrand des Wiener Beckens gewonnen, die im Zuge der Projektierungsphase für die „Staustufe Hainburg" in den frühen achtziger Jahren durchgeführt wurden.

Der taxonomischen Analyse, die den Hauptteil der Publikation ausmacht, ist ein Abriß der regionalen Geologie und mittelmiozänen Paläogeographie des Wiener Beckens im allgemeinen und der Region Bad Deutsch Altenburg – Hainburg/Donau im speziellen vorangestellt. Hier wird insbesondere die wechselhafte fazielle und biogeographische Entwicklung der Zentralen Paratethys als Folge von Meeresspiegelschwankungen und wiederholtem Öffnen und Schließen von Meeresverbindungen zum Mediterran und zur Östlichen Paratethys dargestellt.

Im systematischen Teil erfolgt eine ausführliche Beschreibung und Diskussion der Arten und ihrer stratigraphischen und regionalen Verbreitung, ergänzt durch detaillierte ökologische Diagnosen, die vielfach durch Daten verwandter rezenter Taxa im Mittelmeerraum gestützt werden.

Die taxonomische Arbeit zeichnet sich durch eine umfangreiche und qualitativ hochwertige Bilddokumentation der einzelnen Arten aus. Besonders positiv zu werten ist, dass neben der geschlechtsspezifischen Variabilität auch die oft erheblichen ontogenetischen Veränderungen ausführlich behandelt werden. Außerdem sind die taxonomisch wichtigen internen und externen Feinstrukturen wie Schließmuskelabdrücke, Schlosszähne und flächenständige Porenkanäle durch zahlreiche Detailfotos prägnant dokumentiert. Etwas eingehender hätte dagegen die Analyse der intraspezifischen Variabilität z.B. bei *Callistocythere* und möglicher ökologischer Steuerungsfaktoren sein können. In diesem Zusammenhang wäre auch eine Diskussion der Ökologie der verschiedenen Ostrakodenvergesellschaftungen insbesondere in Bezug zur Paläosalinität und zum Substrat wünschenswert gewesen.

Den Abschluß der Arbeit bildet ein kurzes Kapitel, in dem die biostratigraphische Bedeutung der einzelnen Ostrakodentaxa analysiert und ihre Verwertbarkeit für regionale Korrelationen kritisch beurteilt wird. Es zeigt sich, dass die biostratigraphische Aussagekraft der einzelnen Arten eher begrenzt ist aufgrund der sehr heterogenen Faziesentwicklung und der starken Faziesgebundenheit der meisten Taxa. Abgerundet wird der positive Gesamteindruck durch informative Abbildungen zur Regionalgeologie und Paläogeographie, Tabellen zur Chronostratigraphie, Biozonierung und stratigraphischen Reichweite der Arten sowie einen alphabetischen Index der Arten am Schluß.

Insgesamt handelt es sich also um ein gut gelungenes Werk, das eine wertvolle Basis für weiterführende mikropaläontologische, palökologische und biostratigraphische Forschungen im Neogen des alpinen Raums und angrenzender Gebiete darstellt.

Martin Gross; Werner E. Piller (Hg.) 2006: Mittelmiozäne Ostracoden aus dem Wiener Becken (Badenium/Sarmatium, Österreich). Österreichische Akademie der Wissenschaften, Schriftenreihe der Erdwissenschaftlichen Kommissionen, Sonderband 1, 224 S., 6 Abb., 4 Tab., 55 Taf..

Wolfgang Mette, Institut für Geologie und Paläontologie, Leopold-Franzens-Universität Innsbruck, Innrain 52, a-6020 Innsbruck; e-mail: Wolfgang.Mette@uibk.ac.at

Gredleriana

5

2005

NATURMUSEUM SÜDTIROL
MUSEO SCIENZE NATURALI ALTO ADIGE
MUSEUM NATÖRA SÜDTIROL

Die neue Veröffentlichungsreihe „Gredleriana" des Naturmuseums Südtirol (Bozen) ist ein Forum für naturwissenschaftliche Forschung in und über Südtirol. Sie stellt eine Kommunikationsplattform dar für alle jene, die in Südtirol forschen oder in der Ferne Südtirol und den alpinen Raum als Ziel ihrer naturwissenschaftlichen Forschung haben.
Band 5: 447 Seiten; 25 Euro
Abonnement (1 Band jährlich): 20 Euro

Geo.Alp

Veröffentlichungen des Instituts für Geologie und Paläontologie der Universität Innsbruck
und des
Naturmuseums Südtirol/Museo Scienze Naturali Alto Adige, Bozen/Bolzano

ISSN 1824-7741

Inhalt